How Optic Nerve Head Biomechanics has Clarified the Defining Pathophysiology and OCT Structural Phenotype of Human Glaucoma

The Goldmann Lecture

2024 Glaucoma Research Society Meeting
Siam Reap, Cambodia

November 15, 2024

Claude Burgoyne, MD
Emeritus Van Buskirk Chair for Ophthalmic Research
Past-Director, Optic Nerve Head Research Laboratory
Legacy Devers Eye Institute
Portland, OR
cfburgoyne@gmail.org

How Optic Nerve Head Biomechanics has Clarified the Defining Pathophysiology and OCT Structural Phenotype of Human Glaucoma

The Goldmann Lecture

2024 Glaucoma Research Society Meeting
Siam Reap, Cambodia

November 15, 2024

GRS Website Version - Please request permission to replicate in any form.

Claude Burgoyne, MD
Emeritus Van Buskirk Chair for Ophthalmic Research
Past-Director, Optic Nerve Head Research Laboratory
Legacy Devers Eye Institute
Portland, OR
cfburgoyne@gmail.org

Outline

- Professor Hans Goldmann
- Disclosures and Acknowledgements
- Creating *3D* Optic Nerve Head Histology and Morphology
- The Optic Nerve Head in Glaucoma
- What Defines a Glaucomatous Optic Neuropathy?
- 3D Histomorphometric Structural Phenotyping in Monkey Glaucoma
- 3D OCT Structural Phenotyping in Monkey and Human Glaucoma
- qIHC and 3D SBEM in Monkey EG
- Summary / Implications
- A Final Acknowledgement

Professor Hans Goldmann – Invention – Design – Development - Discovery

1937 - Invented the mirrored gonio-lens

1938 - Developed the modern slit lamp

1941 - Determined the volume of the Anterior Chamber

1945 - Detected the aqueous veins

1945 - Invented the Goldmann perimeter

1949 - Designed the three-mirror fundus lens

1950 - Developed fluorometric methods to measure aqueous flow and outflow facility

1954 - Invented the applanation tonometer

Courtesy of Anders Heijl

Past GRS Goldmann Lecturers

1994 – Stephen Drance, OC, MD

1998 – Anthony A.C.B. Molteno, MD

2003 – Douglas Anderson, MD

2005 – Yoshi Kitazawa, MD, PhD

2006 – Roger Hitchings FRCP, FRCOphth

2008 – George L. Spaeth, MD

2010 – Paul Kaufman, MD

2012 - Elke Lutjen-Drecoll, MD

2014 – Harry A. Quigley, MD

2016 - Anders Heijl, MD

2018 – Wallace L. M. Alward

2022 – Anja Tuulonen, MD

Outline

- Professor Hans Goldmann
- Disclosures and Acknowledgements
- Creating 3D Optic Nerve Head Anatomy and Morphology
- The Optic Nerve Head in Glaucoma
- What Defines a Glaucomatous Optic Neuropathy?
- 3D Histomorphometric Structural Phenotyping in Monkey Glaucoma
- 3D OCT Structural Phenotyping in Monkey and Human Glaucoma
- qIHC and 3D SBEM in Monkey EG
- Summary / Implications
- A Final Acknowledgement

Commercial/Intellectual Disclosures – None Active

Heidelberg Engineering

Previous instruments, software, occasional travel support
Previous Unrestricted research support
Previous Consultant – no personal income, no intellectual property
No travel support or honorarium for this talk

Past Funding

Past Funding

Optic Nerve Head Research Laboratory (ONHRL)

NIH R01EY011610 - NHP ONH Aging and Experimental Glaucoma, PI
NIH R01EY021281 - ONH OCT in Glaucoma, PI
NIH R01EY029087- ONH Glymphatics / Debris Clearance in Glaucoma, Co-I *(Marsh-Armstrong, PI)*

Legacy Good Samaritan, Devers Eye Institute Foundation
Sears Trust for Medical Research
Alcon Research Institute Award Monies
RPB Career Development Award Monies
Whitaker Foundation Award Monies
AHAF – Bright Focus Award Monies
American Glaucoma Society – Mid-Career Award Monies
Lewis Rudin Glaucoma Prize Monies
Association of International Glaucoma Societies (AIGS) Award Monies

Heidelberg Engineering – Instruments and Unrestricted Research Support

ONHRL Members and Collaborators

ONHRL Members
Stephanie Hager, BSc
Tanyo Klyce, BSc
Liqian Qiu, MD
Juan Reynaud, MScE
Hongli Yang, PhD
Jonathan Grimm, BSc
Wenxia Wang, BSc
Galen Williams, MSc
Christy Hardin, MSc
Luke Reyes, BSc
Cheri Stowell, PhD
Howard Lockwood, MScE
Priya Chaudhary, PhD

Devers Eye Institute Collaborators
Jack Cioffi, MD
Lin Wang, MD, PhD
Brad Fortune, OD, PhD
Stuart Gardiner, PhD
Shaban Demirel, OD, PhD
Grant Cull, MSc
Crawford Downs, PhD
Steve Mansberger, MD, MPH
Robert Kinast, MD

DEI ONHRL Doctoral Students and Post-Doctoral Research Fellows
Crawford Downs, PhD
Anthony Bellezza, PhD
Hongli Yang, PhD
Aurora Heickell, MD
Nick Strouthidis, MD, PhD
Ruojin Ren, MD, PhD
Lin (Jonathan) He, OD, PhD
Camila Zangalli, MD, MpH, PhD
Pui Yi Boey, MD
Kevin Ivers, PhD
Haomin Lao, MD
Seungwoo Hong, MD, PhD
Jin Wook Jeoung, MD, PhD
Yaxing Wang, MD, Phd
Anuwat Jiravarnsirikul, MD

Crawford Downs - PhD Students / Post-Doctoral Research Fellows
Hongli Yang, PhD
Michael Girard, PhD
Massimo Fazio, PhD
Mike Roberts, PhD
Ian Sigal, PhD
Rafael Grytz, PhD
Vincent Libertiaux, PhD

External Collaborators
Hilary Thompson, PhD
Chris Girkin, MD
Crawford Downs, PhD
Bal Chauhan, PhD
Marcelo Nicolela, MD
Jaime Vianna, MD
John Crabb, PhD
Ross Ethier, PhD
Andrew Feola, PhD
Nick Marsh-Armstrong, PhD
Mark Ellisman, PhD
Eric Bushong, PhD
Linda Zangwill, PhD
Mark Crawford, PhD
Glaucoma/Myopia OCT Phenotyping Consortium (GMOPC) Investigators

ONHRL Members and Collaborators

ONHRL Members
Stephanie Hager, BSc
Tanyo Klyce, BSc
Liqian Qiu, MD
Juan Reynaud, MScE
Hongli Yang, PhD
Jonathan Grimm, BSc
Wenxia Wang, BSc
Galen Williams, MSc
Christy Hardin, MSc
Luke Reyes, BSc
Cheri Stowell, PhD
Howard Lockwood, MScE
Priya Chaudhary, PhD

Devers Eye Institute Collaborators
Jack Cioffi, MD
Lin Wang, MD, PhD
Brad Fortune, OD, PhD
Stuart Gardiner, PhD
Shaban Demirel, OD, PhD
Grant Cull, MSc
Crawford Downs, PhD
Steve Mansberger, MD, MPH
Robert Kinast, MD

DEI ONHRL Doctoral Students and Post-Doctoral Research Fellows
Crawford Downs, PhD
Anthony Bellezza, PhD
Hongli Yang, PhD
Aurora Heickell, MD
Nick Strouthidis, MD, PhD
Ruojin Ren, MD, PhD
Lin (Jonathan) He, OD, PhD
Camila Zangalli, MD, MpH, PhD
Pui Yi Boey, MD
Kevin Ivers, PhD
Haomin Lao, MD
Seungwoo Hong, MD, PhD
Jin Wook Jeoung, MD, PhD
Yaxing Wang, MD, Phd
Anuwat Jiravarnsirikul, MD

Crawford Downs - PhD Students / Post-Doctoral Research Fellows
Hongli Yang, PhD
Michael Girard, PhD
Massimo Fazio, PhD
Mike Roberts, PhD
Ian Sigal, PhD
Rafael Grytz, PhD
Vincent Libertiaux, PhD

External Collaborators
Hilary Thompson, PhD
Chris Girkin, MD
Crawford Downs, PhD
Bal Chauhan, PhD
Marcelo Nicolela, MD
Jaime Vianna, MD
John Crabb, PhD
Ross Ethier, PhD
Andrew Feola, PhD
Nick Marsh-Armstrong, PhD
Mark Ellisman, PhD
Eric Bushong, PhD
Linda Zangwill, PhD
Mark Crawford, PhD
Glaucoma/Myopia OCT Phenotyping Consortium (GMOPC) Investigators

ONHRL Members

ONHRL Members
Stephanie Hager, BSc
Tanyo Klyce, BSc
Liqian Qiu, MD
Juan Reynaud, MScE
Hongli Yang, PhD
Jonathan Grimm, BSc
Wenxia Wang, BSc
Galen Williams, MSc
Christy Hardin, MSc
Luke Reyes, BSc
Cheri Stowell, PhD
Howard Lockwood, MScE
Priya Chaudhary, PhD

LSU - New Orleans - 1994

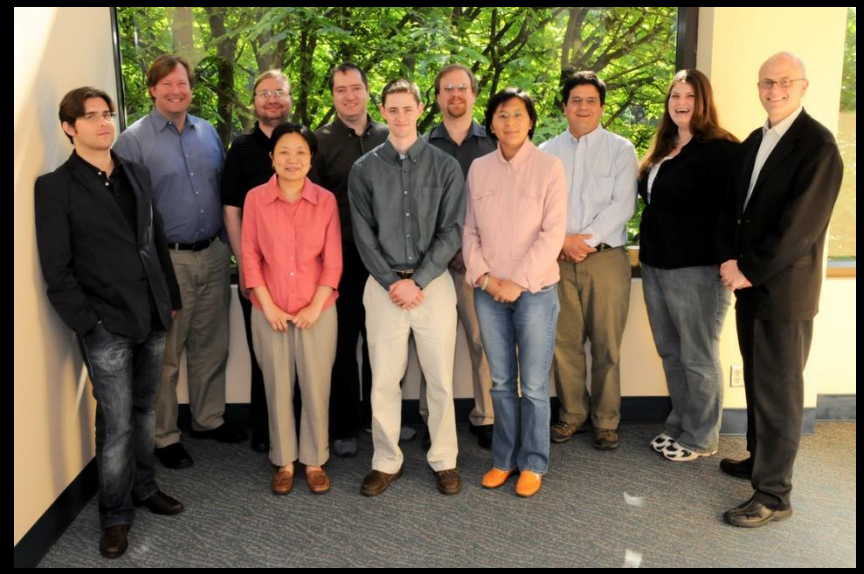

DEI - With Crawford Downs Lab - 2008

DEI -2015

DEI ONHRL Farewell Dinner 2023

Devers Eye Institute

Optic Nerve Head Research Laboratory (ONHRL) Collaborators

ONHRL Members

Stephanie Hager, BSc
Tanyo Klyce, BSc
Liqian Qium, MD
Juan Reynaud, MScE
Hongli Yang, PhD
Jonathan Grimm, BSc
Galen Williams, MSc
Christy Hardin, MSc
Luke Reyes, BSc
Cheri Stowell, PhD
Howard Lockwood, MScE
Priya Chaudhary, PhD

Devers Eye Institute Collaborators

Jack Cioffi, MD
Lin Wang, MD, PhD
Brad Fortune, OD, PhD
Stuart Gardiner, PhD
Shaban Demirel, OD, PhD
Grant Cull, MSc
Crawford Downs, PhD
Steve Mansberger, MD, MPH
Robert Kinast, MD

DEI ONHRL Doctoral Students and Post-Doctoral Research Fellows

Crawford Downs, PhD
Anthony Bellezza, PhD
Hongli Yang, PhD
Aurora Heickell, MD
Nick Strouthidis, MD, PhD
Ruojin Ren, MD, PhD
Lin (Jonathan) He, OD, PhD
Camila Zangalli, MD, MpH, PhD
Pui Yi Boey, MD
Kevin Ivers, PhD
Haomin Lao, MD
Seungwoo Hong, MD, PhD
Jin Wook Jeoung, MD, PhD
Yaxing Wang, MD, Phd
Anuwat Jiravarnsirikul, MD

Crawford Downs - PhD Students / Post-Doctoral Research Fellows

Hongli Yang, PhD
Michael Girard, PhD
Massimo Fazio, PhD
Mike Roberts, PhD
Ian Sigal, PhD
Rafael Grytz, PhD
Vincent Libertiaux, PhD

External Collaborators

Hilary Thompson, PhD
Chris Girkin, MD
Crawford Downs, PhD
Bal Chauhan, PhD
Marcelo Nicolela, MD
Jaime Vianna, MD
John Crabb, PhD
Ross Ethier, PhD
Andrew Feola, PhD
Nick Marsh-Armstrong, PhD
Mark Ellisman, PhD
Eric Bushong, PhD
Linda Zangwill, PhD
Mark Crawford, PhD
Glaucoma/Myopia OCT Phenotyping Consortium (GMOPC) Investigators

Devers Eye Institute (DEI)

Optic Nerve Head Research Laboratory (ONHRL) Collaborators

Devers Eye Institute – Discoveries in Sight Collaborators

Jack Cioffi, MD

Lin Wang, MD, PhD

Brad Fortune OD, PhD

Shaban Demirel BScOptom, PhD

Stuart Gardiner, PhD

Steve Mansberger, MD MPH

ONH Biomechanics

Incomplete list of Contributors to the Field

Engineers

- Ross Ethier, PhD
- Rich Hart, PhD
- Crawford Downs, PhD
- Anthony Bellezza, PhD
- Ian Sigal, PhD
- Michael Girard, PhD
- Hongli Yang, PhD
- Rafael Grytz, PhD
- Michael Roberts, PhD
- Massimo Fazio, PhD
- Vicky Nguyen, PhD
- Baptiste Coudrillier, PhD
- Jonathan Vande Geest, PhD
- Andrew Feola, PhD
- Bryan Samuels, MD, PhD
- Jun Liu, PhD

Clinicians / Scientists

- Harry Quigley, MD
- Ran Zeimer, PhD
- Don Minckler, MD
- John Flanagan, OD, PhD
- Aachal Kotecha, OD, PhD
- Nicholas Strouthidis, MD, PhD
- Lutz Pillunat, MD, PhD
- Chris Girkin, MD
- Joel Schuman, MD
- Gadi Wollstein, MD
- Julie Albon, MD
- Wojciech Karwatowski, MD
- Colm O'Brien
- Mark Lesk, MD
- Tae Woo Kim, MD
- Jost Jonas, MD
- Robert Weinreb, MD
- Joseph Demer, MD, PhD
- Brad Fortune, OD, PhD
- Jeff Liebmann, MD
- Yaxing Wang, MD, PhD
- Eberhard Spoerl, PhD
- Rosario Hernandez, PhD
- Alon Harris, PhD
- Giovanna Guidoboni, PhD
- Mark Johnson, PhD
- All colleagues working on TM / Scleral / Corneal Biomechanics

Burgoyne–2024 Goldmann–GRS Website

ONH Biomechanics

Incomplete list of Contributors to the Field

Engineers

- Ross Ethier, PhD
- Rich Hart, PhD
- Crawford Downs, PhD
- Anthony Bellezza, PhD
- Ian Sigal, PhD
- Michael Girard, PhD
- Hongli Yang, PhD
- Rafael Grytz, PhD
- Michael Roberts, PhD
- Massimo Fazio, PhD
- Vicky Nguyen, PhD
- Baptiste Coudrillier, PhD
- Jonathan Vande Geest, PhD
- Andrew Feola, PhD
- Bryan Samuels, MD, PhD
- Jun Liu, PhD

Clinicians / Scientists

- Harry Quigley, MD
- Ran Zeimer, PhD
- Don Minckler, MD
- John Flanagan, OD, PhD
- Aachal Kotecha, OD, PhD
- Nicholas Strouthidis, MD, PhD
- Lutz Pillunat, MD, PhD
- Chris Girkin, MD
- Joel Schuman, MD
- Gadi Wollstein, MD
- Julie Albon, MD
- Wojciech Karwatowski, MD
- Colm O'Brien
- Mark Lesk, MD
- Tae Woo Kim, MD
- Jost Jonas, MD
- Robert Weinreb, MD
- Joseph Demer, MD, PhD
- Brad Fortune, OD, PhD
- Jeff Liebmann, MD
- Yaxing,Wang, MD, PhD
- Eberhard Spoerl, PhD
- Rosario Hernandez, PhD
- Alon Harris, PhD
- Giovanna Guidoboni, PhD
- Mark Johnson, PhD
- All colleagues working on TM / Scleral / Corneal Biomechanics

Harry Quigley 1990 Lecture at Armed Forces Institute of Pathology – Washington, DC

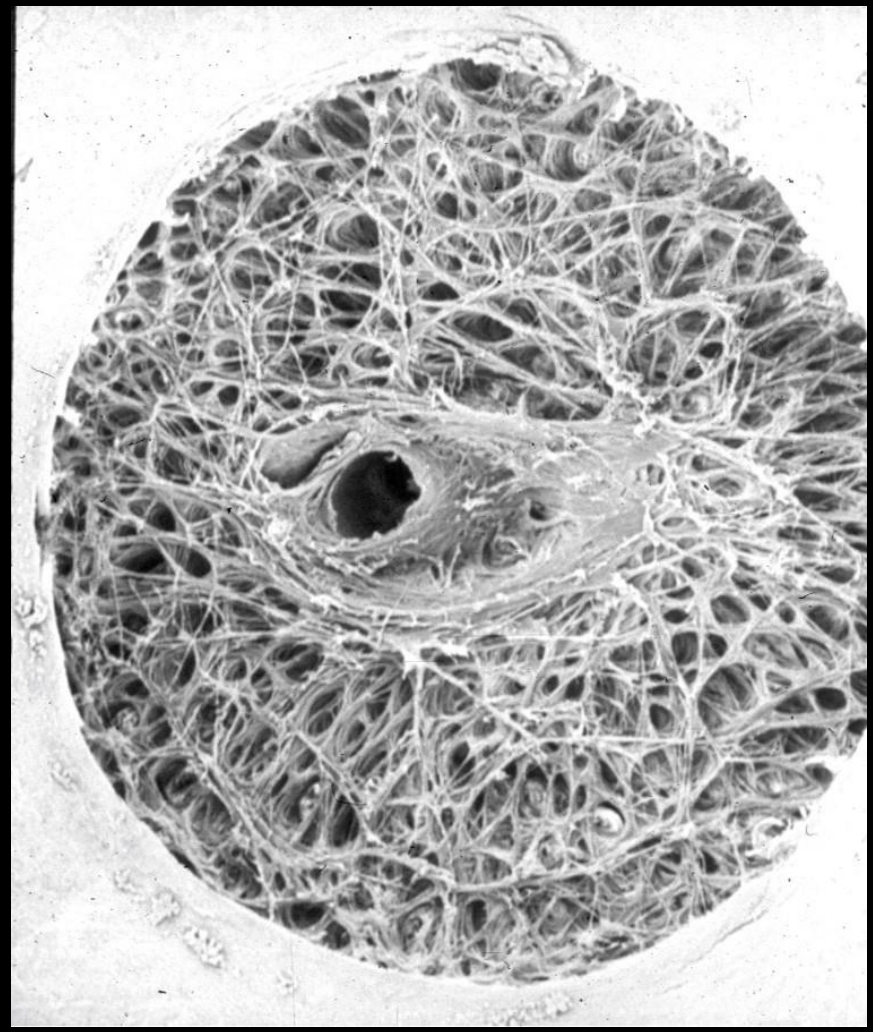

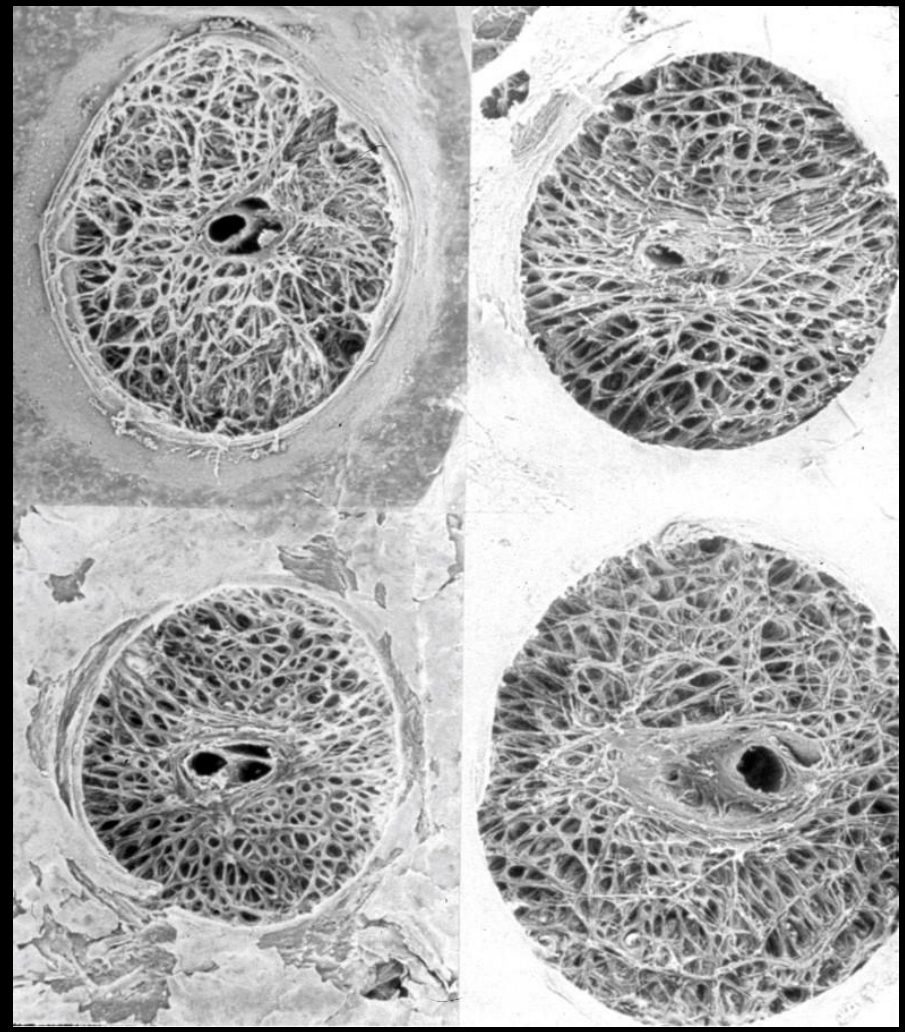

I was filled with a confluence of excitement / enthusiasm / gratitude and urgency!

Harry Quigley 1990 Lecture at Armed Forces Institute of Pathology – Washington, DC

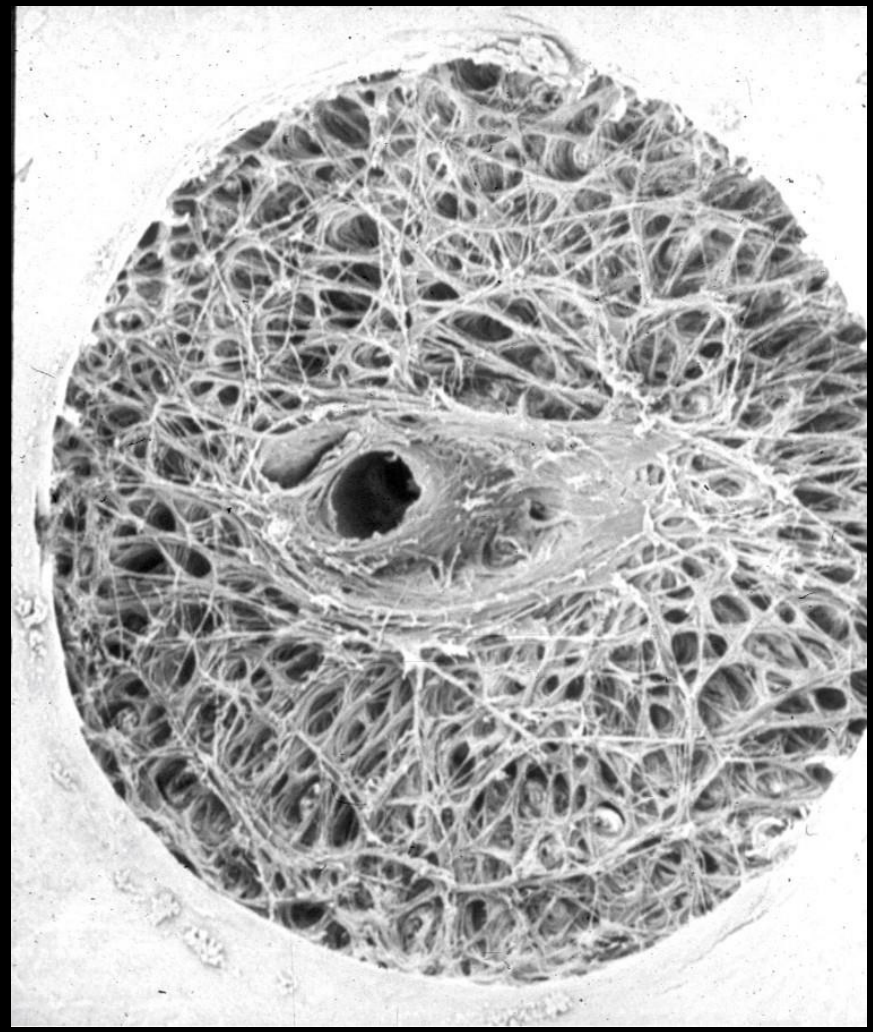

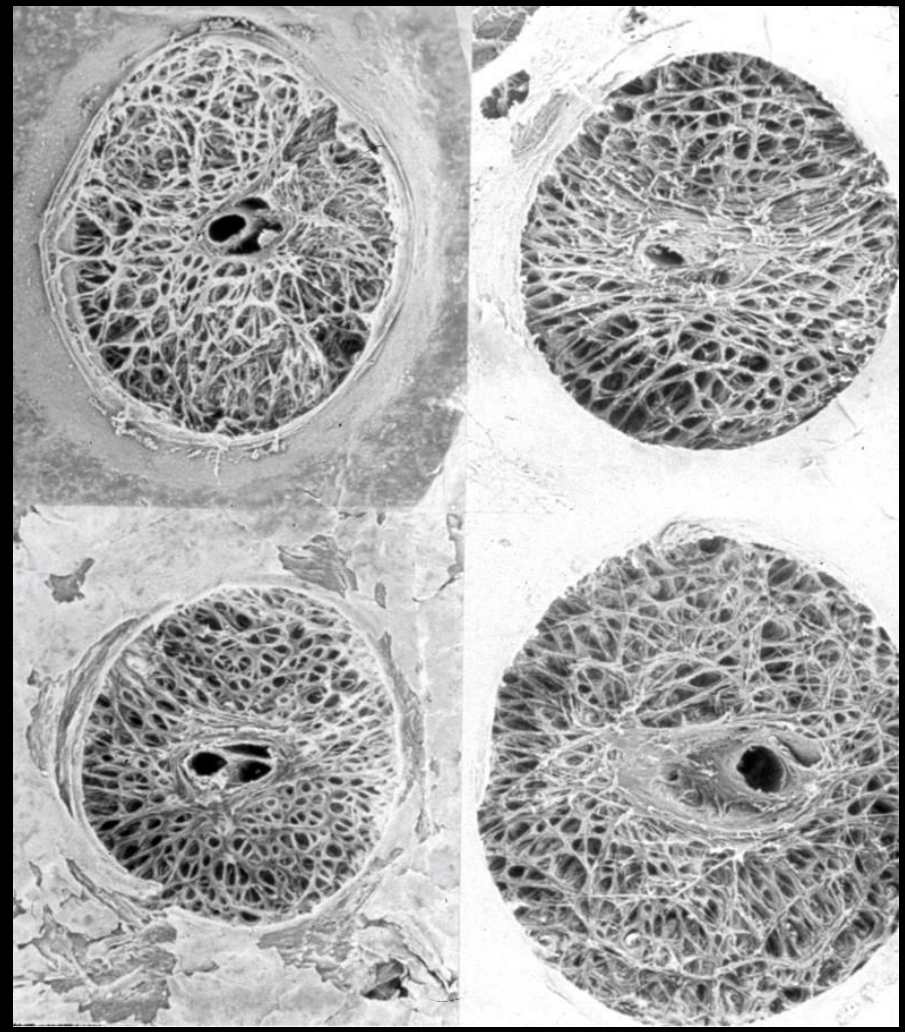

I felt that my exposure to Architecture and Engineering had prepared me to study these tissues – and now knew the next step for doing so…..

Harry Quigley / Don Zack - Wilmer Glaucoma Clinical/Research Fellowship 1991-1993

Longitudinal in-vivo ONH surface hypercompliance then stiffening in Monkey early-endstage experimental glaucoma eyes.

Measurement of Optic Disc Compliance by Digitized Image Analysis in the Normal Monkey Eye

Claude F. Burgoyne, MD,[1,2] Harry A. Quigley, MD,[1,3] Hilary W. Thompson, PhD,[4] Susan Vitale, MHS,[3] Rohit Varma MD, MPH[5]

Purpose: To characterize the compliance of the normal monkey optic disc under conditions of induced short-term fluctuations in intraocular pressure (IOP).

Methods: In 10 monkeys, one eye was compliance tested on three separate days followed by a single test of the contralateral eye (40 compliance tests). In a testing session, the optic disc was imaged at 2 and 47 minutes (baseline time point) after IOP was lowered to 10 mmHg; then at 2, 17, 32, and 47 minutes after IOP was elevated to 45 mmHg; then at 2, 47, and, in some cases, 92 minutes after IOP was lowered back to 10 mmHg. Eight digitized images were analyzed at each time point, yielding two parameters to characterize the position of the disc: the *Mean Position of the Disc* (MPD) and the *Change from* $MPD_{Baseline}$ (the value of MPD at a given time point minus the value for MPD at the baseline time point of that testing session). Analysis of variance (ANOVA) testing was used to evaluate the overall effect of IOP on both parameters while taking into account the effects of variability due to different monkeys and repetitions of the test as well as differences between the two eyes of an individual monkey. With the addition of data from 11 compliance tests performed on eight additional monkeys, the overall results were calculated in terms of the mean *Change from* $MPD_{Baseline}$ at each time point for a total of 51 compliance testing sessions.

Results: The mean *Change from* $MPD_{Baseline}$ was −28 μm (95% confidence interval, −23 to −33 μm) 47 minutes after elevation of IOP. The disc surface returned to its baseline position 92 minutes after IOP was lowered back to 10 mmHg. Elevation of IOP within a compliance test had a significant effect on the position of the optic disc surface ($P = 0.0002$, ANOVA), as characterized by the parameter *Change from* $MPD_{Baseline}$. Neither the difference in the amount of movement between the two eyes of an individual monkey nor the variability within the three repetitions of the test in a given eye was statistically significant.

Conclusion: Small, reversible (elastic) posterior deformations of the optic disc surface follow acute elevations of IOP in the normal monkey eye. Detection of acute IOP-induced deformations of the optic disc surface may represent a means by which to mechanically test the deeper load-bearing tissues of the optic nerve head.

Ophthalmology 1995;102:1790–1799

Burgoyne, et al, Ophthalmology 1995

Early Changes in Optic Disc Compliance and Surface Position in Experimental Glaucoma

Claude F. Burgoyne, MD,[1,2] Harry A. Quigley, MD,[1,3] Hilary W. Thompson, PhD,[4] Susan Vitale, MHS,[3] Rohit Varma, MD, MPH[5]

Purpose: To detect changes in the compliance and baseline position (position at the baseline time point of a compliance test) of the monkey optic disc after the onset of chronic experimental glaucoma.

Methods: Sixty-six compliance tests were performed on 26 eyes of 13 monkeys. *Longitudinal Study.* In seven normal monkeys, compliance tests were performed three times in one eye (study eye) and once in the contralateral eye. In the study eye of five of these monkeys, chronic experimental glaucoma was then induced and compliance tests were performed at some or all of the following postglaucoma testing intervals: 1 to 2 weeks, 3 to 4 weeks, 5 to 8 weeks, 9 to 12 weeks, 13 to 18 weeks, and more than 18 weeks after the onset of elevated intraocular pressure (IOP). In the study eye of the remaining two monkeys, the optic nerve was transected, and compliance was tested at 5, 9, and 13 weeks after transection. An analysis of variance (ANOVA) was performed to detect an increase (hypercompliance) or decrease (rigidity) in the compliance of the glaucomatous eyes at each testing interval. A second ANOVA was performed to detect the onset of chronic posterior deformation of the baseline position of each disc. *Cross-Sectional Study.* In six additional monkeys with pre-existing experimental glaucoma, the glaucomatous study eye was compliance tested at one of the postglaucoma testing intervals used in the longitudinal study. The contralateral normal eye was compliance tested once. These data were then added to the data from the five longitudinally studied monkeys at the appropriate preglaucoma and postglaucoma testing intervals. A third ANOVA was done to compare the compliance of the expanded group of glaucomatous eyes at each postintervention testing interval with the compliance of the 13 normal contralateral eyes.

Results: *Compliance.* In the longitudinally ($Pr > F = 0.0005$) and cross-sectionally ($Pr > F = 0.0001$) studied glaucomatous eyes, optic disc compliance increased significantly by 1 to 2 weeks and then returned to a level statistically indistinguishable from normal within 13 to 18 weeks after the onset of glaucoma. In the transection eyes, the optic discs were significantly less compliant (more rigid) at 5 and 9 weeks after transection compared with the discs in either the normal or the glaucomatous eyes ($Pr > F < 0.05$). *Baseline Optic Disc Position.* Chronic posterior deformation of the disc was detected in one of three eyes tested 1 to 2 weeks and three of four eyes tested 3 to 4 weeks after the onset of glaucoma ($Pr > F < 0.05$). Chronic posterior deformation was not detected in the discs of either of the transection eyes at any of the post-transection testing intervals.

Conclusion: Changes in optic disc compliance and surface position were detected by digitized image analysis within 2 to 4 weeks of the onset of experimental glaucoma in the monkey eye. These findings are unlikely to be due to axon loss alone, because they did not occur in optic nerve transection eyes (which constitute a model of axon loss in which intraocular pressures remain normal). The results suggest that IOP-related damage to the load-bearing connective tissues of the optic nerve head may occur early in the course of experimental glaucoma.

Ophthalmology 1995;102:1800–1809

Burgoyne, et al, Ophthalmology 1995

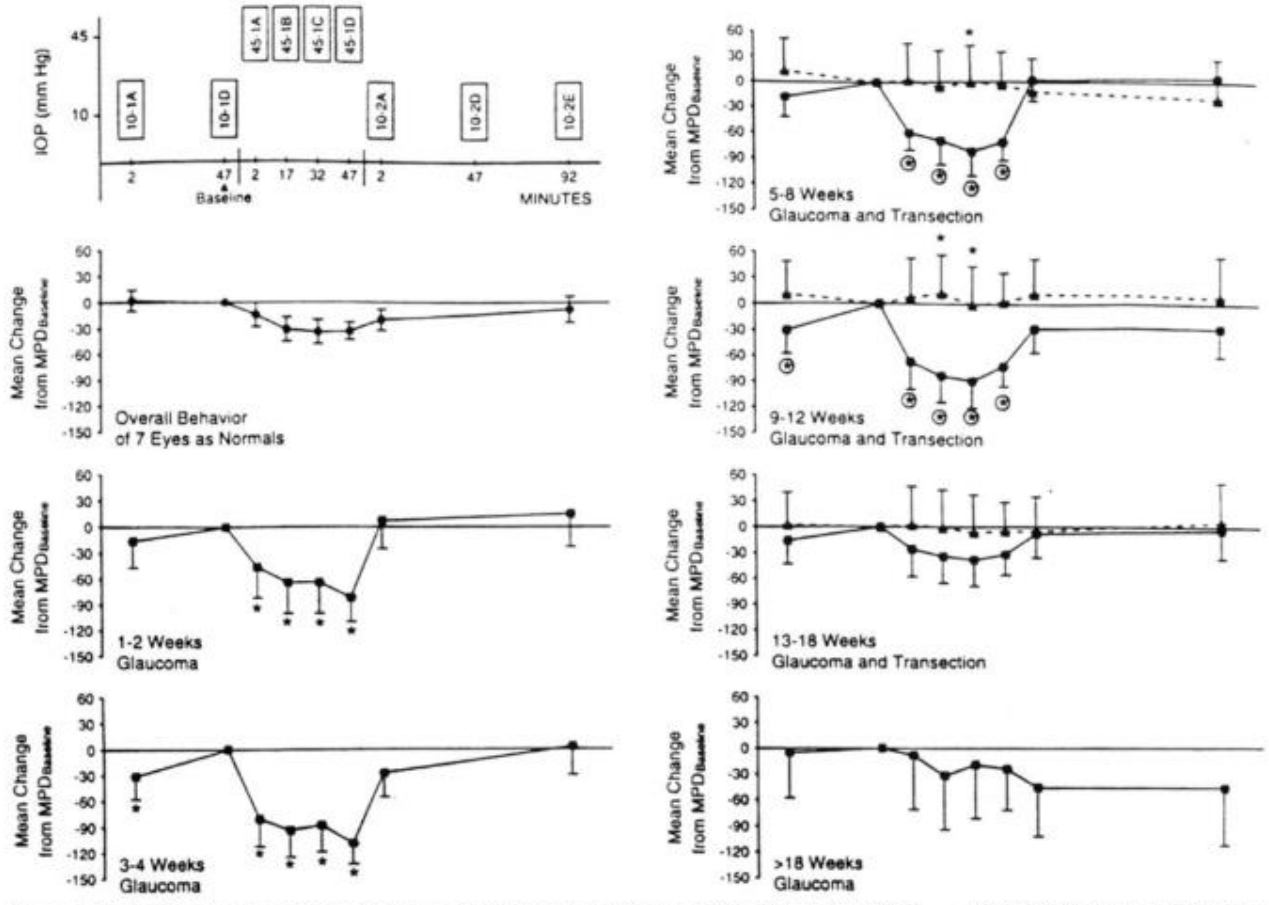

Figure 1. Optic disc compliance changes within the longitudinally studied eyes. Mean *Change from* $MPD_{Baseline}$ and ANOVA-generated 95% CI at each compliance test time point for glaucomatous eyes (■), transection eyes (▲), and study eyes as normal (●). An asterisk denotes a compliance test time point at which the mean *Change from* $MPD_{Baseline}$ was significantly different ($P < 0.05$, ANOVA) from the mean *Change from* $MPD_{Baseline}$ for the study eyes tested as normal at the same time point. A circle around the asterisk denotes time points at which the mean *Change from* $MPD_{Baseline}$ for the glaucomatous eyes was significantly greater ($P < 0.05$, ANOVA) than the corresponding mean *Change from* $MPD_{Baseline}$ for the transection eyes.

Burgoyne–2024 Goldmann–GRS Website

Harry Quigley / Don Zack - Wilmer Glaucoma Clinical/Research Fellowship 1991-1993

Progressive Stiffening (only) in Transection Eyes

Measurement of Optic Disc Compliance by Digitized Image Analysis in the Normal Monkey Eye

Claude F. Burgoyne, MD,[1,2] Harry A. Quigley, MD,[1,3]
Hilary W. Thompson, PhD,[4] Susan Vitale, MHS,[3] Rohit Varma MD, MPH[5]

Purpose: To characterize the compliance of the normal monkey optic disc under conditions of induced short-term fluctuations in intraocular pressure (IOP).

Methods: In 10 monkeys, one eye was compliance tested on three separate days followed by a single test of the contralateral eye (40 compliance tests). In a testing session, the optic disc was imaged at 2 and 47 minutes (baseline time point) after IOP was lowered to 10 mmHg; then at 2, 17, 32, and 47 minutes after IOP was elevated to 45 mmHg; then at 2, 47, and, in some cases, 92 minutes after IOP was lowered back to 10 mmHg. Eight digitized images were analyzed at each time point, yielding two parameters to characterize the position of the disc: the *Mean Position of the Disc* (MPD) and the *Change from* $MPD_{Baseline}$ (the value of MPD at a given time point minus the value for MPD at the baseline time point of that testing session). Analysis of variance (ANOVA) testing was used to evaluate the overall effect of IOP on both parameters while taking into account the effects of variability due to different monkeys and repetitions of the test as well as differences between the two eyes of an individual monkey. With the addition of data from 11 compliance tests performed on eight additional monkeys, the overall results were calculated in terms of the mean *Change from* $MPD_{Baseline}$ at each time point for a total of 51 compliance testing sessions.

Results: The mean *Change from* $MPD_{Baseline}$ was −28 μm (95% confidence interval, −23 to −33 μm) 47 minutes after elevation of IOP. The disc surface returned to its baseline position 92 minutes after IOP was lowered back to 10 mmHg. Elevation of IOP within a compliance test had a significant effect on the position of the optic disc surface ($P = 0.0002$, ANOVA), as characterized by the parameter *Change from* $MPD_{Baseline}$. Neither the difference in the amount of movement between the two eyes of an individual monkey nor the variability within the three repetitions of the test in a given eye was statistically significant.

Conclusion: Small, reversible (elastic) posterior deformations of the optic disc surface follow acute elevations of IOP in the normal monkey eye. Detection of acute IOP-induced deformations of the optic disc surface may represent a means by which to mechanically test the deeper load-bearing tissues of the optic nerve head.

Ophthalmology 1995;102:1790–1799

Burgoyne, et al, Ophthalmology 1995

Early Changes in Optic Disc Compliance and Surface Position in Experimental Glaucoma

Claude F. Burgoyne, MD,[1,2] Harry A. Quigley, MD,[1,3]
Hilary W. Thompson, PhD,[4] Susan Vitale, MHS,[3] Rohit Varma, MD, MPH[5]

Purpose: To detect changes in the compliance and baseline position (position at the baseline time point of a compliance test) of the monkey optic disc after the onset of chronic experimental glaucoma.

Methods: Sixty-six compliance tests were performed on 26 eyes of 13 monkeys. *Longitudinal Study.* In seven normal monkeys, compliance tests were performed three times in one eye (study eye) and once in the contralateral eye. In the study eye of five of these monkeys, chronic experimental glaucoma was then induced and compliance tests were performed at some or all of the following postglaucoma testing intervals: 1 to 2 weeks, 3 to 4 weeks, 5 to 8 weeks, 9 to 12 weeks, 13 to 18 weeks, and more than 18 weeks after the onset of elevated intraocular pressure (IOP). In the study eye of the remaining two monkeys, the optic nerve was transected, and compliance was tested at 5, 9, and 13 weeks after transection. An analysis of variance (ANOVA) was performed to detect an increase (hypercompliance) or decrease (rigidity) in the compliance of the glaucomatous eyes at each testing interval. A second ANOVA was performed to detect the onset of chronic posterior deformation of the baseline position of each disc. *Cross-Sectional Study.* In six additional monkeys with pre-existing experimental glaucoma, the glaucomatous study eye was compliance tested at one of the postglaucoma testing intervals used in the longitudinal study. The contralateral normal eye was compliance tested once. These data were then added to the data from the five longitudinally studied monkeys at the appropriate preglaucoma and postglaucoma testing intervals. A third ANOVA was done to compare the compliance of the expanded group of glaucomatous eyes at each postintervention testing interval with the compliance of the 13 normal contralateral eyes.

Results: *Compliance.* In the longitudinally ($Pr > F = 0.0005$) and cross-sectionally ($Pr > F = 0.0001$) studied glaucomatous eyes, optic disc compliance increased significantly by 1 to 2 weeks and then returned to a level statistically indistinguishable from normal within 13 to 18 weeks after the onset of glaucoma. In the transection eyes, the optic discs were significantly less compliant (more rigid) at 5 and 9 weeks after transection compared with the discs in either the normal or the glaucomatous eyes ($Pr > F < 0.05$). *Baseline Optic Disc Position.* Chronic posterior deformation of the disc was detected in one of three eyes tested 1 to 2 weeks and three of four eyes tested 3 to 4 weeks after the onset of glaucoma ($Pr > F < 0.05$). Chronic posterior deformation was not detected in the discs of either of the transection eyes at any of the post-transection testing intervals.

Conclusion: Changes in optic disc compliance and surface position were detected by digitized image analysis within 2 to 4 weeks of the onset of experimental glaucoma in the monkey eye. These findings are unlikely to be due to axon loss alone, because they did not occur in optic nerve transection eyes (which constitute a model of axon loss in which intraocular pressures remain normal). The results suggest that IOP-related damage to the load-bearing connective tissues of the optic nerve head may occur early in the course of experimental glaucoma.

Ophthalmology 1995;102:1800–1809

Burgoyne, et al, Ophthalmology 1995

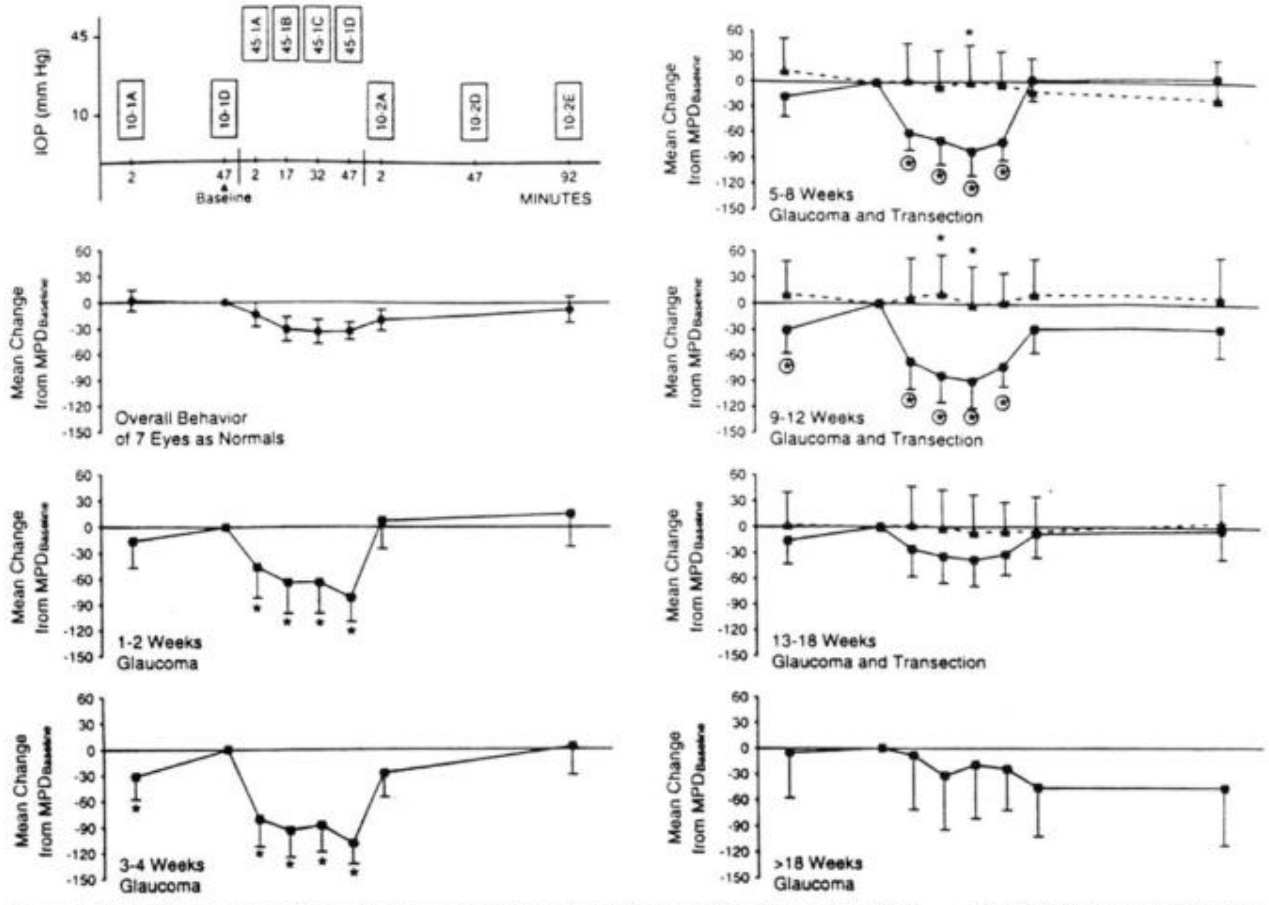

Figure 1. Optic disc compliance changes within the longitudinally studied eyes. Mean *Change from* $MPD_{Baseline}$ and ANOVA-generated 95% CI at each compliance test time point for glaucomatous eyes (■), transection eyes (▲), and study eyes as normal (●). An asterisk denotes a compliance test time point at which the mean *Change from* $MPD_{Baseline}$ was significantly different ($P < 0.05$, ANOVA) from the mean *Change from* $MPD_{Baseline}$ for the study eyes tested as normal at the same time point. A circle around the asterisk denotes time points at which the mean *Change from* $MPD_{Baseline}$ for the glaucomatous eyes was significantly greater ($P < 0.05$, ANOVA) than the corresponding mean *Change from* $MPD_{Baseline}$ for the transection eyes.

Burgoyne–2024 Goldmann–GRS Website

Harry Quigley/ Don Zack - Wilmer Glaucoma Clinical/Research Fellowship 1991-1993

But all of this was based on the ONH surface!!!

Measurement of Optic Disc Compliance by Digitized Image Analysis in the Normal Monkey Eye

Claude F. Burgoyne, MD,[1,2] Harry A. Quigley, MD,[1,3] Hilary W. Thompson, PhD,[4] Susan Vitale, MHS,[3] Rohit Varma MD, MPH[5]

Purpose: To characterize the compliance of the normal monkey optic disc under conditions of induced short-term fluctuations in intraocular pressure (IOP).

Methods: In 10 monkeys, one eye was compliance tested on three separate days followed by a single test of the contralateral eye (40 compliance tests). In a testing session, the optic disc was imaged at 2 and 47 minutes (baseline time point) after IOP was lowered to 10 mmHg; then at 2, 17, 32, and 47 minutes after IOP was elevated to 45 mmHg; then at 2, 47, and, in some cases, 92 minutes after IOP was lowered back to 10 mmHg. Eight digitized images were analyzed at each time point, yielding two parameters to characterize the position of the disc: the *Mean Position of the Disc* (MPD) and the *Change from* $MPD_{Baseline}$ (the value of MPD at a given time point minus the value for MPD at the baseline time point of that testing session). Analysis of variance (ANOVA) testing was used to evaluate the overall effect of IOP on both parameters while taking into account the effects of variability due to different monkeys and repetitions of the test as well as differences between the two eyes of an individual monkey. With the addition of data from 11 compliance tests performed on eight additional monkeys, the overall results were calculated in terms of the mean *Change from* $MPD_{Baseline}$ at each time point for a total of 51 compliance testing sessions.

Results: The mean *Change from* $MPD_{Baseline}$ was −28 μm (95% confidence interval, −23 to −33 μm) 47 minutes after elevation of IOP. The disc surface returned to its baseline position 92 minutes after IOP was lowered back to 10 mmHg. Elevation of IOP within a compliance test had a significant effect on the position of the optic disc surface ($P = 0.0002$, ANOVA), as characterized by the parameter *Change from* $MPD_{Baseline}$. Neither the difference in the amount of movement between the two eyes of an individual monkey nor the variability within the three repetitions of the test in a given eye was statistically significant.

Conclusion: Small, reversible (elastic) posterior deformations of the optic disc surface follow acute elevations of IOP in the normal monkey eye. Detection of acute IOP-induced deformations of the optic disc surface may represent a means by which to mechanically test the deeper load-bearing tissues of the optic nerve head.

Ophthalmology 1995;102:1790–1799

Burgoyne, et al, Ophthalmology 1995

Early Changes in Optic Disc Compliance and Surface Position in Experimental Glaucoma

Claude F. Burgoyne, MD,[1,2] Harry A. Quigley, MD,[1,3] Hilary W. Thompson, PhD,[4] Susan Vitale, MHS,[3] Rohit Varma, MD, MPH[5]

Purpose: To detect changes in the compliance and baseline position (position at the baseline time point of a compliance test) of the monkey optic disc after the onset of chronic experimental glaucoma.

Methods: Sixty-six compliance tests were performed on 26 eyes of 13 monkeys. *Longitudinal Study.* In seven normal monkeys, compliance tests were performed three times in one eye (study eye) and once in the contralateral eye. In the study eye of five of these monkeys, chronic experimental glaucoma was then induced and compliance tests were performed at some or all of the following postglaucoma testing intervals: 1 to 2 weeks, 3 to 4 weeks, 5 to 8 weeks, 9 to 12 weeks, 13 to 18 weeks, and more than 18 weeks after the onset of elevated intraocular pressure (IOP). In the study eye of the remaining two monkeys, the optic nerve was transected, and compliance was tested at 5, 9, and 13 weeks after transection. An analysis of variance (ANOVA) was performed to detect an increase (hypercompliance) or decrease (rigidity) in the compliance of the glaucomatous eyes at each testing interval. A second ANOVA was performed to detect the onset of chronic posterior deformation of the baseline position of each disc. *Cross-Sectional Study.* In six additional monkeys with pre-existing experimental glaucoma, the glaucomatous study eye was compliance tested at one of the postglaucoma testing intervals used in the longitudinal study. The contralateral normal eye was compliance tested once. These data were then added to the data from the five longitudinally studied monkeys at the appropriate preglaucoma and postglaucoma testing intervals. A third ANOVA was done to compare the compliance of the expanded group of glaucomatous eyes at each postintervention testing interval with the compliance of the 13 normal contralateral eyes.

Results: *Compliance.* In the longitudinally ($Pr > F = 0.0005$) and cross-sectionally ($Pr > F = 0.0001$) studied glaucomatous eyes, optic disc compliance increased significantly by 1 to 2 weeks and then returned to a level statistically indistinguishable from normal within 13 to 18 weeks after the onset of glaucoma. In the transection eyes, the optic discs were significantly less compliant (more rigid) at 5 and 9 weeks after transection compared with the discs in either the normal or the glaucomatous eyes ($Pr > F < 0.05$). *Baseline Optic Disc Position.* Chronic posterior deformation of the disc was detected in one of three eyes tested 1 to 2 weeks and three of four eyes tested 3 to 4 weeks after the onset of glaucoma ($Pr > F < 0.05$). Chronic posterior deformation was not detected in the discs of either of the transection eyes at any of the post-transection testing intervals.

Conclusion: Changes in optic disc compliance and surface position were detected by digitized image analysis within 2 to 4 weeks of the onset of experimental glaucoma in the monkey eye. These findings are unlikely to be due to axon loss alone, because they did not occur in optic nerve transection eyes (which constitute a model of axon loss in which intraocular pressures remain normal). The results suggest that IOP-related damage to the load-bearing connective tissues of the optic nerve head may occur early in the course of experimental glaucoma.

Ophthalmology 1995;102:1800–1809

Burgoyne, et al, Ophthalmology 1995

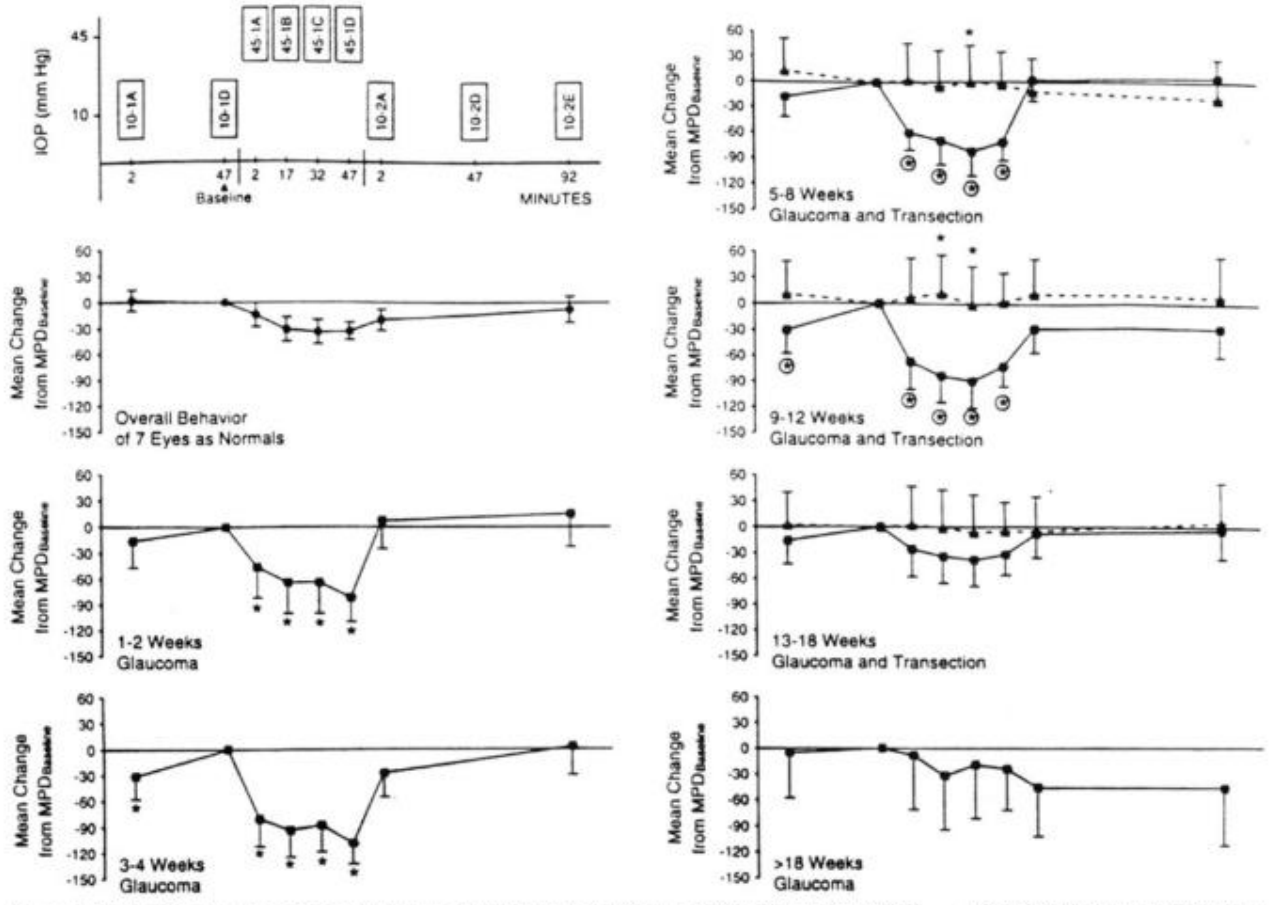

Figure 1. Optic disc compliance changes within the longitudinally studied eyes. Mean *Change from* $MPD_{Baseline}$ and ANOVA-generated 95% CI at each compliance test time point for glaucomatous eyes (■), transection eyes (▲), and study eyes as normal (●). An asterisk denotes a compliance test time point at which the mean *Change from* $MPD_{Baseline}$ was significantly different ($P < 0.05$, ANOVA) from the mean *Change from* $MPD_{Baseline}$ for the study eyes tested as normal at the same time point. A circle around the asterisk denotes time points at which the mean *Change from* $MPD_{Baseline}$ for the glaucomatous eyes was significantly greater ($P < 0.05$, ANOVA) than the corresponding mean *Change from* $MPD_{Baseline}$ for the transection eyes.

Burgoyne–2024 Goldmann–GRS Website

Harry Quigley / Don Zack - Wilmer Glaucoma Clinical/Research Fellowship 1991-1993

I wanted to generate digital 3D Optic Nerve Head Anatomy / Morphology / Electron Microscopy

Measurement of Optic Disc Compliance by Digitized Image Analysis in the Normal Monkey Eye

Claude F. Burgoyne, MD,[1,2] Harry A. Quigley, MD,[1,3]
Hilary W. Thompson, PhD,[4] Susan Vitale, MHS,[3] Rohit Varma MD, MPH[5]

Purpose: To characterize the compliance of the normal monkey optic disc under conditions of induced short-term fluctuations in intraocular pressure (IOP).

Methods: In 10 monkeys, one eye was compliance tested on three separate days followed by a single test of the contralateral eye (40 compliance tests). In a testing session, the optic disc was imaged at 2 and 47 minutes (baseline time point) after IOP was lowered to 10 mmHg; then at 2, 17, 32, and 47 minutes after IOP was elevated to 45 mmHg; then at 2, 47, and, in some cases, 92 minutes after IOP was lowered back to 10 mmHg. Eight digitized images were analyzed at each time point, yielding two parameters to characterize the position of the disc: the *Mean Position of the Disc* (MPD) and the *Change from* $MPD_{Baseline}$ (the value of MPD at a given time point minus the value for MPD at the baseline time point of that testing session). Analysis of variance (ANOVA) testing was used to evaluate the overall effect of IOP on both parameters while taking into account the effects of variability due to different monkeys and repetitions of the test as well as differences between the two eyes of an individual monkey. With the addition of data from 11 compliance tests performed on eight additional monkeys, the overall results were calculated in terms of the mean *Change from* $MPD_{Baseline}$ at each time point for a total of 51 compliance testing sessions.

Results: The mean *Change from* $MPD_{Baseline}$ was −28 μm (95% confidence interval, −23 to −33 μm) 47 minutes after elevation of IOP. The disc surface returned to its baseline position 92 minutes after IOP was lowered back to 10 mmHg. Elevation of IOP within a compliance test had a significant effect on the position of the optic disc surface ($P = 0.0002$, ANOVA), as characterized by the parameter *Change from* $MPD_{Baseline}$. Neither the difference in the amount of movement between the two eyes of an individual monkey nor the variability within the three repetitions of the test in a given eye was statistically significant.

Conclusion: Small, reversible (elastic) posterior deformations of the optic disc surface follow acute elevations of IOP in the normal monkey eye. Detection of acute IOP-induced deformations of the optic disc surface may represent a means by which to mechanically test the deeper load-bearing tissues of the optic nerve head.

Ophthalmology 1995;102:1790–1799

Burgoyne, et al, Ophthalmology 1995

Early Changes in Optic Disc Compliance and Surface Position in Experimental Glaucoma

Claude F. Burgoyne, MD,[1,2] Harry A. Quigley, MD,[1,3]
Hilary W. Thompson, PhD,[4] Susan Vitale, MHS,[3] Rohit Varma, MD, MPH[5]

Purpose: To detect changes in the compliance and baseline position (position at the baseline time point of a compliance test) of the monkey optic disc after the onset of chronic experimental glaucoma.

Methods: Sixty-six compliance tests were performed on 26 eyes of 13 monkeys. *Longitudinal Study.* In seven normal monkeys, compliance tests were performed three times in one eye (study eye) and once in the contralateral eye. In the study eye of five of these monkeys, chronic experimental glaucoma was then induced and compliance tests were performed at some or all of the following postglaucoma testing intervals: 1 to 2 weeks, 3 to 4 weeks, 5 to 8 weeks, 9 to 12 weeks, 13 to 18 weeks, and more than 18 weeks after the onset of elevated intraocular pressure (IOP). In the study eye of the remaining two monkeys, the optic nerve was transected, and compliance was tested at 5, 9, and 13 weeks after transection. An analysis of variance (ANOVA) was performed to detect an increase (hypercompliance) or decrease (rigidity) in the compliance of the glaucomatous eyes at each testing interval. A second ANOVA was performed to detect the onset of chronic posterior deformation of the baseline position of each disc. *Cross-Sectional Study.* In six additional monkeys with pre-existing experimental glaucoma, the glaucomatous study eye was compliance tested at one of the postglaucoma testing intervals used in the longitudinal study. The contralateral normal eye was compliance tested once. These data were then added to the data from the five longitudinally studied monkeys at the appropriate preglaucoma and postglaucoma testing intervals. A third ANOVA was done to compare the compliance of the expanded group of glaucomatous eyes at each postintervention testing interval with the compliance of the 13 normal contralateral eyes.

Results: *Compliance.* In the longitudinally ($Pr > F = 0.0005$) and cross-sectionally ($Pr > F = 0.0001$) studied glaucomatous eyes, optic disc compliance increased significantly by 1 to 2 weeks and then returned to a level statistically indistinguishable from normal within 13 to 18 weeks after the onset of glaucoma. In the transection eyes, the optic discs were significantly less compliant (more rigid) at 5 and 9 weeks after transection compared with the discs in either the normal or the glaucomatous eyes ($Pr > F < 0.05$). *Baseline Optic Disc Position.* Chronic posterior deformation of the disc was detected in one of three eyes tested 1 to 2 weeks and three of four eyes tested 3 to 4 weeks after the onset of glaucoma ($Pr > F < 0.05$). Chronic posterior deformation was not detected in the discs of either of the transection eyes at any of the post-transection testing intervals.

Conclusion: Changes in optic disc compliance and surface position were detected by digitized image analysis within 2 to 4 weeks of the onset of experimental glaucoma in the monkey eye. These findings are unlikely to be due to axon loss alone, because they did not occur in optic nerve transection eyes (which constitute a model of axon loss in which intraocular pressures remain normal). The results suggest that IOP-related damage to the load-bearing connective tissues of the optic nerve head may occur early in the course of experimental glaucoma.

Ophthalmology 1995;102:1800–1809

Burgoyne, et al, Ophthalmology 1995

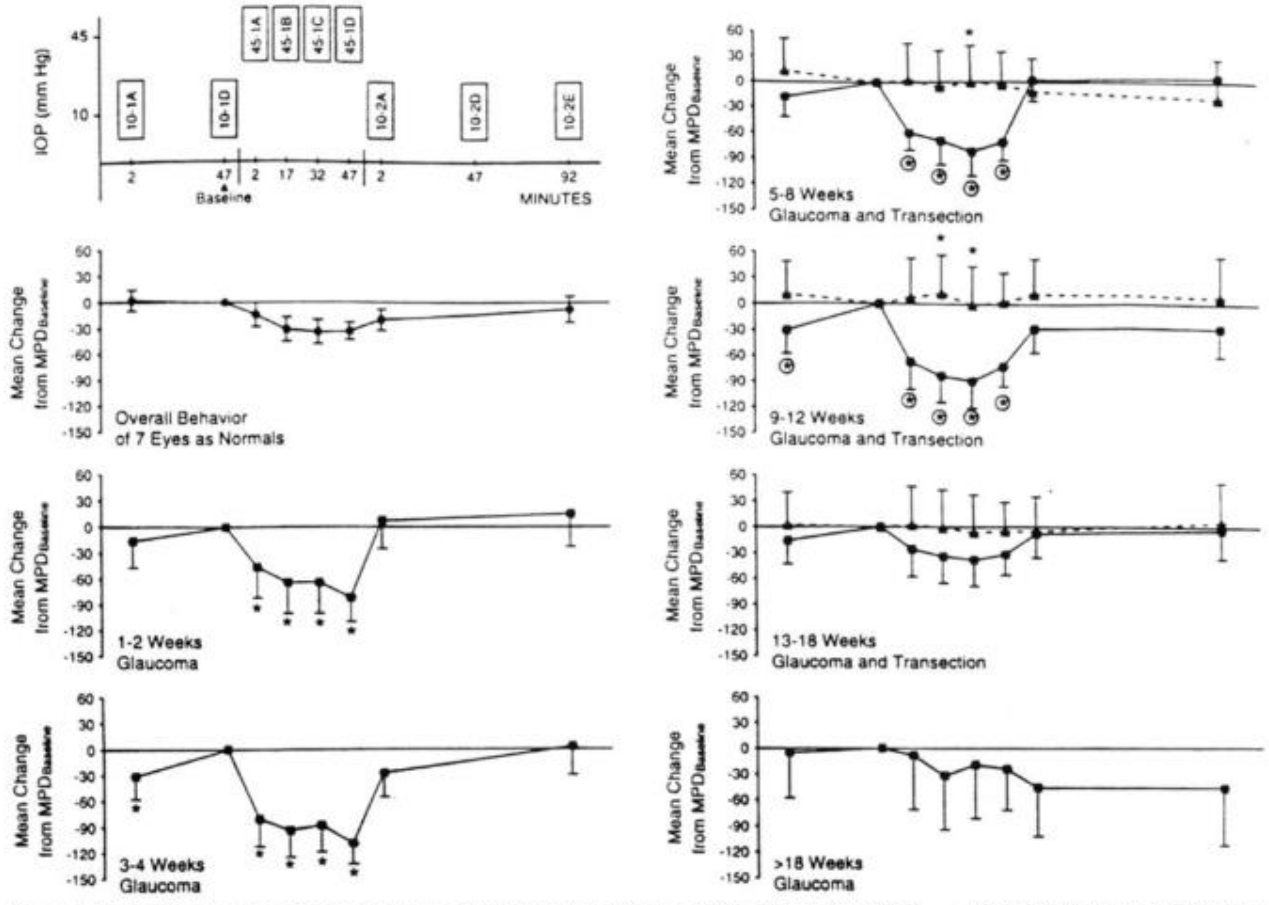

Figure 1. Optic disc compliance changes within the longitudinally studied eyes. Mean *Change from* $MPD_{Baseline}$ and ANOVA-generated 95% CI at each compliance test time point for glaucomatous eyes (■), transection eyes (▲), and study eyes as normal (●). An asterisk denotes a compliance test time point at which the mean *Change from* $MPD_{Baseline}$ was significantly different ($P < 0.05$, ANOVA) from the mean *Change from* $MPD_{Baseline}$ for the study eyes tested as normal at the same time point. A circle around the asterisk denotes time points at which the mean *Change from* $MPD_{Baseline}$ for the glaucomatous eyes was significantly greater ($P < 0.05$, ANOVA) than the corresponding mean *Change from* $MPD_{Baseline}$ for the transection eyes.

Burgoyne–2024 Goldmann–GRS Website

Outline

- Professor Hans Goldmann
- Disclosures and Acknowledgements
- Digital *3D* Optic Nerve Head Anatomy and Morphology
- The Optic Nerve Head in Glaucoma
- What Defines a Glaucomatous Optic Neuropathy?
- FoBMO 3D Histomorphometric Structural Phenotyping in Monkey Glaucoma
- FoBMO 3D OCT Structural Phenotyping in Monkey and Human Glaucoma
- FoBMO qIHC and 3D SBEM in Monkey EG
- Summary / Implications
- A Final Acknowledgement

VISUALIZATION IS A HYPOTHESIS FORMING STEP!!!

3D VISUALIZATION
of ONH Anatomy and Morphology
is ESSENTIAL to
understanding its complexity.

Digital 3D ONH Anatomy / Morphology / Electron Microscopy

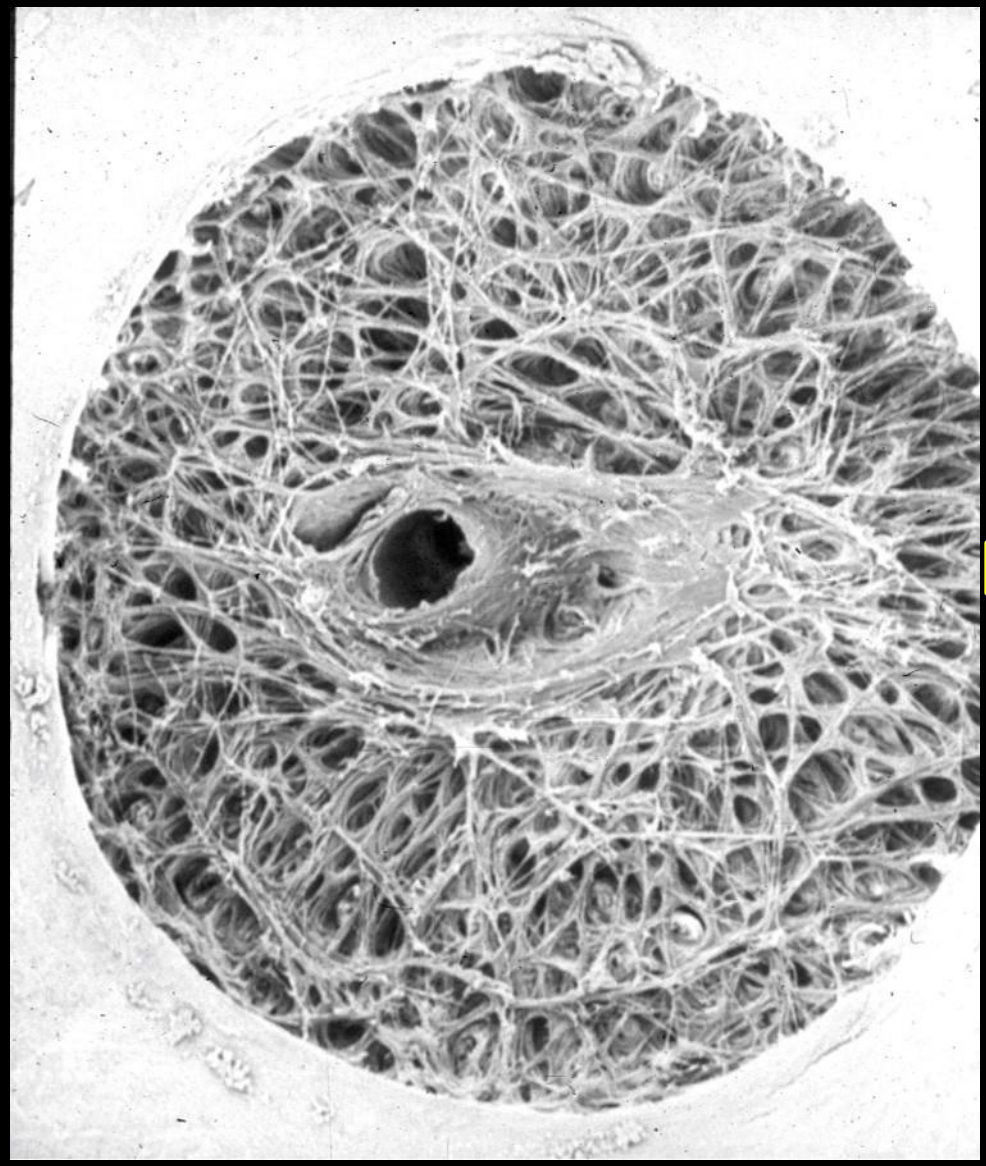

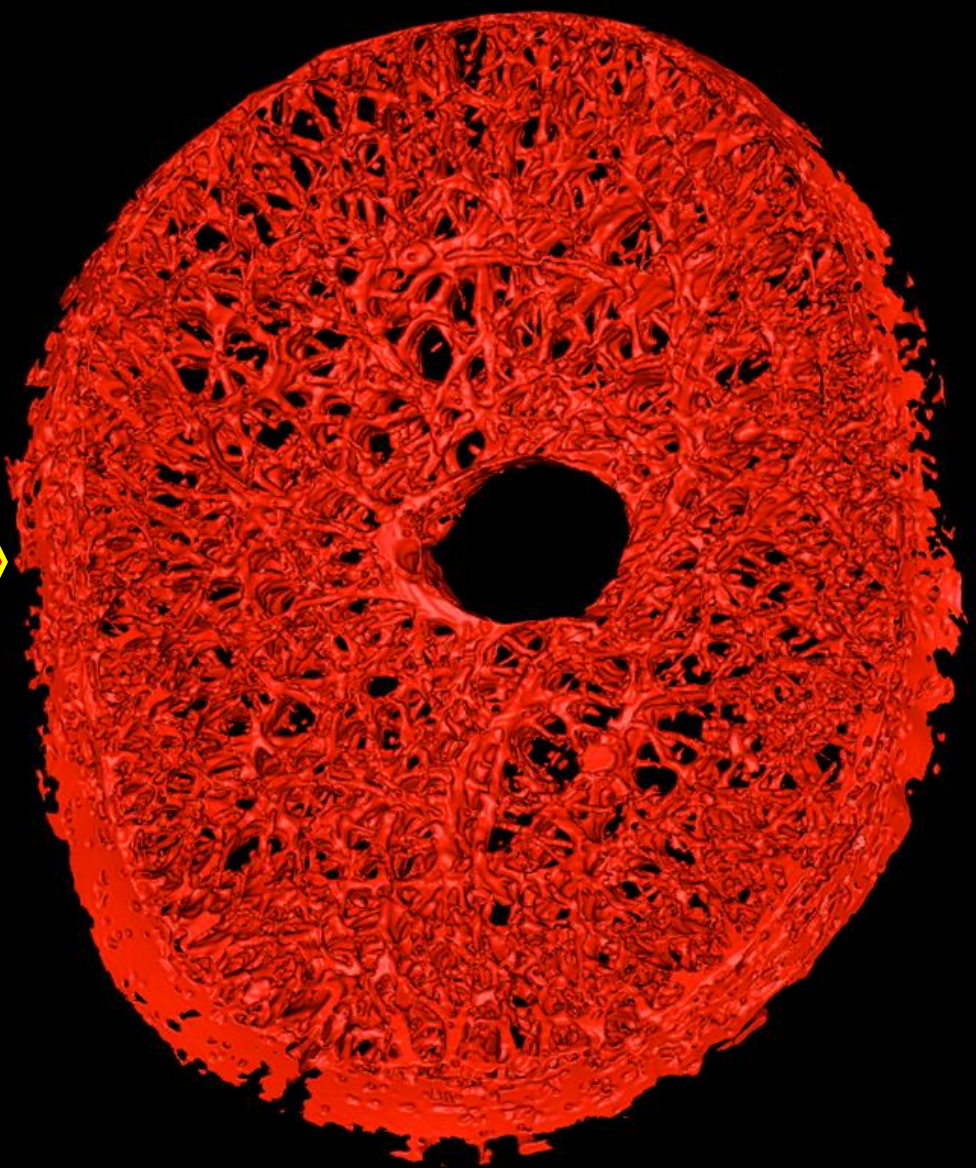

From 2D ONH SEM 1980s

To High Resolution Digital 3D HMRN

Burgoyne–2024 Goldmann–GRS Website

ONH Biomechanics

Incomplete list of Contributors to the Field

Engineers

- Ross Ethier, PhD
- Richard Hart, PhD 1995-2005
- Crawford Downs, PhD 1995-2012
- Anthony Bellezza, PhD 1995-2003
- Ian Sigal, PhD
- Michael Girard, PhD
- Hongli Yang, PhD
- Rafael Grytz, PhD
- Michael Roberts, PhD
- Massimo Fazio, PhD
- Vick Nguyen, PhD
- Baptiste Coudrillier, PhD
- Jonathan Vande Geest, PhD
- Andrew Feola, PhD
- Bryan Samuels, MD, PhD
- Jun Liu, PhD

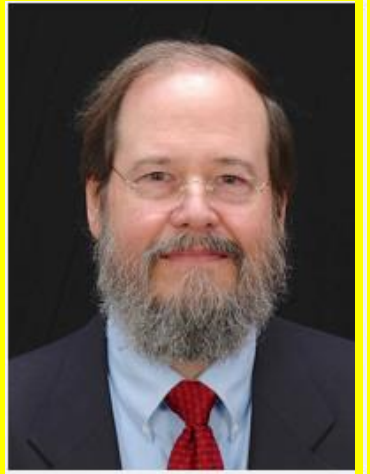

Richard Hart, PhD
Chairman Department of
Biomechanical Engineering
Tulane University – New Orleans, LA

Crawford Downs, PhD **Anthony Bellezza, PhD**

ARVO – New Orleans - 2023

In New Orleans in 1995 I was given the Gift of a Generous Engineering Collaborator

Burgoyne–2024 Goldmann–GRS Website

To Build Biomechanical Engineering Finite Element Models of the ONH tissues we needed high-resolution, digital 3D Histomorphometric reconstructions (3D HMRNs) of the ONH Connective Tissues

Monkey and Human ONH 3D Histomorphometric Reconstruction

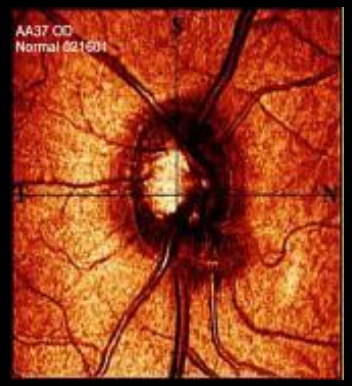

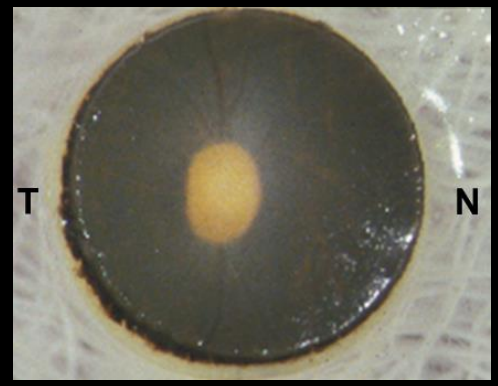

6 mm ONH trephine

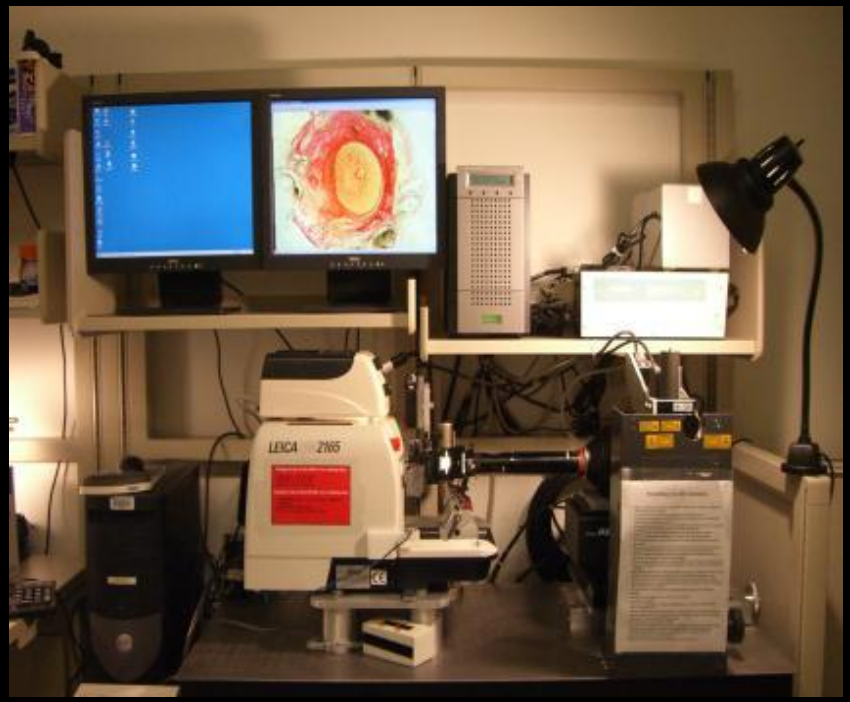

900 serial, 1.5 micron sections

900 serial, collagen-stained, block-face images

Juan Reynaud, MScE

Crawford Downs, PhD Anthony Bellezza, PhD

ARVO – New Orleans - 2023

Ponceau S/Acid Fuchsin Block Surface Staining
Developed by Anthony Bellezza / Crawford Downs

<u>Technically</u> <u>Accomplished</u> by
Juan Reynaud, MScE

Monkey and Human ONH 3D Histomorphometric Reconstruction

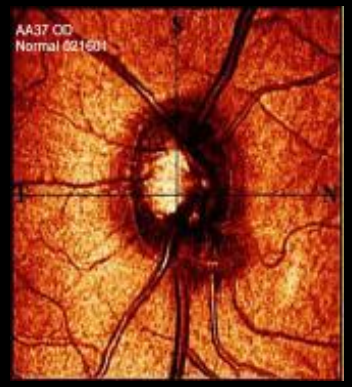

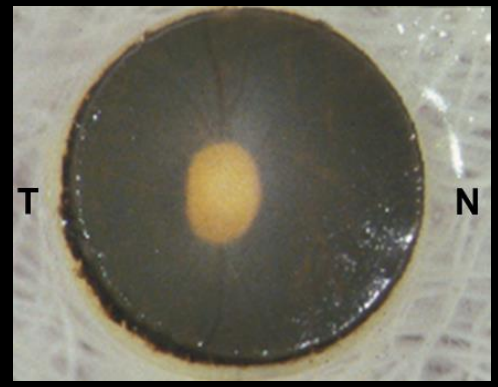

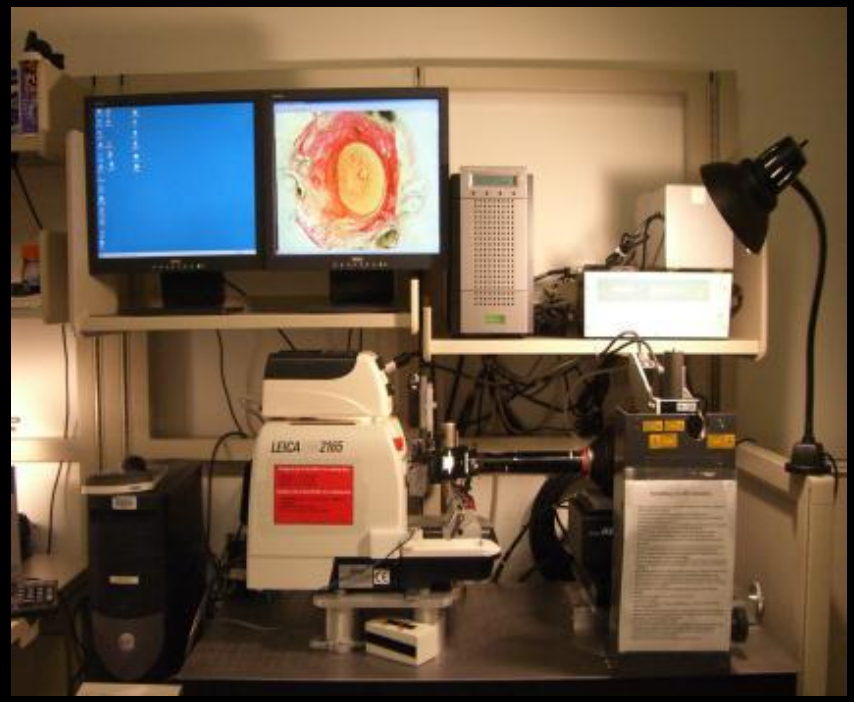

900 serial, 1.5 micron sections

900 serial, collagen-stained, block-face images

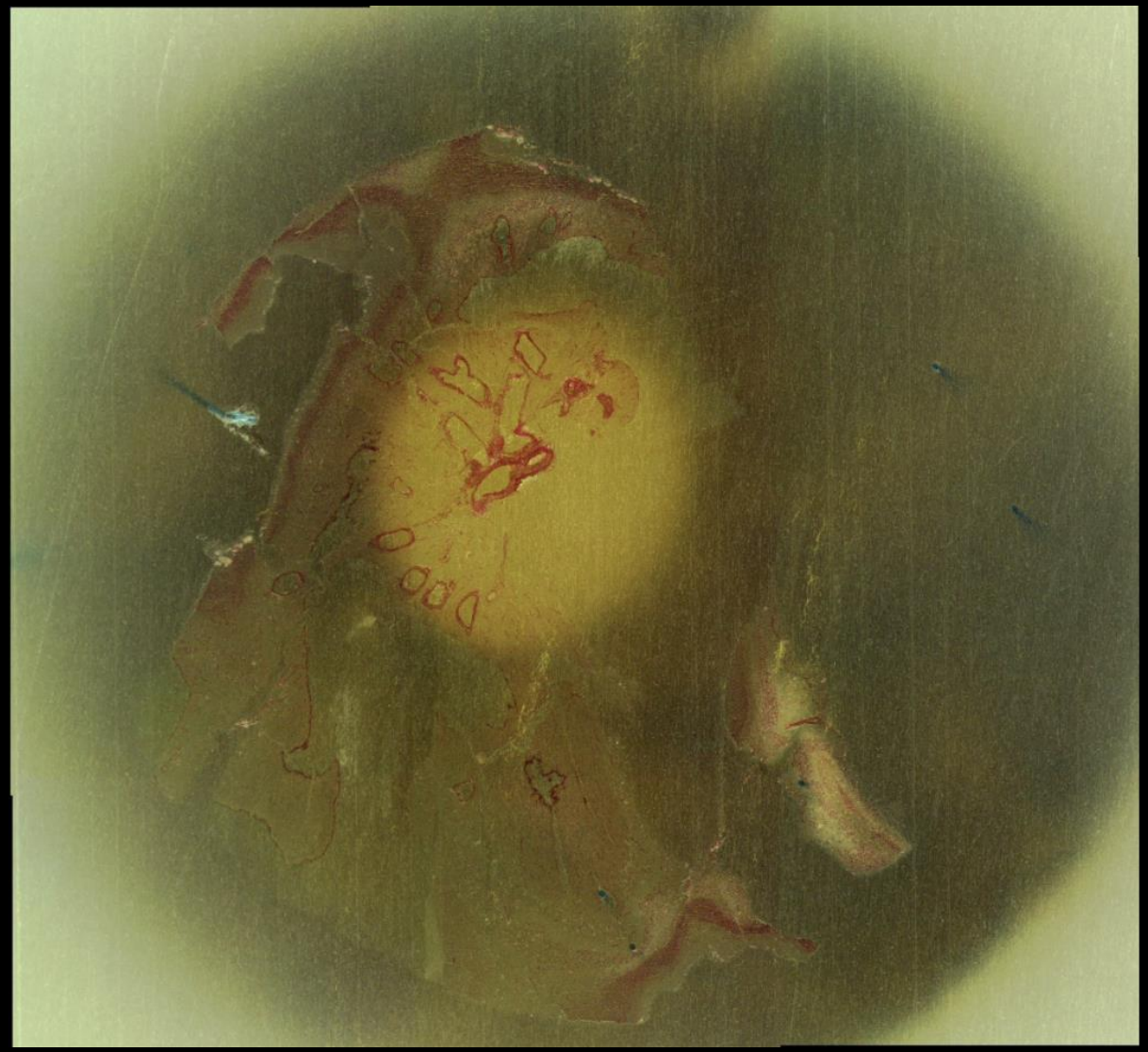

1.5 x 1.5 micron section image pixel resolution

1.5 x 1.5 x 1.5 µm voxel resolution

(Human Eye Tissue Courtesy Chris Girkin, MD)

Click Here for Human Eye Digital Serial Block-Face Section Images

From Vitreous through the orbital optic nerve

PENDING AS OF 111524

Burgoyne
2024 Goldman
GRS Website
Human Eye Courtesy Chris Girkin, MD

3D Histomorphometric Review of ONH Anatomy/Morphology

3D Histomorphometric Review of ONH Anatomy/Morphology

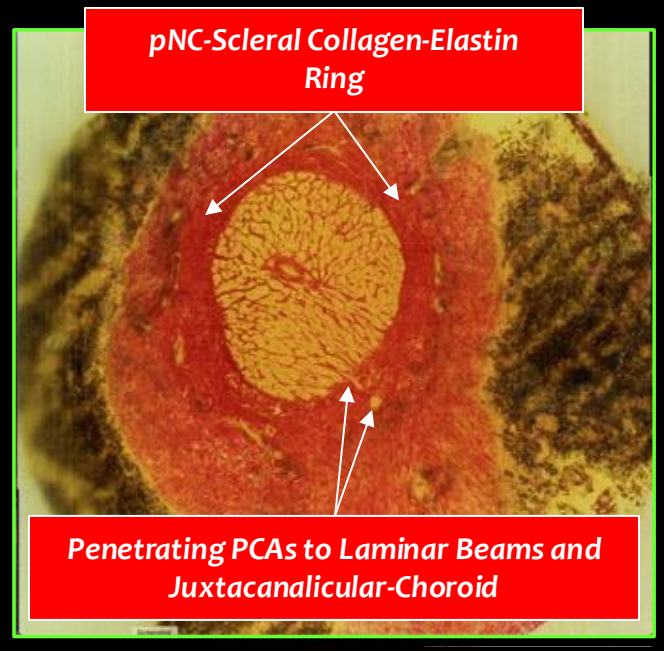

3D Histomorphometric Review of ONH Anatomy/Morphology

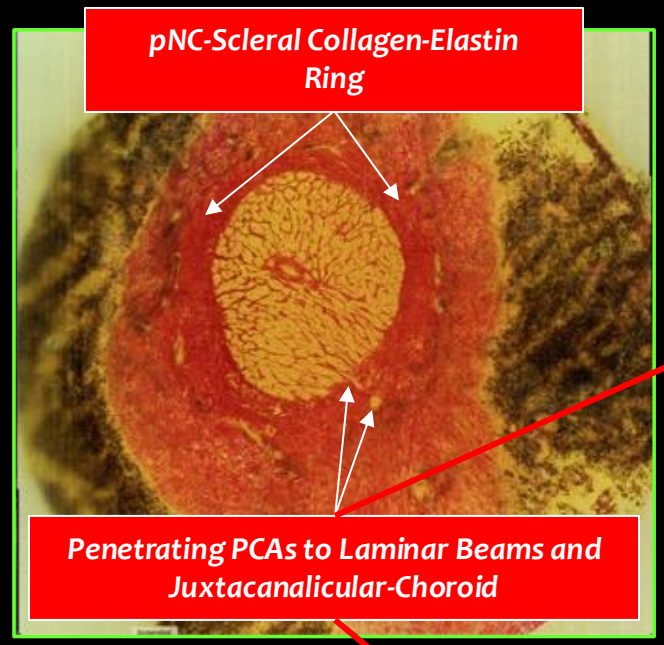

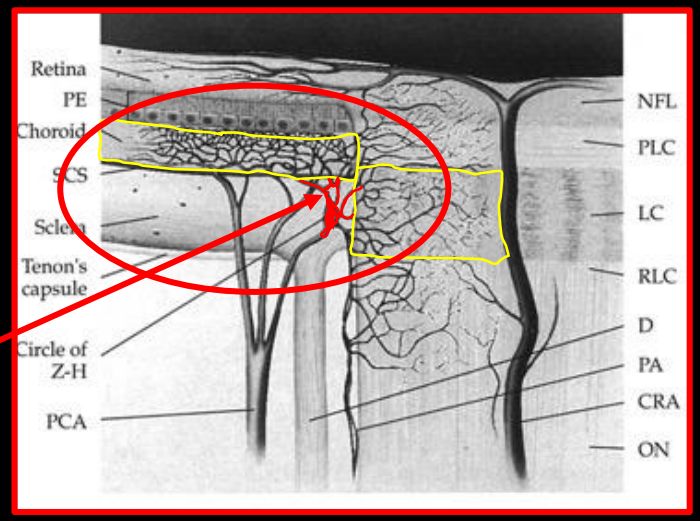

Cioffi and Van Buskirk. The Glaucomas: Basic Science. 1996

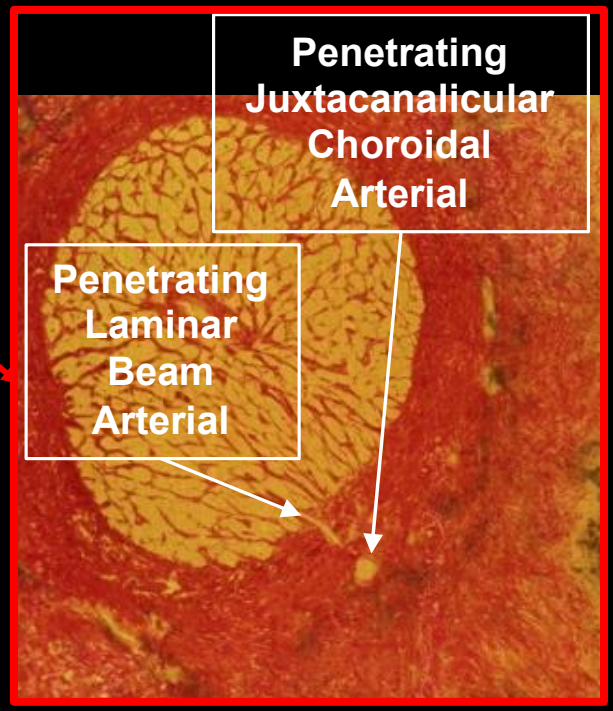

3D Histomorphometric Review of ONH Anatomy/Morphology

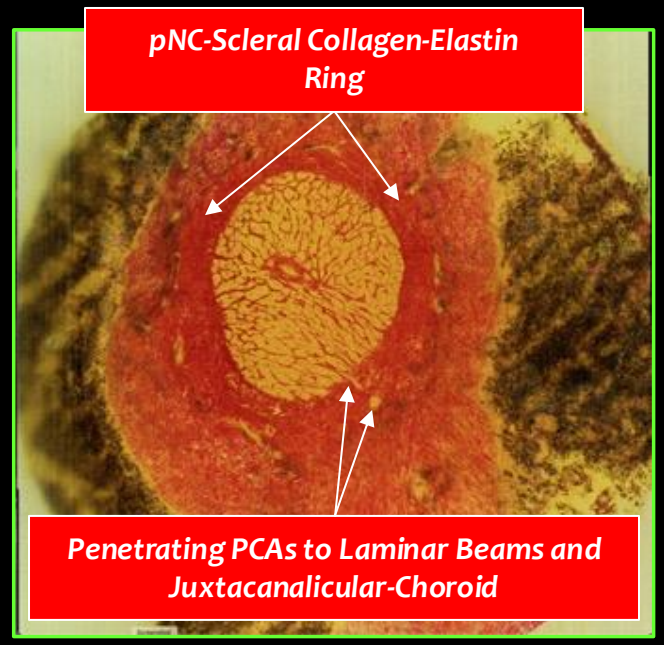

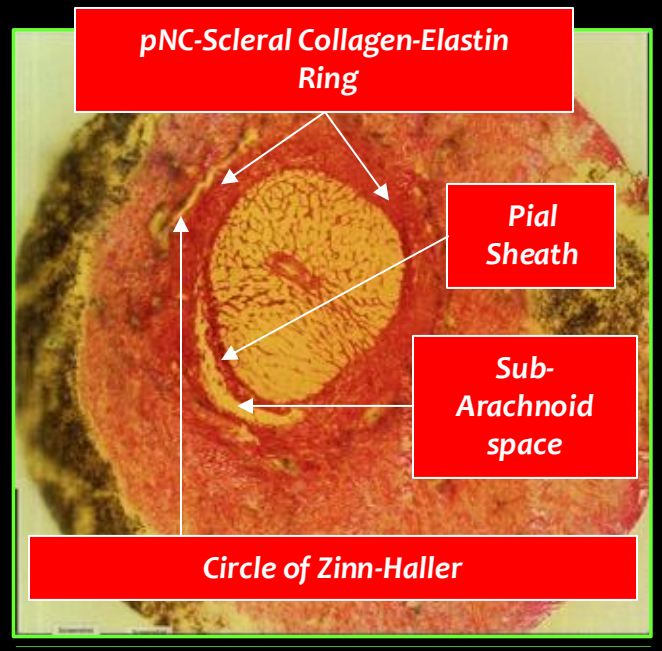

3D Histomorphometric Review of ONH Anatomy/Morphology

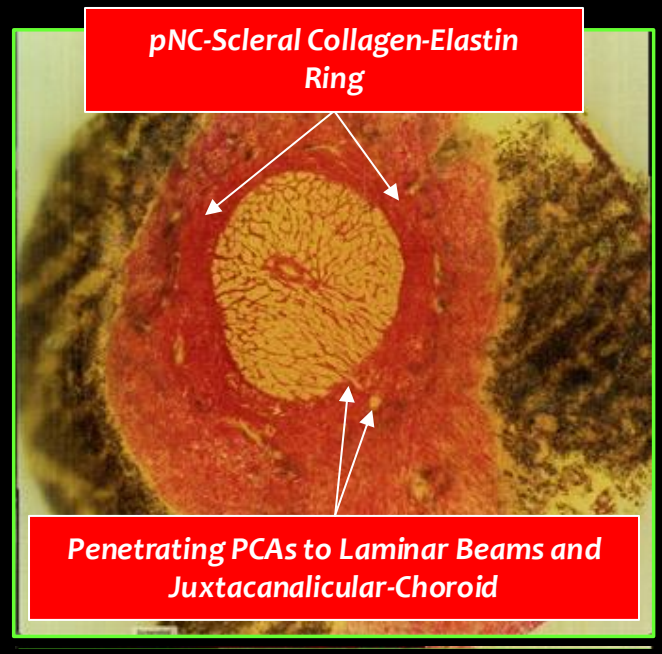

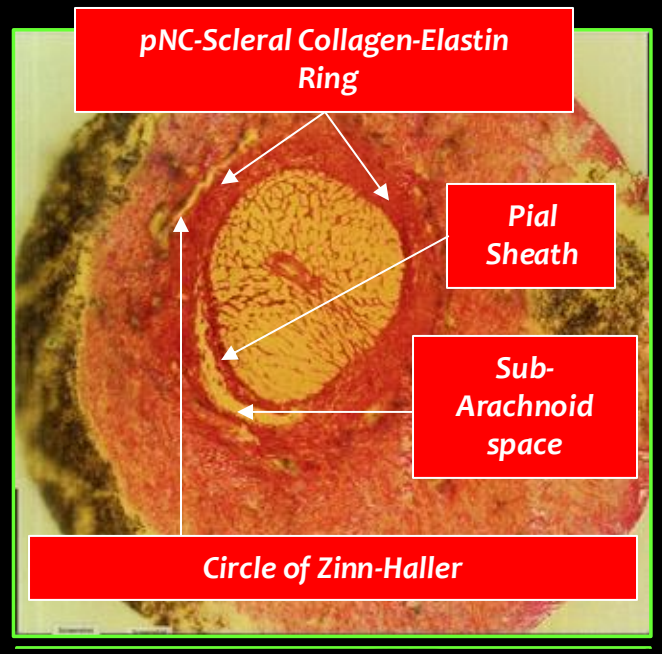

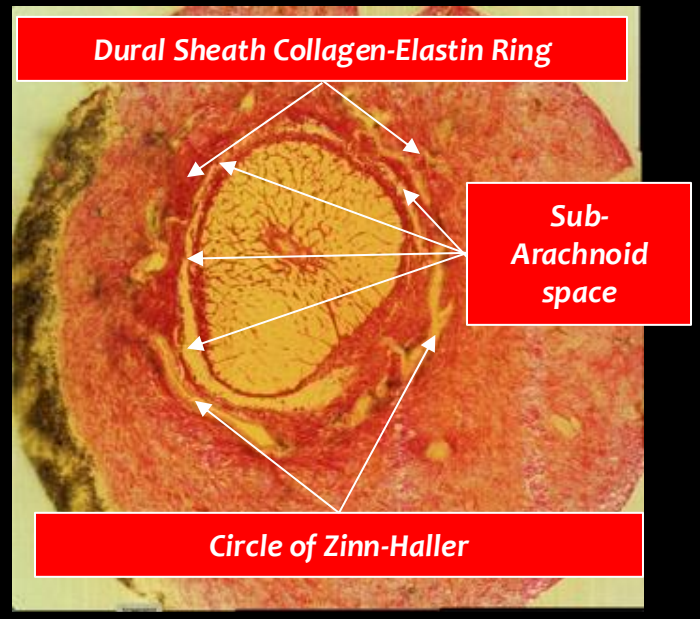

3D Histomorphometric Review of ONH Anatomy/Morphology

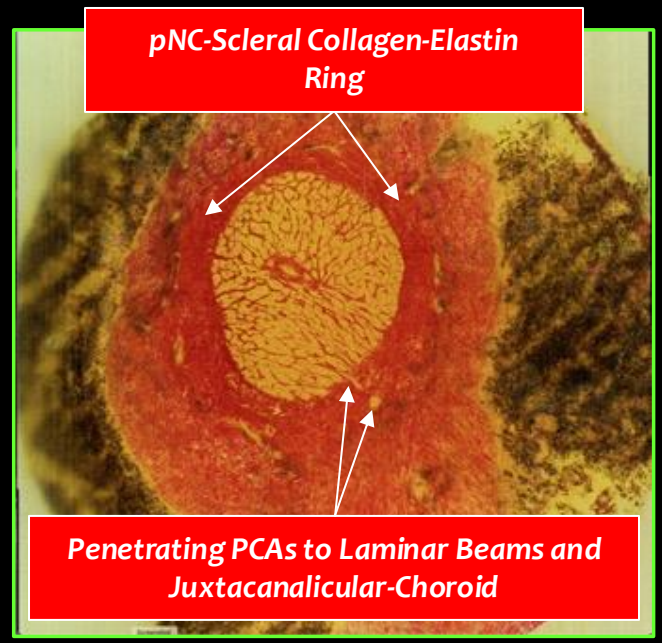

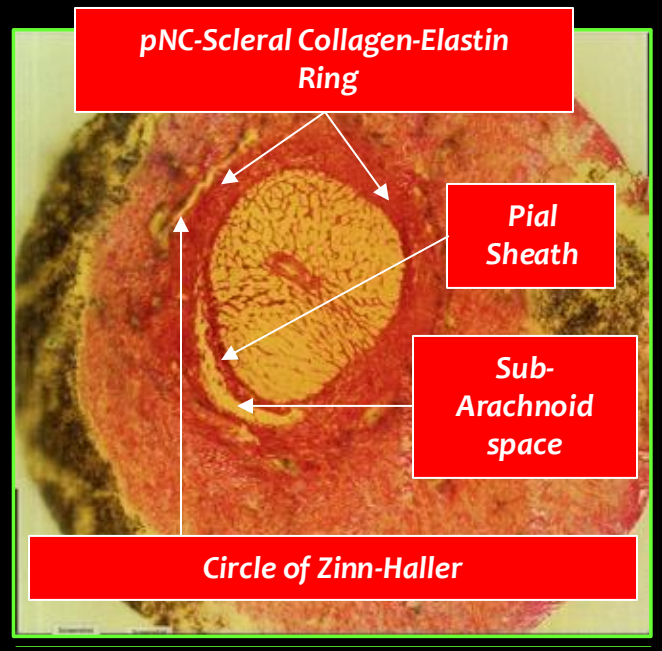

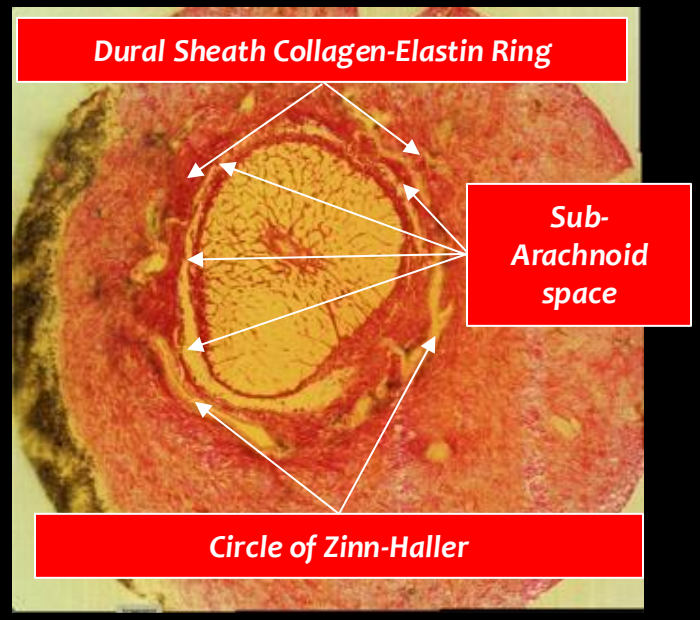

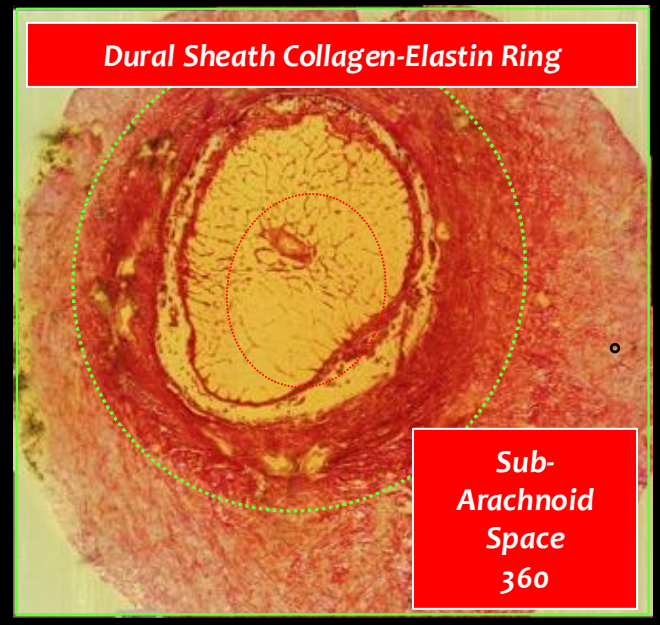

Burgoyne–2024 Goldmann–GRS Website

3D Histomorphometric Review of ONH Anatomy/Morphology

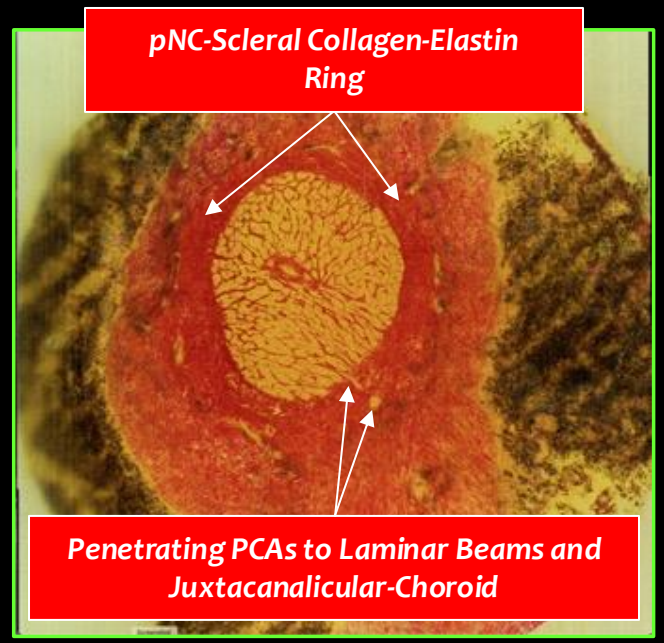

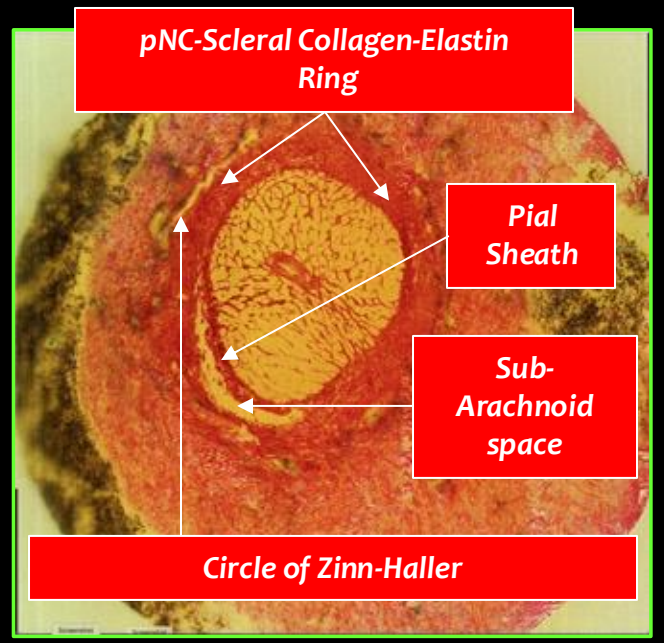

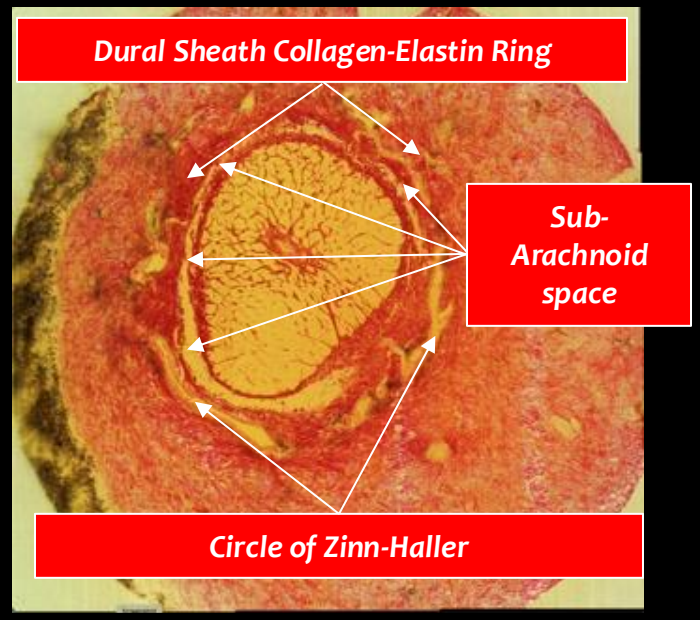

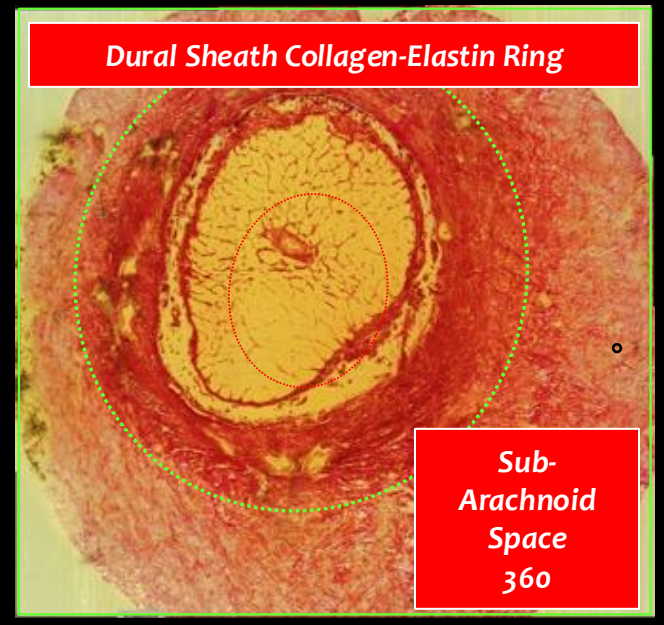

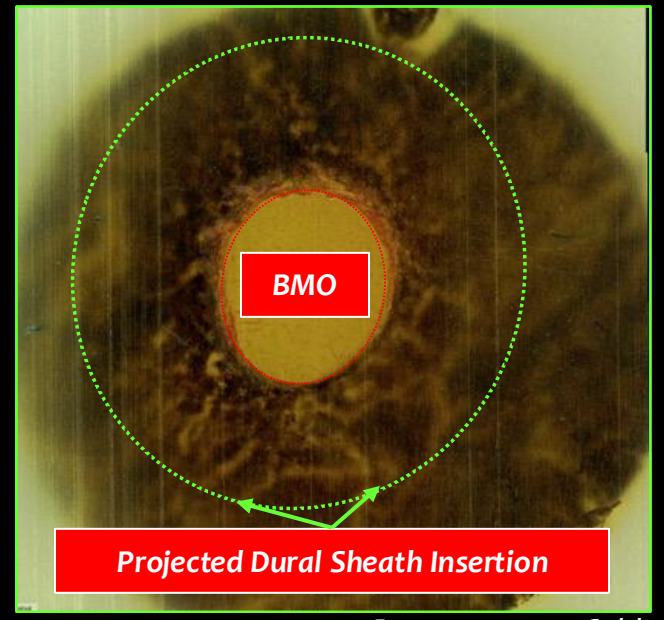

The ONH is much LARGER than the Clinical "Optic Disc"

Morphologically *the lateral boundary of the ONH is a continuum that can be estimated by the optic nerve dural sheath insertion.*

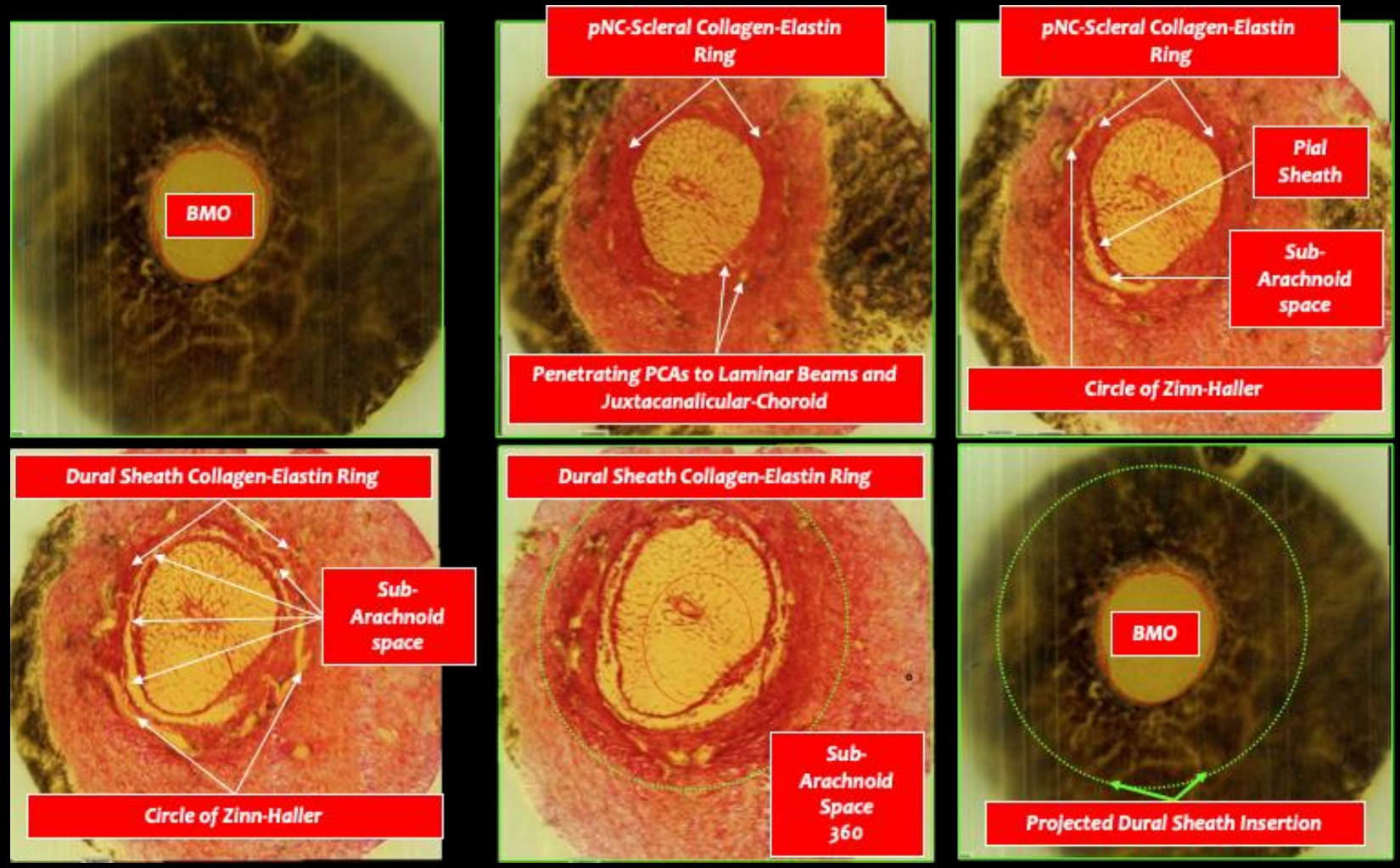

The ONH is much LARGER than the Clinical "Optic Disc"

Biomechanically *the ONH should include the pNC-collagen-elastin ring, the posterior ciliary vasculature and the retrolaminar dural sheath and optic nerve*

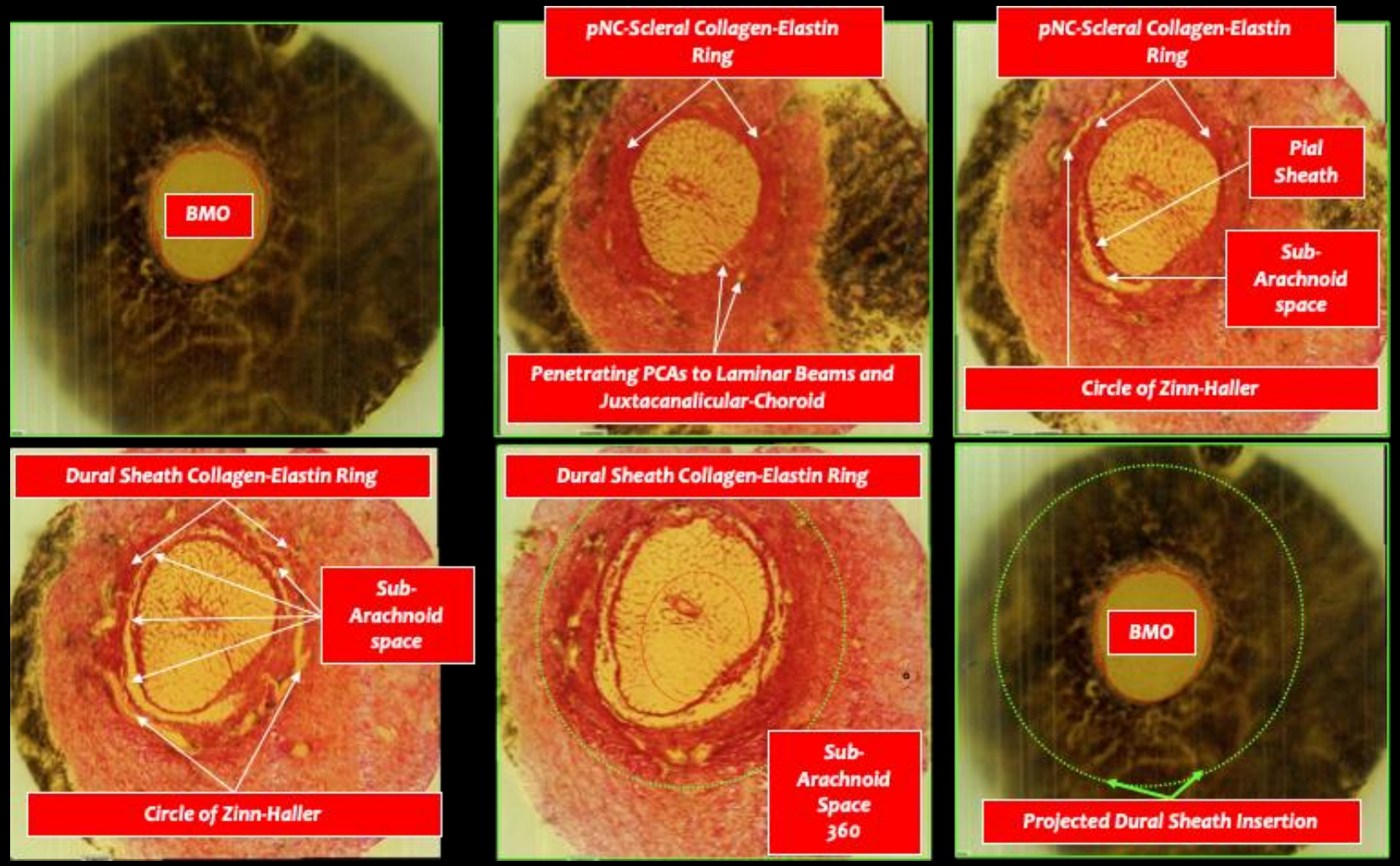

Burgoyne–2024 Goldmann–GRS Website

Paradigm Change From the Clinical "Optic Disc" to ONH Anatomic Terminology

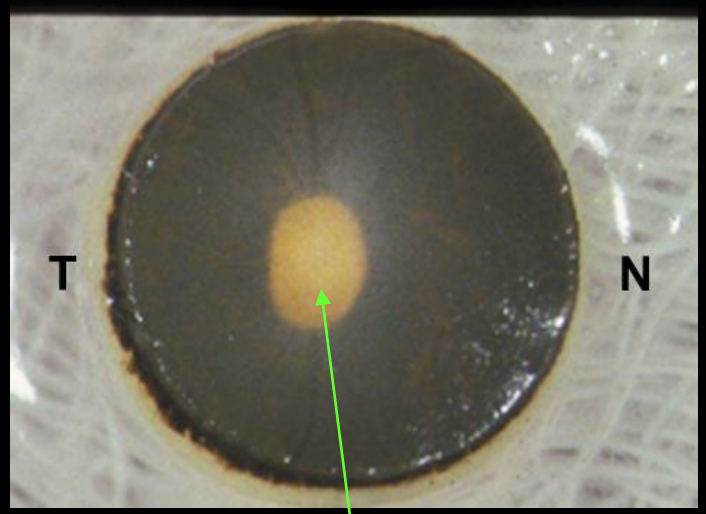

Clinical "Optic Disc"

Iconic Clinical Exam Landmark since Helmholtz's Direct Ophthalmoscope (1851)

Helmholtz – Description of the Ophthalmoscope - 1851

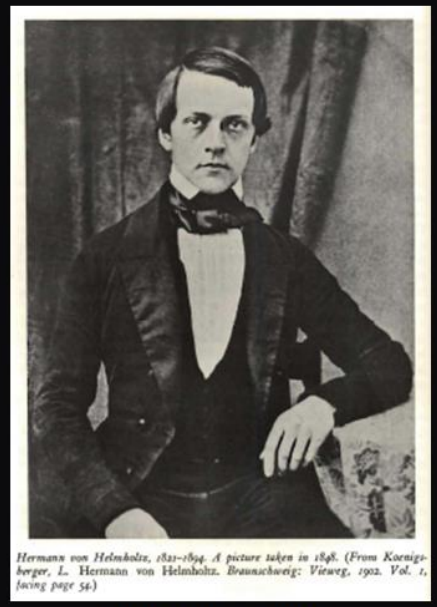

Hermann von Helmholtz, 1821–1894. A picture taken in 1848. (From Koenigsberger, L. Hermann von Helmholtz. Braunschweig: Vieweg, 1902. Vol. 1, facing page 54.)

Helmholtz in 1848

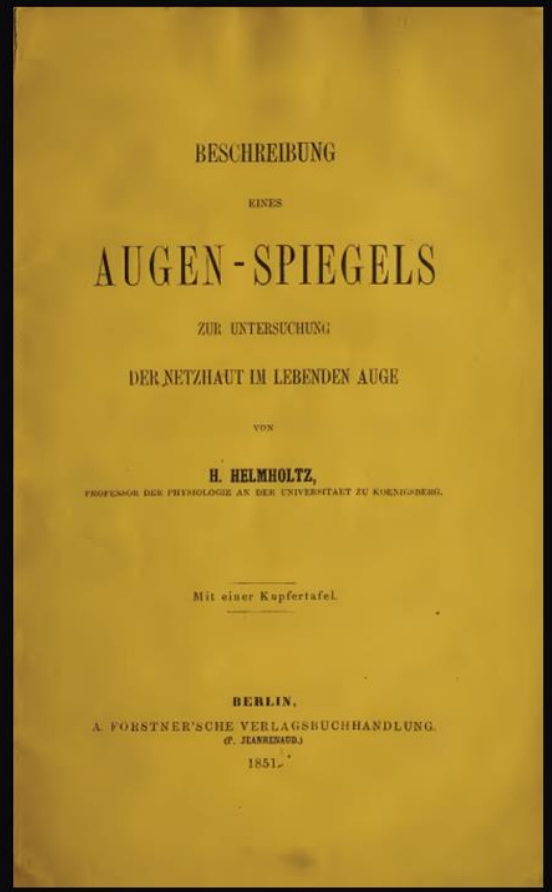

BESCHREIBUNG

EINES

AUGEN-SPIEGELS

ZUR UNTERSUCHUNG

DER NETZHAUT IM LEBENDEN AUGE

VON

H. HELMHOLTZ,

PROFESSOR DER PHYSIOLOGIE AN DER UNIVERSITÄT ZU KÖNIGSBERG.

Mit einer Kupfertafel.

BERLIN.

A. FORSTNER'SCHE VERLAGSBUCHHANDLUNG.

(P. JEANRENAUD.)

1851.

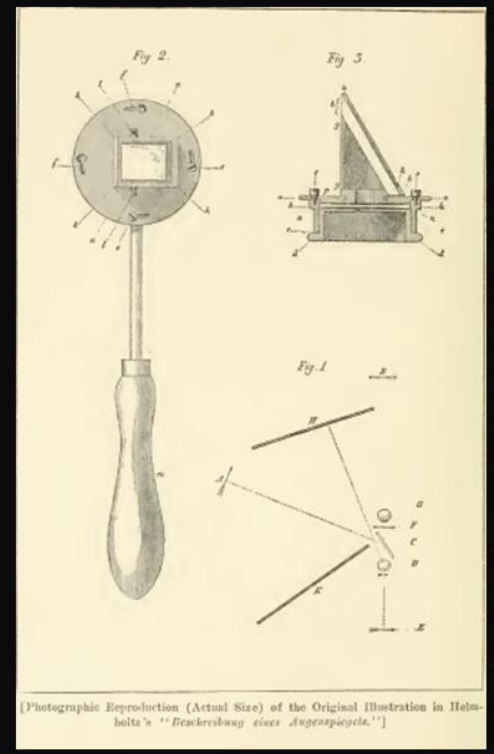

[Photographic Reproduction (Actual Size) of the Original Illustration in Helmholtz's "Beschreibung eines Augenspiegels."]

Paradigm Change From the Clinical "Optic Disc" to ONH Anatomic Terminology

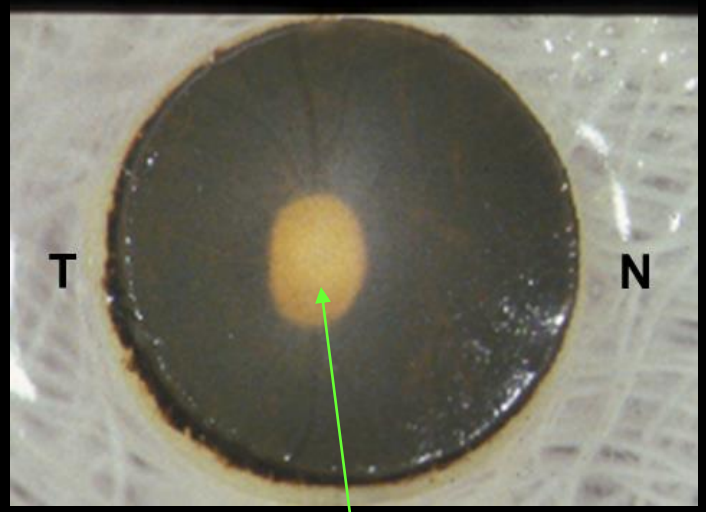

Clinical "Optic Disc"

Iconic Clinical Exam Landmark since Helmholtz's Direct Ophthalmoscope (1851)

No Consistent Anatomic Foundation by Histology / OCT

Helmholtz – Description of the Ophthalmoscope - 1851

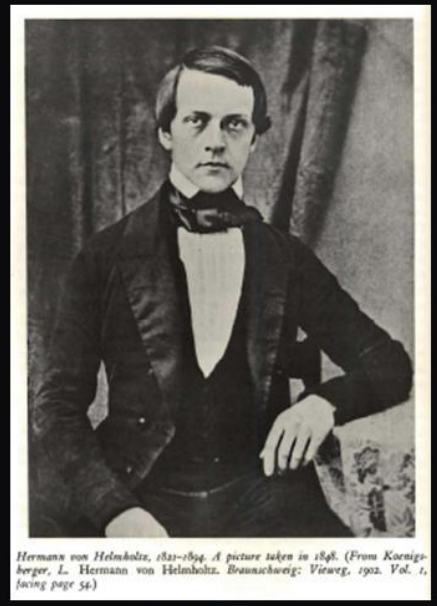

Hermann von Helmholtz, 1821–1894. A picture taken in 1848. (From Koenigsberger, L. Hermann von Helmholtz. Braunschweig: Vieweg, 1902. Vol. 1, facing page 54.)

Helmholtz in 1848

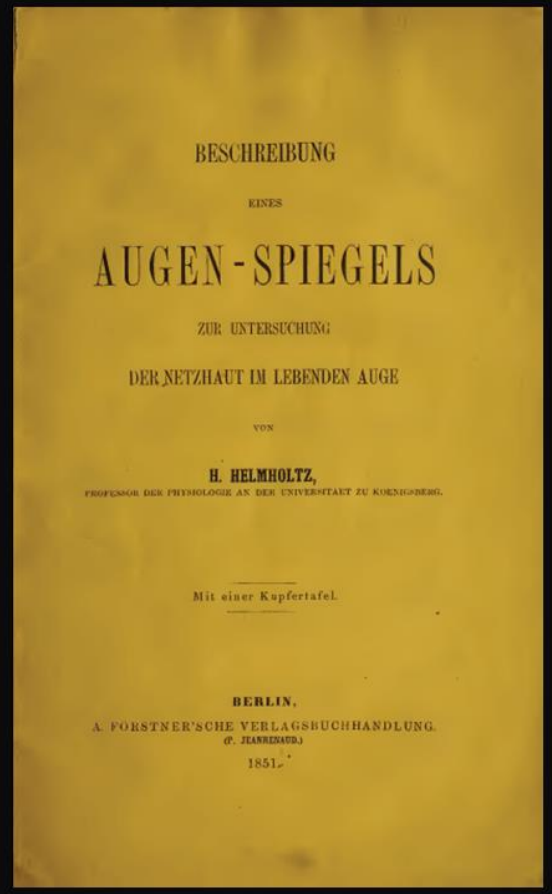

BESCHREIBUNG

EINES

AUGEN-SPIEGELS

ZUR UNTERSUCHUNG

DER NETZHAUT IM LEBENDEN AUGE

VON

H. HELMHOLTZ,

PROFESSOR DER PHYSIOLOGIE AN DER UNIVERSITÄT ZU KÖNIGSBERG.

Mit einer Kupfertafel.

BERLIN.

A. FORSTNER'SCHE VERLAGSBUCHHANDLUNG.

(P. JEANRENAUD.)

1851.

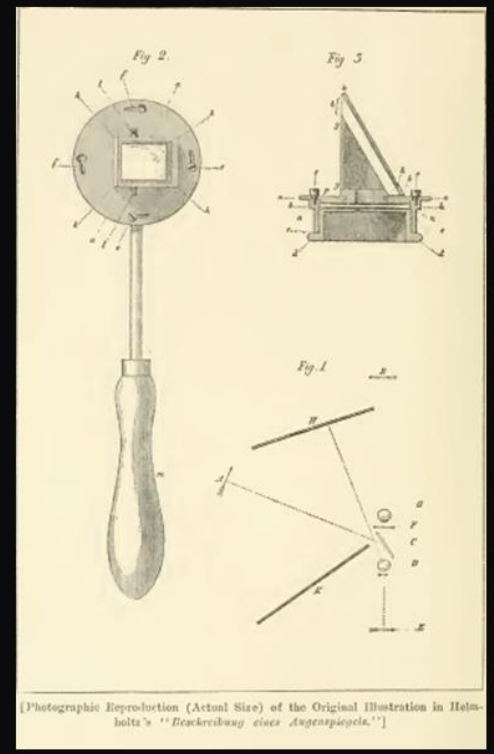

[Photographic Reproduction (Actual Size) of the Original Illustration in Helmholtz's "Beschreibung eines Augenspiegels."]

Paradigm Change From the Clinical "Optic Disc" to ONH Anatomic Terminology

OCT-Detected BMO
(ONH neural canal entrance)

Histologic
Bruch's Membrane Opening (BMO)
(ONH neural canal entrance)

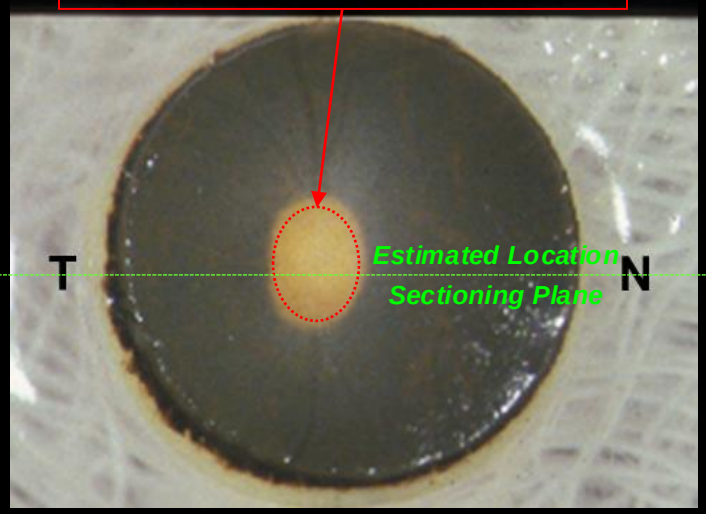

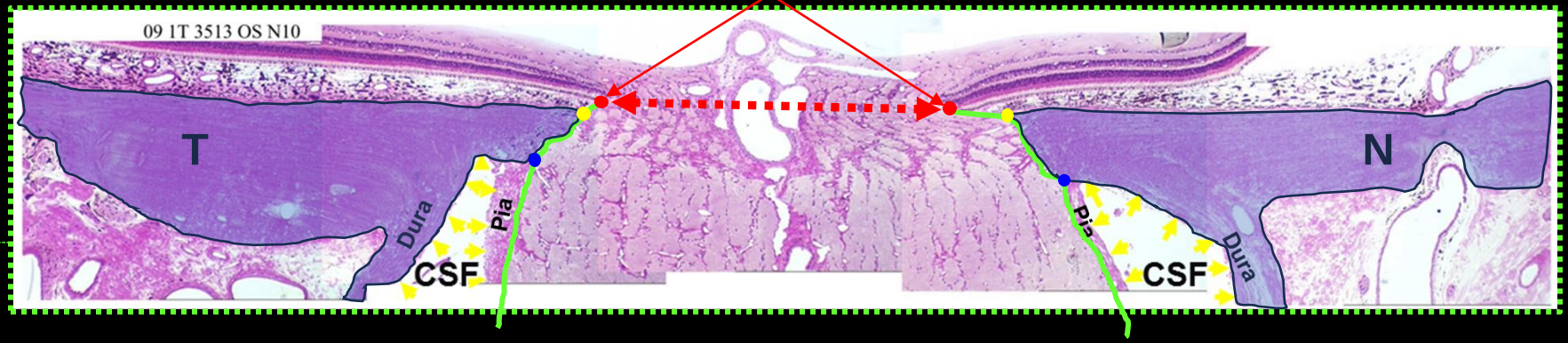

Paradigm Change From the Clinical "Optic Disc" to ONH Anatomic Terminology

OCT-Detected BMO

(ONH neural canal entrance)

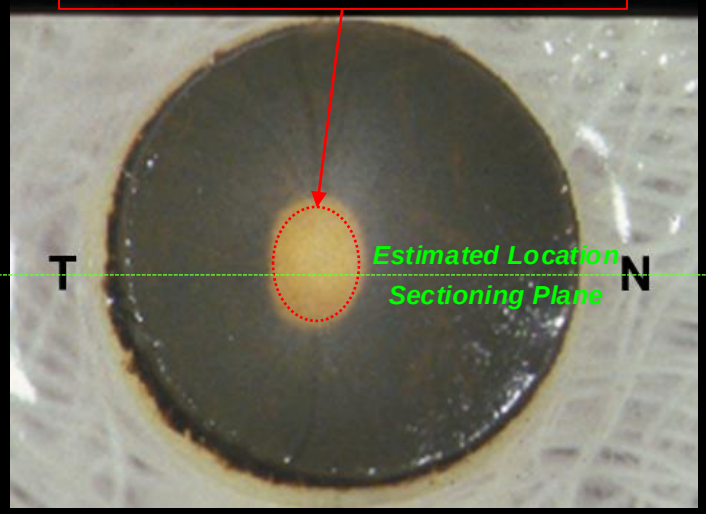

ONH Neural Canal

(RGC axon pathway through the sclera)

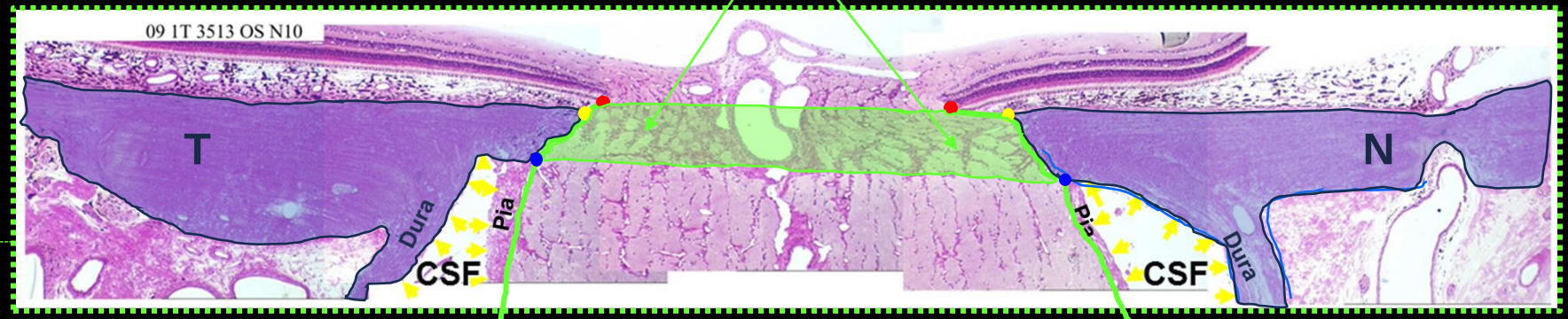

- BMO – Bruch's Membrane Opening
- ASCO – Anterior Scleral Canal Opening
- PSCO – Posterior Scleral Canal Opening
- Neural Canal

Paradigm Change From the Clinical "Optic Disc" to ONH Anatomic Terminology

OCT-Detected BMO

(ONH neural canal entrance)

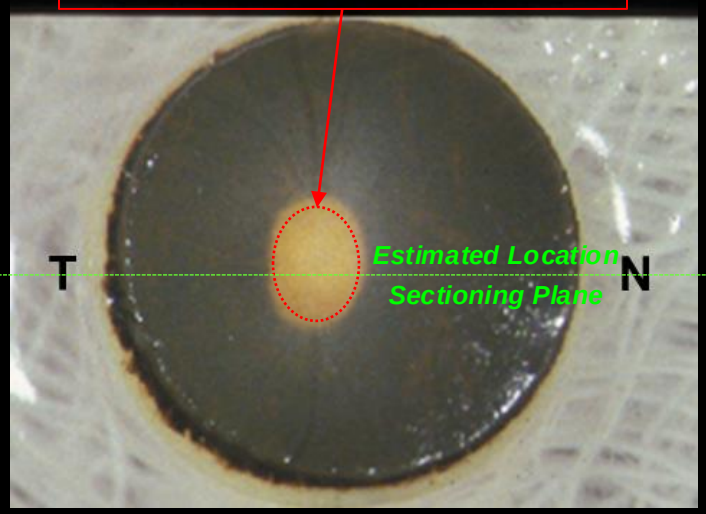

ONH Neural Canal

(3 anatomic openings)

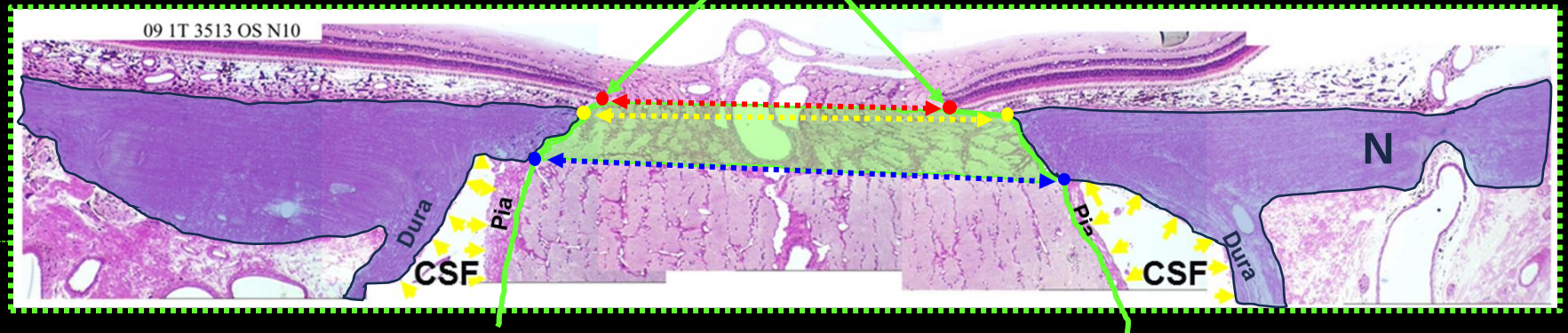

- **BMO – Bruch's Membrane Opening**
- **ASCO – Anterior Scleral Canal Opening**
- **PSCO – Posterior Scleral Canal Opening**

Paradigm Change From the Clinical "Optic Disc" to ONH Anatomic Terminology

OCT-Detected BMO
(ONH neural canal entrance)

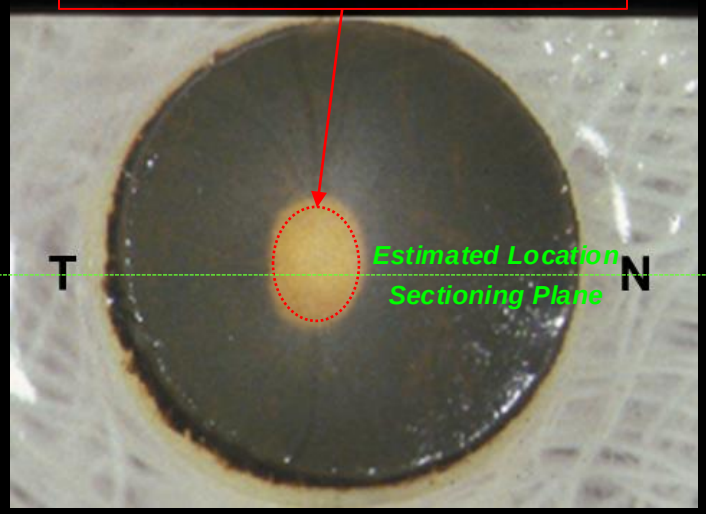

ONH Retrolaminar Optic Nerve
(Retrolaminar Myelinated RGC axons)

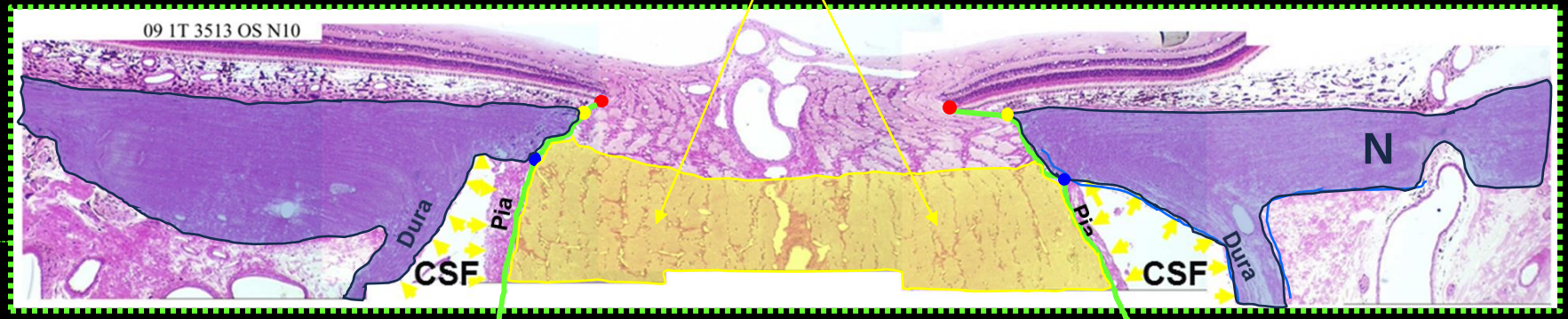

- BMO – Bruch's Membrane Opening
- ASCO – Anterior Scleral Canal Opening
- PSCO – Posterior Scleral Canal Opening
- Retrolaminar Optic Nerve (axon myelination)

Paradigm Change From the Clinical "Optic Disc" to ONH Anatomic Terminology

ONH Peri-Neural Canal (pNC) Tissues

Retina – Choroid – Sclera

(No anatomically precise lateral boundary)

OCT-Detected BMO

(ONH neural canal entrance)

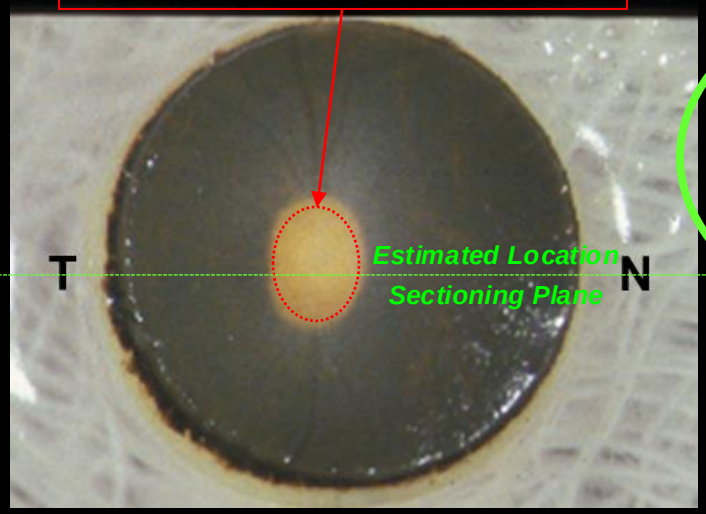

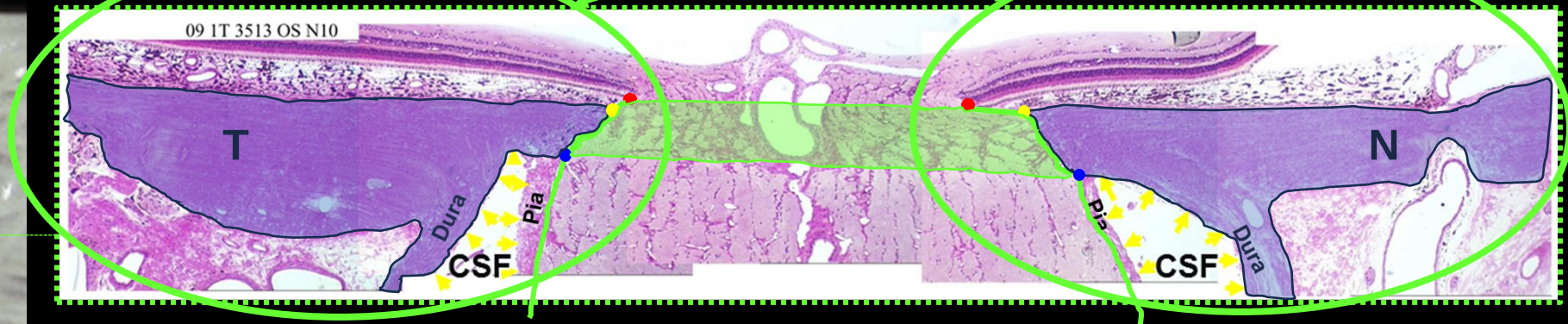

- BMO – Bruch's Membrane Opening
- ASCO – Anterior Scleral Canal Opening
- PSCO – Posterior Scleral Canal Opening
- Neural Canal

Paradigm Change From the Clinical "Optic Disc" to ONH Anatomic Terminology

ONH Peri-Neural Canal (pNC) Tissues

Retina – Choroid – Sclera

(No anatomically precise lateral boundary)

OCT-Detected BMO

(ONH neural canal entrance)

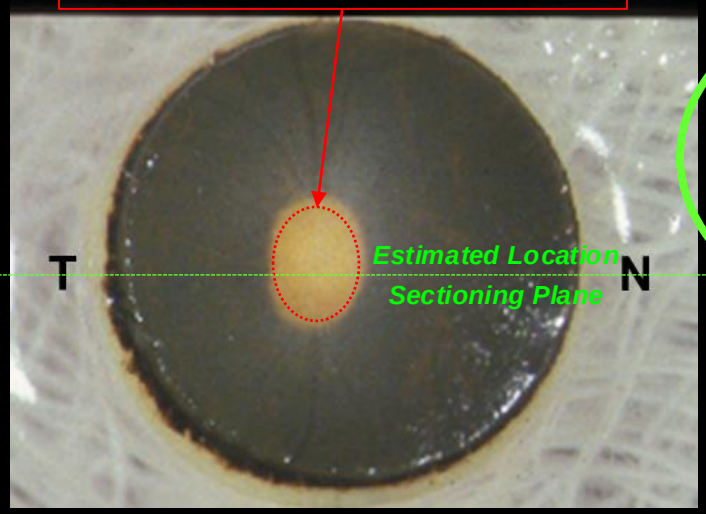

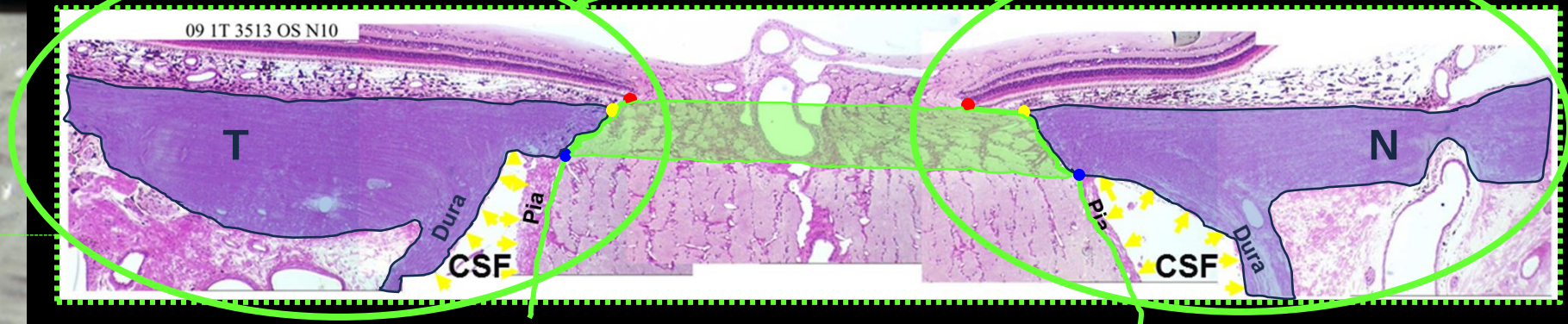

- BMO – Bruch's Membrane Opening
- ASCO – Anterior Scleral Canal Opening
- PSCO – Posterior Scleral Canal Opening
- Neural Canal

Distinguishes the tissues adjacent to the ONH neural canal from those of the Posterior Scleral Shell and Macula

Paradigm Change From the Clinical "Optic Disc" to ONH Anatomic Terminology

ONH Peri-Neural Canal (pNC) Tissues

Retina – Choroid – Sclera

(No anatomically precise lateral boundary)

OCT-Detected BMO

(ONH neural canal entrance)

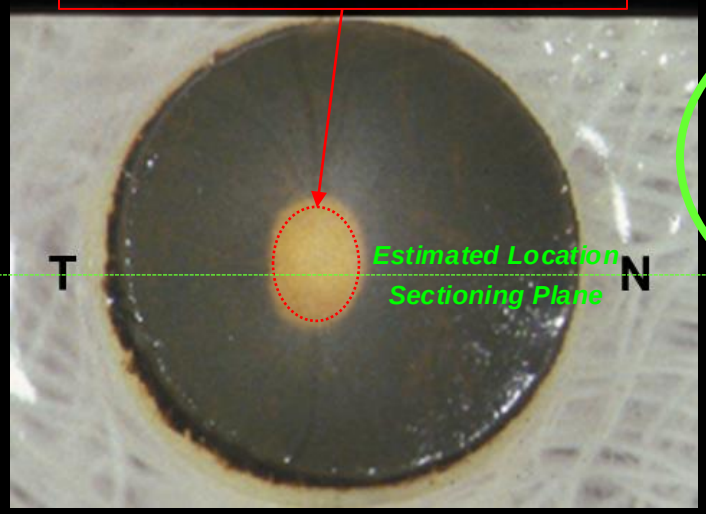

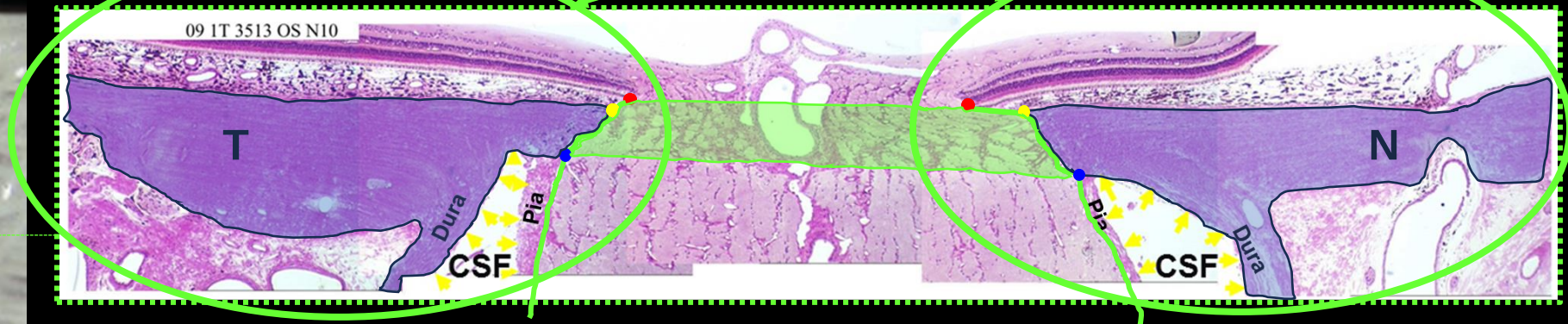

- BMO – Bruch's Membrane Opening
- ASCO – Anterior Scleral Canal Opening
- PSCO – Posterior Scleral Canal Opening
- Neural Canal

Replaces the clinical term "para" or "peripapillary" because the "papilla" or "optic disc" has no consistent anatomic foundation.

Paradigm Change From the Clinical "Optic Disc" to ONH Anatomic Terminology

OCT-Detected BMO
(ONH neural canal entrance)

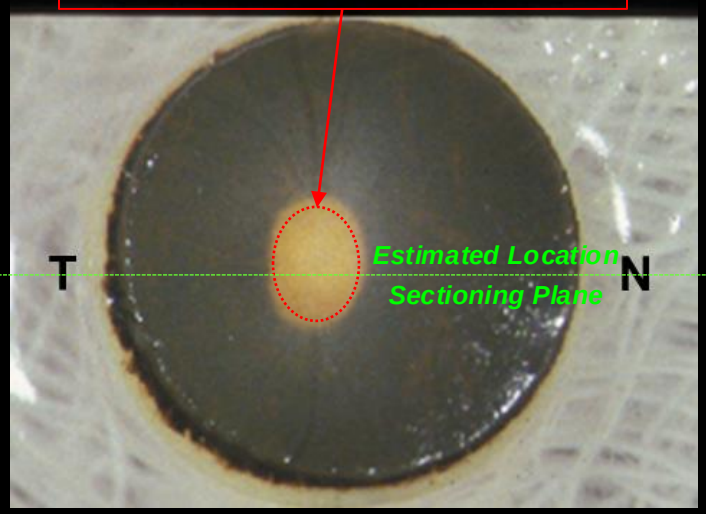

ONH Juxta-Canalicular Tissues
Retina – Choroid – Sclera
(Immediately adjacent to/abutting the neural canal)

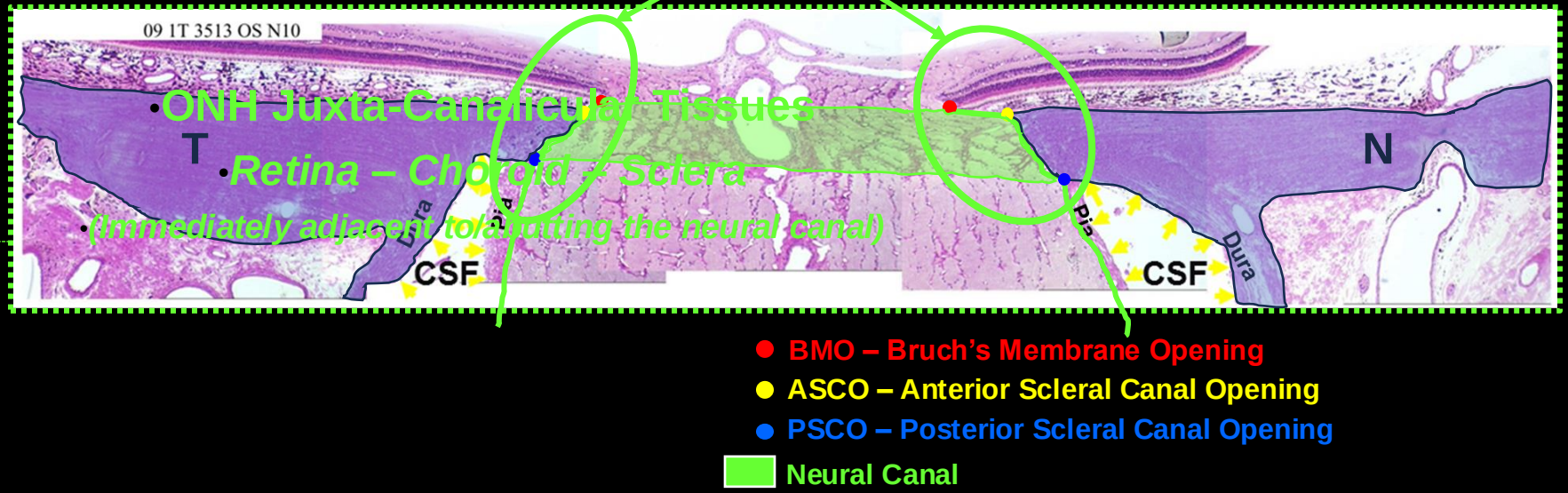

The *"juxta-canalicular"* pNC-tissues are immediately adjacent to or abut the neural canal wall

Paradigm Change From the Clinical "Optic Disc" to ONH Anatomic Terminology

ONH Juxta-Canalicular Tissues

Scleral Flange

(pNC-sclera internal to the Dural Sheath Insertion)

OCT-Detected BMO

(ONH neural canal entrance)

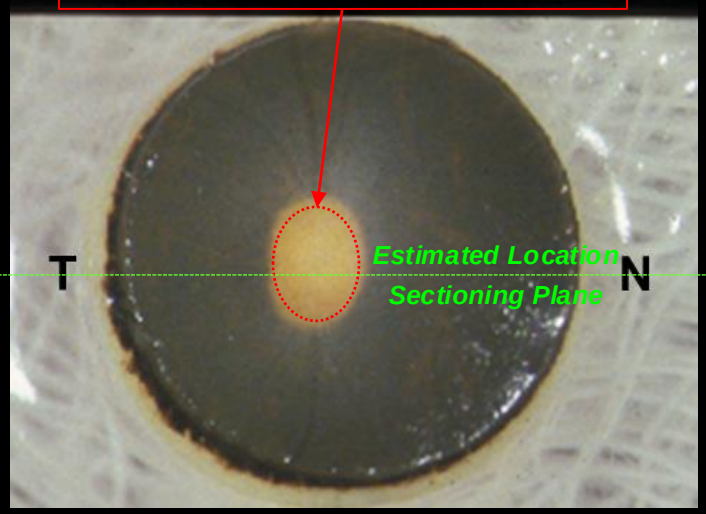

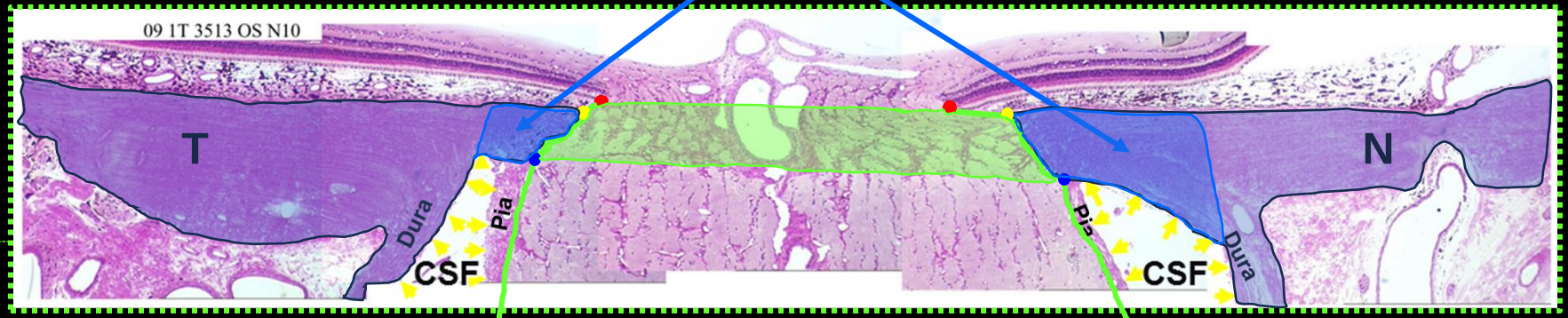

- BMO – Bruch's Membrane Opening
- ASCO – Anterior Scleral Canal Opening
- PSCO – Posterior Scleral Canal Opening
- Neural Canal

Jonas' histologic concept of the scleral flange - defined by the dural sheath insertion in "normal" eyes

Scleral Flange

Scleral flange is 1/3rd to 1/2 perineural canal scleral thickness

Dural sheath adds 1/2 to 2/3rds peripapillary scleral thickness

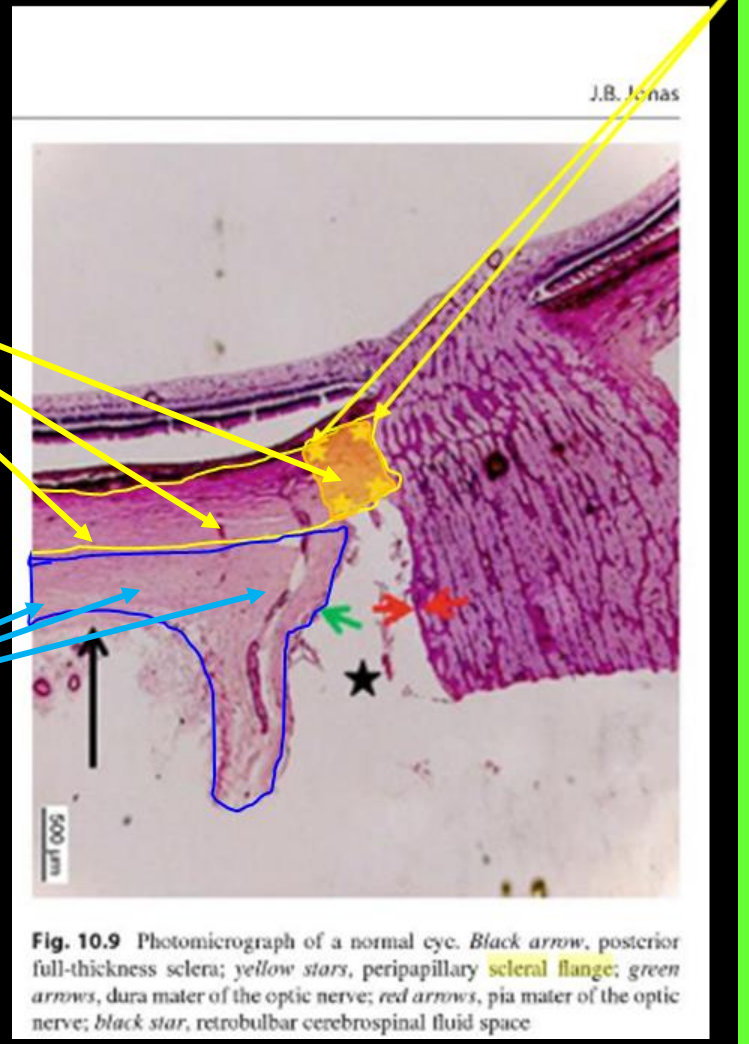

Fig. 10.9 Photomicrograph of a normal eye. *Black arrow*, posterior full-thickness sclera; *yellow stars*, peripapillary scleral flange; *green arrows*, dura mater of the optic nerve; *red arrows*, pia mater of the optic nerve; *black star*, retrobulbar cerebrospinal fluid space

"Normal"

Jonas' also described profound scleral flange thinning, stretching and bowing in "highly myopic" eyes

Scleral Flange

Scleral flange is 1/3rd to 1/2 perineural canal scleral thickness

Dural sheath adds 1/2 to 2/3rds peripapillary scleral thickness

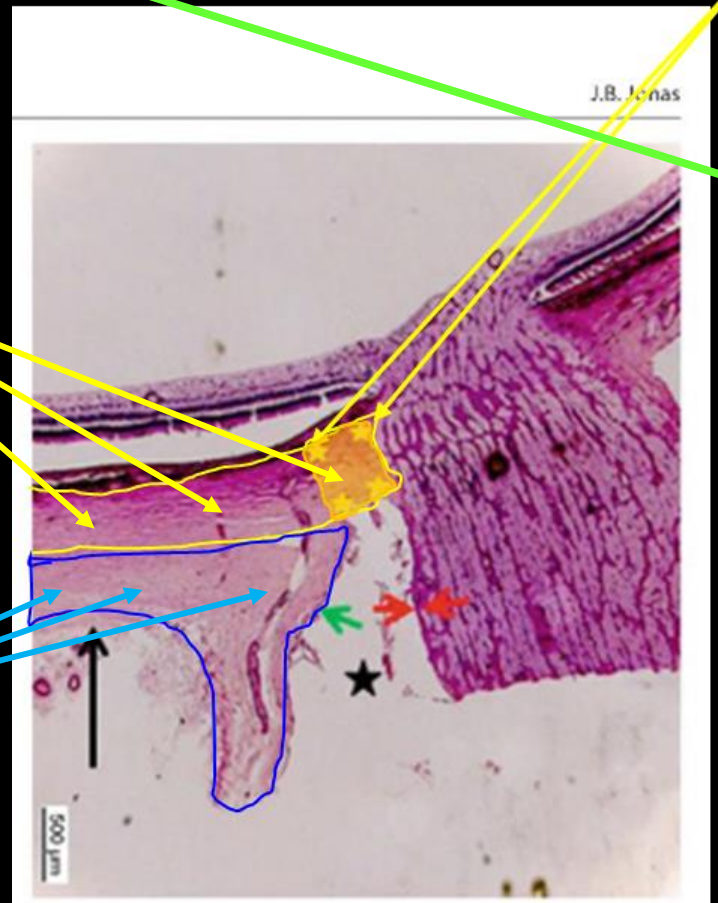

Fig. 10.9 Photomicrograph of a normal eye. *Black arrow*, posterior full-thickness sclera; *yellow stars*, peripapillary scleral flange; *green arrows*, dura mater of the optic nerve; *red arrows*, pia mater of the optic nerve; *black star*, retrobulbar cerebrospinal fluid space

"Normal"

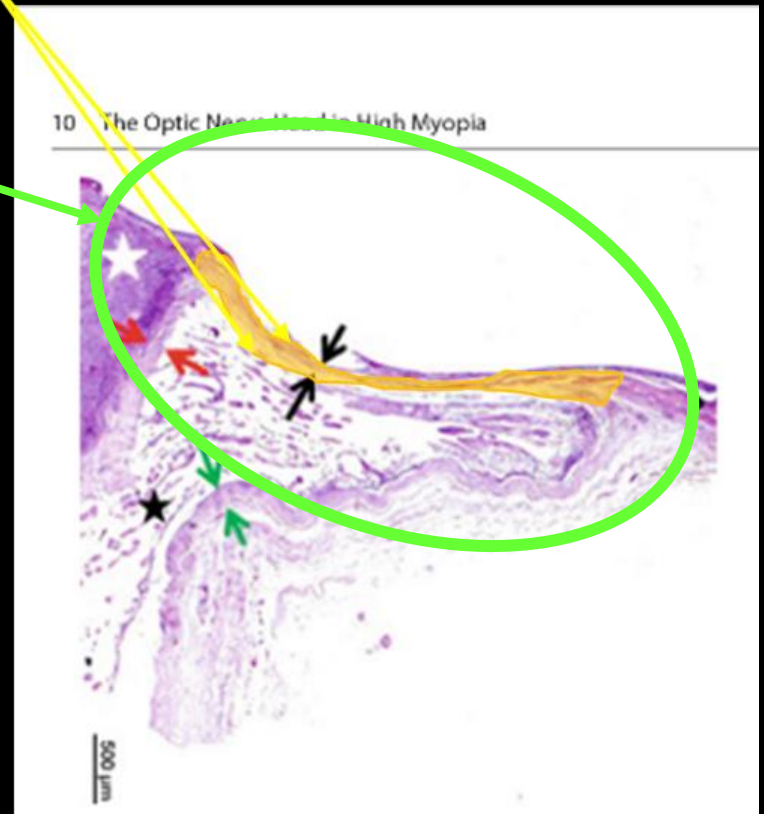

Fig. 10.8 Photomicrograph of a highly myopic eye. *Black arrows*, elongated peripapillary scleral flange ("delta zone"); *green arrows*, dura mater of the optic nerve; *red arrows*, pia mater of the optic nerve; *black star*, retrobulbar cerebrospinal fluid space; *white arrow*, optic nerve

"Highly Myopic / Staphylomatous"

The Scleral Flange and ONH Blood Flow - emphasized by Hayreh - refined by Cioffi and others

Small penetrating Posterior Ciliary arterioles pass through the *scleral flange* to supply the juxta-canalicular choroid and laminar beams

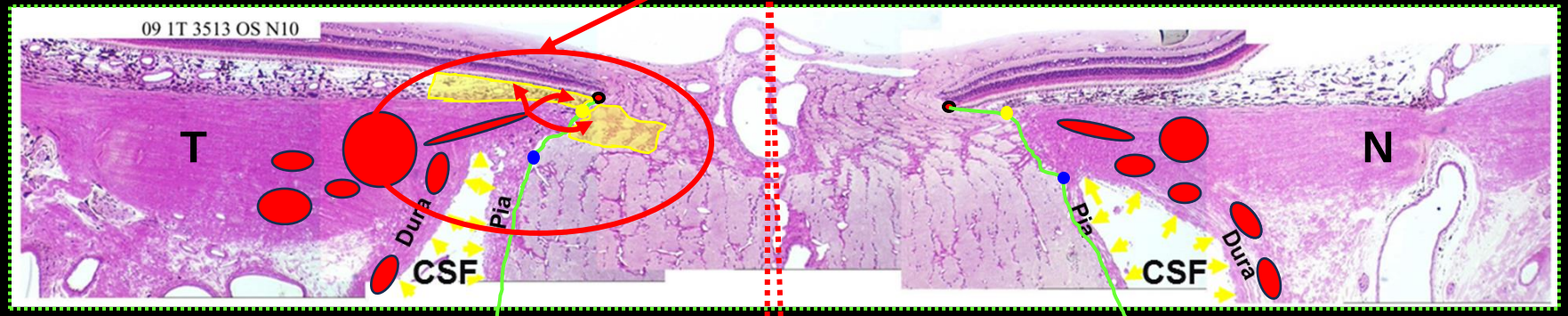

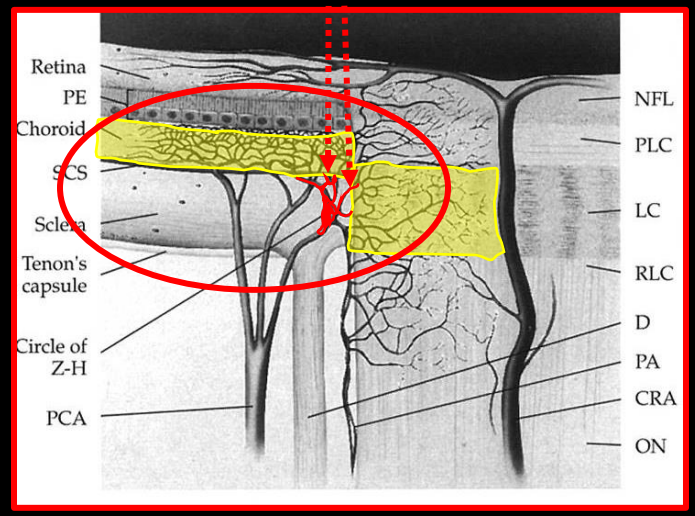

Cioffi and Van Buskirk. The Glaucomas: Basic Science. 1996

Hayreh articulated the susceptibility of this vasculature to IOP fluctuations and its relationship to clinical pNC- Choroidal and RPE atrophy

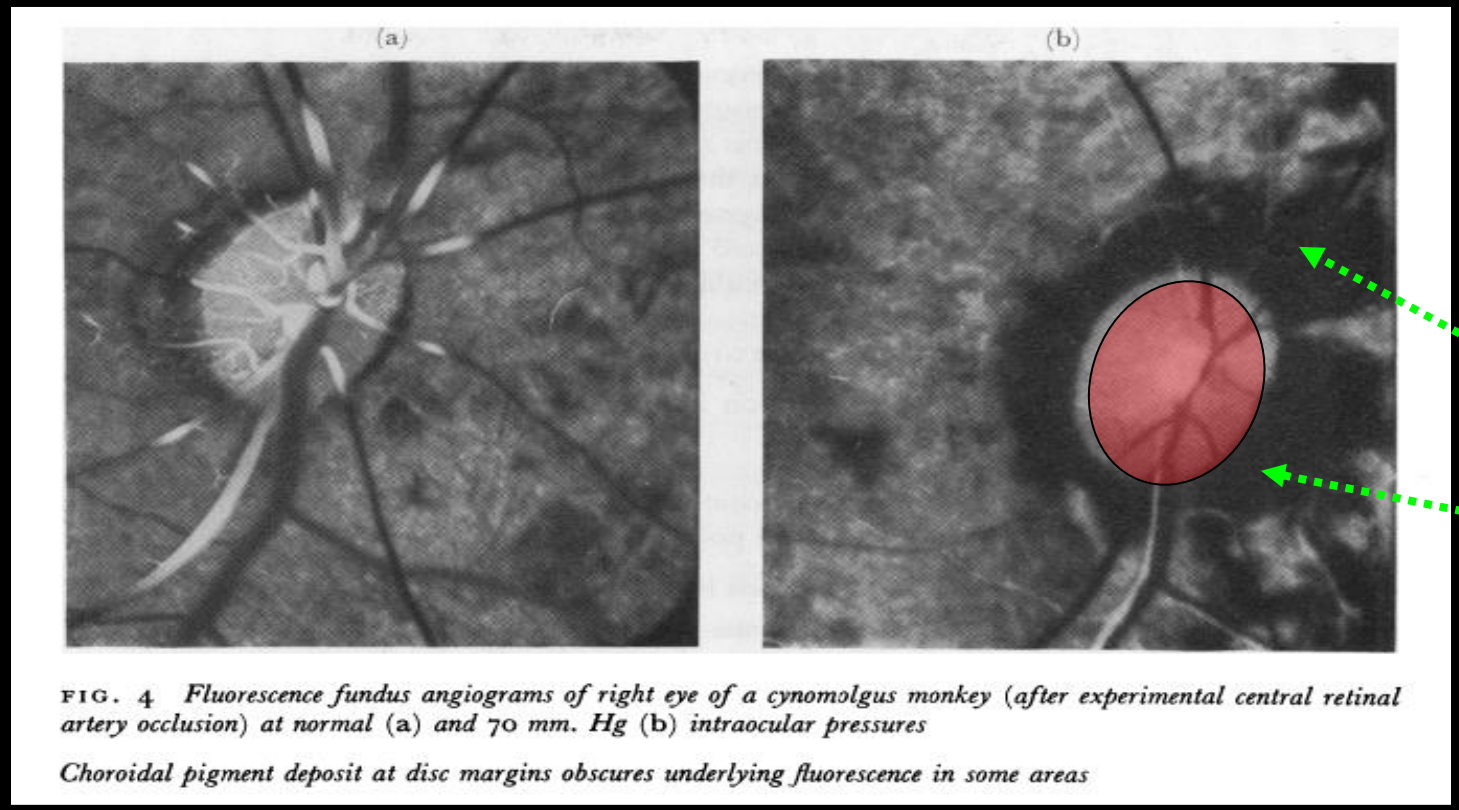

FIG. 4 *Fluorescence fundus angiograms of right eye of a cynomolgus monkey (after experimental central retinal artery occlusion) at normal (a) and 70 mm. Hg (b) intraocular pressures*

Choroidal pigment deposit at disc margins obscures underlying fluorescence in some areas

Hayreh, BJO 2000

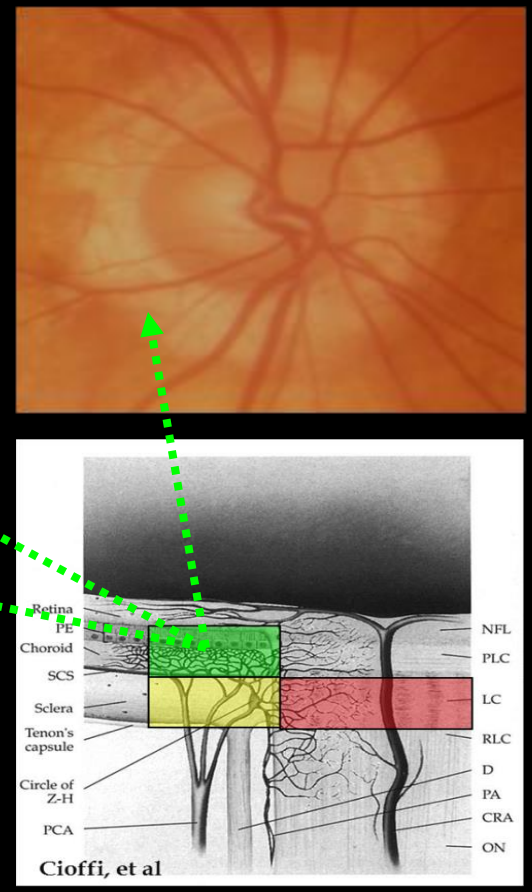

But Hayreh did not emphasize the importance of IOP-related loading of the scleral flange connective tissues through which the small vasculature passed

Small penetrating arterioles pass through the *scleral flange* *to supply the juxta-canalicular choroid and laminar beams*

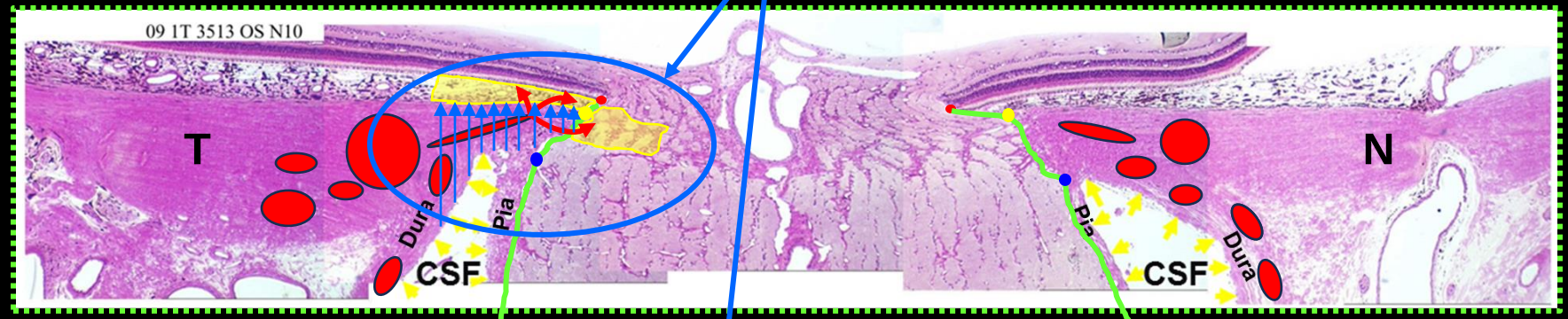

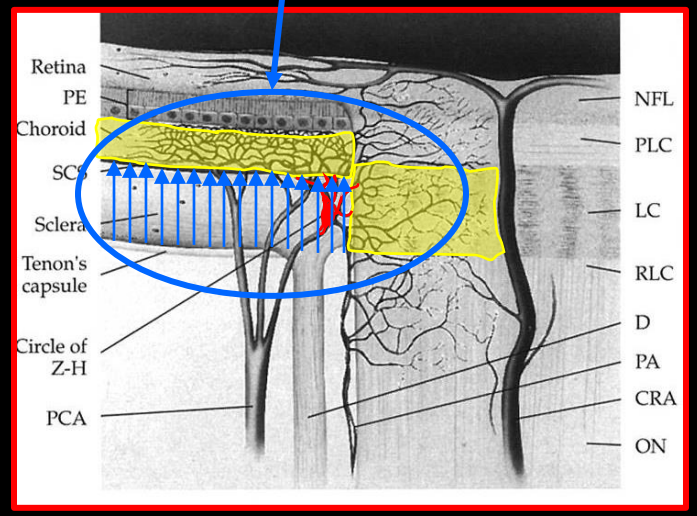

Cioffi and Van Buskirk. The Glaucomas: Basic Science. 1996

In 1993 - "Mechanical" versus "Vascular" Conceptual Warfare Confounded Glaucoma Research and Clinical Practice

Small penetrating arterioles pass through the *scleral flange* to supply the juxta-canalicular choroid and laminar beams

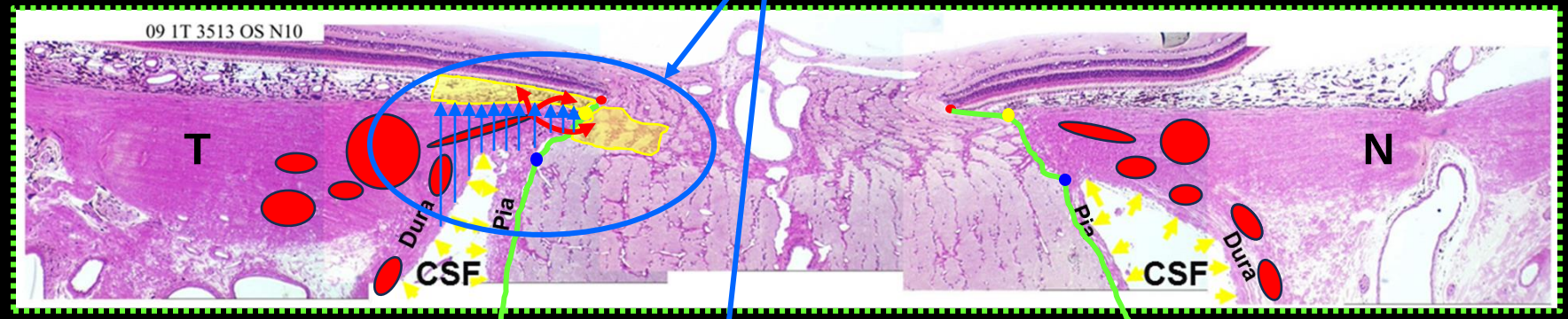

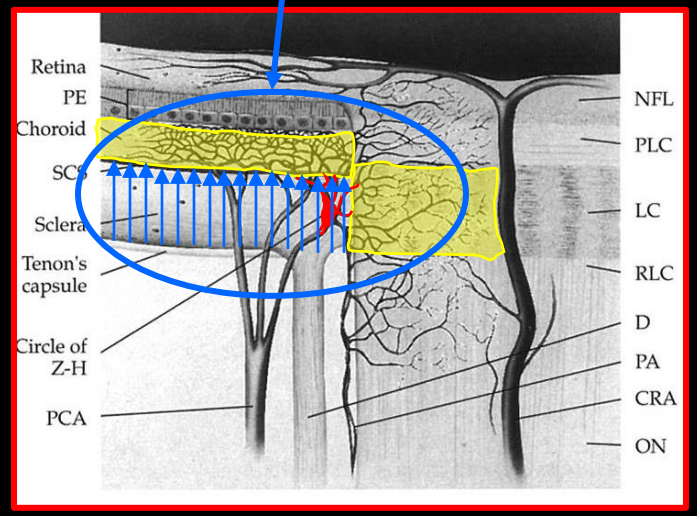

Cioffi and Van Buskirk. The Glaucomas: Basic Science. 1996

ONH Biomechanics provided a Conceptual Framework for how IOP-related connective tissue loading could influence ONH blood flow within the Scleral Flange, Choroid and Lamina

Available online at www.sciencedirect.com
SCIENCE DIRECT®
Progress in RETINAL AND EYE RESEARCH
ELSEVIER
Progress in Retinal and Eye Research 24 (2005) 39–73
www.elsevier.com/locate/prer

The optic nerve head as a biomechanical structure: a new paradigm for understanding the role of IOP-related stress and strain in the pathophysiology of glaucomatous optic nerve head damage

Claude F. Burgoyne[a,b,*], J. Crawford Downs[a,b], Anthony J. Bellezza[a,b], J.-K. Francis Suh[b], Richard T. Hart[b]

[a]*LSU Eye Center, Louisiana State University Health Sciences Center, 2020 Gravier Street, Suite B, New Orleans, LA 70112, USA*
[b]*Department of Biomedical Engineering, Tulane University, New Orleans, LA, USA*

Abstract

We propose here a conceptual framework for understanding the optic nerve head (ONH) as a biomechanical structure. Basic principles of biomechanical engineering are used to propose a central role for intraocular pressure (IOP)-related stress and strain in the physiology of ONH aging and the pathophysiology of glaucomatous damage. Our paradigm suggests that IOP-related stress and strain (1) are substantial within the load-bearing connective tissues of the ONH even at low levels of IOP and (2) underlie both ONH aging and the two central pathophysiologies of glaucomatous damage—mechanical failure of the connective tissues of the lamina cribrosa, scleral canal wall, and peripapillary sclera, and axonal compromise within the lamina cribrosa by a variety of mechanisms. Modeling the ONH as a biomechanical structure generates a group of testable hypotheses regarding the central mechanisms of glaucomatous damage and provides a logic for classifying the principal components of the susceptibility of an individual ONH to a given level of IOP.
© 2004 Elsevier Ltd. All rights reserved.

Burgoyne et al. PRER 2005

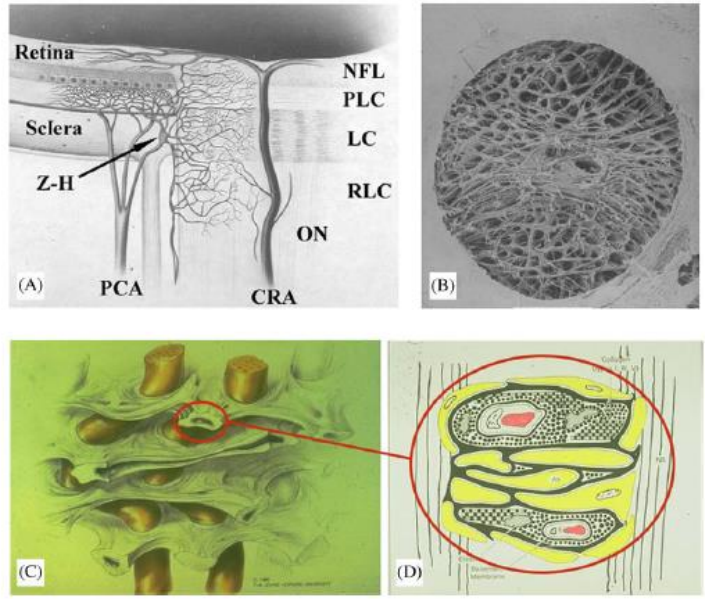

Fig. 6. IOP-related stress may have acute and chronic effects on the delivery of blood-borne nutrients to the axons within the lamina cribrosa. (A) The blood supply to the ONH. The traditional extra-bulbar determinants of ONH laminar capillary volume flow are fluctuations in systemic blood pressure and vasospasm. However, laminar volume flow may additionally be diminished by a compressive effect on volume flow within the branches of the posterior ciliary arteries that penetrate to the choroid, prelaminar, laminar, and post-laminar regions from IOP-related stress within the peripapillary sclera. Separate from these effects, IOP-related stress within each individual laminar trabecula (B and C) may have acute compressive effects on laminar capillary volume flow (solid red, D). Separate from considerations of volume flow, axonal nutrition within the lamina (D) requires diffusion of nutrients from the laminar capillaries (solid red), across the endothelial and pericyte basement membranes, through the extracellular matrix of the laminar beam (stippled), across the basement membranes of the astrocytes (thick black), into the astrocytes (yellow), and across their processes (not shown) to the adjacent axons (vertical lines). Chronic age-related changes in the endothelial cell and astrocyte basement membranes, as well as IOP-induced changes in the laminar extracellular matrix and astrocyte basement membranes, may diminish nutrient diffusion to the axons in the presence of a stable level of laminar capillary volume flow. Z−H = circle of Zinn–Haller; PCA = posterior ciliary arteries; NFL = nerve fiber layer; PLC = prelaminar region; LC = lamina cribrosa; RLC = retrolaminar region; ON = optic nerve; CRA = central retinal artery. (A) Reprinted with permission from Cioffi, G.A., Van Buskirk, E.M., 1996. Vasculature of the optic nerve and peripapillary choroid. Chapter 8. In: Ritch, R., Shields, M.B., Krupin, T. (Eds.), The Glaucomas, Second ed. Mosby-Year Book, St. Louis. (B) Reprinted with permission from Quigley, H.A., Brown, A.E., Morrison, J.D., Drance, S.M., 1990. The size and shape of the optic disc in normal human eyes. Arch. Ophthalmol. 108, 51–57, Copyright, 1990, American Medical Association. (C) Reprinted with permission from Quigley, H.A., 1995. Overview and introduction to session on connective tissue of the optic nerve in glaucoma. Chapter 2. In: Drance, S.M., Anderson, D.R. (Eds.) Optic Nerve in Glaucoma. Kugler Publications, Amsterdam/New York. (D) Reprinted with permission from Morrison, J.C., L'Hernault, N.L., Jerdan, J.A., Quigley, H.A., 1989. Ultrastructural location of extracellular matrix components in the optic nerve head. Arch. Ophthalmol. 107, 123–129, Copyright, 1989, American Medical Association.

"Figure 6: IOP-related stress may have acute and chronic effects on the delivery of blood-borne nutrients to the axons within the Lamina cribrosa."

Specifically hypothesizing that "IOP-related" and "Vascular" risk factors could be expected to interact within these tissues in "Aging", "Glaucoma" and "High Myopia"

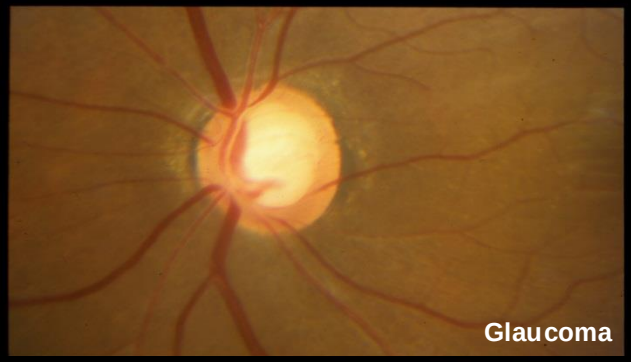

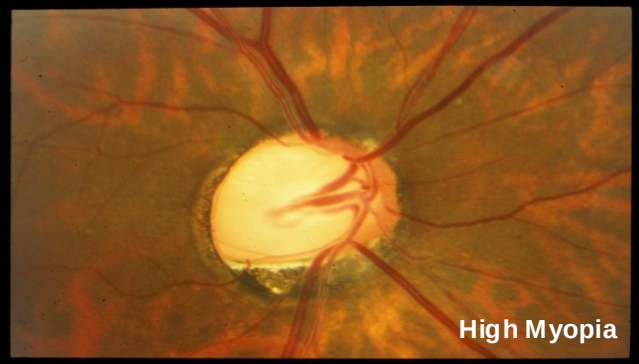

Small penetrating arterioles pass through the *scleral flange* to supply the juxta-canalicular choroid and laminar beams

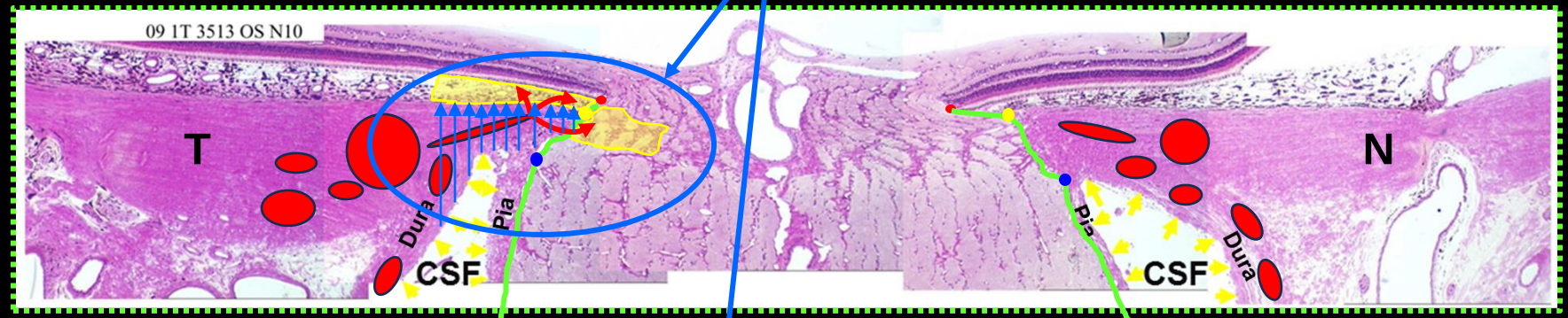

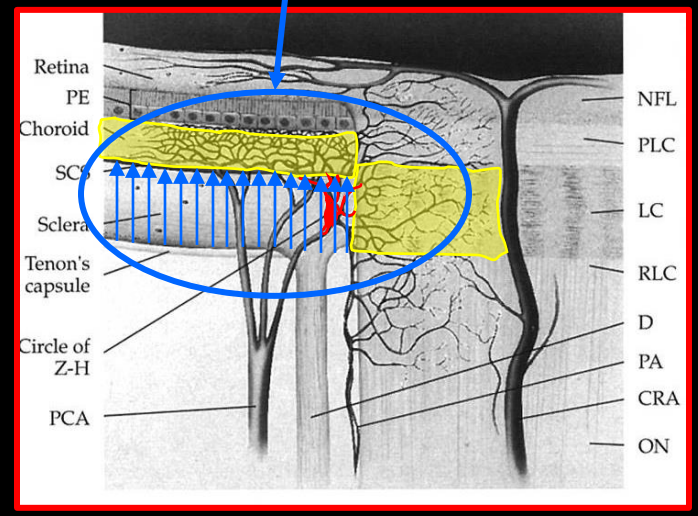

Cioffi and Van Buskirk. The Glaucomas: Basic Science. 1996

While it is still not possible to directly measure blood flow within the scleral flange, changes in this blood supply should indirectly manifest as microvascular dropout within, and thinning of, the juxta-canalicular choroid

SCIENTIFIC REPORTS
nature research
Check for updates

Focal lamina cribrosa defects are not associated with steep lamina cribrosa curvature but with choroidal microvascular dropout

Seung Hyen Lee[1], Tae-Woo Kim[2] ✉, Eun Ji Lee[2], Michaël J. A. Girard[3,4] & Jean Martial Mari[5]

Focal lamina cribrosa (LC) defects have been found to play an important role in the development and progression of glaucomatous optic neuropathy. However, the mechanism of generation of focal LC defects is largely unknown. This cross-sectional study was performed to investigate LC curvature and the frequency of parapapillary choroidal microvascular dropout (MvD) in glaucomatous eyes with focal LC defects. This study was conducted by a retrospective review of patients with primary open-angle glaucoma (POAG) included in an ongoing prospective study being performed at the Seoul National University Bundang Hospital (Investigating Glaucoma Progression Study). A total of 118 eyes of 118 patients with POAG, 59 with and 59 without focal LC defects, with eyes matched by age, axial length, and severity of visual field (VF) damage were included. Posterior LC bowing was assessed by calculating LC curvature index (LCCI), as the inflection of a curve representing a section of the LC, on the optic nerve head images obtained by enhanced-depth-imaging (EDI) spectral-domain optical coherence tomography (OCT). MvD was detected by OCT angiography. LCCI and MvD frequency were compared between eyes with and without focal LC defects. Mean LCCI was significantly smaller than in eyes with than without focal LC defects (9.75 ± 1.29 vs. 11.25 ± 1.39, $P < 0.001$). MvD was significantly more frequent in eyes with than without focal LC defects (84.7% vs. 49.2%, $P < 0.001$). MvD in eyes with focal LC defects showed a strong topographic correlation with the focal LC defects. These findings suggest that focal LC defects may primarily result from vascular factors rather than from mechanical strain.

Lee SH, et al. Sci Reports. 2020

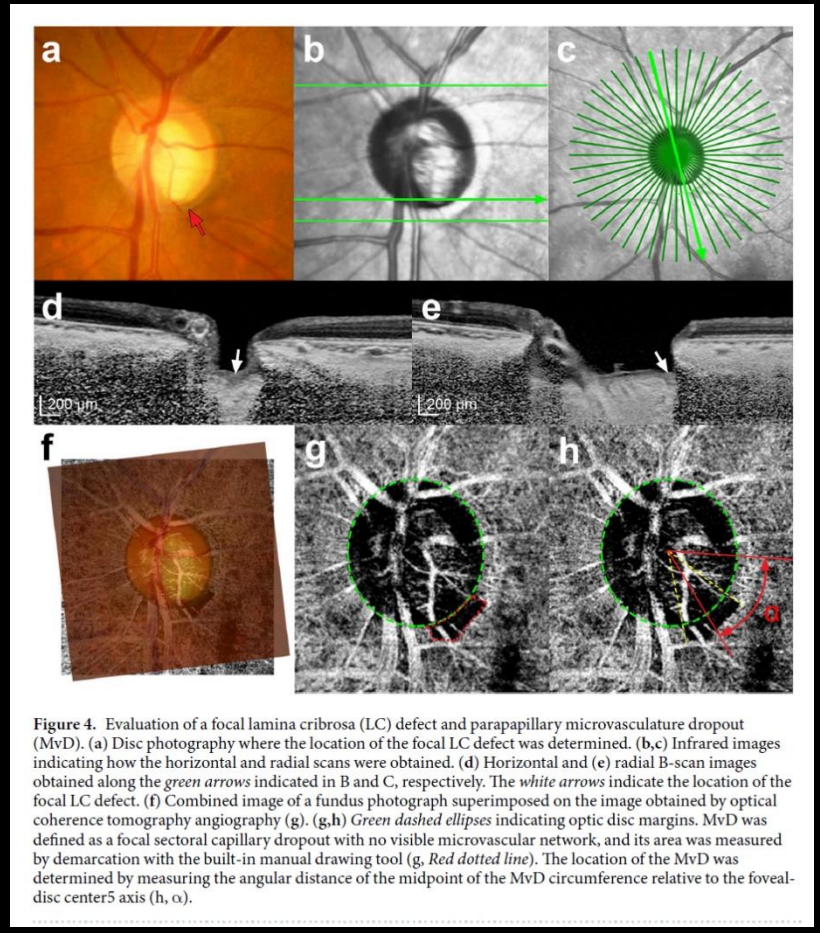

Figure 4. Evaluation of a focal lamina cribrosa (LC) defect and parapapillary microvasculature dropout (MvD). (**a**) Disc photography where the location of the focal LC defect was determined. (**b**,**c**) Infrared images indicating how the horizontal and radial scans were obtained. (**d**) Horizontal and (**e**) radial B-scan images obtained along the *green arrows* indicated in B and C, respectively. The *white arrows* indicate the location of the focal LC defect. (**f**) Combined image of a fundus photograph superimposed on the image obtained by optical coherence tomography angiography (**g**). (**g**,**h**) *Green dashed ellipses* indicating optic disc margins. MvD was defined as a focal sectoral capillary dropout with no visible microvascular network, and its area was measured by demarcation with the built-in manual drawing tool (g, *Red dotted line*). The location of the MvD was determined by measuring the angular distance of the midpoint of the MvD circumference relative to the foveal-disc center5 axis (h, α).

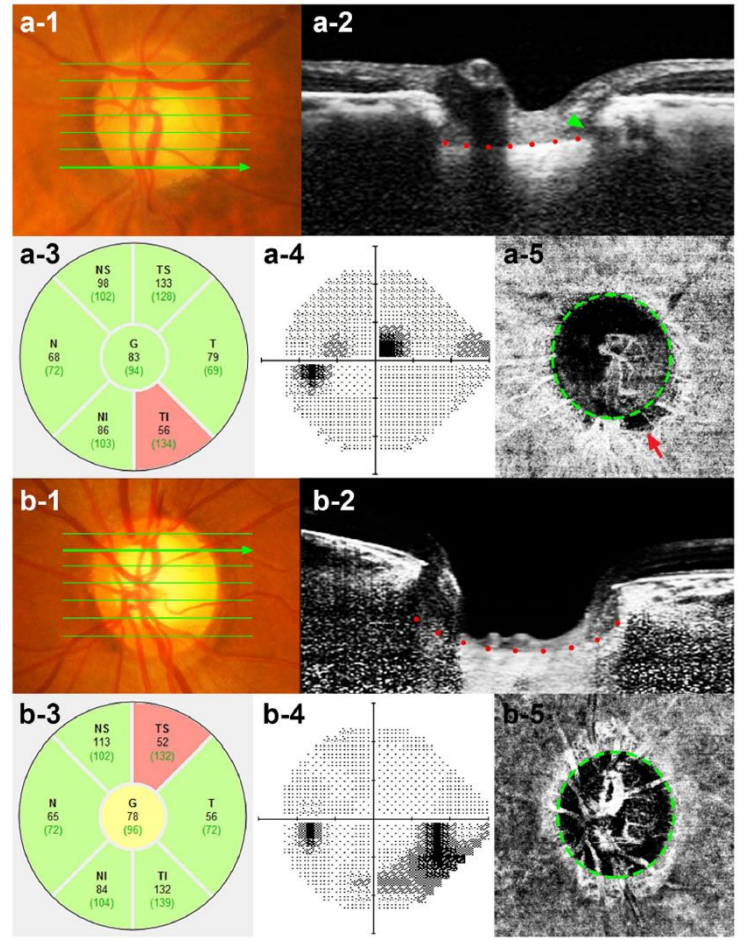

Figure 2. Representative eyes with (**a**) and without a (**b**) a focal LC defect. (a-1, b-1) Disc photographs of the left eye of a 75-year-old man (**a**), and a 50-year-old woman (**b**). (a-2, b-2) B-scan images obtained at the locations indicated by the *green arrows* in a-1and b-1, respectively. The focal LC defect is indicated by the *green arrow head* (b-2). Note that LCCI was smaller in the eye with (a-2, *red dots*) than without (b-2, *red dots*) a focal LC defect. However, retinal nerve fiber layer thickness (a-3, b-3) and visual field damage (a-4, b-4) did not differ between these two eyes. (a-5, b-5) *Green dashed lines* indicate the optic disc margin, and the *red arrow* indicates MvD (a-5). Note that the parapapillary MvD was located at the same sector as the focal LC defect.

Burgoyne–2024 Goldmann–GRS Website

Peri–Neural Canal Scleral Bowing increases with age and is inversely related to pNC-CT in Non-Highly Myopic Health Eyes

Glaucoma

Variation of Peripapillary Scleral Shape With Age

Tin A. Tun,[1,2] Xiaofei Wang,[2,3] Mani Baskaran,[1,4] Monisha E. Nongpiur,[1,4] Yih-Chung Tham,[1] Shamira A. Perera,[1,4] Nicholas G. Strouthidis,[1,5,6] Tin Aung,[1,4,7] Ching-Yu Cheng,[1,4,7] and Michaël J. A. Girard[1,2]

[1]Singapore Eye Research Institute and Singapore National Eye Centre, Singapore
[2]Ophthalmic Engineering & Innovation Laboratory, Department of Biomedical Engineering, National University of Singapore, Singapore
[3]Beijing Advanced Innovation Center for Biomedical Engineering, School of Biological Science and Medical Engineering, Beihang University, Beijing, China
[4]Duke-NUS Medical School, Singapore
[5]NIHR Biomedical Research Centre, Moorfields Eye Hospital NHS Foundation Trust and UCL Institute of Ophthalmology, London, United Kingdom
[6]Discipline of Clinical Ophthalmology and Eye Health, University of Sydney, Sydney, New South Wales, Australia
[7]Department of Ophthalmology, Yong Loo Lin School of Medicine, National University of Singapore, Singapore

Correspondence: Michaël J. A. Girard, Ophthalmic Engineering & Innovation Laboratory (OEIL), Department of Biomedical Engineering, National University of Singapore, 4 Engineering Drive 3, E4-04-08, 117583, Singapore; mgirard@nus.edu.sg.

TAT and XW contributed equally to the work presented here and should therefore be regarded as equivalent authors.

Submitted: February 9, 2019
Accepted: June 18, 2019

Citation: Tun TA, Wang X, Baskaran M, et al. Variation of peripapillary scleral shape with age. *Invest Ophthalmol Vis Sci.* 2019;60:3275–3282. https://doi.org/10.1167/iovs.19-26777

Purpose. To define the shape of the anterior surface of the peripapillary sclera (PPS) and evaluate its relationship with age and ocular determinants in a population-based Chinese cohort.

Methods. The optic nerve heads of 619 healthy Chinese subjects were imaged with spectral-domain optical coherence tomography. To assess the shape of the PPS/Bruch's membrane (BM), we measured the angle between a line parallel to the nasal anterior PPS/BM boundary and one parallel to the temporal side. A negative value indicated that the PPS/BM followed an inverted v-shaped configuration (peak pointing toward the vitreous), whereas a positive value indicated that it followed a v-shaped configuration (peak pointing toward the orbital tissues). A linear regression model was used to evaluate the relationship between the PPS angle and other ocular parameters.

Results. The mean PPS angle was 3.68° ± 6.73° and the BM angle was 9.69° ± 5.05°. The PPS angle increased on average by 0.233 deg/y. A v-shaped PPS was significantly associated with age ($\beta = 0.087$, $P = 0.004$), peripapillary choroidal thickness ($\beta = -0.479$, $P < 0.001$), lamina cribrosa depth ($\beta = 0.307$, $P < 0.001$), and BM angle ($\beta = 0.487$, $P < 0.001$) after adjusting for best corrected visual acuity, central corneal thickness, and axial length.

Conclusions. The anterior surface of PPS of an elderly adult population had a v-shaped configuration and was more pronounced with increasing age, thin peripapillary choroid, and a deep cup. Such a change in shape with age could have an impact on the biomechanical environment of the optic nerve head.

Keywords: peripapillary sclera, age, choroidal thickness, laminar depth

Tun et al. IOVS. 2019

IOVS | August 2019 | Vol. 60 | No. 10 | 3276

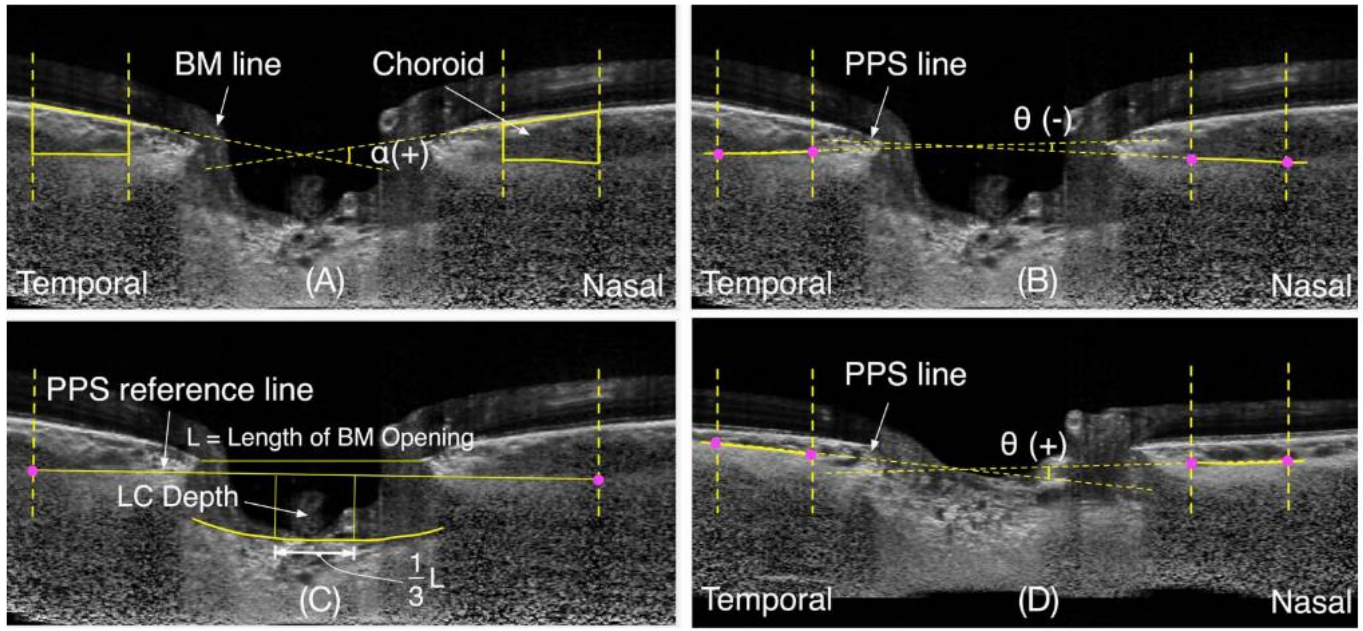

Figure 1. Illustration of measurement of Bruch's membrane angle and of the peripapillary scleral angle. (**A**) Illustration of a v-shaped Bruch's membrane angle, α; (**B**) Illustration of an inverted-v shaped PPS angle, θ(–); (**C**) The measurement of the depth of anterior surface of the lamina cribrosa (LC depth) from the peripapillary sclera reference plane; (**D**) Illustration of a v-shaped PPS angle, θ(+).

Peri–Neural Canal Scleral Bowing (pNC-SB) Increases with Age and Colocalizes with Choroidal Thinning in Normal and Highly Myopic Eyes

Peripapillary Scleral Bowing Increases with Age and Is Inversely Associated with Peripapillary Choroidal Thickness in Healthy Eyes

YA XING WANG, HONGLI YANG, HAOMIN LUO, SEUNG WOO HONG, STUART K. GARDINER, JIN WOOK JEOUNG, CHRISTY HARDIN, GLEN P. SHARPE, KOUROS NOURI-MAHDAVI, JOSEPH CAPRIOLI, SHABAN DEMIREL, CHRISTOPHER A. GIRKIN, JEFFREY M. LIEBMANN, CHRISTIAN Y. MARDIN, HARRY A. QUIGLEY, ALEXANDER F. SCHEUERLE, BRAD FORTUNE, BALWANTRAY C. CHAUHAN, AND CLAUDE F. BURGOYNE

• PURPOSE: To use optical coherence tomography (OCT) to 3-dimensionally characterize the optic nerve head (ONH) in peripapillary scleral bowing in non-highly myopic healthy eyes.
• DESIGN: Cross-sectional, multicenter study.
• METHODS: A total of 362 non-highly myopic (+6 diopters [D] > spherical equivalent > −6D) eyes of 362 healthy subjects from 20-90 years old underwent OCT ONH radial B-scan imaging. Bruch's membrane (BM), BM opening (BMO), anterior scleral canal opening (ASCO), and the peripapillary scleral surface were segmented. BMO and ASCO planes were fit, and their centroids, major axes, ovality, areas and offsets were determined. Peripapillary scleral bowing was characterized by 2 parameters: peripapillary scleral slope (ppSS) of 3 anterior peripapillary scleral segments (0-300, 300-700, and 700-1,000 μm from the ASCO centroid); and ASCO depth relative to a peripapillary scleral reference plane (*ASCOD-ppScleral*). Peripapillary choroidal thickness (*ppCT*) was calculated relative to the ASCO as the minimum distance between the anterior scleral surface and BM.
• RESULTS: Both ppSS and *ASCOD-ppScleral* ranged from slightly inward through profoundly outward in direction. Both parameters increased with age and were independently associated with decreased *ppCT*.
• CONCLUSIONS: In non-highly myopic healthy eyes, outward peripapillary scleral bowing achieved substantial levels, was markedly increased with age, and was independently associated with decreased peripapillary choroidal thickness. These findings provide a normative foundation for characterizing this anatomy in cases of high myopia and glaucoma and in eyes with optic disc tilt, torsion, and peripapillary atrophy. (Am J Ophthalmol 2020;217:91–103. © 2020 Elsevier Inc. All rights reserved.)

AJO.com Supplemental Material available at AJO.com.
Accepted for publication Mar 31, 2020.
From the Devers Eye Institute Optic Nerve Head Research Laboratory (Y.X.W., H.Y., H.L., S.W.H., J.W.J., C.H., C.F.B.), Legacy Research Institute, Portland, Oregon, USA; Devers Eye Institute Discoveries in

Wang et al. AJO. 2020

OCT Optic Nerve Head Morphology in Myopia II: Peri-Neural Canal Scleral Bowing and Choroidal Thickness in High Myopia—An American Ophthalmological Society Thesis

CLAUDE F. BURGOYNE, YA XING WANG, JIN WOOK JEOUNG, SEUNGWOO HONG, STUART GARDINER, JUAN REYNAUD, BRAD FORTUNE, MICHAËL J.A. GIRARD, GLEN SHARPE, MARCELO NICOLELA, BALWANTRAY C. CHAUHAN, AND HONGLI YANG

• PURPOSE: To use optical coherence tomography (OCT) to characterize optic nerve head (ONH) peri-neural canal (pNC) scleral bowing (pNC-SB) and pNC choroidal thickness (pNC-CT) in 69 highly myopic and 138 healthy, age-matched, control eyes.
• DESIGN: Cross-sectional, case control study.
• METHODS: Within ONH radial B-scans, Bruch membrane (BM), BM opening (BMO), anterior scleral canal opening (ASCO), and pNC scleral surface were segmented. BMO and ASCO planes and centroids were determined. pNC-SB was characterized within 30° foveal-BMO (FoBMO) sectors by 2 parameters: pNC-SB-scleral slope (pNC-SB-SS), measured within 3 pNC segments (0-300, 300-700, and 700-1000 μm from the ASCO centroid); and pNC-SB-ASCO depth relative to a pNC scleral reference plane (pNC-SB-ASCOD). pNC-CT was calculated as the minimum distance between the scleral surface and BM at 3 pNC locations (300, 700, and 1100 μm from the ASCO).
• RESULTS: pNC-SB increased and pNC-CT decreased with axial length ($P < .0133$; $P < .0001$) and age ($P < .0211$; $P < .0004$) among all study eyes. pNC-SB was increased ($P < .001$) and pNC-CT was decreased ($P < .0279$) in the highly myopic compared to control eyes, and these differences were greatest in the inferior quadrant sectors ($P < .0002$). Sectoral pNC-SB was not related to sectoral pNC-CT in control eyes, but was inversely related to sectoral pNC-CT ($P < .0001$) in the highly myopic eyes.
• CONCLUSIONS: Our data suggest that pNC-SB is increased and pNC-CT is decreased in highly myopic eyes and that these phenomena are greatest in the inferior sectors. They support the hypothesis that sectors of maximum pNC-SB may predict sectors of greatest susceptibility to aging and glaucoma in future longitudinal studies of highly myopic eyes. (Am J Ophthalmol 2023;252:225–252. © 2023 Elsevier Inc. All rights reserved.)

THE PURPOSE OF THIS STUDY IS TO CHARACTERIZE PERI-neural canal (pNC) scleral bowing (pNC-SB) and choroidal thickness (pNC-CT) in highly myopic vs age-matched non–highly myopic (control) eyes. To do so, our study uses a conceptual framework for clinically evaluating the optic nerve head (ONH) tissues (Figure 1) using optical coherence tomography (OCT).[1] We argue that this conceptual framework represents a paradigm change from 2-dimensionally examining the "clinical disc" as defined by the clinical disc margin to 3-dimensionally examining the ONH tissues based on the Bruch membrane opening (BMO) and the neural canal (Figure 2). We therefore start with definitions that are central to this paradigm change and to the execution of this study.

We define the ONH anatomically and morphologically

Burgoyne et al. AJO. 2023

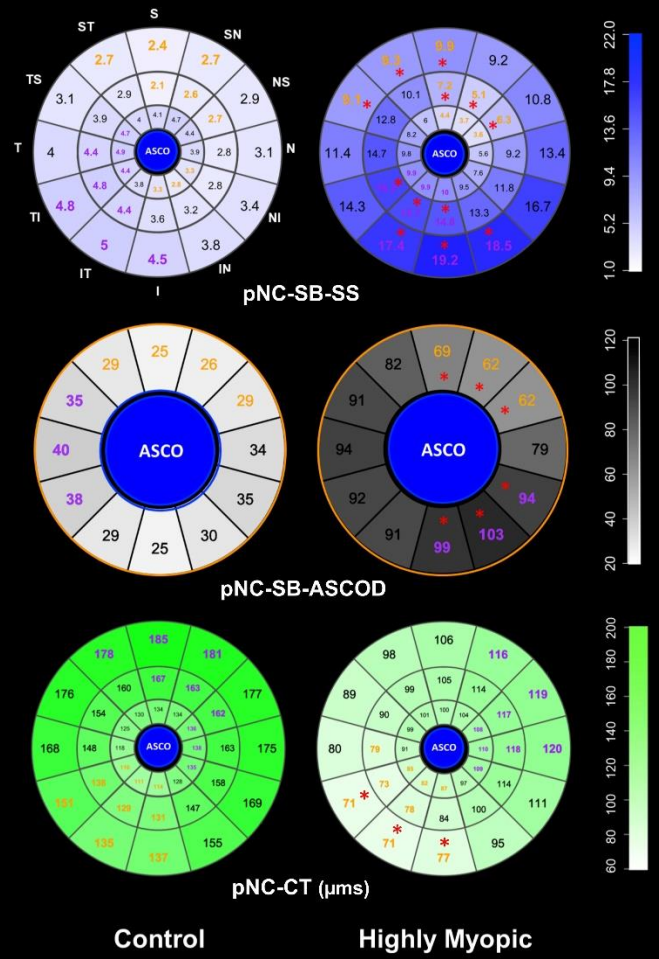

Burgoyne–2024 Goldmann–GRS Website

But even before the scleral flange – the vascular Circle of Zinn Haller passes through the Circumferential Collagen / Elastin Ring

Schematically-Depicted
pNC-Scleral Circumferential Collagen/Elastin Ring

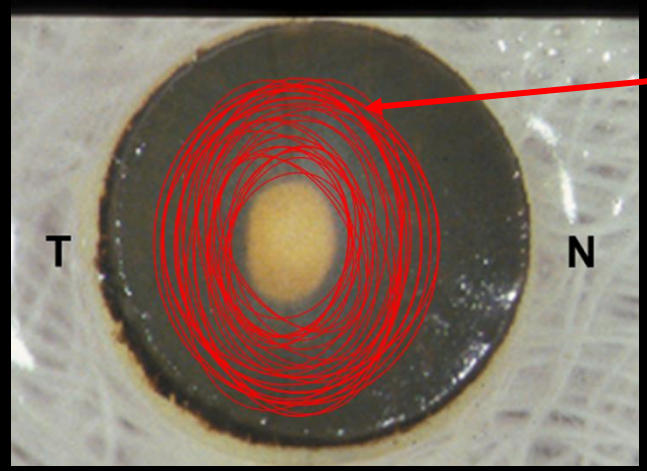

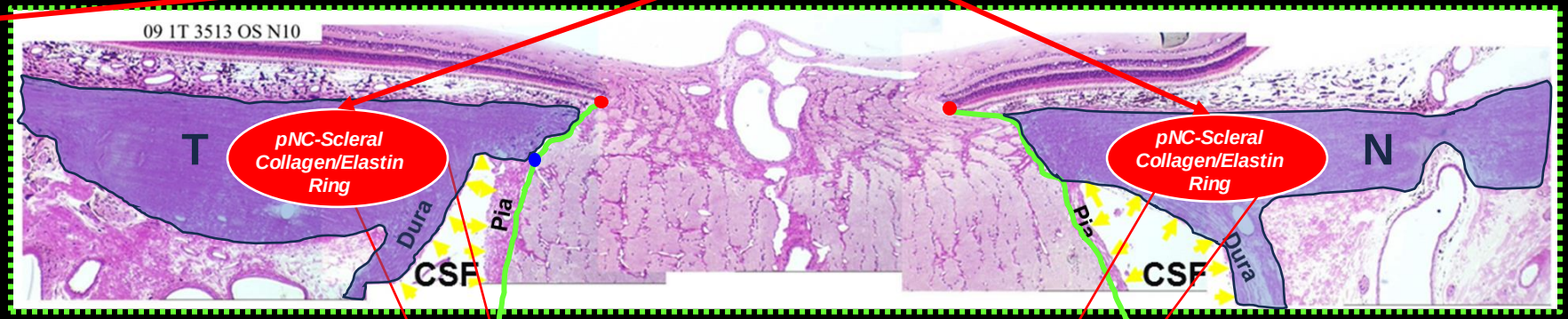

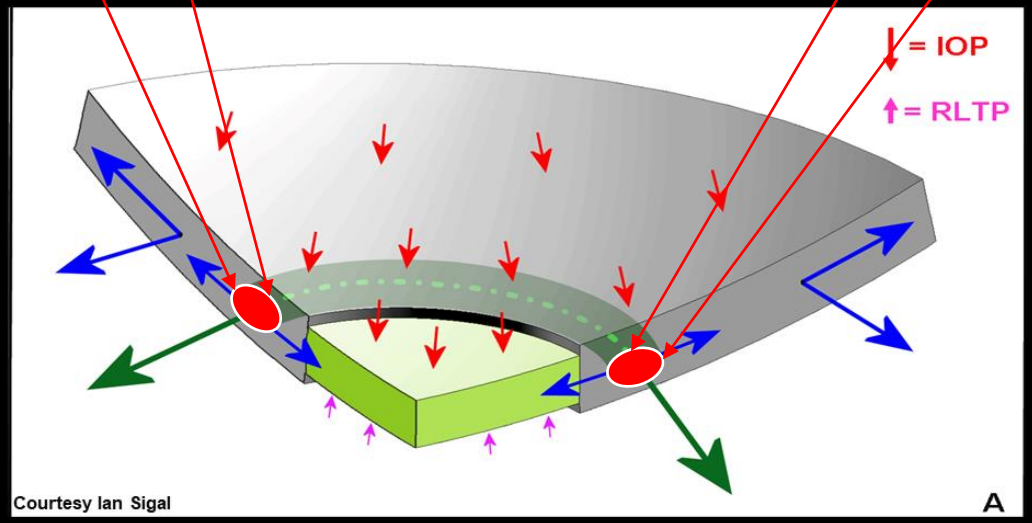

The pNC-Scleral Circumferential Collagen/Elastin Ring

Which is a central determinant of
ONH Biomechanical Loading and Behavior

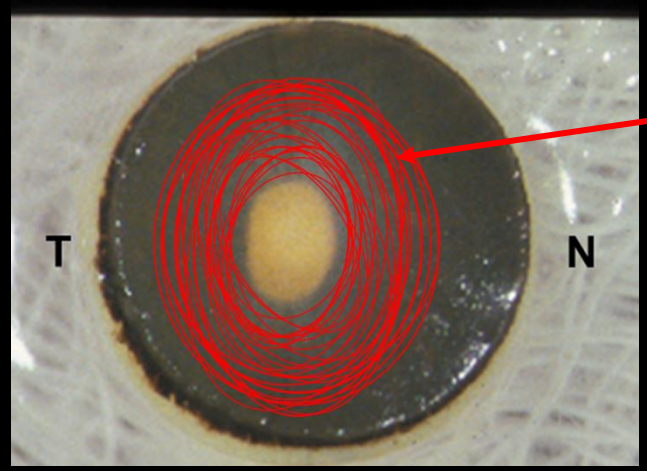

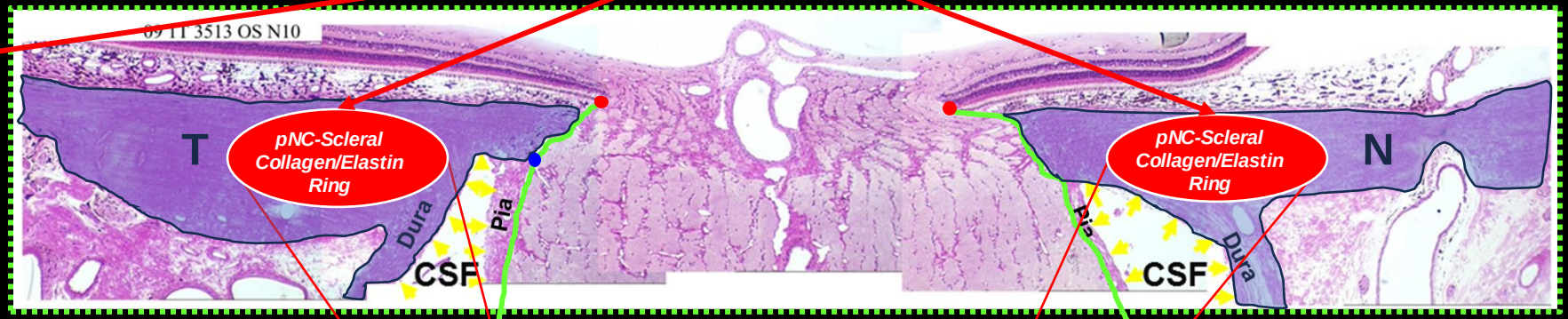

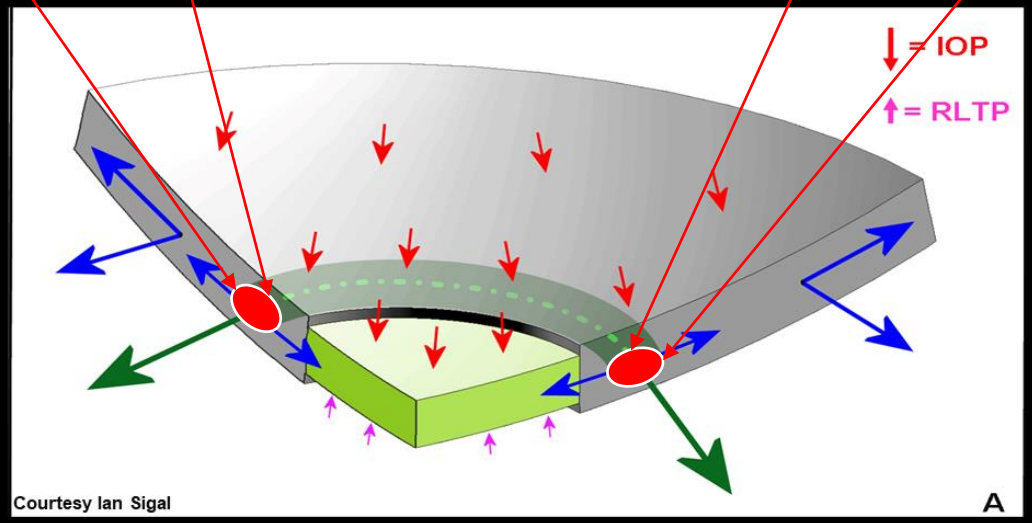

The pNC-Scleral Circumferential Collagen/Elastin Ring

The laminar beams insert into the

Circumferential Collagen/Elastin Ring

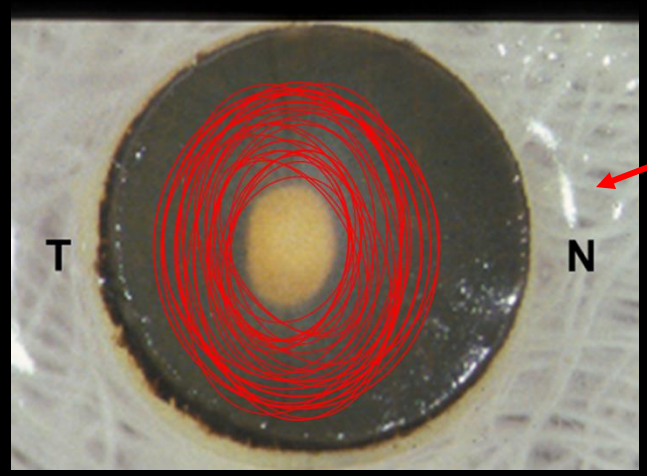

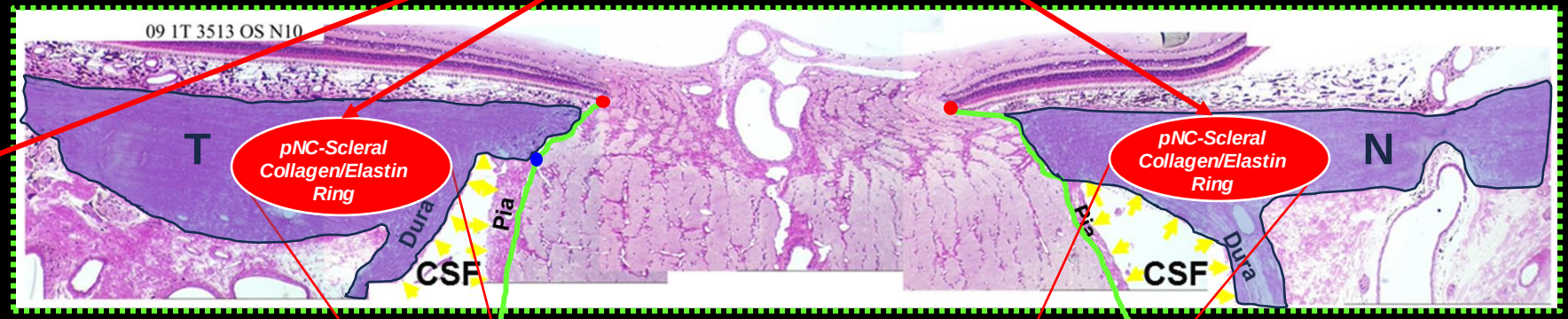

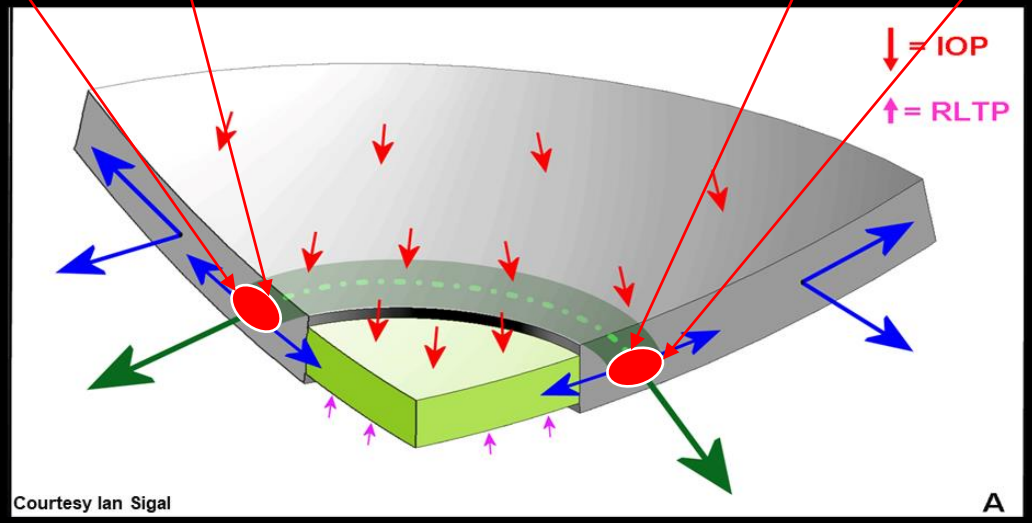

The pNC-Scleral Circumferential Collagen/Elastin Ring

Eye-specific architecture and material properties likely highly variable and affected by age-related/glaucomatous/myopic remodeling

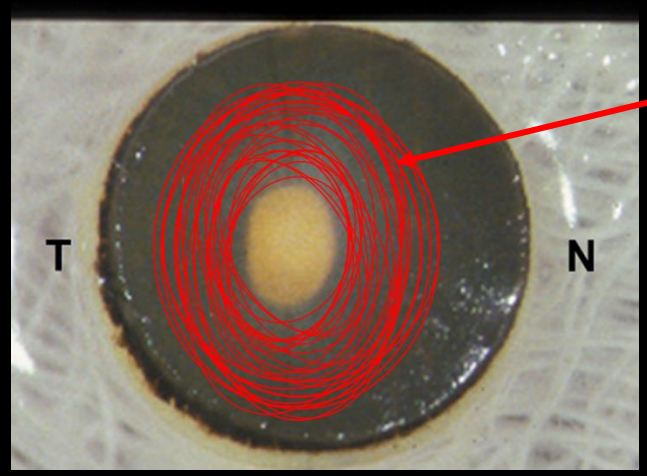

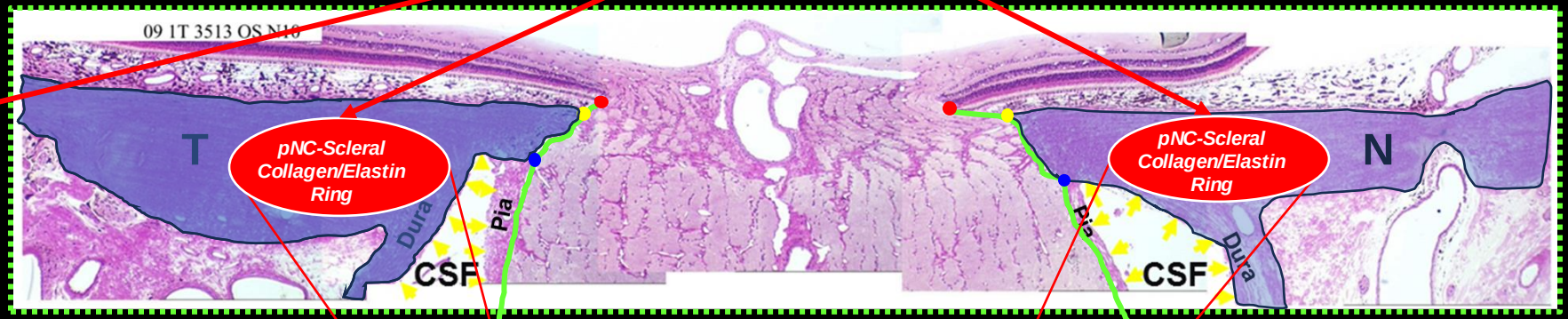

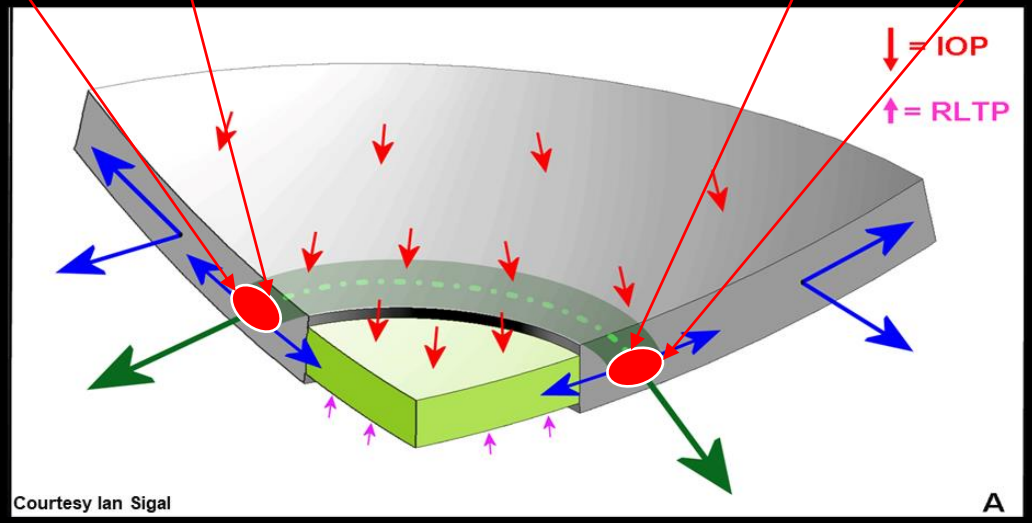

The pNC-Scleral and Dural Circumferential Collagen/Elastin Ring are contiguous

Schematically Depicted pNC-Scleral Collagen Ring

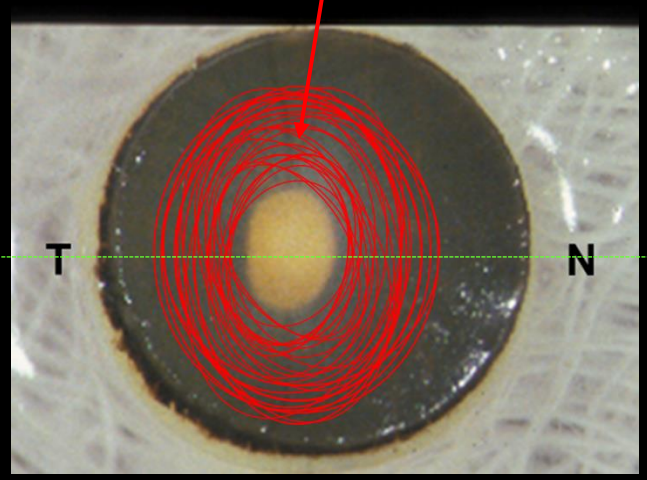

Dural Sheath Circumferential Collagen Ring / Peri-Neural Canal (pNC) Scleral Collagen Ring Are Contiguous

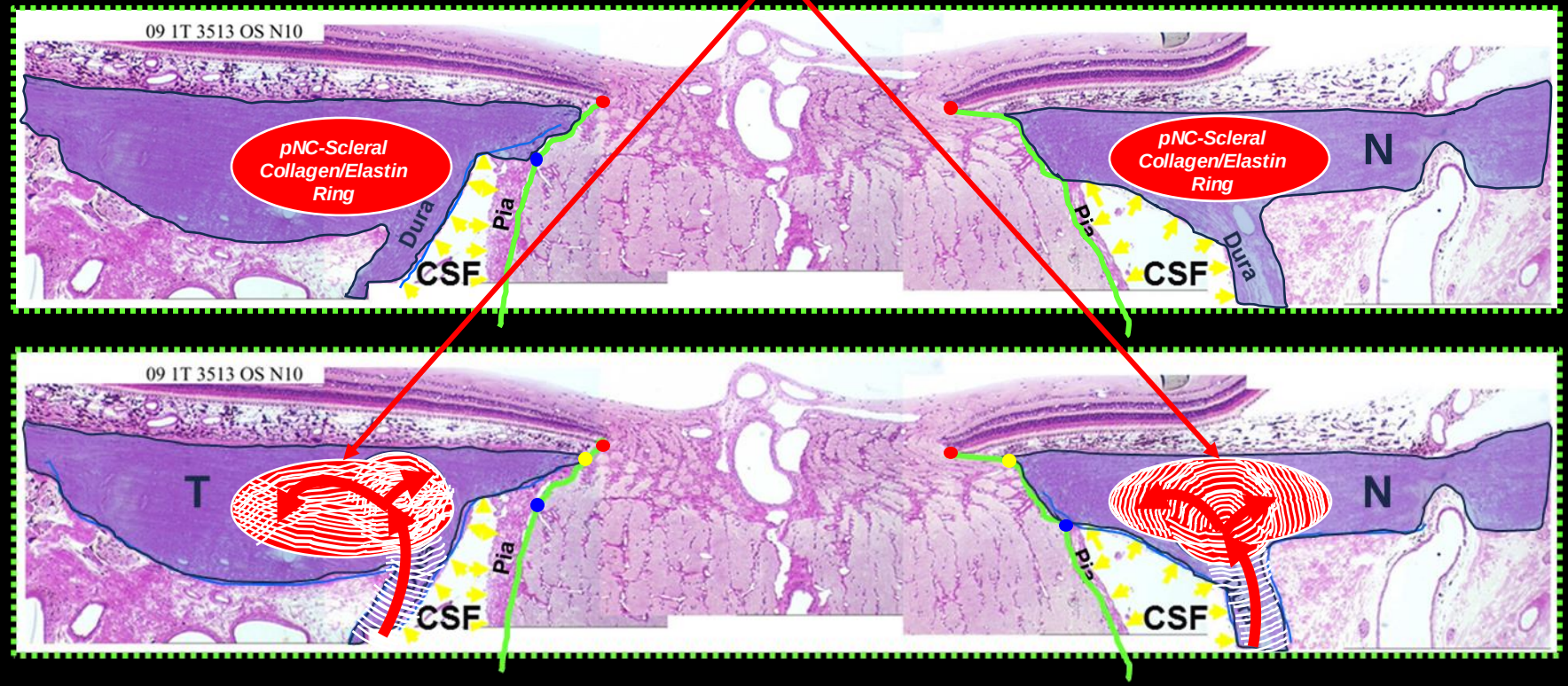

The pNC-Scleral and Dural Circumferential Collagen/Elastin Ring are contiguous

Schematically Depicted pNC-Scleral Collagen Ring

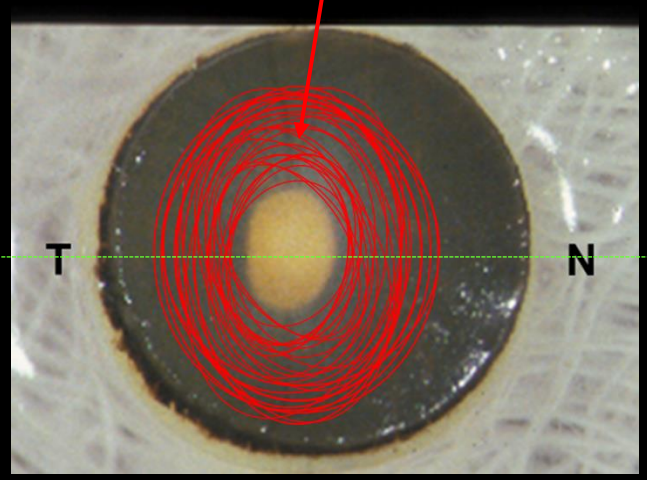

Biomechanically the Dural Sheath Circumferential Collagen Ring and the Peri-Neural Canal Scleral Collagen Ring may behave as one structure

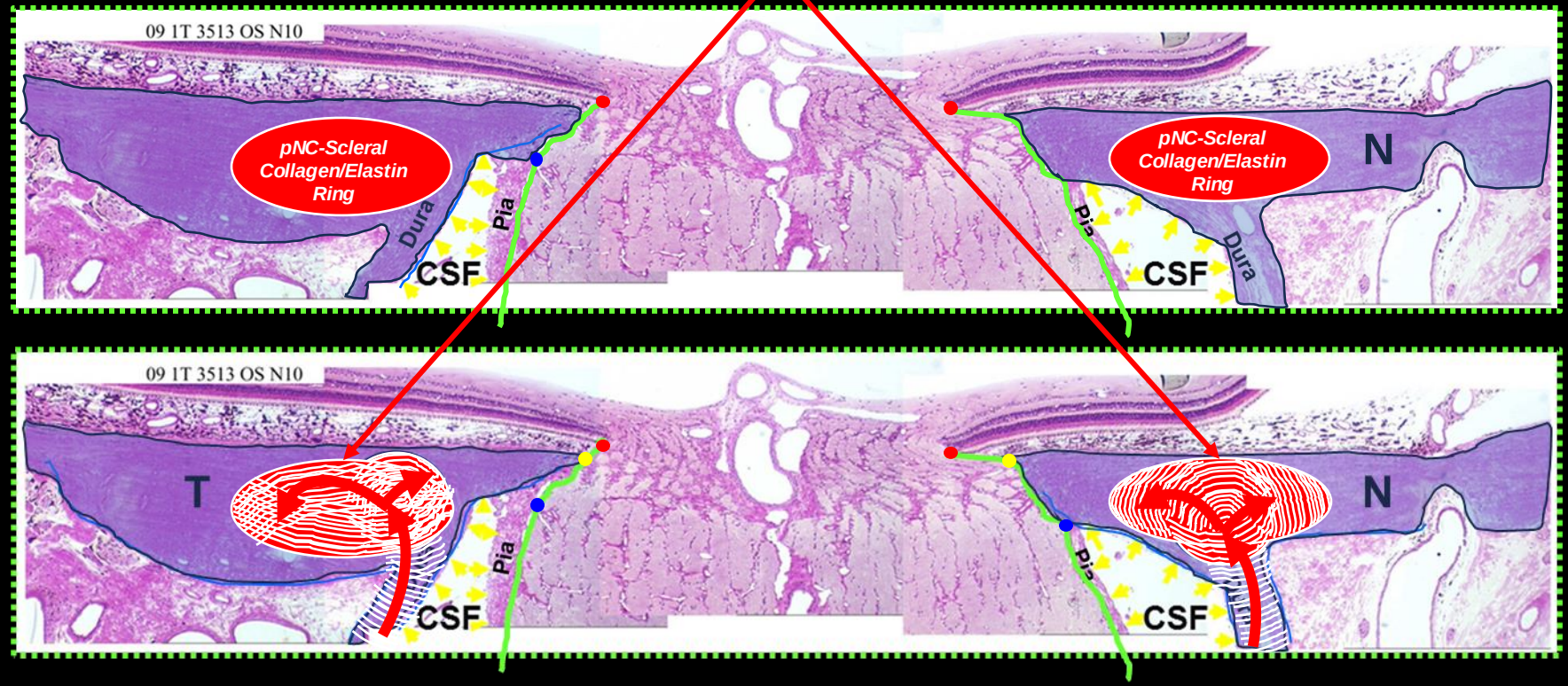

Eye-movement (Dural Sheath) related changes in IOP-related loading of the human pNC–Sclera and Scleral Flange may contribute to ONH susceptibility in Aging, Myopia and Glaucoma????

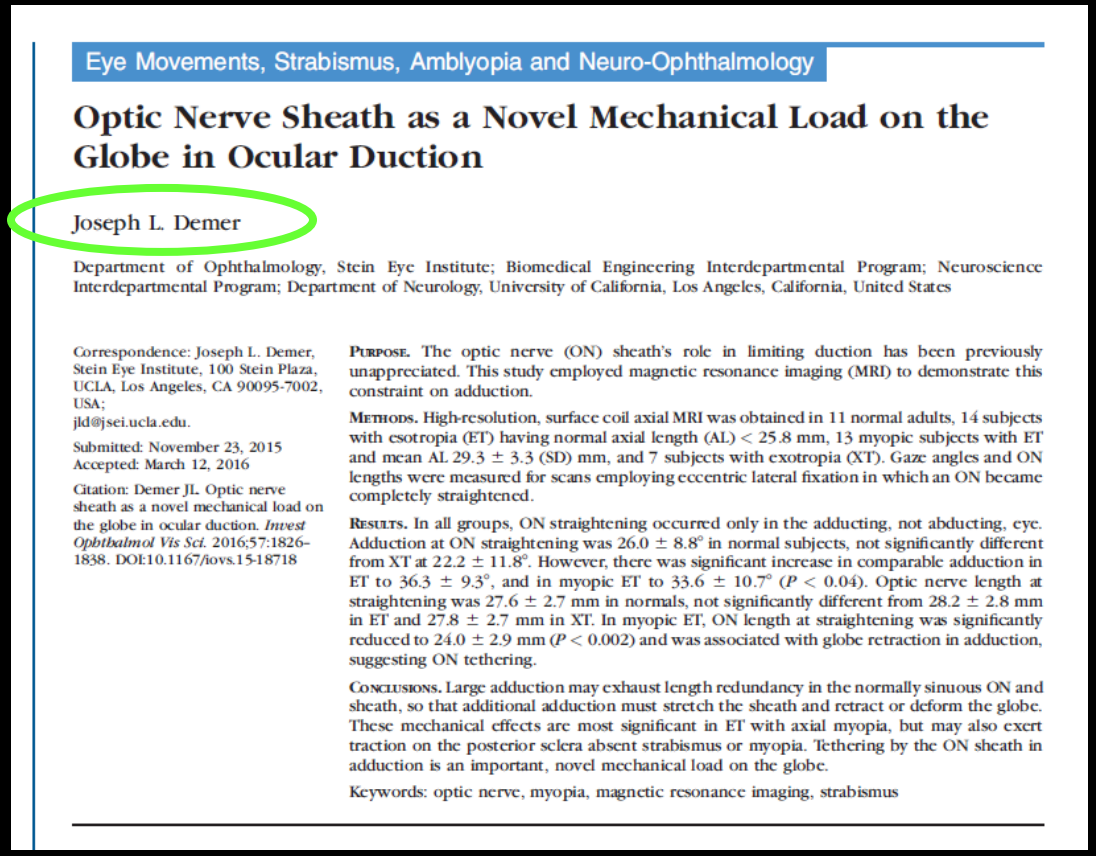

Eye Movements, Strabismus, Amblyopia and Neuro-Ophthalmology

Optic Nerve Sheath as a Novel Mechanical Load on the Globe in Ocular Duction

Joseph L. Demer

Department of Ophthalmology, Stein Eye Institute; Biomedical Engineering Interdepartmental Program; Neuroscience Interdepartmental Program; Department of Neurology, University of California, Los Angeles, California, United States

Correspondence: Joseph L. Demer, Stein Eye Institute, 100 Stein Plaza, UCLA, Los Angeles, CA 90095-7002, USA; jld@jsei.ucla.edu.

Submitted: November 23, 2015
Accepted: March 12, 2016

Citation: Demer JL. Optic nerve sheath as a novel mechanical load on the globe in ocular duction. *Invest Ophthalmol Vis Sci.* 2016;57:1826–1838. DOI:10.1167/iovs.15-18718

Purpose. The optic nerve (ON) sheath's role in limiting duction has been previously unappreciated. This study employed magnetic resonance imaging (MRI) to demonstrate this constraint on adduction.

Methods. High-resolution, surface coil axial MRI was obtained in 11 normal adults, 14 subjects with esotropia (ET) having normal axial length (AL) < 25.8 mm, 13 myopic subjects with ET and mean AL 29.3 ± 3.3 (SD) mm, and 7 subjects with exotropia (XT). Gaze angles and ON lengths were measured for scans employing eccentric lateral fixation in which an ON became completely straightened.

Results. In all groups, ON straightening occurred only in the adducting, not abducting, eye. Adduction at ON straightening was 26.0 ± 8.8° in normal subjects, not significantly different from XT at 22.2 ± 11.8°. However, there was significant increase in comparable adduction in ET to 36.3 ± 9.3°, and in myopic ET to 33.6 ± 10.7° ($P < 0.04$). Optic nerve length at straightening was 27.6 ± 2.7 mm in normals, not significantly different from 28.2 ± 2.8 mm in ET and 27.8 ± 2.7 mm in XT. In myopic ET, ON length at straightening was significantly reduced to 24.0 ± 2.9 mm ($P < 0.002$) and was associated with globe retraction in adduction, suggesting ON tethering.

Conclusions. Large adduction may exhaust length redundancy in the normally sinuous ON and sheath, so that additional adduction must stretch the sheath and retract or deform the globe. These mechanical effects are most significant in ET with axial myopia, but may also exert traction on the posterior sclera absent strabismus or myopia. Tethering by the ON sheath in adduction is an important, novel mechanical load on the globe.

Keywords: optic nerve, myopia, magnetic resonance imaging, strabismus

Demer. IOVS. 2016

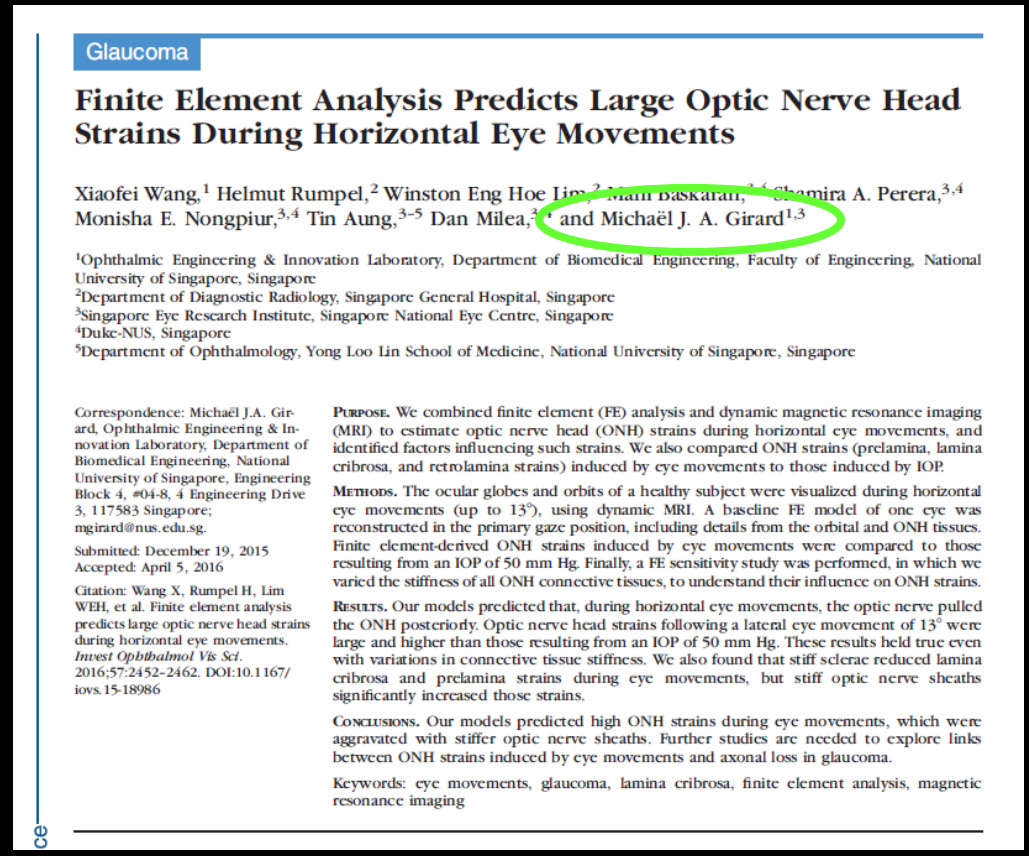

Glaucoma

Finite Element Analysis Predicts Large Optic Nerve Head Strains During Horizontal Eye Movements

Xiaofei Wang,[1] Helmut Rumpel,[2] Winston Eng Hoe Lim,[2] Mani Baskaran,[3,4] Shamira A. Perera,[3,4] Monisha E. Nongpiur,[3,4] Tin Aung,[3–5] Dan Milea,[3,4] and Michaël J. A. Girard[1,3]

[1]Ophthalmic Engineering & Innovation Laboratory, Department of Biomedical Engineering, Faculty of Engineering, National University of Singapore, Singapore
[2]Department of Diagnostic Radiology, Singapore General Hospital, Singapore
[3]Singapore Eye Research Institute, Singapore National Eye Centre, Singapore
[4]Duke-NUS, Singapore
[5]Department of Ophthalmology, Yong Loo Lin School of Medicine, National University of Singapore, Singapore

Correspondence: Michaël J.A. Girard, Ophthalmic Engineering & Innovation Laboratory, Department of Biomedical Engineering, National University of Singapore, Engineering Block 4, #04-8, 4 Engineering Drive 3, 117583 Singapore; mgirard@nus.edu.sg.

Submitted: December 19, 2015
Accepted: April 5, 2016

Citation: Wang X, Rumpel H, Lim WEH, et al. Finite element analysis predicts large optic nerve head strains during horizontal eye movements. *Invest Ophthalmol Vis Sci.* 2016;57:2452–2462. DOI:10.1167/iovs.15-18986

Purpose. We combined finite element (FE) analysis and dynamic magnetic resonance imaging (MRI) to estimate optic nerve head (ONH) strains during horizontal eye movements, and identified factors influencing such strains. We also compared ONH strains (prelamina, lamina cribrosa, and retrolamina strains) induced by eye movements to those induced by IOP.

Methods. The ocular globes and orbits of a healthy subject were visualized during horizontal eye movements (up to 13°), using dynamic MRI. A baseline FE model of one eye was reconstructed in the primary gaze position, including details from the orbital and ONH tissues. Finite element-derived ONH strains induced by eye movements were compared to those resulting from an IOP of 50 mm Hg. Finally, a FE sensitivity study was performed, in which we varied the stiffness of all ONH connective tissues, to understand their influence on ONH strains.

Results. Our models predicted that, during horizontal eye movements, the optic nerve pulled the ONH posteriorly. Optic nerve head strains following a lateral eye movement of 13° were large and higher than those resulting from an IOP of 50 mm Hg. These results held true even with variations in connective tissue stiffness. We also found that stiff sclerae reduced lamina cribrosa and prelamina strains during eye movements, but stiff optic nerve sheaths significantly increased those strains.

Conclusions. Our models predicted high ONH strains during eye movements, which were aggravated with stiffer optic nerve sheaths. Further studies are needed to explore links between ONH strains induced by eye movements and axonal loss in glaucoma.

Keywords: eye movements, glaucoma, lamina cribrosa, finite element analysis, magnetic resonance imaging

Wang, et al. IOVS. 2016

The Circumferential Collagen/Elastin Ring may be much more complicated than this

Appears Circumferential but may be Tangential (?)

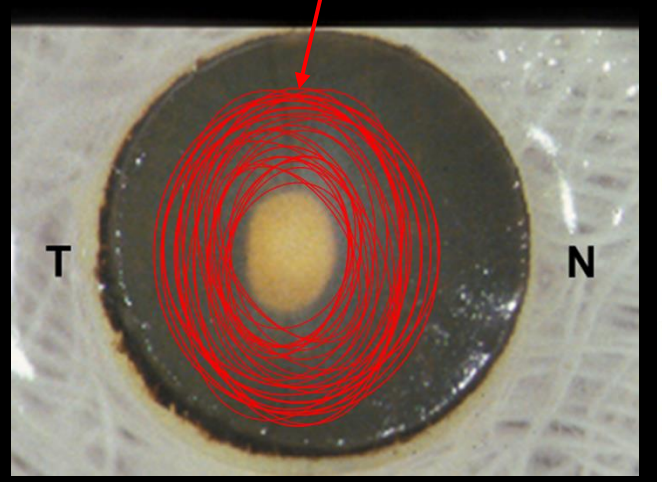

Acta Biomaterialia 79 (2018) 113–122

Contents lists available at ScienceDirect

Acta Biomaterialia

journal homepage: www.elsevier.com/locate/actabiomat

Full length article

Peripapillary sclera architecture revisited: A tangential fiber model and its biomechanical implications

Andrew P. Voorhees [a], Ning-Jiun Jan [a,b], Yi Hua [a], Bin Yang [c], Ian A. Sigal [a,b,c,*]

[a] Department of Ophthalmology, University of Pittsburgh, Pittsburgh, PA, USA
[b] Department of Bioengineering, University of Pittsburgh, Pittsburgh, PA, USA
[c] McGowan Institute for Regenerative Medicine, University of Pittsburgh, Pittsburgh, PA, USA

ARTICLE INFO

Article history:
Received 25 March 2018
Received in revised form 9 August 2018
Accepted 17 August 2018
Available online 21 August 2018

Keywords:
Biomechanics
Optic nerve head
Peripapillary sclera
Collagen architecture

ABSTRACT

The collagen fiber architecture of the peripapillary sclera (PPS), which surrounds the scleral canal, is a critical factor in determining the mechanical response of the optic nerve head (ONH) to variations in intraocular pressure (IOP). Experimental and clinical evidence point to IOP-induced deformations within the scleral canal as important contributing factors of glaucomatous neural tissue damage and consequent vision loss. Hence, it is imperative to understand PPS architecture and biomechanics. Current consensus is that the fibers of the PPS form a closed ring around the canal to support the delicate neural tissues within. We propose an alternative fiber architecture for the PPS, in which the scleral canal is supported primarily by long-running fibers oriented tangentially to the canal. We present evidence that this tangential model is consistent with histological observations in multiple species, and with quantitative measurements of fiber orientation obtained from small angle light scattering and wide-angle X-ray scattering. Using finite element models, we investigated the biomechanical implications of a tangential fiber PPS architecture. We found that the tangential arrangement of fibers afforded better mechanical support to the tissues within the scleral canal as compared to a simple circumferential ring of fibers or a combination of fibers oriented radially and circumferentially. We also found that subtle variations from a tangential orientation could reproduce clinically observed ONH behavior which has yet to be explained using current theories of PPS architecture and simulation, namely, the contraction of the scleral canal under elevated IOP.

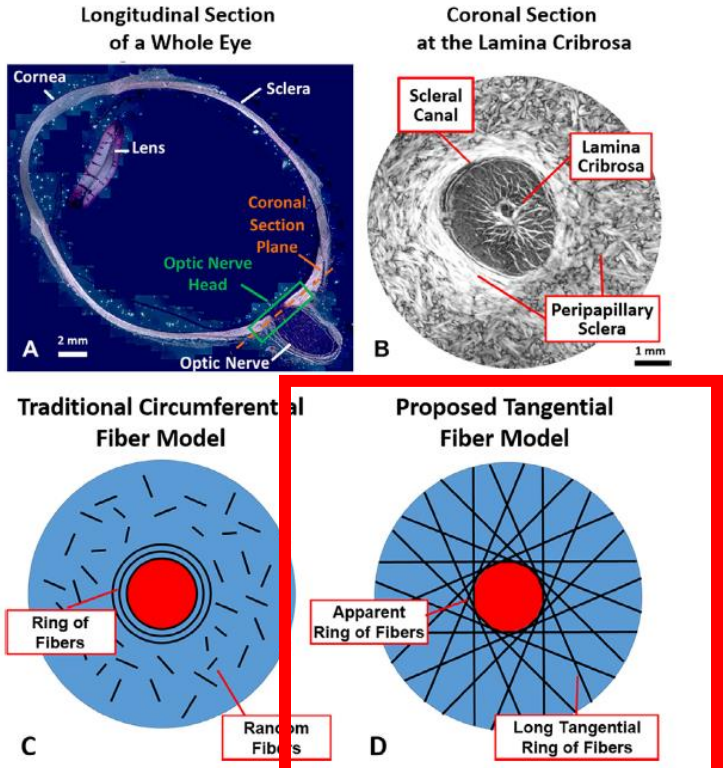

Fig. 1. The anatomy of the eye and models of fiber orientation. (A) A longitudinal cross-section of a whole eye, with the location of the optic nerve head (ONH) shown. (B) A coronal section of the ONH showing the peripapillary sclera (PPS) and lamina cribrosa located within the scleral canal. (C) The current consensus opinion as to the organization of collagen fibers in the PPS is a closed ring of fibers surrounded by short randomly oriented fibers. (D) Our proposed organization of fibers is a collection of long fibers oriented tangentially to the canal edge, giving the appearance of a closed ring of fibers around the canal. A&B Adapted from Voorhees et al, 2017.

Appears Circumferential but may be Tangential (?)

Circumferential Collagen/Elastin Ring importantly contributes to the "laminar/scleral" dynamic

Underlies the
"Laminar/Scleral Dynamic"

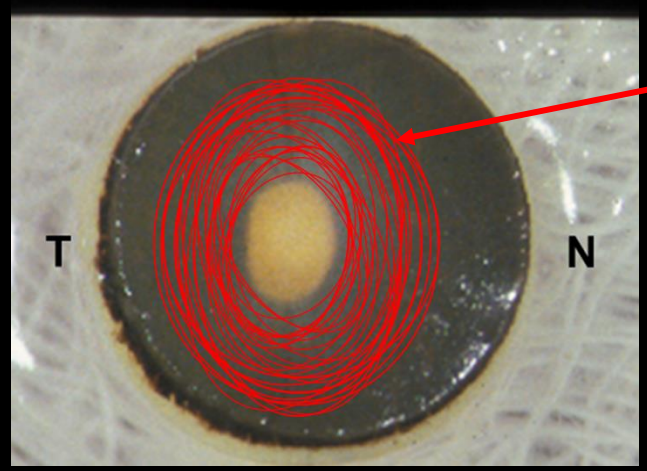

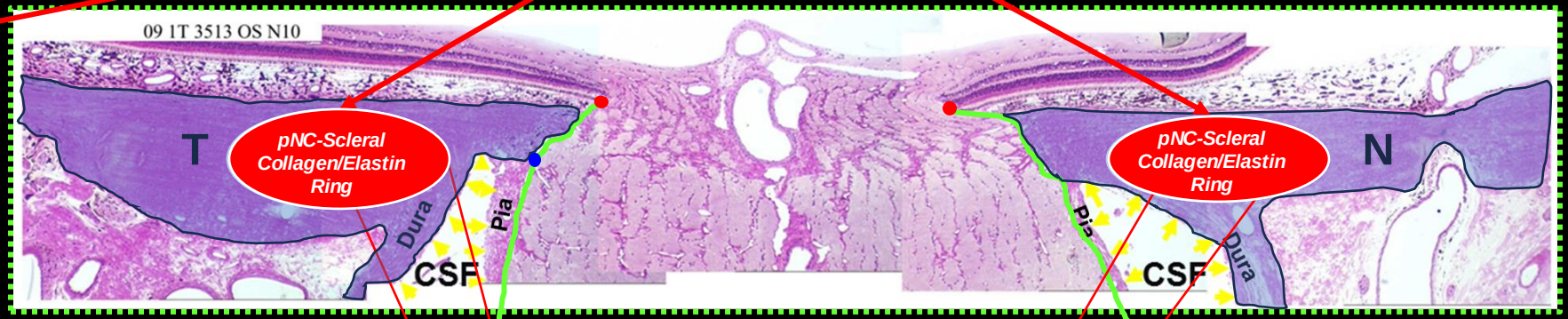

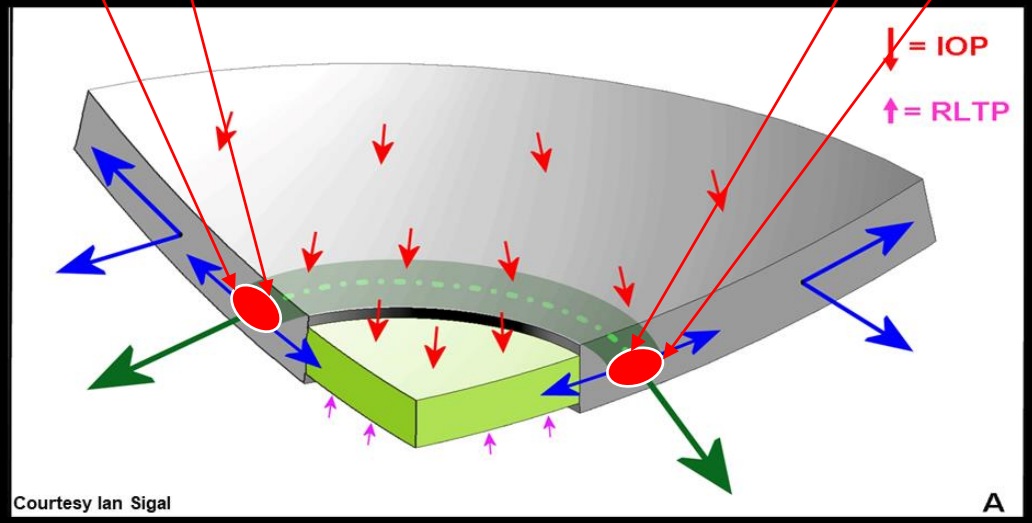

Circumferential Collagen/Elastin Ring likely underlies the "laminar/scleral" dynamic

If you elevate IOP it pushes out on the lamina but it also expands the scleral shell creating strain in the sclera that pulls the lamina taut.

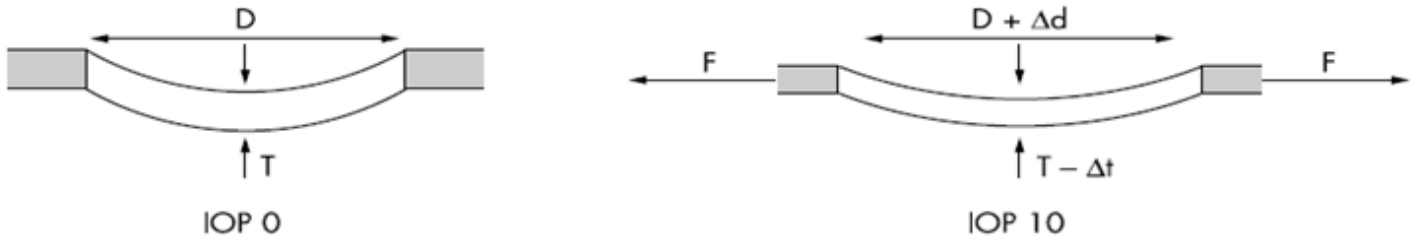

Figure 4 Schematic representation of the lamina cribrosa and scleral canal in a non-pressurised (IOP 0) and pressurised (IOP 10) eye. Left: Thickness (T) of the lamina cribrosa and diameter (D) of the scleral canal opening in an unpressurised (IOP 0) eye. Right: Pressure within the globe generates an expansion of the scleral shell which, in turn, generates (and is resisted by) tensile forces within the sclera. These forces (F) act on the scleral canal wall, causing the scleral canal opening to expand (Δd), which in turn stretches the lamina within the canal. Thus, the lamina is taut (more anteriorly positioned) and thinned (Δt) in the IOP 10 eye, compared with the IOP 0 eye.

Bellezza et al. Br J Ophthalmol 2003;87:1284–1290

Circumferential Collagen/Elastin Ring likely underlies the "laminar/scleral" dynamic

Human Cadaver Eye Finite Element Models

Factors Influencing Optic Nerve Head Biomechanics

Ian A. Sigal,[1,2] John G. Flanagan,[3,4] and C. Ross Ethier[1,2,3]

TABLE 3. Rankings of Input Factors as Determined by Sensitivity Analysis

Input Factor	Outcome measure group: Strain: All	Strain: Peak	Strain: Mean	Stress: All	Stress: Peak	Stress: Mean	Geometry: All	Geometry: Non-observable	Geometry: Observable	Mean
Eye Radius	2	2	4	2	2	4	3	2	2	2.6
Scleral Canal Thickness	11	6	8	7	10	11	11	10	12	9.6
Lamina Thickness	14	12	11	12	14	13	14	7	17	12.7
Retina Thickness Shell	21	17	19	18	18	19	18	21	19	18.9
Sclera Thickness Shell	5	5	6	5	8	8	8	8	4	6.3
Lamina Width / Radius	6	9	5	6	11	10	9	6	3	7.2
Pia Thickness	17	14	15	15	16	17	17	18	21	16.7
Lamina Depth below rim	10	10	12	11	12	14	13	5	8	10.6
Cup to Disc ratio	18	19	20	20	19	20	20	17	7	17.8
Angle Scleral Canal Wall	15	15	14	14	15	15	15	13	14	14.4
Angle Optic Nerve	16	16	13	13	17	16	16	19	20	16.2
Sclera Thin Factor	13	8	10	9	9	12	12	12	15	11.1
Ram Height	20	21	18	19	20	18	19	20	18	19.2
Cup Depth	19	20	21	21	21	21	21	16	9	18.8
IOP	4	3	2	3	4	3	4	4	5	3.6
Ret Poisson ratio	12	18	17	17	13	9	10	9	6	12.3
Modulus Pia	7	7	9	8	5	5	5	14	16	8.4
Modulus Lamina	3	4	3	4	3	2	2	3	10	3.8
Modulus Sclera	1	1	1	1	1	1	1	1	1	1.0
Modulus Retina	9	13	16	16	7	7	7	11	11	10.8
Modulus Optic Nerve	8	11	7	10	6	6	6	15	13	9.1

2

1

1

A rank of 1 means that the input factor had the largest total influence (see text for definition of total influence), 2 means that the input factor had the second-largest total influence, and so forth. Cells are shaded green when the rank is within the top five, and orange when the rank is within the bottom five. Factor ranking depends on the set of outcome measures considered. Columns 2–10 represent different sets of outcome measures. Column 2 considers all outcome measures. The ranks in column 3 were computed using peak strains within all tissues as outcome measures. Column 4 contains similar rankings when considering mean strains. Column 5 considers both peak and mean strains. Columns 6–8 are similar, with stress replacing strain. Columns 9 and 10 consider only outcome measures related to model geometry (see text for definitions of groups). The numbers in column 10 are the mean rank averaged over all outcome measure sets (i.e., over columns 3–10). All ranks in this table were computed using input factor full ranges.

Sigal, et al., IOVS 2005

Sigal, et al, IOVS 2005

Monkeys post-mortem 3D histomorphometry

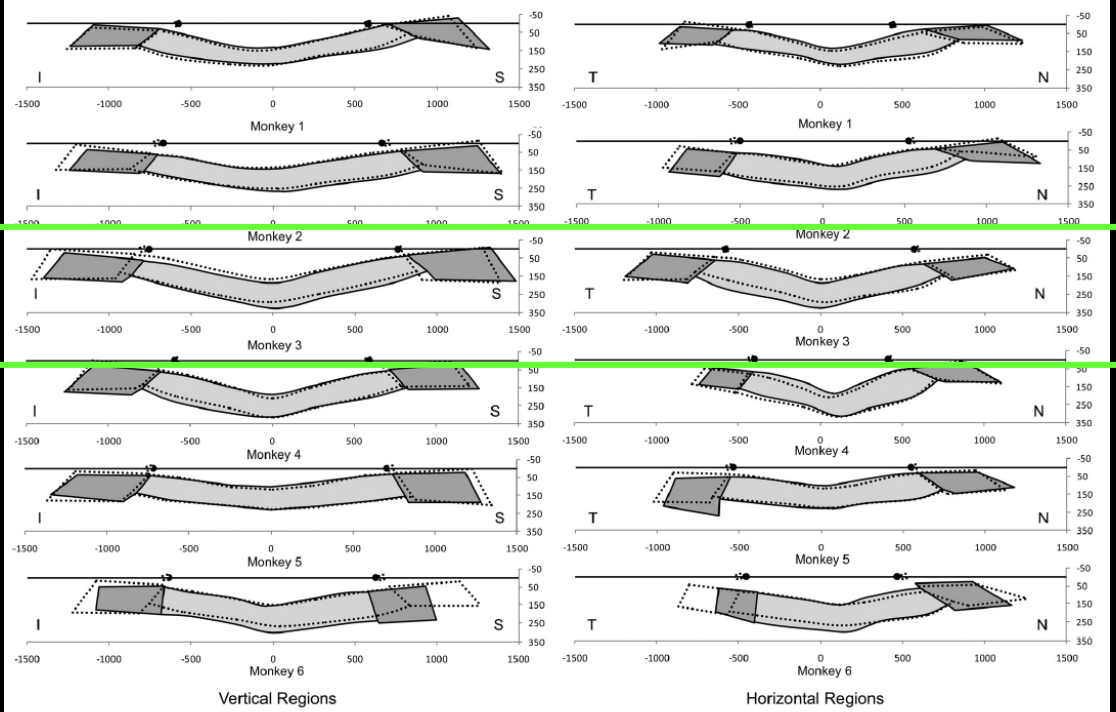

FIGURE 5. Schematic representation of the vertical and horizontal regional deformation data for the low (*solid colors*)- and high (*dotted lines*)-IOP ONHs of each monkey. Mean data from the superior and inferior (*left*) and nasal and temporal (*right*). Regions of both eyes of each animal are schematically overlaid as central vertical (*left*) and horizontal (*right*) sections. The net regional canal expansion can now be seen in monkeys 2, 3, 5, and 6 (although in monkey 1, there was contraction of the superior canal). Small overall posterior bowing of the peripapillary sclera was present in most animals. Small anterior and posterior deformations of the lamina cribrosa accompanied by laminar thinning were also present in most high-IOP eyes. The canal, laminar, and peripapillary sclera deformations were not symmetrical to the center of the NCO in some animals because of the true asymmetric deformation and asymmetric neural canal architecture within the two eyes of an animal. Although the recorded intereye differences are accurate, they are a likely combination of true connective tissue deformation plus some reference-plane-induced artifacts in the subset of high-IOP eyes, in which true connective tissue deformation led to shifts and/or tilts in the position of the reference plane relative to the structures being measured. All data are plotted in right eye configuration.

Yang et al. IOVS. 2009

Outline

- Professor Hans Goldmann
- Disclosures and Acknowledgements
- Creating 3D Optic Nerve Head Anatomy and Morphology
- The Optic Nerve Head in Glaucoma
- What Defines a Glaucomatous Optic Neuropathy?
- FoBMO 3D Histomorphometric Structural Phenotyping in Monkey Glaucoma
- FoBMO 3D OCT Structural Phenotyping in Monkey and Human Glaucoma
- FoBMO qIHC and 3D SBEM in Monkey EG
- Summary / Implications
- A Final Acknowledgement

The optic nerve head in Glaucoma

A primary site of injury to the RGC axon in glaucoma – by multiple mechanisms – *at all all levels of IOP*

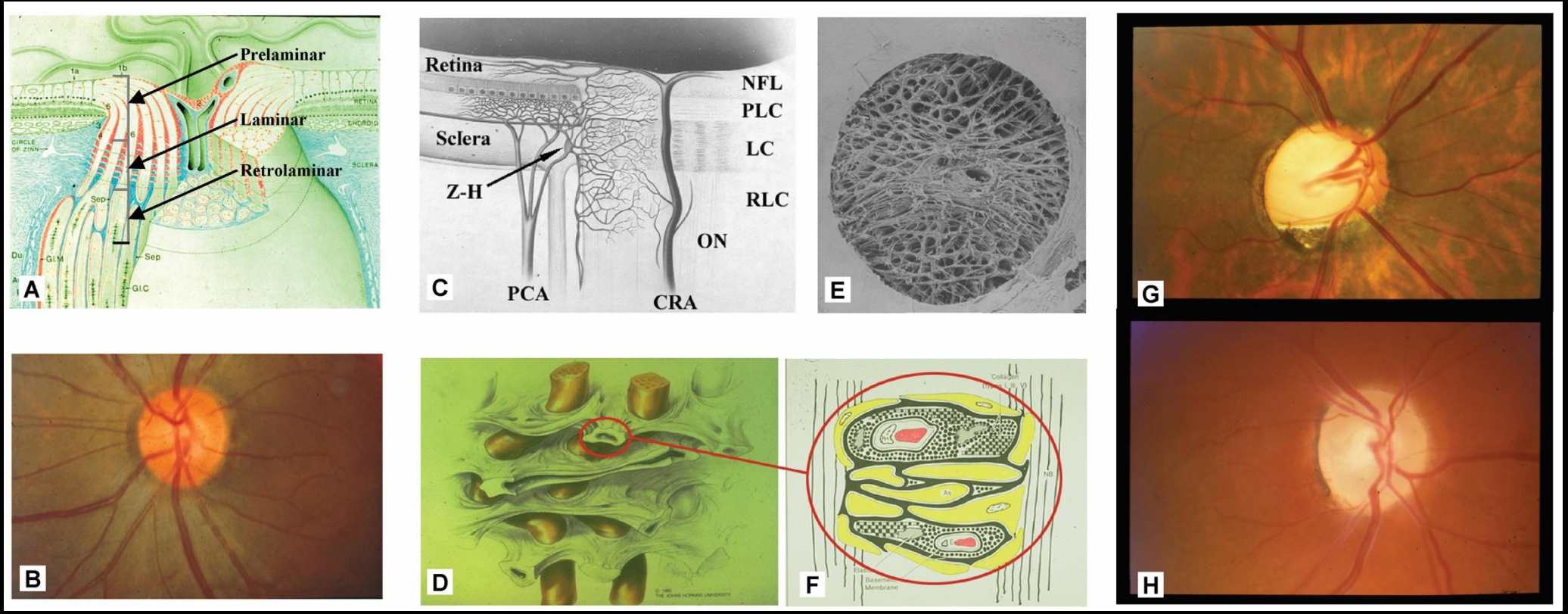

(A) Reprinted with permission from Arch Ophthalmol 1969;82:506-530. Copyright © 1969 American Medical Association. All rights reserved.36 (B) Reprinted with permission from Journal of glaucoma By Lippincott Williams & Wilkins, J Glaucoma 2008;17:318-328.37 (C) reprinted with permission from Dr G. A. Cioffi. In: The Glaucomas. Mosby: Basic Sciences; 1996:177–197.38 (D) Reprinted with permission from Optic Nerve in Glaucoma. Amsterdam: Kugler Publications; 1995:15–36.39 (E) Reprinted with permission from Arch Ophthalmol 1990;108:51–57. Copyright © 1990 American Medical Association. All rights reserved.40 (F) Reprinted with permission from Arch Ophthalmol 1989;107:123–129. Copyright © 1989 American Medical Association. All rights reserved.41 (G, H) Reprinted with permission from Journal of glaucoma By Lippincott Williams & Wilkins, J Glaucoma 2008;17:318-328.37

The optic nerve head in Glaucoma

A primary site of injury to the RGC axon in glaucoma – by multiple mechanisms – *at all all levels of IOP*

A complex and challenging biomechanical environment - *at all levels of IOP*

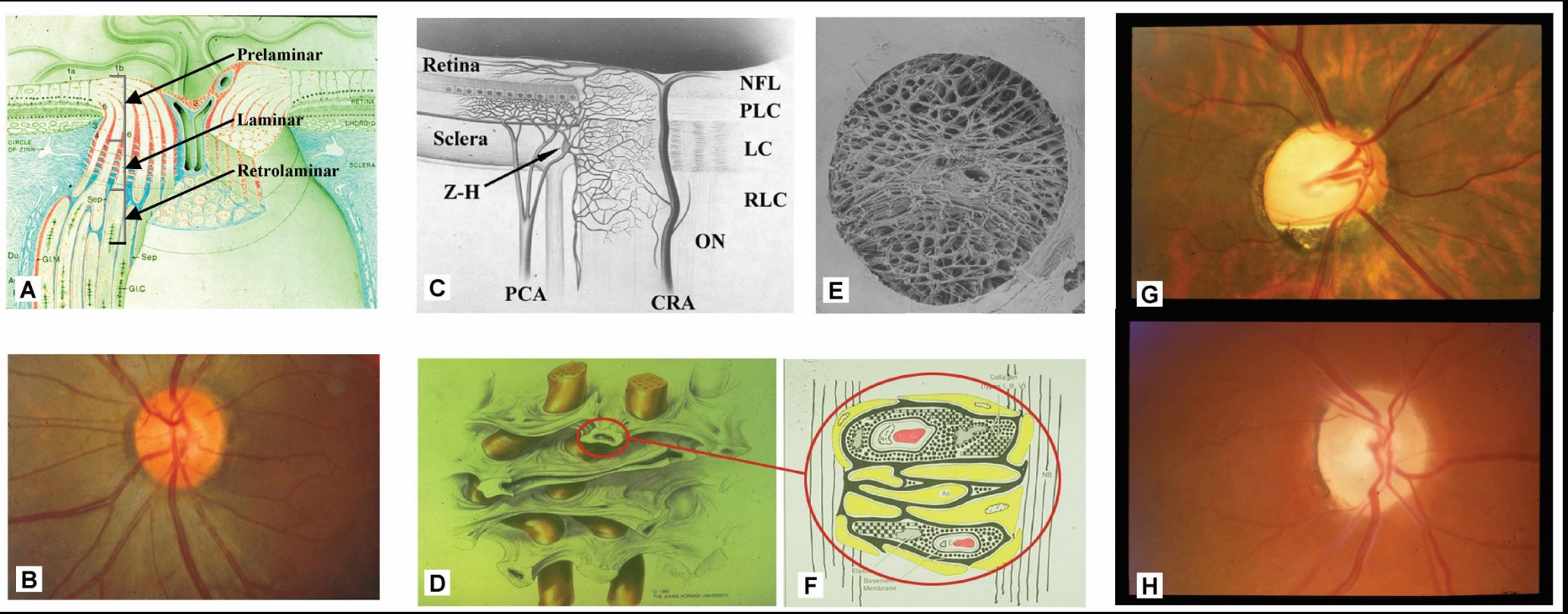

(A) Reprinted with permission from Arch Ophthalmol 1969;82:506-530. Copyright © 1969 American Medical Association. All rights reserved.36 (B) Reprinted with permission from Journal of glaucoma By Lippincott Williams & Wilkins, J Glaucoma 2008;17:318-328.37 (C) reprinted with permission from Dr G. A. Cioffi. In: The Glaucomas. Mosby: Basic Sciences; 1996:177–197.38 (D) Reprinted with permission from Optic Nerve in Glaucoma. Amsterdam: Kugler Publications; 1995:15–36.39 (E) Reprinted with permission from Arch Ophthalmol 1990;108:51–57. Copyright © 1990 American Medical Association. All rights reserved.40 (F) Reprinted with permission from Arch Ophthalmol 1989;107:123–129. Copyright © 1989 American Medical Association. All rights reserved.41 (G, H) Reprinted with permission from Journal of glaucoma By Lippincott Williams & Wilkins, J Glaucoma 2008;17:318-328.37

As demonstrated by a series of important axon transport studies

Optic Nerve Head
(Entire Dynamic Structure)

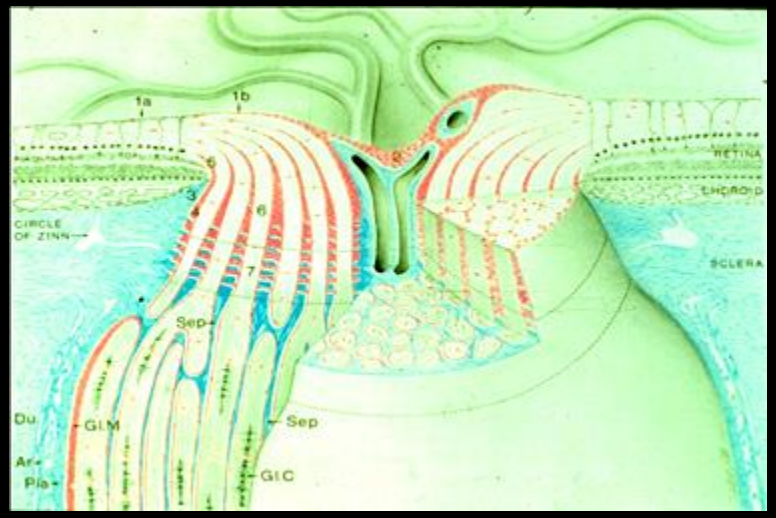

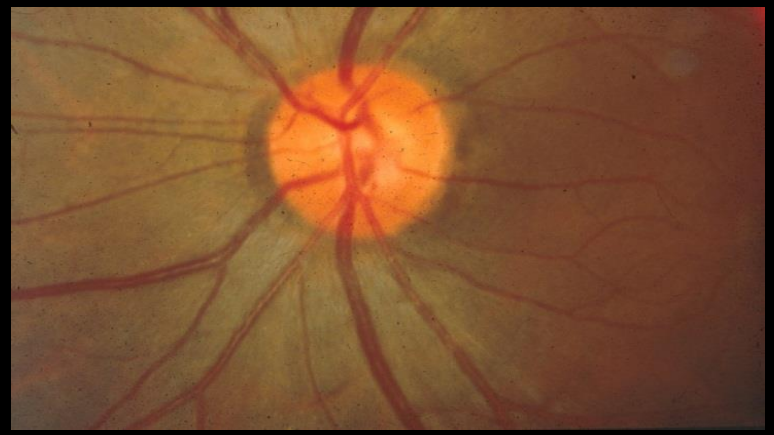

Optic Disc
(Clinically Visible Surface)

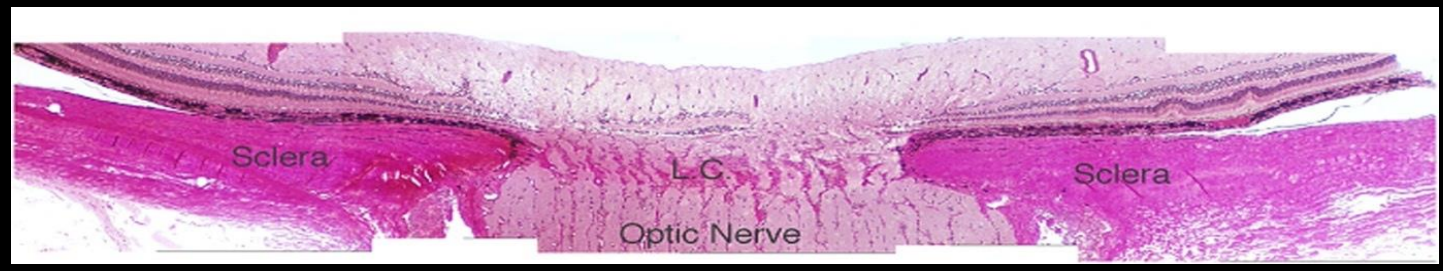

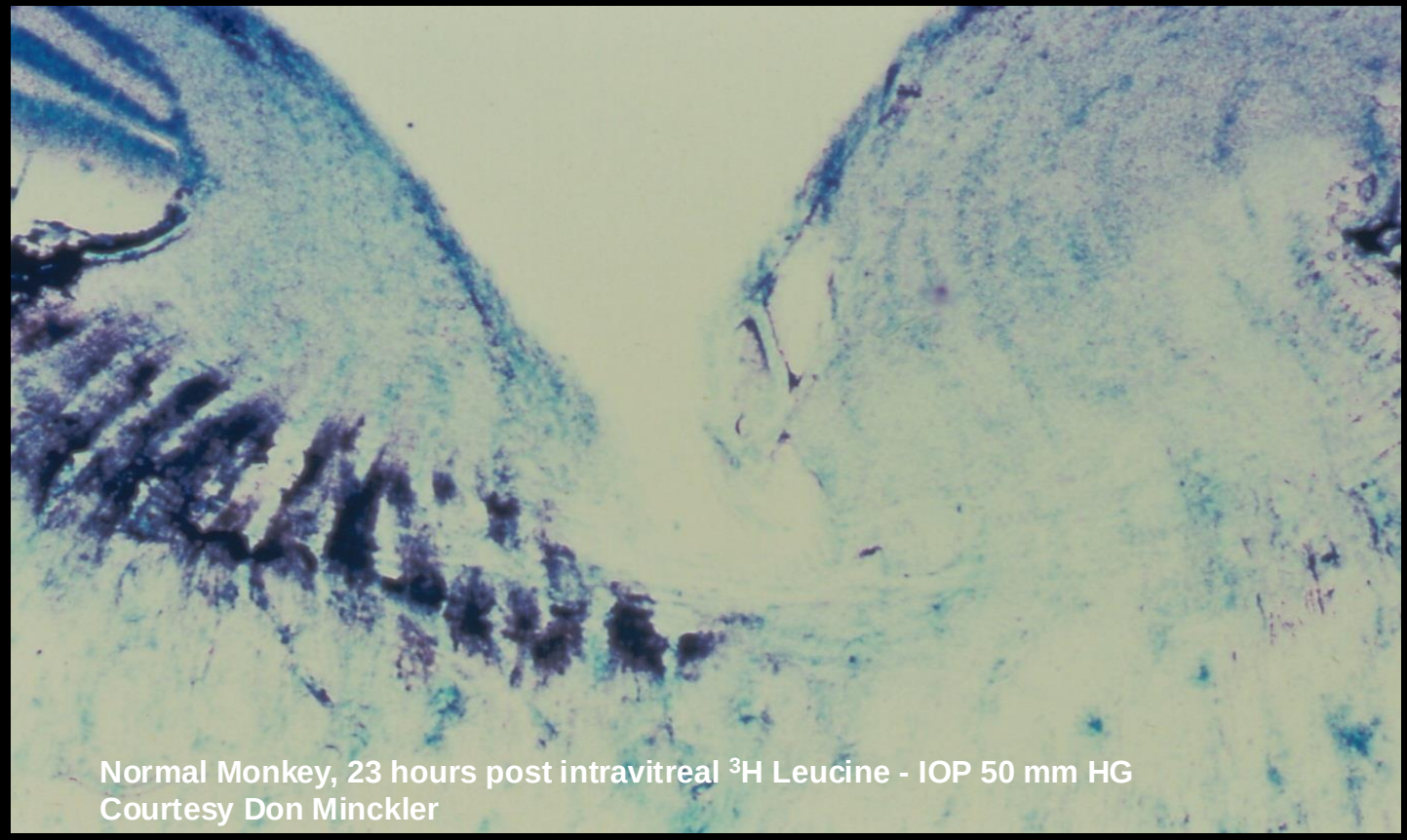

Normal Monkey, 23 hours post intravitreal ^{3}H Leucine - IOP 50 mm HG
Courtesy Don Minckler

As demonstrated by a series of important axon transport studies

Optic Nerve Head
(Entire Dynamic Structure)

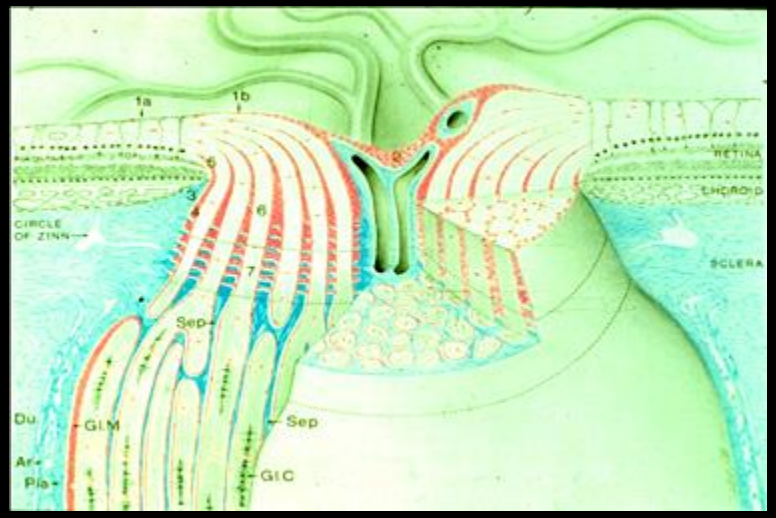

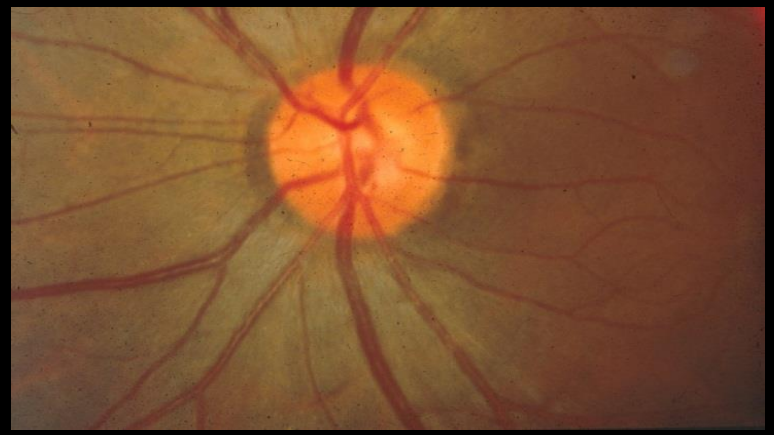

Optic Disc
(Clinically Visible Surface)

Normal IOP (Physiologic Blockade)

As demonstrated by a series of important axon transport studies

Optic Nerve Head
(Entire Dynamic Structure)

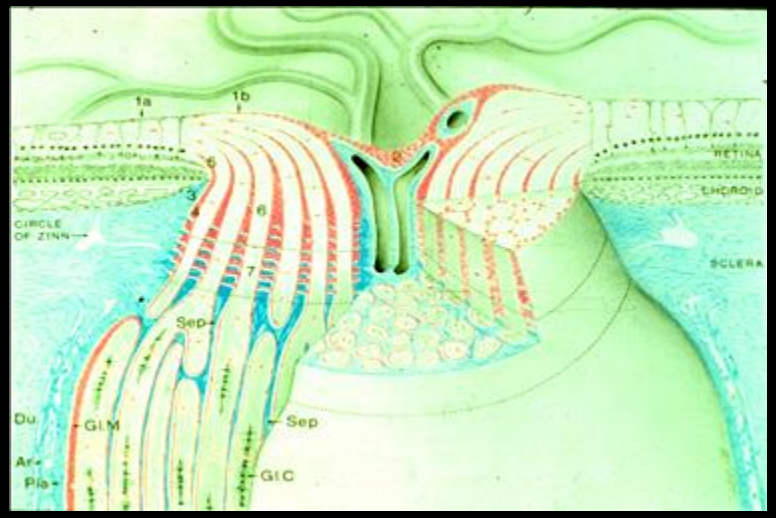

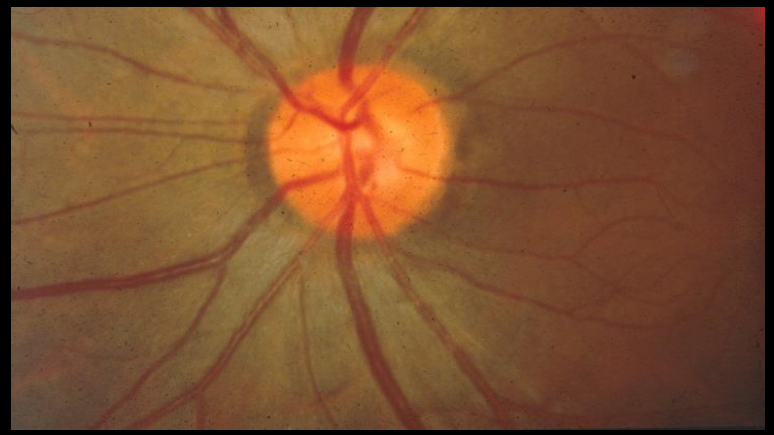

Optic Disc
(Clinically Visible Surface)

Normal IOP (Physiologic Blockade)

Acute and chronic IOP elevation

As demonstrated by a series of important axon transport studies

Optic Nerve Head
(Entire Dynamic Structure)

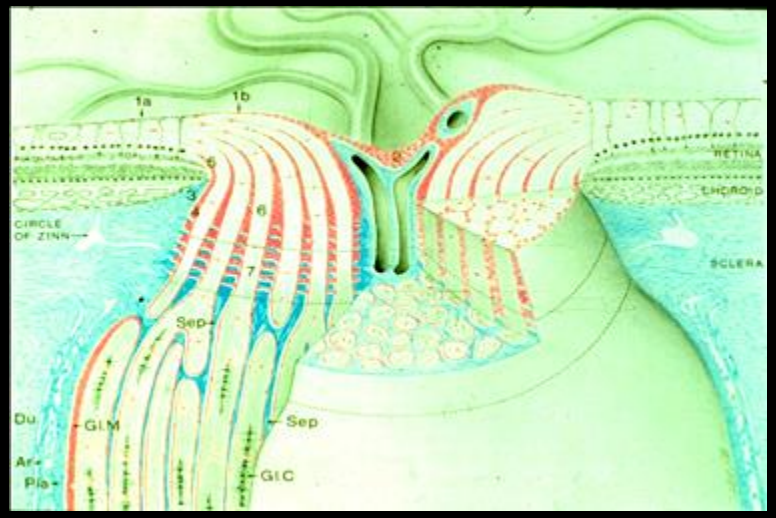

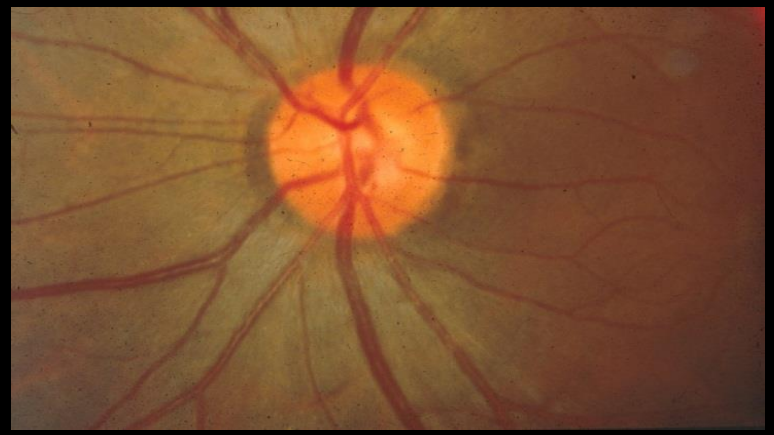

Optic Disc
(Clinically Visible Surface)

Normal IOP (Physiologic Blockade)

Acute and chronic IOP elevation

Mouse, rat, pig, dog, cat, monkey, human

As demonstrated by a series of important axon transport studies

Optic Nerve Head
(Entire Dynamic Structure)

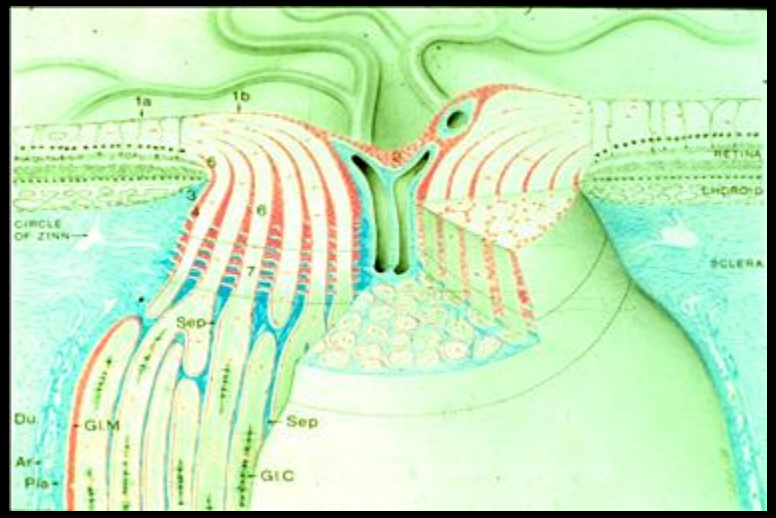

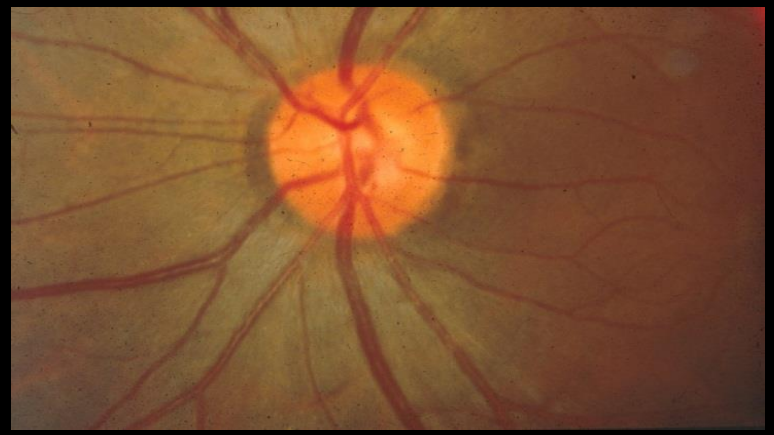

Optic Disc
(Clinically Visible Surface)

Normal IOP (Physiologic Blockade)

Acute and chronic IOP elevation

Mouse, rat, pig, dog, cat, monkey, human

Multiple Investigators – Important Studies

- **Minckler and Bunt**
- **Anderson**
- **Quigley**
- **Howell, John, Jakobs, Marsh-Armstrong, Calkins**
- **Morrison and Johnson**
- **James Morgan**
- **Bill Morgan**
- **many others**

But what about the RGC soma / Peripheral RGC Synapse???

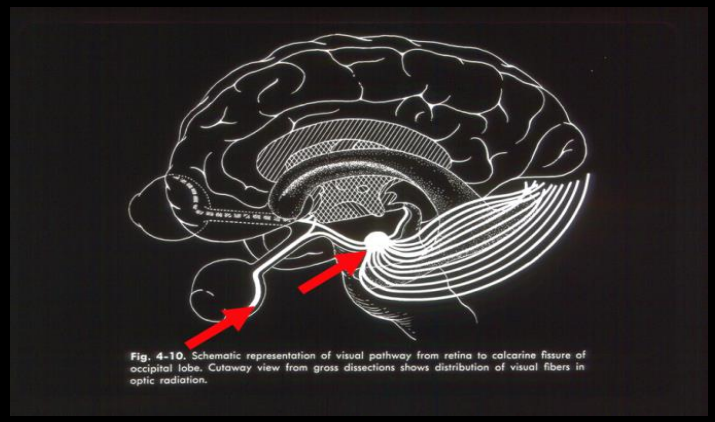

Lateral Geniculate (LGN) / Superior Colliculus (SC)

- **Yucel /Gupta – LGN changes in monkey/human glaucoma**
- **Quigley – preferential layer change in LGN**
- **Calkins – pre-synaptic pruning precedes ONH change - mice**

Retinal Ganglion Cell (RGC) and non RGC Retina

- **Weber – RGC Dendritic Shrinkage**
- **Cordeiro – Prevent RGC Dendritic shrinkage**
- **Leung – In vivo Imaging Dendritic shrinkage**

But what about the RGC soma / Peripheral RGC Synapse???

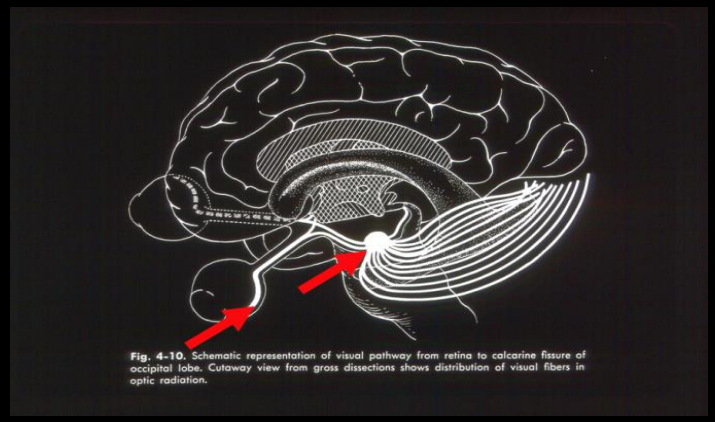

Lateral Geniculate (LGN) / Superior Colliculus (SC)

- **Yucel /Gupta – LGN changes in monkey/human glaucoma**
- **Quigley – preferential layer change in LGN**
- **Calkins – pre-synaptic pruning precedes ONH change - mice**

Retinal Ganglion Cell (RGC) and non RGC Retina

- **Weber – RGC Dendritic Shrinkage**
- **Cordeiro – Prevent RGC Dendritic shrinkage**
- **Leung – In vivo Imaging Dendritic shrinkage**

Many studies report important pathophysiologies within both tissues that may precede or coincide with ONH change.

But what about the RGC soma / Peripheral RGC Synapse???

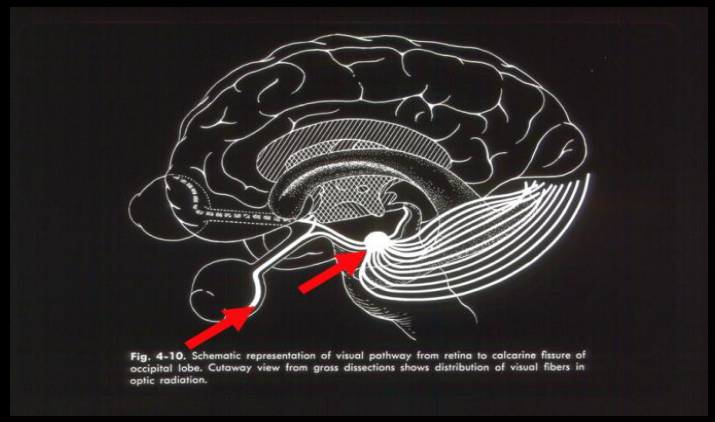

Lateral Geniculate (LGN) / Superior Colliculus (SC)

- **Yucel /Gupta – LGN changes in monkey/human glaucoma**
- **Quigley – preferential layer change in LGN**
- **Calkins – pre-synaptic pruning precedes ONH change - mice**

Retinal Ganglion Cell (RGC) and non RGC Retina

- **Weber – RGC Dendritic Shrinkage**
- **Cordeiro – Prevent RGC Dendritic shrinkage**
- **Leung – In vivo Imaging Dendritic shrinkage**

From a Biomechanical Standpoint

The RGC soma, the LGN and SC are *POTENTIAL* SITES OF IMPORTANT, TREATABLE SOMAL/AXONAL PATHOPHYSIOLOGY BUT THEY ARE *NOT* THE CAUSE OF ONH PATHOPHYSIOLOGY

But what about the RGC soma / Peripheral RGC Synapse???

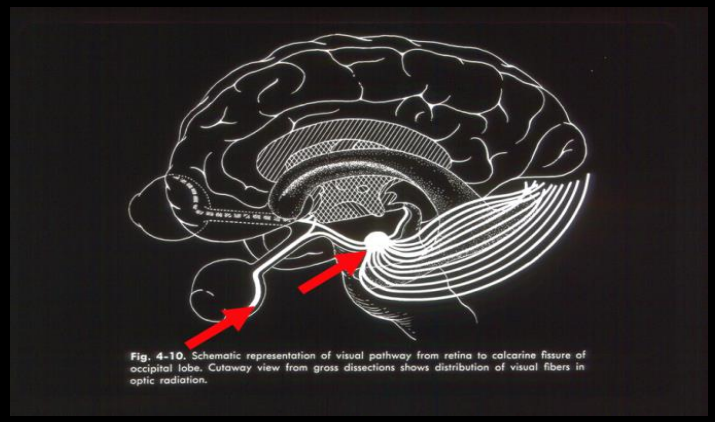

Lateral Geniculate (LGN) / Superior Colliculus (SC)

- **Yucel /Gupta – LGN changes in monkey/human glaucoma**
- **Quigley – preferential layer change in LGN**
- **Calkins – pre-synaptic pruning precedes ONH change - mice**

Retinal Ganglion Cell (RGC) and non RGC Retina

- **Weber – RGC Dendritic Shrinkage**
- **Cordeiro – Prevent RGC Dendritic shrinkage**
- **Leung – In vivo Imaging Dendritic shrinkage**

No primary experimental insult to the RGC, LGN or SC has been shown to generate a "glaucomatous" optic neuropathy.

But what about the RGC soma / Peripheral RGC Synapse???

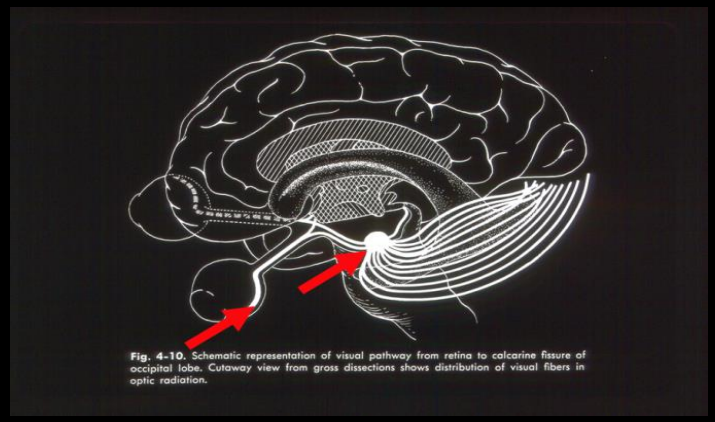

Lateral Geniculate (LGN) / Superior Colliculus (SC)

- **Yucel /Gupta – LGN changes in monkey/human glaucoma**
- **Quigley – preferential layer change in LGN**
- **Calkins – pre-synaptic pruning precedes ONH change - mice**

Retinal Ganglion Cell (RGC) and non RGC Retina

- **Weber – RGC Dendritic Shrinkage**
- **Cordeiro – Prevent RGC Dendritic shrinkage**
- **Leung – In vivo Imaging Dendritic shrinkage**

More Specifically –

No primary experimental insult to any of these sites has ever created "glaucomatous" "cupping" of the ONH.

Outline

- Professor Hans Goldmann
- Disclosures and Acknowledgements
- Creating 3D Optic Nerve Head Anatomy and Morphology
- The Optic Nerve Head in Glaucoma
- What Defines a Glaucomatous Optic Neuropathy?
- FoBMO 3D Histomorphometric Structural Phenotyping in Monkey Glaucoma
- FoBMO 3D OCT Structural Phenotyping in Monkey and Human Glaucoma
- FoBMO qIHC and 3D SBEM in Monkey EG
- Summary / Implications
- A Final Acknowledgement

So what defines a glaucomatous optic neuropathy?

How Optic Nerve Head Biomechanics has Clarified the Defining Pathophysiology and OCT Structural Phenotype of Human Glaucoma

The Goldmann Lecture

2024 Glaucoma Research Society Meeting
Siam Reap, Cambodia

November 15, 2024

…and how has ONH Biomechanics clarified it ???

Claude Burgoyne, MD
Emeritus Van Buskirk Chair in Ophthalmic Research
Past-Director, Optic Nerve Head Research Laboratory
Legacy Devers Eye Institute
Portland, OR
cfburgoyne@gmail.org

"Glaucomatous" cupping is a defining clinical feature of a glaucomatous optic neuropathy

1982

1997

1999

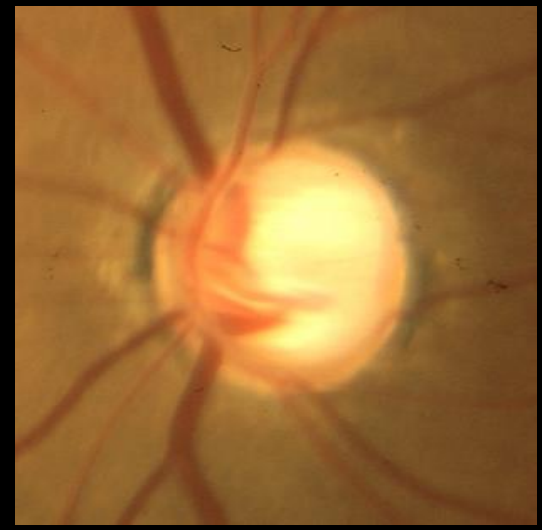

2001

"Glaucomatous" cupping is a defining clinical feature of a glaucomatous optic neuropathy

But it is *NOT* the pathophysiology itself!!!!

1982

1997

1999

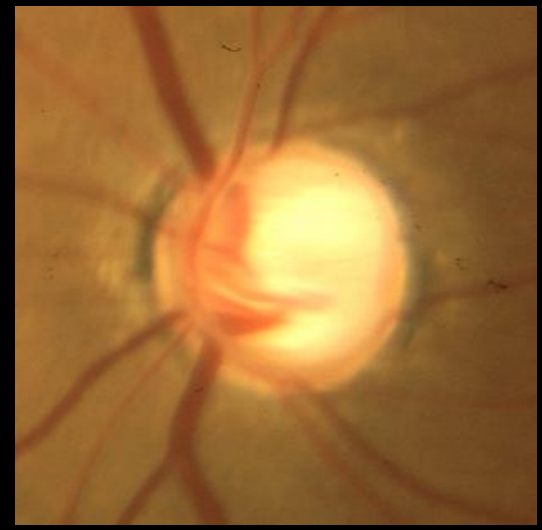

2001

"Glaucomatous" cupping is a defining clinical feature of a glaucomatous optic neuropathy

But it is *NOT* the pathophysiology itself!!!!

1982

1997

1999

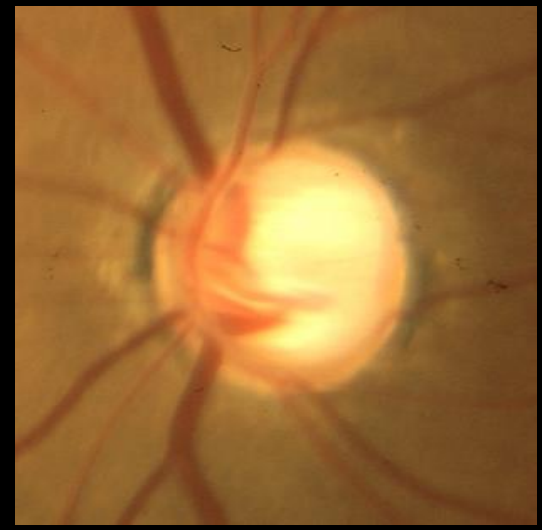

2001

It is a clinical manifestation of the defining pathophysiology

In the same way -the clinical patterns of RGC axon bundle damage and visual field loss are also clinical manifestations of the defining pathophysiology

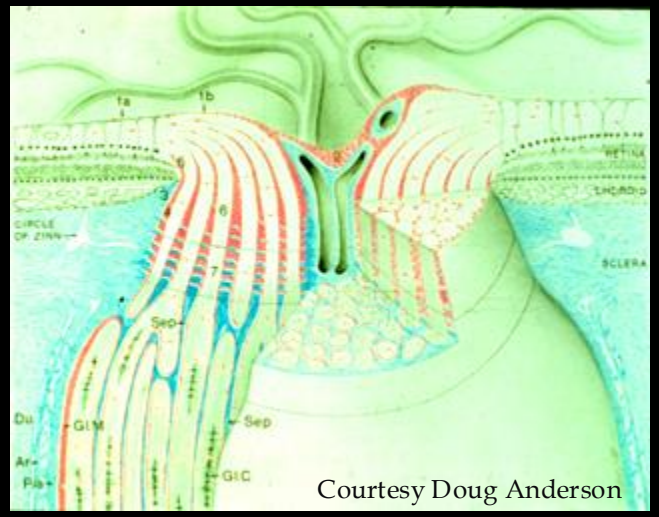

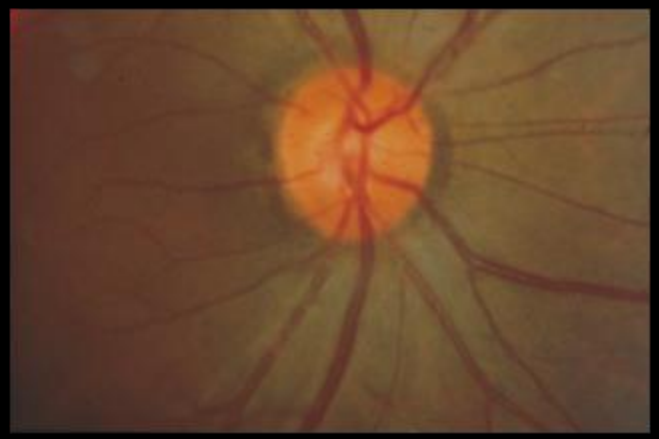

Optic Disc
(Clinically Visible Surface)

1997

2001

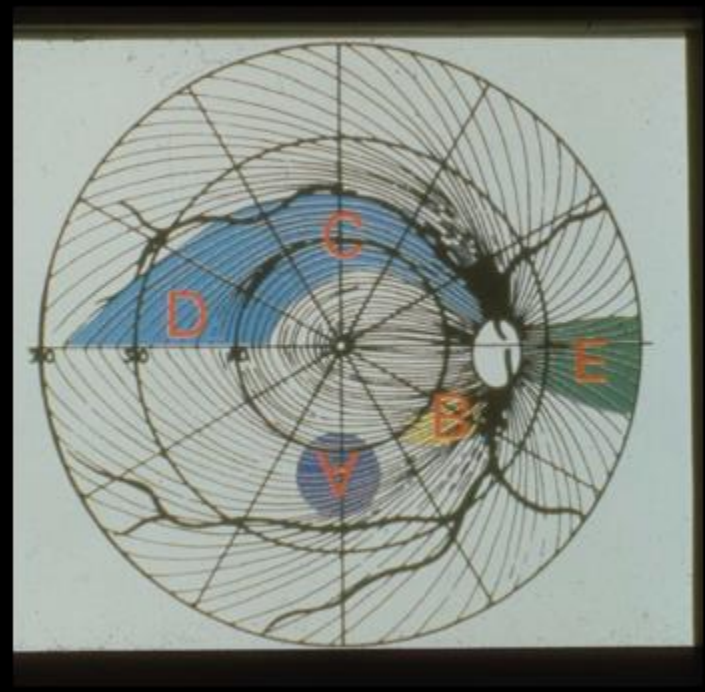

Not the pathophysiology itself!!!!

A Deliberately Controversial Premise

It's the *optic nerve head connective tissues/cells* not the RGC soma/axons that define both the clinical appearance (cupping) and behavior (pattern of RGC axon/visual field loss) in a glaucomatous optic neuropathy.

ONH Biomechanics clarifying contribution to this Discussion

Altered ONH connective tissue mechanobiology **is the defining pathophysiology of a glaucomatous optic neuropathy at whatever level of IOP it occurs.**

Mechanobiology – a definition

"Mechanobiology" links cellular and tissue behavior to the surrounding biomechanical environment they directly experience

ONH Mechanobiology in Glaucoma is Unique

While ONH connective tissue mechanobiology (itself) may be altered by all forms of optic neuropathy in which the RGC somas and or axons are damaged primarily……..

ONH Mechanobiology in Glaucoma is Unique

While ONH connective tissue mechanobiology (itself) may be altered by all forms of optic neuropathy in which the RGC somas and or axons are damaged primarily……

To date no form of primary insult to the RGC soma or axons produces a "glaucomatous" form of connective tissue deformation / remodeling / repair and/or failure.

ONH Mechanobiology in Glaucoma is Unique

While ONH connective tissue mechanobiology (itself) may be altered by all forms of optic neuropathy in which the RGC somas and or axons are damaged primarily……

To date no form of primary insult to the RGC soma or axons produces a "glaucomatous" form of connective tissue deformation / remodeling / repair and/or failure.

NONE

ONH Mechanobiology in Glaucoma is Unique

While ONH connective tissue mechanobiology (itself) may be altered by all forms of optic neuropathy in which the RGC somas and or axons are damaged primarily……

To date no form of primary insult to the RGC soma or axons produces a *"glaucomatous" form of connective tissue deformation / remodeling / repair and/or failure*.

I will talk more about this in a moment

Three Monkey Experimental Optic Neuropathy Models that do not create "Glaucomatous" Cupping because the ONH connective tissues do not deform / remodel / repair or fail.

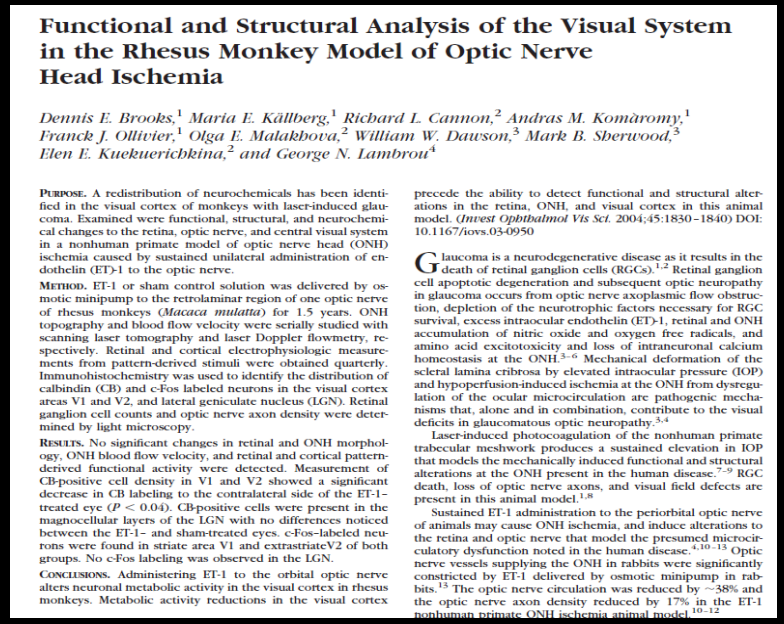

Functional and Structural Analysis of the Visual System in the Rhesus Monkey Model of Optic Nerve Head Ischemia

Dennis E. Brooks,[1] Maria E. Källberg,[1] Richard L. Cannon,[2] Andras M. Komáromy,[1] Franck J. Ollivier,[1] Olga E. Malakhova,[2] William W. Dawson,[3] Mark B. Sherwood,[3] Elen E. Kuekuerichkina,[2] and George N. Lambrou[4]

PURPOSE. A redistribution of neurochemicals has been identified in the visual cortex of monkeys with laser-induced glaucoma. Examined were functional, structural, and neurochemical changes to the retina, optic nerve, and central visual system in a nonhuman primate model of optic nerve head (ONH) ischemia caused by sustained unilateral administration of endothelin (ET)-1 to the optic nerve.

METHOD. ET-1 or sham control solution was delivered by osmotic minipump to the retrolaminar region of one optic nerve of rhesus monkeys (*Macaca mulatta*) for 1.5 years. ONH topography and blood flow velocity were serially studied with scanning laser tomography and laser Doppler flowmetry, respectively. Retinal and cortical electrophysiologic measurements from pattern-derived stimuli were obtained quarterly. Immunohistochemistry was used to identify the distribution of calbindin (CB) and c-Fos labeled neurons in the visual cortex areas V1 and V2, and lateral geniculate nucleus (LGN). Retinal ganglion cell counts and optic nerve axon density were determined by light microscopy.

RESULTS. No significant changes in retinal and ONH morphology, ONH blood flow velocity, and retinal and cortical pattern-derived functional activity were detected. Measurement of CB-positive cell density in V1 and V2 showed a significant decrease in CB labeling to the contralateral side of the ET-1–treated eye ($P < 0.04$). CB-positive cells were present in the magnocellular layers of the LGN with no differences noticed between the ET-1– and sham-treated eyes. c-Fos–labeled neurons were found in striate area V1 and extrastriateV2 of both groups. No c-Fos labeling was observed in the LGN.

CONCLUSIONS. Administering ET-1 to the orbital optic nerve alters neuronal metabolic activity in the visual cortex in rhesus monkeys. Metabolic activity reductions in the visual cortex precede the ability to detect functional and structural alterations in the retina, ONH, and visual cortex in this animal model. (*Invest Ophthalmol Vis Sci.* 2004;45:1830–1840) DOI: 10.1167/iovs.03-0950

Glaucoma is a neurodegenerative disease as it results in the death of retinal ganglion cells (RGCs).[1,2] Retinal ganglion cell apoptotic degeneration and subsequent optic neuropathy in glaucoma occurs from optic nerve axoplasmic flow obstruction, depletion of the neurotrophic factors necessary for RGC survival, excess intraocular endothelin (ET)-1, retinal and ONH accumulation of nitric oxide and oxygen free radicals, and amino acid excitotoxicity and loss of intraneuronal calcium homeostasis at the ONH.[3–6] Mechanical deformation of the scleral lamina cribrosa by elevated intraocular pressure (IOP) and hypoperfusion-induced ischemia at the ONH from dysregulation of the ocular microcirculation are pathogenic mechanisms that, alone and in combination, contribute to the visual deficits in glaucomatous optic neuropathy.[3,4]

Laser-induced photocoagulation of the nonhuman primate trabecular meshwork produces a sustained elevation in IOP that models the mechanically induced functional and structural alterations at the ONH present in the human disease.[7–9] RGC death, loss of optic nerve axons, and visual field defects are present in this animal model.[1,8]

Sustained ET-1 administration to the periorbital optic nerve of animals may cause ONH ischemia, and induce alterations to the retina and optic nerve that model the presumed microcirculatory dysfunction noted in the human disease.[4,10–13] Optic nerve vessels supplying the ONH in rabbits were significantly constricted by ET-1 delivered by osmotic minipump in rabbits.[13] The optic nerve circulation was reduced by ~38% and the optic nerve axon density reduced by 17% in the ET-1 nonhuman primate ONH ischemia animal model.[10–12]

Brooks et al. IOVS. 2004

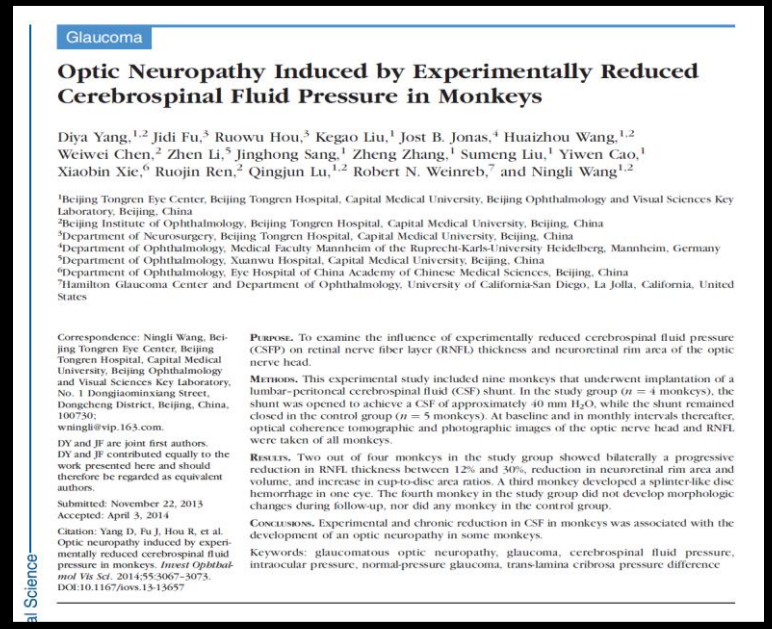

Glaucoma

Optic Neuropathy Induced by Experimentally Reduced Cerebrospinal Fluid Pressure in Monkeys

Diya Yang,[1,2] Jidi Fu,[3] Ruowu Hou,[3] Kegao Liu,[1] Jost B. Jonas,[4] Huaizhou Wang,[1,2] Weiwei Chen,[2] Zhen Li,[5] Jinghong Sang,[1] Zheng Zhang,[1] Sumeng Liu,[1] Yiwen Cao,[1] Xiaobin Xie,[6] Ruojin Ren,[2] Qingjun Lu,[1,2] Robert N. Weinreb,[7] and Ningli Wang[1,2]

[1]Beijing Tongren Eye Center, Beijing Tongren Hospital, Capital Medical University, Beijing Ophthalmology and Visual Sciences Key Laboratory, Beijing, China
[2]Beijing Institute of Ophthalmology, Beijing Tongren Hospital, Capital Medical University, Beijing, China
[3]Department of Neurosurgery, Beijing Tongren Hospital, Capital Medical University, Beijing, China
[4]Department of Ophthalmology, Medical Faculty Mannheim of the Ruprecht-Karls-University Heidelberg, Mannheim, Germany
[5]Department of Ophthalmology, Xuanwu Hospital, Capital Medical University, Beijing, China
[6]Department of Ophthalmology, Eye Hospital of China Academy of Chinese Medical Sciences, Beijing, China
[7]Hamilton Glaucoma Center and Department of Ophthalmology, University of California-San Diego, La Jolla, California, United States

Correspondence: Ningli Wang, Beijing Tongren Eye Center, Beijing Tongren Hospital, Capital Medical University, Beijing Ophthalmology and Visual Sciences Key Laboratory, No. 1 Dongjiaominxiang Street, Dongcheng District, Beijing, China, 100730; wningli@vip.163.com.

DY and JF are joint first authors. DY and JF contributed equally to the work presented here and should therefore be regarded as equivalent authors.

Submitted: November 22, 2013
Accepted: April 3, 2014

Citation: Yang D, Fu J, Hou R, et al. Optic neuropathy induced by experimentally reduced cerebrospinal fluid pressure in monkeys. *Invest Ophthalmol Vis Sci.* 2014;55:3067–3073. DOI:10.1167/iovs.13-13657

PURPOSE. To examine the influence of experimentally reduced cerebrospinal fluid pressure (CSFP) on retinal nerve fiber layer (RNFL) thickness and neuroretinal rim area of the optic nerve head.

METHODS. This experimental study included nine monkeys that underwent implantation of a lumbar–peritoneal cerebrospinal fluid (CSF) shunt. In the study group ($n = 4$ monkeys), the shunt was opened to achieve a CSF of approximately 40 mm H_2O, while the shunt remained closed in the control group ($n = 5$ monkeys). At baseline and in monthly intervals thereafter, optical coherence tomographic and photographic images of the optic nerve head and RNFL were taken of all monkeys.

RESULTS. Two out of four monkeys in the study group showed bilaterally a progressive reduction in RNFL thickness between 12% and 30%, reduction in neuroretinal rim area and volume, and increase in cup-to-disc area ratios. A third monkey developed a splinter-like disc hemorrhage in one eye. The fourth monkey in the study group did not develop morphologic changes during follow-up, nor did any monkey in the control group.

CONCLUSIONS. Experimental and chronic reduction in CSF in monkeys was associated with the development of an optic neuropathy in some monkeys.

Keywords: glaucomatous optic neuropathy, glaucoma, cerebrospinal fluid pressure, intraocular pressure, normal-pressure glaucoma, trans-lamina cribrosa pressure difference

Yang et al. IOVS. 2014

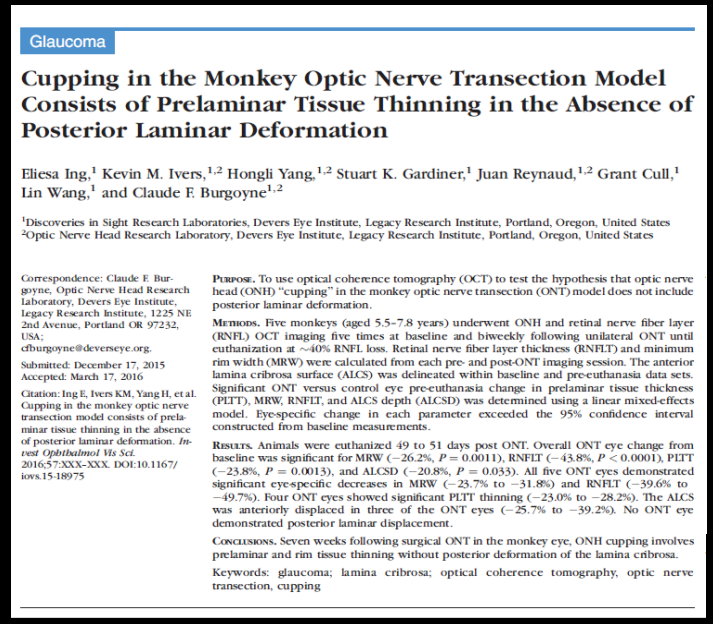

Glaucoma

Cupping in the Monkey Optic Nerve Transection Model Consists of Prelaminar Tissue Thinning in the Absence of Posterior Laminar Deformation

Eliesa Ing,[1] Kevin M. Ivers,[1,2] Hongli Yang,[1,2] Stuart K. Gardiner,[1] Juan Reynaud,[1,2] Grant Cull,[1] Lin Wang,[1] and Claude F. Burgoyne[1,2]

[1]Discoveries in Sight Research Laboratories, Devers Eye Institute, Legacy Research Institute, Portland, Oregon, United States
[2]Optic Nerve Head Research Laboratory, Devers Eye Institute, Legacy Research Institute, Portland, Oregon, United States

Correspondence: Claude F. Burgoyne, Optic Nerve Head Research laboratory, Devers Eye Institute, legacy Research Institute, 1225 NE 2nd Avenue, Portland OR 97232, USA; cfburgoyne@deverseye.org.

Submitted: December 17, 2015
Accepted: March 17, 2016

Citation: Ing E, Ivers KM, Yang H, et al. Cupping in the monkey optic nerve transection model consists of prelaminar tissue thinning in the absence of posterior laminar deformation. *Invest Ophthalmol Vis Sci.* 2016;57:XXX–XXX. DOI:10.1167/iovs.15-18975

PURPOSE. To use optical coherence tomography (OCT) to test the hypothesis that optic nerve head (ONH) "cupping" in the monkey optic nerve transection (ONT) model does not include posterior laminar deformation.

METHODS. Five monkeys (aged 5.5–7.8 years) underwent ONH and retinal nerve fiber layer (RNFL) OCT imaging five times at baseline and biweekly following unilateral ONT until euthanization at ~40% RNFL loss. Retinal nerve fiber layer thickness (RNFLT) and minimum rim width (MRW) were calculated from each pre- and post-ONT imaging session. The anterior lamina cribrosa surface (ALCS) was delineated within baseline and pre-euthanasia data sets. Significant ONT versus control eye pre-euthanasia change in prelaminar tissue thickness (PLTT), MRW, RNFLT, and ALCS depth (ALCSD) was determined using a linear mixed-effects model. Eye-specific change in each parameter exceeded the 95% confidence interval constructed from baseline measurements.

RESULTS. Animals were euthanized 49 to 51 days post ONT. Overall ONT eye change from baseline was significant for MRW (−26.2%, $P = 0.0011$), RNFLT (−43.8%, $P < 0.0001$), PLTT (−23.8%, $P = 0.0013$), and ALCSD (−20.8%, $P = 0.033$). All five ONT eyes demonstrated significant eye-specific decreases in MRW (−23.7% to −31.8%) and RNFLT (−39.6% to −49.7%). Four ONT eyes showed significant PLTT thinning (−23.0% to −28.2%). The ALCS was anteriorly displaced in three of the ONT eyes (−25.7% to −39.2%). No ONT eye demonstrated posterior laminar displacement.

CONCLUSIONS. Seven weeks following surgical ONT in the monkey eye, ONH cupping involves prelaminar and rim tissue thinning without posterior deformation of the lamina cribrosa.

Keywords: glaucoma; lamina cribrosa; optical coherence tomography, optic nerve transection, cupping

Ing et al. IOVS. 2016

Endothelin

(ischemia vs astrocyte activation????)

No glaucomatous "Cupping"

Primary CSF Lowering

(increased translaminar pressure difference)

(without elevated IOP-related scleral effects)

No Glaucomatous "Cupping"

Surgical Optic Nerve Transection

(primary RGC axotomy)

No Glaucomatous "Cupping"

Outline

- Professor Hans Goldmann
- Disclosures and Acknowledgements
- Creating 3D Optic Nerve Head Histology and Morphology
- The Optic Nerve Head in Glaucoma
- What Defines a Glaucomatous Optic Neuropathy?
- 3D Histomorphometric Structural Phenotyping in Monkey Glaucoma
- 3D OCT Structural Phenotyping in Monkey and Human Glaucoma
- qIHC and 3D SBEM in Monkey EG
- Summary / Implications
- A Final Acknowledgement

3D Manual Segmentation of ONH landmarks/surfaces

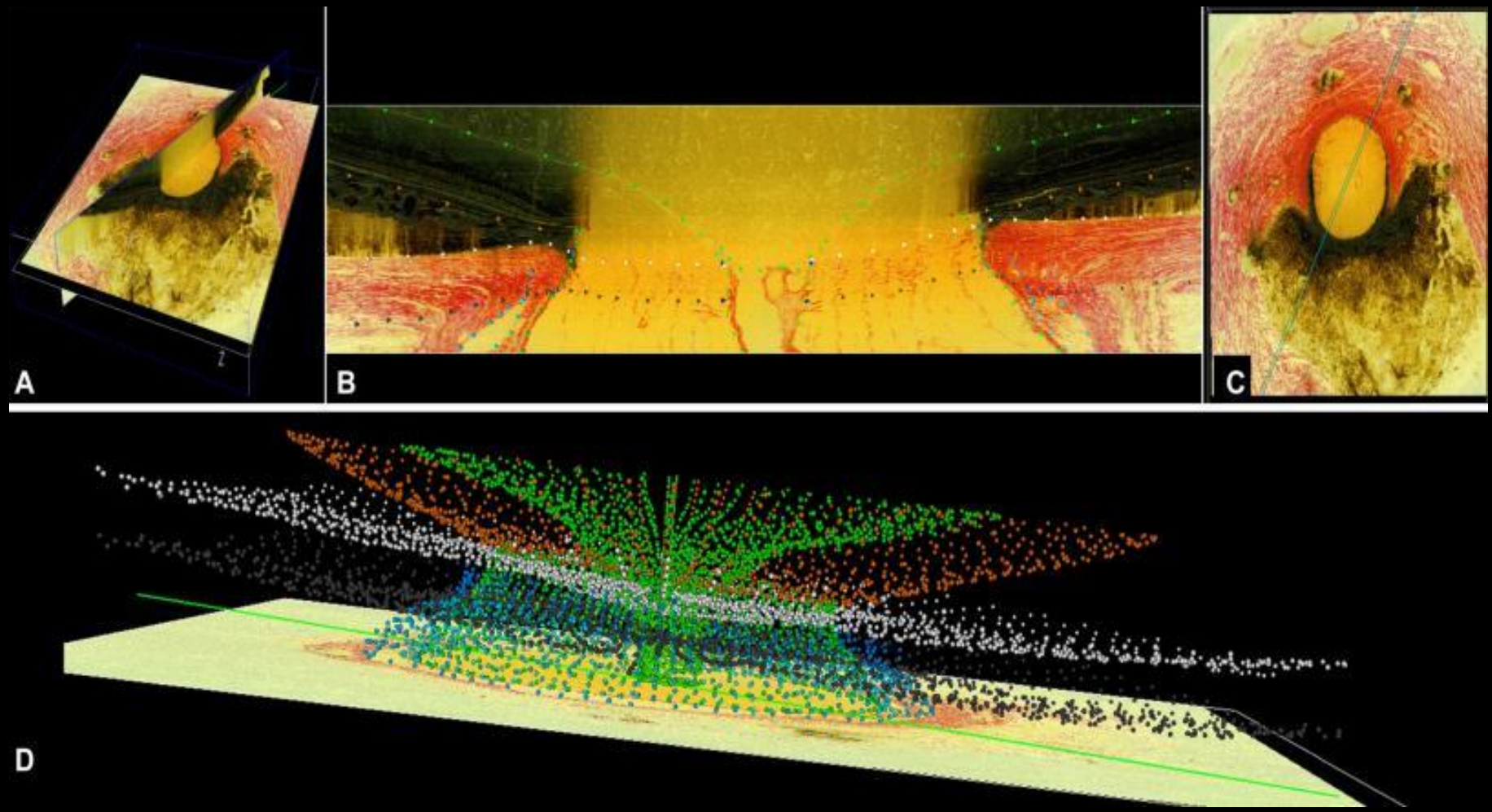

3D Histomorphometric ONH Structural Phenotyping in Monkey Glaucoma

Hongli Yang, PhD

Progress in Retinal and Eye Research 59 (2017) 1–52

Contents lists available at ScienceDirect

Progress in Retinal and Eye Research

journal homepage: www.elsevier.com/locate/prer

The connective tissue phenotype of glaucomatous cupping in the monkey eye - Clinical and research implications

Hongli Yang [a, b, 1], Juan Reynaud [a, b, 1], Howard Lockwood [a, b, 1], Galen Williams [a, b, 1], Christy Hardin [a, b, 1], Luke Reyes [a, b, 1], Cheri Stowell [a, b, 1], Stuart K. Gardiner [b, 1], Claude F. Burgoyne, MD [a, b, *, 1]

[a] Devers Eye Institute, Optic Nerve Head Research Laboratory, Legacy Research Institute, Portland, OR, United States
[b] Devers Eye Institute, Discoveries in Sight Research Laboratories, Legacy Research Institute, Portland, OR, United States

ARTICLE INFO

Article history:
Received 17 November 2016
Received in revised form
14 February 2017
Accepted 6 March 2017
Available online 12 March 2017

Keywords:
Glaucoma
Optic nerve head
Lamina cribrosa
Monkey
Astrocyte

ABSTRACT

In a series of previous publications we have proposed a framework for conceptualizing the optic nerve head (ONH) as a biomechanical structure. That framework proposes important roles for intraocular pressure (IOP), IOP-related stress and strain, cerebrospinal fluid pressure (CSFp), systemic and ocular determinants of blood flow, inflammation, auto-immunity, genetics, and other non-IOP related risk factors in the physiology of ONH aging and the pathophysiology of glaucomatous damage to the ONH. The present report summarizes 20 years of technique development and study results pertinent to the characterization of ONH connective tissue deformation and remodeling in the unilateral monkey experimental glaucoma (EG) model. In it we propose that the defining pathophysiology of a glaucomatous optic neuropathy involves deformation, remodeling, and mechanical failure of the ONH connective tissues. We view this as an active process, driven by astrocyte, microglial, fibroblast and oligodendrocyte mechanobiology. These cells, and the connective tissue phenomena they propagate, have primary and secondary effects on retinal ganglion cell (RGC) axon, laminar beam and retrolaminar capillary homeostasis that may initially be "protective" but eventually lead to RGC axonal injury, repair and/or cell death. The primary goal of this report is to summarize our 3D histomorphometric and optical coherence tomography (OCT)-based evidence for the early onset and progression of ONH connective tissue deformation and remodeling in monkey EG. A second goal is to explain the importance of including ONH connective tissue processes in characterizing the phenotype of a glaucomatous optic neuropathy in all species. A third goal is to summarize our current efforts to move from ONH morphology to the cell biology of connective tissue remodeling and axonal insult early in the disease. A final goal is to facilitate the translation of our findings and ideas into neuroprotective interventions that target these ONH phenomena for therapeutic effect.

© 2017 Elsevier Ltd. All rights reserved.

Yang et al. PRER 2017

Our strategies for Structurally Phenotypying the optic neuropathy of experimental glaucoma in the monkey eye using

3D Histomorphometry

have been lead by Hongli Yang, PhD and are summarized in this 2017 PRER review paper.

ONH Connective Tissue Change – Early through Severe Experimental Glaucoma

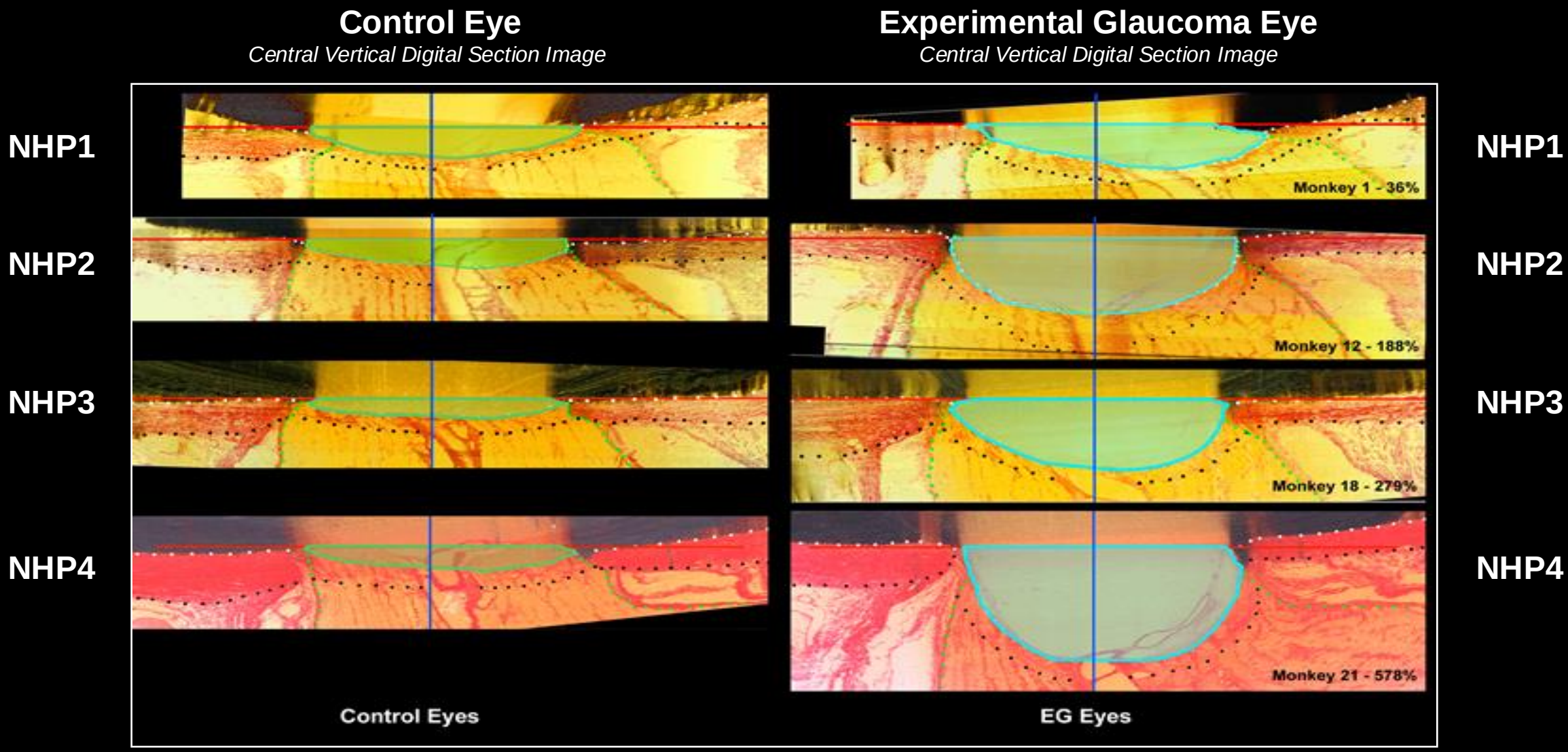

Yang, et al. IOVS, 2015.

ONH Connective Tissue Change – Early Experimental Glaucoma

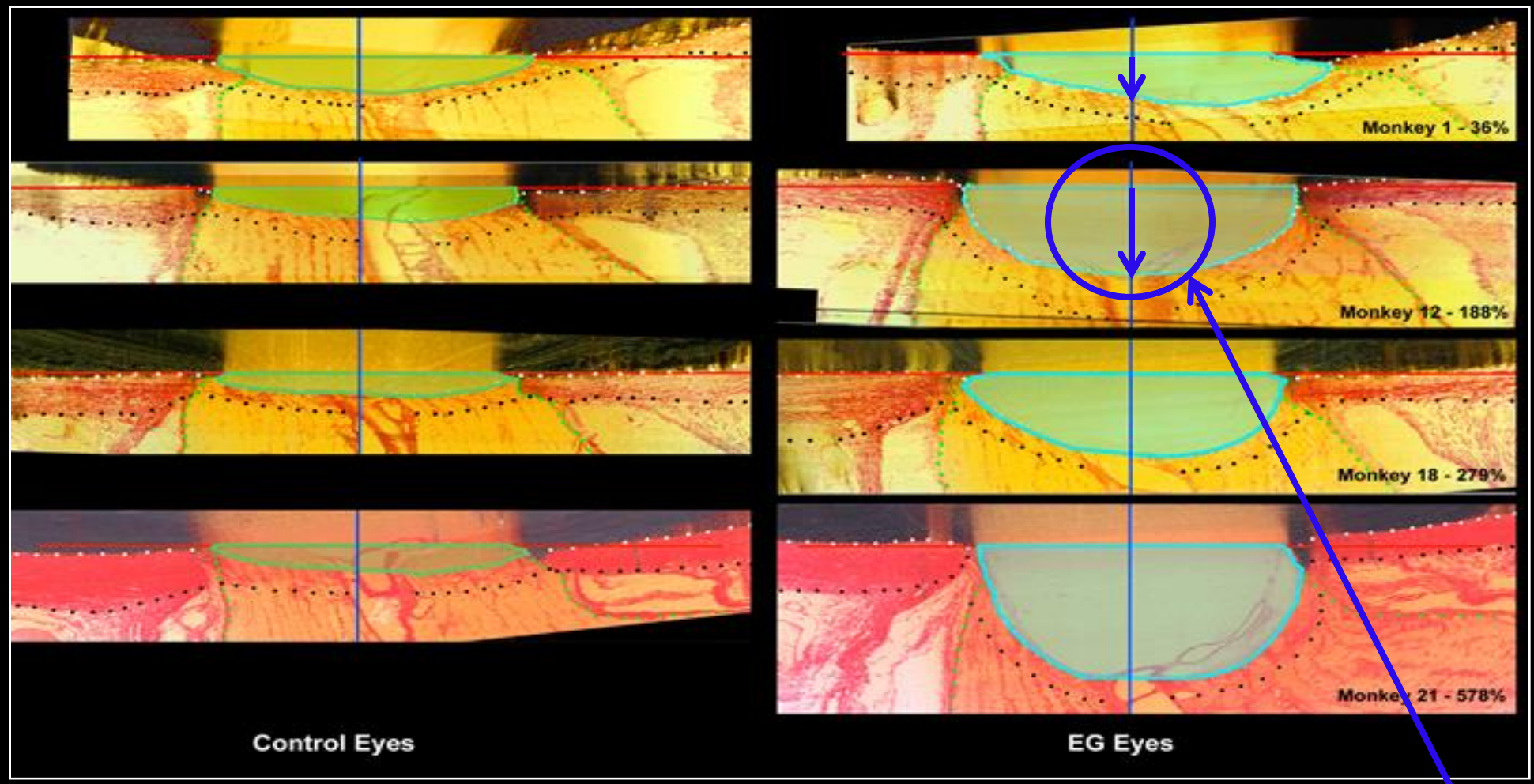

Yang, et al. IOVS, 2015.

ONH Connective Tissue Change – Early Experimental Glaucoma

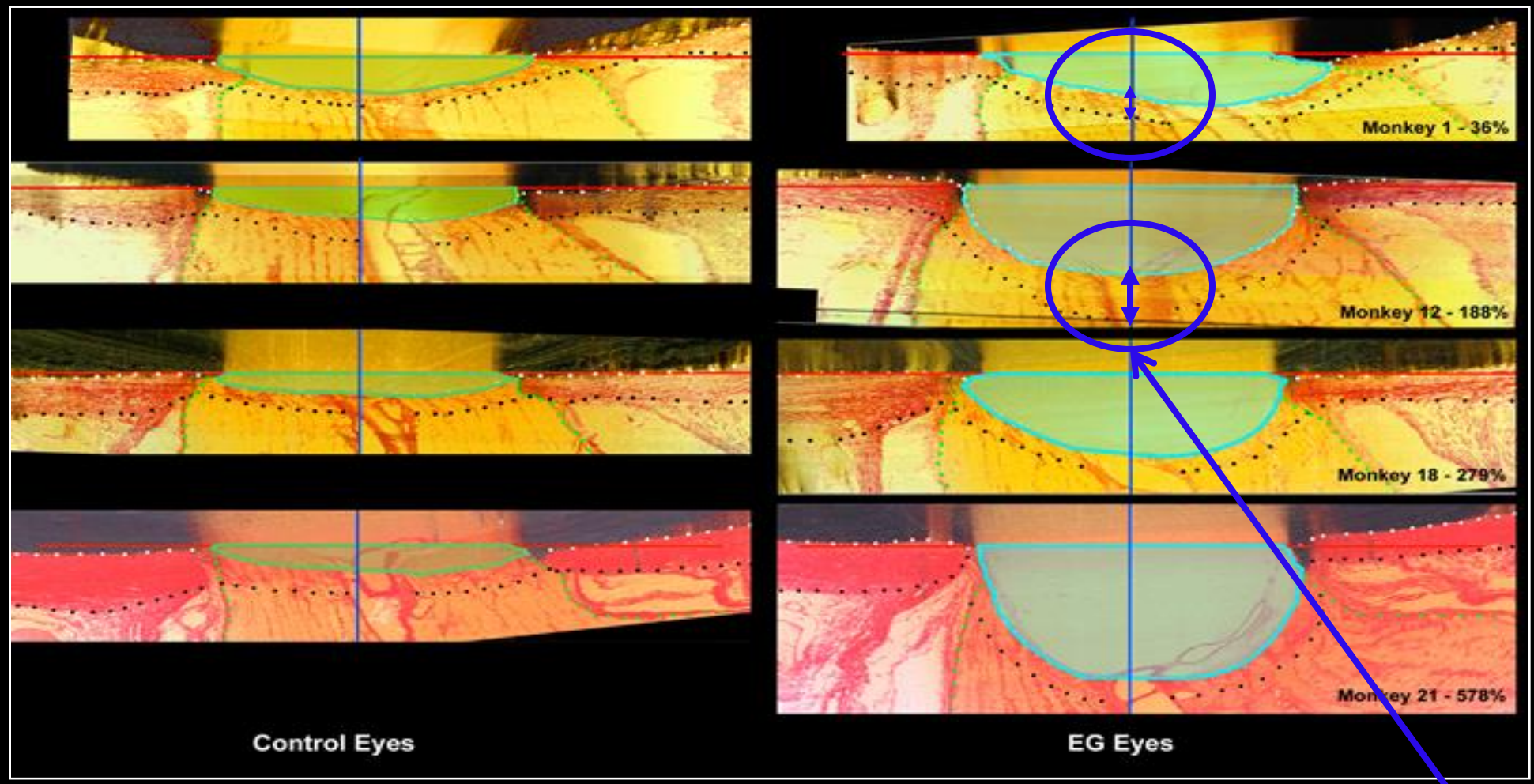

Yang, et al. IOVS, 2015.

ONH Connective Tissue Change – Early Experimental Glaucoma

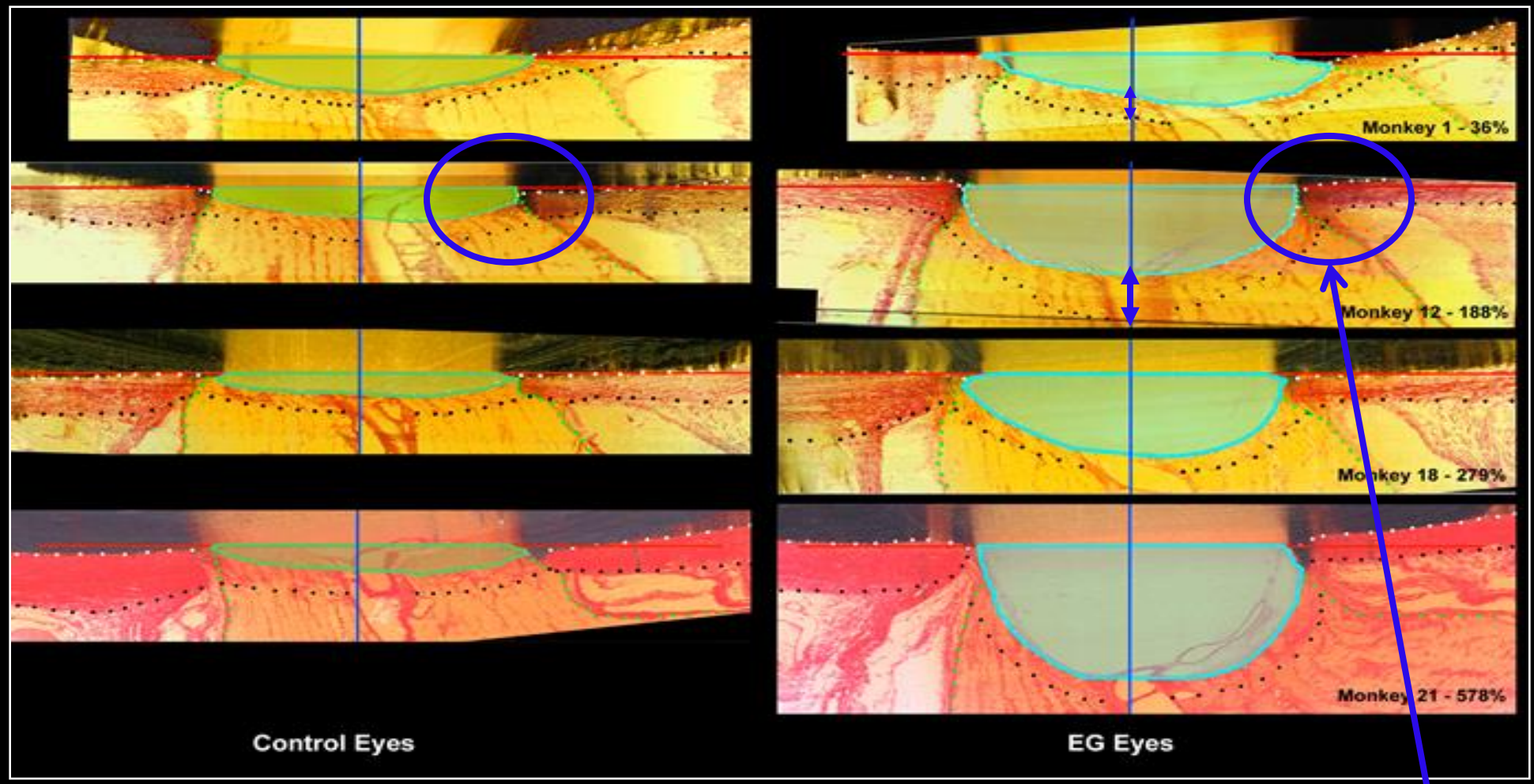

Yang, et al. IOVS, 2015.

ONH Connective Tissue Change – Progressive Experimental Glaucoma

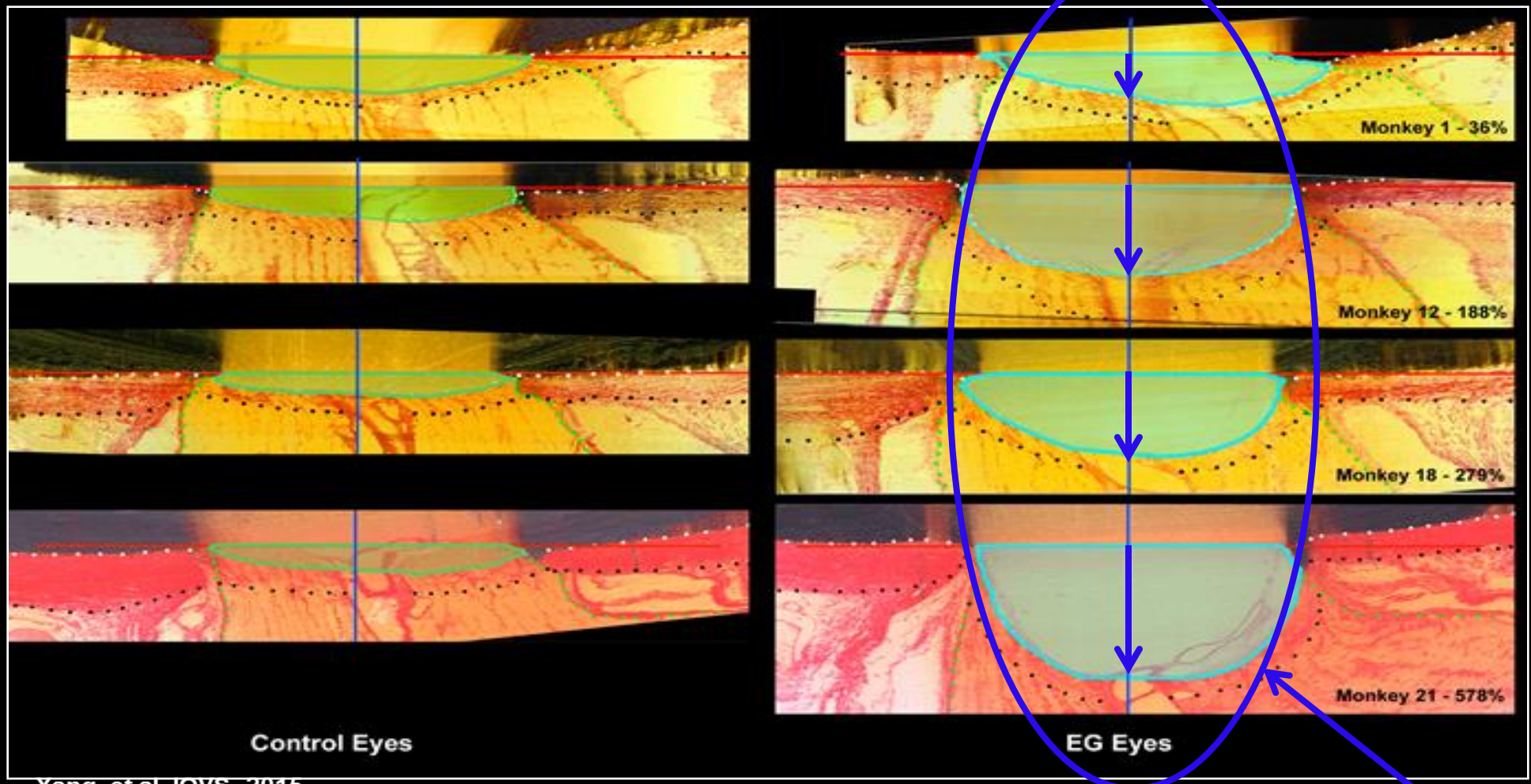

Yang, et al. IOVS, 2015.

Progressive Laminar Deformation

ONH Connective Tissue Change – Progressive Experimental Glaucoma

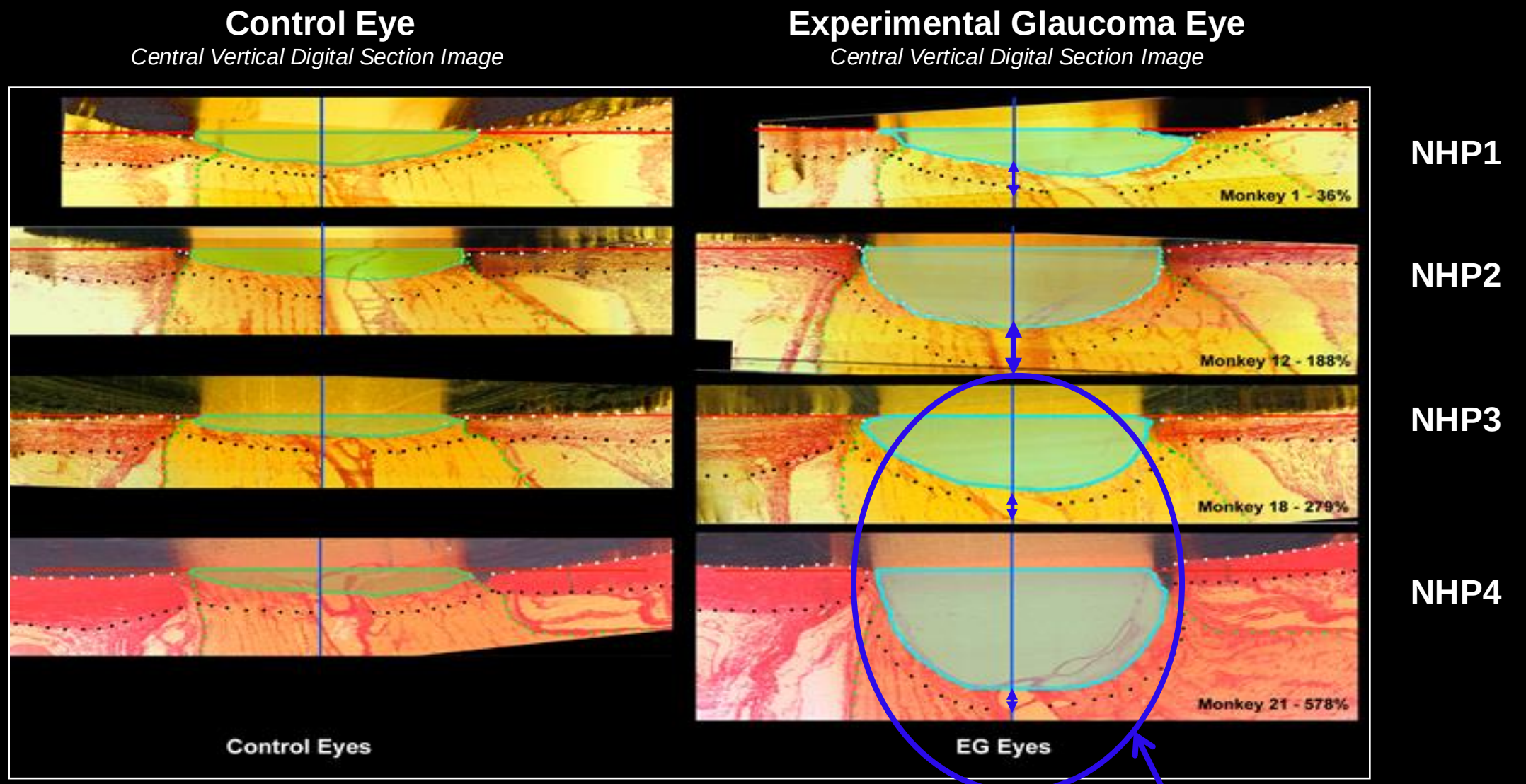

ONH Connective Tissue Change – Progressive Experimental Glaucoma

Control Eye
Central Vertical Digital Section Image

Experimental Glaucoma Eye
Central Vertical Digital Section Image

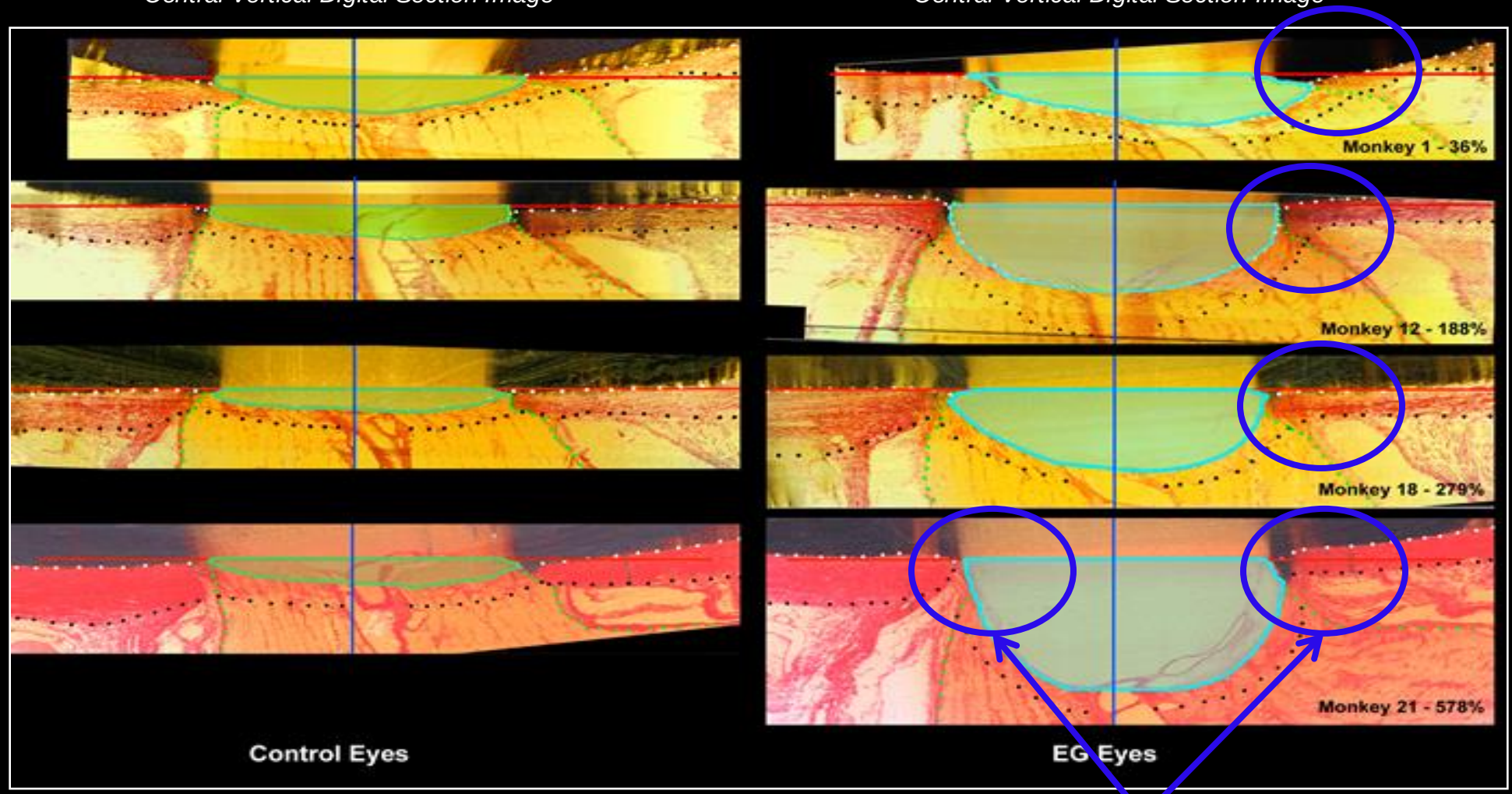

Yang, et al. IOVS, 2015.

Progressive Migration of the Lamina into the Pial Sheath

Laminar Microarchitecture Change in Monkey Early Experimental Glaucoma is complex, profound and EG eye-specific

Glaucoma

Lamina Cribrosa Microarchitecture in Normal Monkey Eyes Part 1: Methods and Initial Results

Howard Lockwood,[1,2] Juan Reynaud,[1,2] Stuart Gardiner,[2] Jonathan Grimm,[3] Vincent Libertiaux,[4] J. Crawford Downs,[4] Hongli Yang,[1,2] and Claude F. Burgoyne[1,2]

[1]Optic Nerve Head Research Laboratory, Discoveries in Sight Research Laboratories, Devers Eye Institute, Legacy Health, Portland, Oregon, United States
[2]Discoveries in Sight Research Laboratories of the Devers Eye Institute, Legacy Health, Portland, Oregon, United States
[3]Ocular Biomechanics Laboratory, Department of Ophthalmology, UPMC Eye Center, Ophthalmology and Visual Science Research Center, University of Pittsburgh School of Medicine, Pittsburgh, Pennsylvania, United States
[4]Department of Ophthalmology, University of Alabama at Birmingham School of Medicine, Birmingham, Alabama, United States

Correspondence: Claude F. Burgoyne, Optic Nerve Head Research Laboratory, Devers Eye Institute, Legacy Research Institute, 1225 NE 2nd Avenue, Portland, OR 97232, USA; cfburgoyne@deverseye.org.

HL and JR contributed equally to the work presented here and should therefore be regarded as equivalent authors.

Submitted: October 29, 2014
Accepted: January 14, 2015

Citation: Lockwood H, Reynaud J, Gardiner S, et al. Lamina cribrosa microarchitecture in normal monkey eyes part 1: methods and initial results. *Invest Ophthalmol Vis Sci*. 2015;56:1618–1637. DOI:10.1167/iovs.14-15967

Purpose. To introduce quantitative postmortem lamina cribrosa (LC) microarchitecture (LMA) assessment and characterize beam diameter (BD), pore diameter (PD), and connective tissue volume fraction (CTVF) in 21 normal monkey eyes.

Methods. Optic nerve heads (ONHs) underwent digital three-dimensional (3D) reconstruction and LC beam segmentation. Each beam and pore voxel was assigned a diameter based on the largest sphere that contained it before transformation to one of twelve 30° sectors in a common cylinder. Mean BD, PD, and CTVF within 12 central and 12 peripheral subsectors and within inner, middle, and outer LC depths were assessed for sector, subsector, and depth effects by analysis of variance using general estimating equations. Eye-specific LMA discordance (the pattern of lowest connective tissue density) was plotted for each parameter.

Results. The ranges of mean BD, PD, and CTVF were 14.0 to 23.1 µm, 20.0 to 35.6 µm, and 0.247 to 0.638, respectively. Sector, subsector, and depth effects were significant ($P < 0.01$) for all parameters except subsector on CTVF. Beam diameter and CTVF were smaller and PD was larger within the superior-temporal (ST) and inferior-temporal (IT) sectors ($P < 0.05$). These differences were enhanced within the central versus peripheral subsectors. Beam diameter and CTVF were larger and PD was smaller ($P < 0.05$) within the middle LC layer. Lamina cribrosa microarchitecture discordance most commonly occurred within the ST and IT sectors, varied by eye, and generally diminished as CTVF increased.

Conclusions. Our data support previous characterizations of diminished connective tissue density within the ST and IT ONH regions. The clinical importance of eye-specific LMA discordance warrants further study.

Keywords: glaucoma, optic nerve head, lamina cribrosa

Lockwood, et al. IOVS. 2015

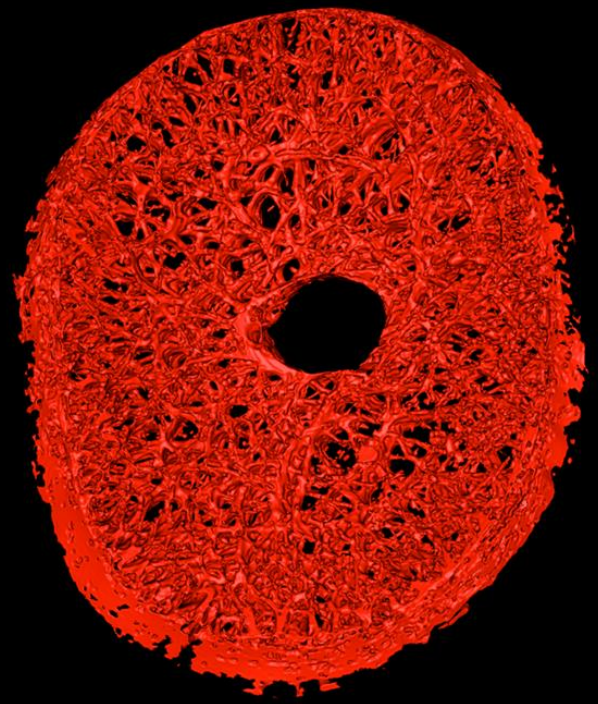

Howard Lockwood

Juan Reynaud

Hongli Yang

Glaucoma

Lamina Cribrosa Microarchitecture in Monkey Early Experimental Glaucoma: Global Change

Juan Reynaud,[1,2] Howard Lockwood,[1,2] Stuart K. Gardiner,[2] Galen Williams,[1,2] Hongli Yang,[1,2] and Claude F. Burgoyne[1,2]

[1]Optic Nerve Head Research Laboratory, Devers Eye Institute, Legacy Research Institute, Portland, Oregon, United States
[2]Discoveries in Sight Research Laboratories, Devers Eye Institute, Legacy Research Institute, Portland, Oregon, United States

Correspondence: Claude F. Burgoyne, Optic Nerve Head Research Laboratory, Devers Eye Institute, Legacy Research Institute, 1225 NE 2nd Avenue, Portland, OR 97232, USA; cfburgoyne@deverseye.org.

JR and HL contributed equally to the work presented here and should therefore be regarded as equivalent authors.

Submitted: March 1, 2016
Accepted: May 14, 2016

Citation: Reynaud J, Lockwood H, Gardiner SK, Williams G, Yang H, Burgoyne CF. Lamina cribrosa microarchitecture in monkey early experimental glaucoma: global change. *Invest Ophthalmol Vis Sci*. 2016;57:3451–3469. DOI:10.1167/iovs.16-19474

Purpose. The purpose of this study was to characterize experimental glaucoma (EG) versus control eye differences in lamina cribrosa (LC), beam diameter (BD), pore diameter (PD), connective tissue volume fraction (CTVF), connective tissue volume (CTV), and LC volume (LV) in monkey early EG.

Methods. Optic nerve heads (ONHs) of 14 unilateral EG and 6 bilateral normal (BN) monkeys underwent three-dimensional reconstruction and LC beam segmentation. Each beam and pore voxel was assigned a diameter based on the largest sphere that contained it before transformation to a common cylinder with inner, middle, and outer layers. Full-thickness and layer averages for BD, PD, CTVF, CTV, and LV were calculated for each ONH. Beam diameter and PD distributions for each ONH were fit to a gamma distribution and summarized by scale and shape parameters. Experimental glaucoma and depth effects were assessed for each parameter by linear mixed-effects (LME) modeling. Animal-specific EG versus control eye differences that exceeded the maximum intereye difference among the six BN animals were considered significant.

Results. Overall EG eye mean PD was 12.8% larger (28.2 ± 5.6 vs. 25.0 ± 3.3 µm), CTV was 26.5% larger (100.06 ± 47.98 vs. 79.12 ± 28.35 × 10^6 µm^3), and LV was 40% larger (229.29 ± 98.19 vs. 163.63 ± 39.87 × 10^6 µm^3) than control eyes ($P \leq 0.05$, LME). Experimental glaucoma effects were significantly different by layer for PD ($P = 0.0097$) and CTVF ($P < 0.0001$). Pore diameter expanded consistently across all PDs. Experimental glaucoma eye-specific parameter change was variable in magnitude and direction.

Conclusions. Pore diameter, CTV, and LV increase in monkey early EG; however, EG eye-specific change is variable and includes both increases and decreases in BD and CTVF.

Keywords: glaucoma, optic nerve head, lamina cribrosa

Reynaud, et al. IOVS. 2015

pNC / Posterior Scleral Connective Tissue Change – is also complex, eye specific and related to baseline geometry and material properties

Glaucoma

Biomechanical Changes in the Sclera of Monkey Eyes Exposed to Chronic IOP Elevations

Michaël J. A. Girard,[1,2,3] J.-K. Francis Suh,[2,4] Michael Bottlang,[5] Claude F. Burgoyne,[2,6] and J. Crawford Downs[1,2]

Purpose. To characterize scleral biomechanics in both eyes of eight monkeys in which chronic intraocular pressure (IOP) elevation was induced in one eye.

Methods. Each posterior sclera was mounted on a pressurization apparatus, IOP was elevated from 5 to 45 mm Hg while the 3D displacements of the scleral surface were measured by speckle interferometry. Finite element (FE) models of each scleral shell were constructed that incorporated stretch-induced stiffening and multidirectionality of the collagen fibers. FE model predictions were then iteratively matched to experimental displacements to extract unique sets of scleral biomechanical properties.

Results. For all eyes, the posterior sclera exhibited inhomogeneous, anisotropic, nonlinear biomechanical behavior. Biomechanical changes caused by chronic IOP elevation were complex and specific to each subject. Specifically: (1) Glaucomatous eyes in which the contralateral normal eyes displayed large modulus or thickness were less prone to biomechanical changes; (2) glaucomatous scleral modulus associated with an IOP of 10 mm Hg decreased (when compared with that of the contralateral normal) after minimal chronic IOP elevation; (3) glaucomatous scleral modulus associated with IOPs of 30 and 45 mm Hg increased (when compared with that of the contralateral normal) after moderate IOP elevation; and (4) FE-based estimates of collagen fiber orientation demonstrated no change in the glaucomatous eyes.

Conclusions. Significant stiffening of the sclera follows exposure to moderate IOP elevations in most eyes. Scleral hypercompliance may precede stiffening or be a unique response to minimal chronic IOP elevation in some eyes. These biomechanical changes are likely to be the result of scleral extracellular matrix remodeling. (*Invest Ophthalmol Vis Sci.* 2011;52:5656–5669) DOI:10.1167/iovs.10-6927

Glaucoma is the second leading cause of blindness worldwide[1,2] and leads to vision loss through irreversible damage to retinal ganglion cell axons as they pass through the scleral canal at the optic nerve head (ONH). Although glaucoma pathogenesis is not well understood and could also involve direct damage to the retinal ganglion cells or lateral geniculate, the biomechanical environment of the ONH has been hypothesized to play an important role in the neuropathy. The sclera is an important factor in ONH biomechanics, and recent work strongly suggests that the biomechanics of the posterior sclera and lamina cribrosa are tightly coupled.[3–6] The sclera is the stiffest tissue of the eye and provides the mechanical boundary conditions for the lamina cribrosa at its insertion into the scleral canal wall. Computational models have shown that scleral stiffness[7] and scleral collagen fiber organization[3,4] dictate the IOP-induced deformation exhibited by the ONH. Of note, the sclera exhibits significant biomechanical changes with age[8] and after exposure to chronic IOP elevation, as shown herein, both of which are major risk factors in glaucoma.

To investigate scleral biomechanics as a factor in glaucomatous damage, it is important to quantify its mechanical response to IOP. The stresses and strains in the sclera are significant at normal IOPs,[8,9] and exposure to elevated IOP could lead to changes in scleral biomechanics that precede the onset of glaucoma or occur very early in disease progression. We therefore focused this work on the scleral changes that are present at the early stages of the disease in nonhuman primates, which could indicate that scleral biomechanics and its IOP-induced changes contribute to both the individual susceptibility to glaucoma and its pathogenesis.

We recently described our ex vivo method to experimentally measure the 3-D deformation pattern and thickness of posterior sclera from both eyes of four young and four old

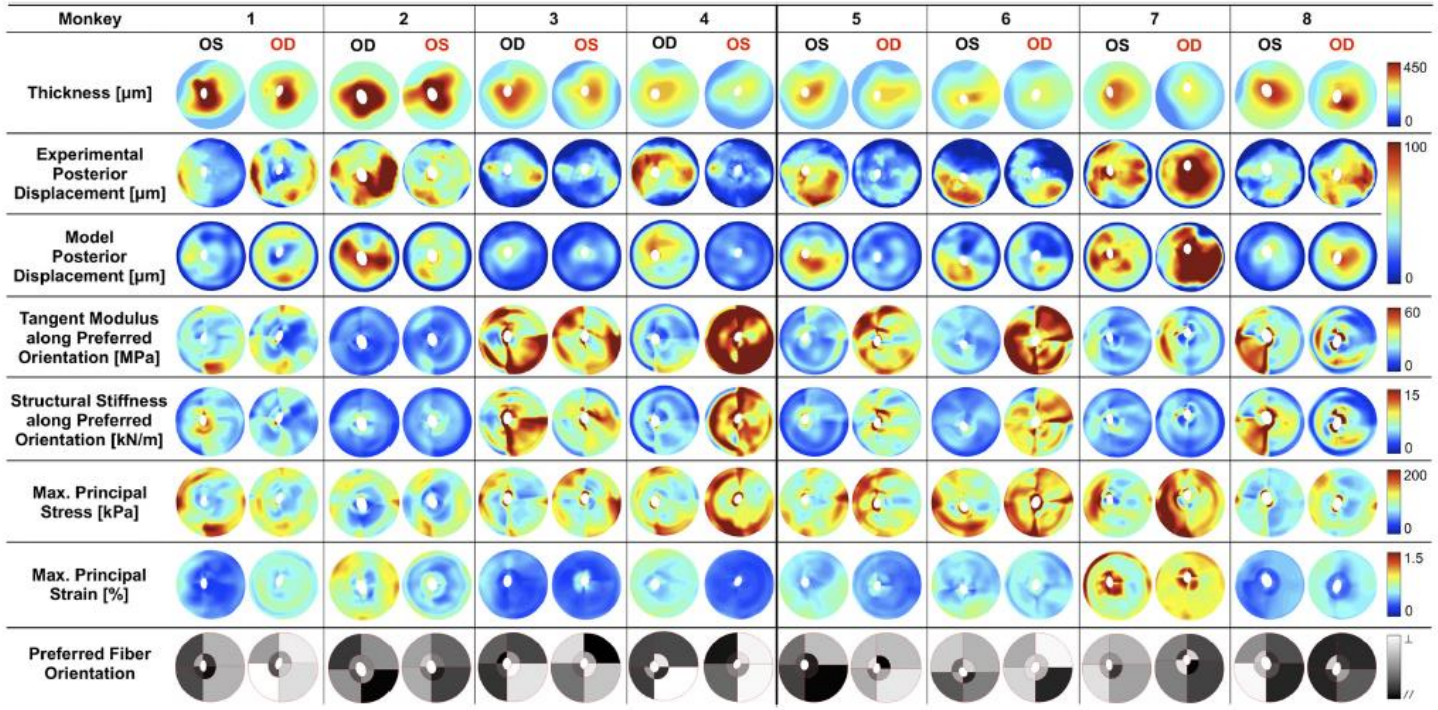

Figure 4. Experimental and modeling results for all posterior scleral shells as viewed from the back of the eye (superior is on *top*, all eyes are in OD configuration with temporal on the *right*). For each monkey, the glaucomatous eye is shown in *red* on the *right*. Scleral thickness was experimentally measured at an IOP of 5 mm Hg and interpolated to obtain continuous thickness maps. Tangent modulus, structural stiffness, and maximum principal stress and strain are shown for all eyes at a single IOP of 30 mm Hg. Good agreements were observed between the FE-computed and the experimentally measured posterior displacements (plotted for an IOP range, 5–30 mm Hg). Finally the preferred fiber orientation is shown for all eight regions of each eye, where // (*black*) corresponds to a collagen fiber organization tangent to the scleral canal (circumferential, $\theta_p = 0°$) and ⊥ (*white*) corresponds to a fiber organization that is perpendicular to the scleral canal (meridional, $\theta_p = 90°$).

Burgoyne–2024 Goldmann–GRS Website

Outline

- Professor Hans Goldmann
- Disclosures and Acknowledgements
- Revisiting 3D Optic Nerve Head Anatomy and Morphology
- The Optic Nerve Head in Glaucoma
- What Defines a Glaucomatous Optic Neuropathy?
- 3D Histomorphometric Structural Phenotyping in Monkey Glaucoma
- 3D *OCT* Structural Phenotyping in *Monkey* and *Human* Glaucoma
- qIHC and 3D SBEM in Monkey EG
- Summary / Implications
- A Final Acknowledgement

3D OCT ONH Structural Phenotyping in Monkey Experimental Glaucoma

Hongli Yang, PhD

Progress in Retinal and Eye Research 59 (2017) 1–52

Contents lists available at ScienceDirect

Progress in Retinal and Eye Research

journal homepage: www.elsevier.com/locate/prer

The connective tissue phenotype of glaucomatous cupping in the monkey eye - Clinical and research implications

Hongli Yang [a, b, 1], Juan Reynaud [a, b, 1], Howard Lockwood [a, b, 1], Galen Williams [a, b, 1], Christy Hardin [a, b, 1], Luke Reyes [a, b, 1], Cheri Stowell [a, b, 1], Stuart K. Gardiner [b, 1], Claude F. Burgoyne, MD [a, b, *, 1]

[a] Devers Eye Institute, Optic Nerve Head Research Laboratory, Legacy Research Institute, Portland, OR, United States
[b] Devers Eye Institute, Discoveries in Sight Research Laboratories, Legacy Research Institute, Portland, OR, United States

ARTICLE INFO

Article history:
Received 17 November 2016
Received in revised form
14 February 2017
Accepted 6 March 2017
Available online 12 March 2017

Keywords:
Glaucoma
Optic nerve head
Lamina cribrosa
Monkey
Astrocyte

ABSTRACT

In a series of previous publications we have proposed a framework for conceptualizing the optic nerve head (ONH) as a biomechanical structure. That framework proposes important roles for intraocular pressure (IOP), IOP-related stress and strain, cerebrospinal fluid pressure (CSFp), systemic and ocular determinants of blood flow, inflammation, auto-immunity, genetics, and other non-IOP related risk factors in the physiology of ONH aging and the pathophysiology of glaucomatous damage to the ONH. The present report summarizes 20 years of technique development and study results pertinent to the characterization of ONH connective tissue deformation and remodeling in the unilateral monkey experimental glaucoma (EG) model. In it we propose that the defining pathophysiology of a glaucomatous optic neuropathy involves deformation, remodeling, and mechanical failure of the ONH connective tissues. We view this as an active process, driven by astrocyte, microglial, fibroblast and oligodendrocyte mechanobiology. These cells, and the connective tissue phenomena they propagate, have primary and secondary effects on retinal ganglion cell (RGC) axon, laminar beam and retrolaminar capillary homeostasis that may initially be "protective" but eventually lead to RGC axonal injury, repair and/or cell death. The primary goal of this report is to summarize our 3D histomorphometric and optical coherence tomography (OCT)-based evidence for the early onset and progression of ONH connective tissue deformation and remodeling in monkey EG. A second goal is to explain the importance of including ONH connective tissue processes in characterizing the phenotype of a glaucomatous optic neuropathy in all species. A third goal is to summarize our current efforts to move from ONH morphology to the cell biology of connective tissue remodeling and axonal insult early in the disease. A final goal is to facilitate the translation of our findings and ideas into neuroprotective interventions that target these ONH phenomena for therapeutic effect.

© 2017 Elsevier Ltd. All rights reserved.

Yang et al. PRER 2017

Our strategies for Structurally Phenotyping the optic neuropathy of experimental glaucoma in the monkey eye using

3D OCT

have also been lead by Hongli Yang, PhD and are also summarized in this 2017 PRER review paper.

3D OCT ONH Structural Phenotyping in Human Glaucoma

- We may never need more than topographically-correspondent:
  - ONH Rim / pNC-RNFLT and Macular Retinal Thickness parameters
  - ROTA and other higher order analyses of the RNFL signal
  - OCT Angiography
  - AI derivations thereof

- But to detect early ONH connective tissue alterations that may precede/predict subsequent RGC axon/rim/retinal change we needed parameters to characterize and stage deep ONH connective tissue structural normality and abnormality in Glaucoma

3D OCT ONH Structural Phenotyping in Human Glaucoma

- We may never need more than topographically-correspondant
  - ONH Rim / pNC-RNFLT and Macular Retinal Thickness parameters
  - Chris Leung's ROTA analysis may be importantly additive to above
  - Angiography may be further additive
  - AI derivations thereof

- But to cross-sectionally or longitudinally detect early ONH connective tissue alterations that may precede/predict subsequent RGC axon/rim/retinal change - parameters to characterize and stage deep ONH connective tissue structural normality and abnormality in Glaucoma are needed

3D OCT ONH Structural Phenotyping in Human Glaucoma

- Many investigators and studies are now detecting phenomenon in human eyes that are evidence of the structural remodeling or failed remodeling we have described in Monkeys

- Our own work focused on understanding human OCT-detected ONH anatomy and parameterizing it in a way that can be deployed in cross-sectional and longitudinal studies

3D OCT Deep ONH Structural Phenotyping in <u>Human</u> Glaucoma is detecting <u>Human</u> <u>ONH</u> <u>Mechanobiology</u> in action!!!

- Laminar Depth / Curvature / Shape
- Laminar Anterior Insertion Migration
- Laminar Thickness
- Laminar Defects / Disinsertions
- Laminar Micro-architecture
- pNC-Hemorrhages and Choroidal Microvascular Drop Out
- pNC-Scleral Flange Remodeling
- pNC–Scleral Bowing
- pNC–Choroidal Thinning

3D OCT Deep ONH Structural Phenotyping in Human Glaucoma is detecting Human ONH Mechanobiology!!!

- Laminar Depth / Curvature / Shape
- Laminar Anterior Insertion Migration
- Laminar Thickness
- Laminar Defects / Disinsertions
- Laminar Micro-architecture
- pNC-Hemorrhages and Choroidal Microvascular Drop Out
- pNC-Scleral Flange Remodeling
- pNC–Scleral Bowing
- pNC–Choroidal Thinning

These are
NOT *just curiosities!*

3D OCT Deep ONH Structural Phenotyping in Human Glaucoma is detecting Human ONH Mechanobiology in action!!!

- Laminar Depth / Curvature / Shape
- Laminar Anterior Insertion Migration
- Laminar Thickness
- Laminar Defects / Disinsertions
- Laminar Micro-architecture
- pNC-Hemorrhages and Choroidal Microvascular Drop Out
- pNC-Scleral Flange Remodeling
- pNC–Scleral Bowing
- pNC–Choroidal Thinning

These are evidence of glaucomatous or myopic remodeling / failed-remodeling until proven otherwise.

Laminar Insertion Migration requires Profound Vascular/Connective Tissue Remodeling within the Scleral Flange and Peripheral Laminar Beams!

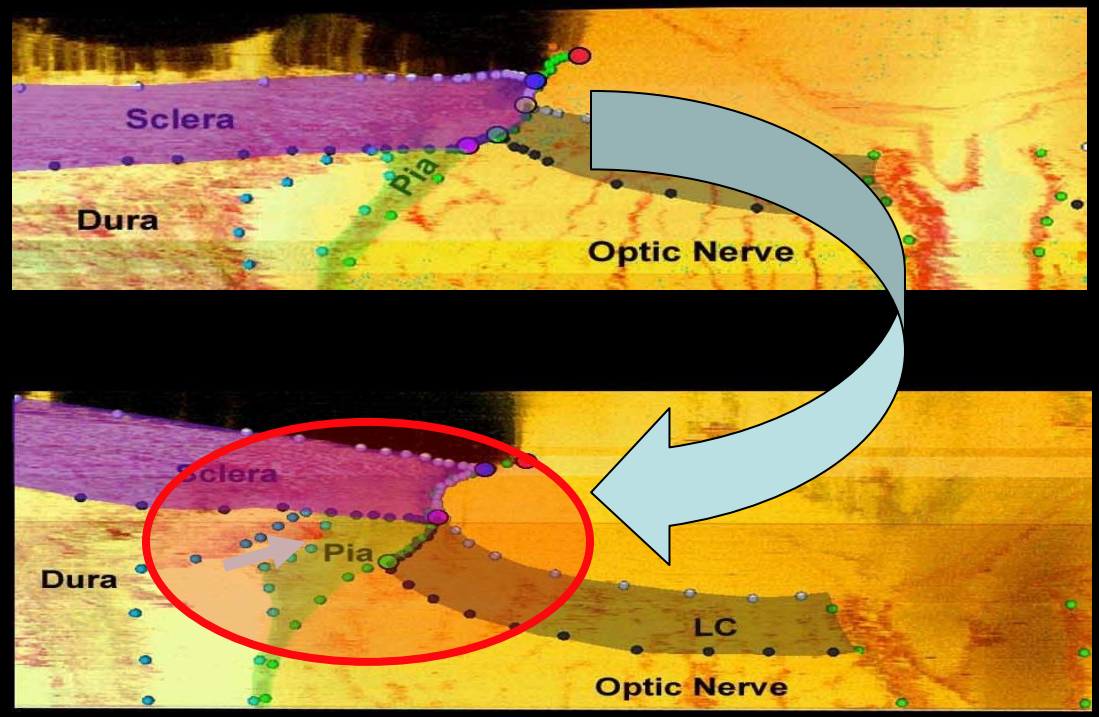

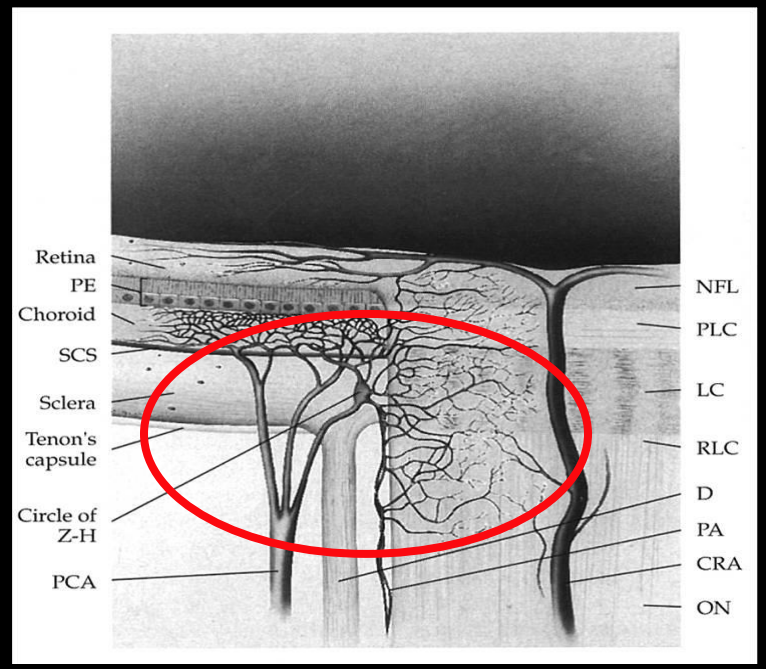

Cioffi and Van Buskirk. The Glaucomas: Basic Science. 1996

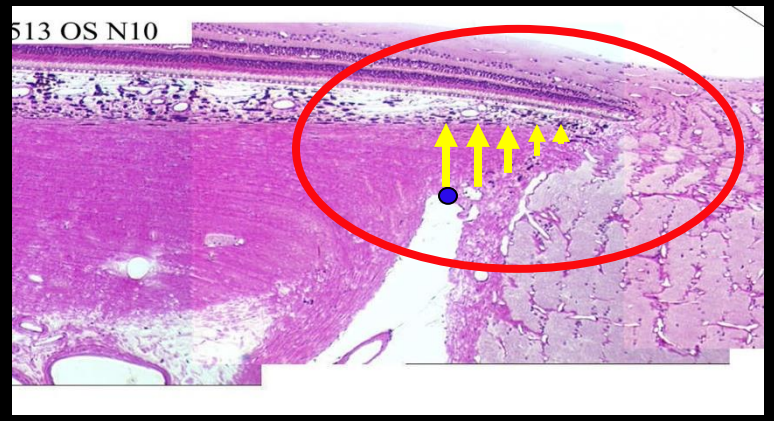

Profound Vascular/Connective Tissue Remodeling within the Scleral Flange should be a contributing cause of NFL Heme and Peripheral Neural Canal RGC axon susceptibility

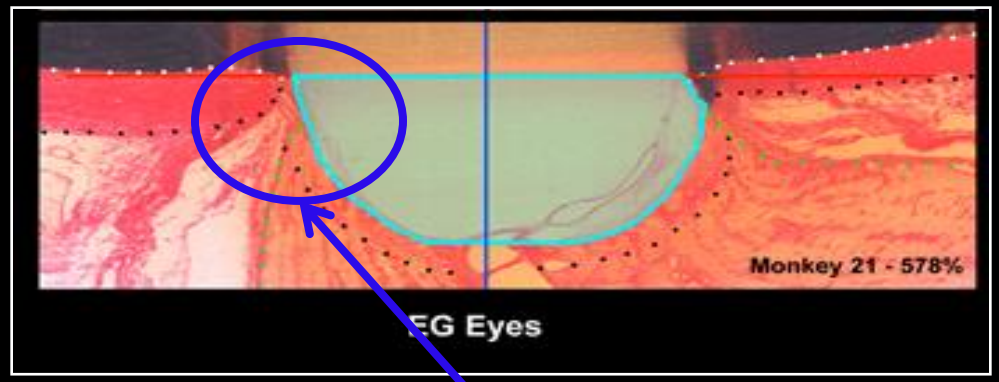

NFL Heme
Acquired Laminar Pits
OCT Laminar/Scleral Disinsertions
Focal Rim / RNFL Loss
Peripheral Axon Susceptibility

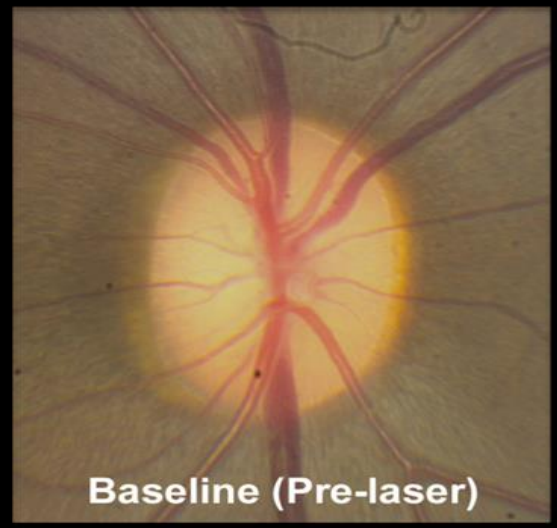

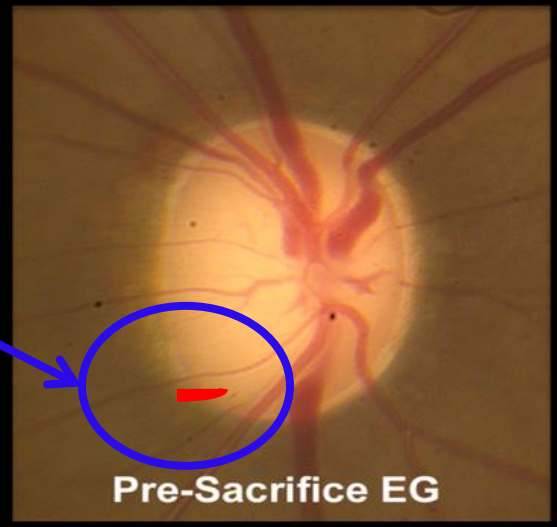

Monkey Experimental Glaucoma (EG)

FoBMO 3D OCT Structural Phenotyping in Human Glaucoma

- Many investigators and studies are detecting phenomenon that are in fact evidence of the structural changes we have described in Monkeys

- Our own work focused on understanding human OCT-detected *DEEP* ONH anatomy and parameterizing it in a way that can be deployed in cross-sectional and longitudinal studies to assess this anatomy's predictive power.

From FoBMO 3D HMRN in Monkeys to FoBMO 3D Monkey/Human OCT!

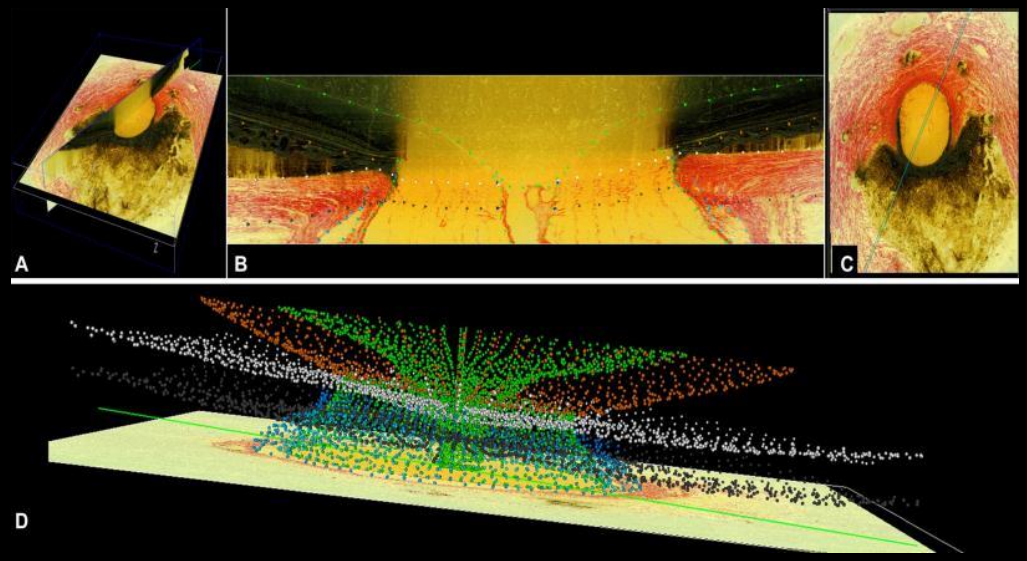

3D HMRN

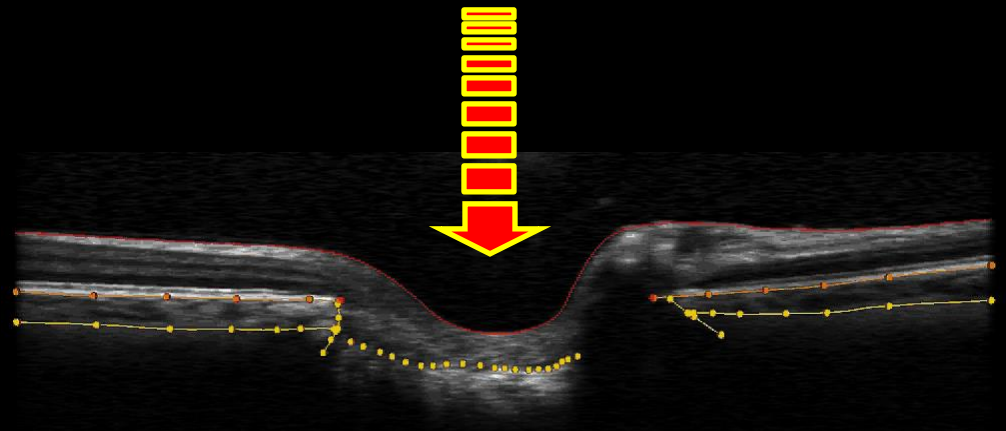

3D OCT

Balwantray Chauhan, PhD
Mathers Professor of Ophthalmology
Dalhousie University

The gift of a long collaboration with a dear friend.

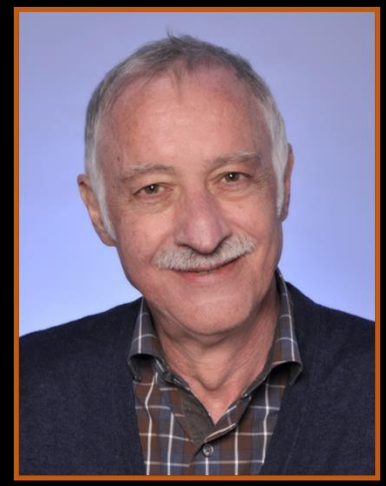

Gerhard Zinser, PhD
Co-Founder Heidelberg Engineering
1954-2017

The gift of having our ideas incorporated into a powerful clinical instrument.

FoBMO Deep ONH / pNC OCT Structural Phenotyping – Healthy Eyes

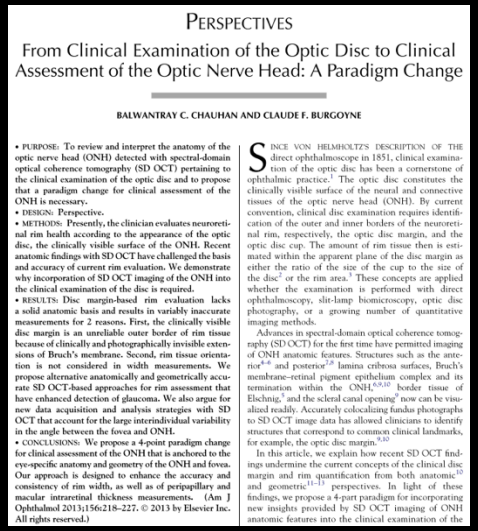

PERSPECTIVES

From Clinical Examination of the Optic Disc to Clinical Assessment of the Optic Nerve Head: A Paradigm Change

BALWANTRAY C. CHAUHAN AND CLAUDE F. BURGOYNE

Chauhan and Burgoyne, AJO 2013

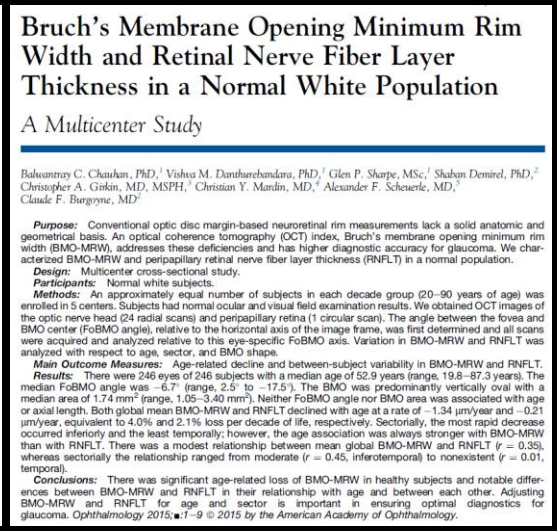

Bruch's Membrane Opening Minimum Rim Width and Retinal Nerve Fiber Layer Thickness in a Normal White Population

A Multicenter Study

Chauhan et al, Ophthalmology 2015

Glaucoma

Determinants and Characteristics of Bruch's Membrane Opening and Bruch's Membrane Opening–Minimum Rim Width in a Normal Japanese Population

Araie et al, IOVS 2017

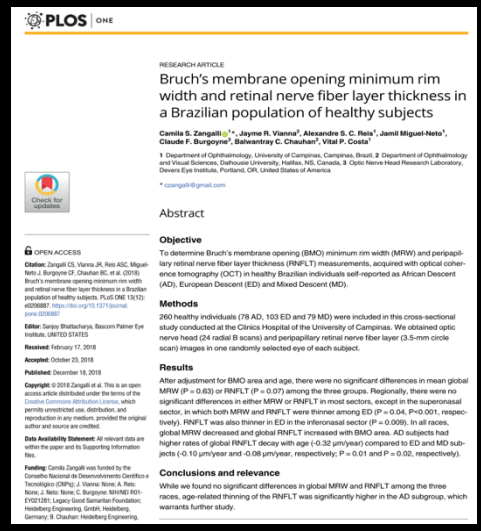

PLOS ONE

Bruch's membrane opening minimum rim width and retinal nerve fiber layer thickness in a Brazilian population of healthy subjects

Zangalli et al, IOVS 2020

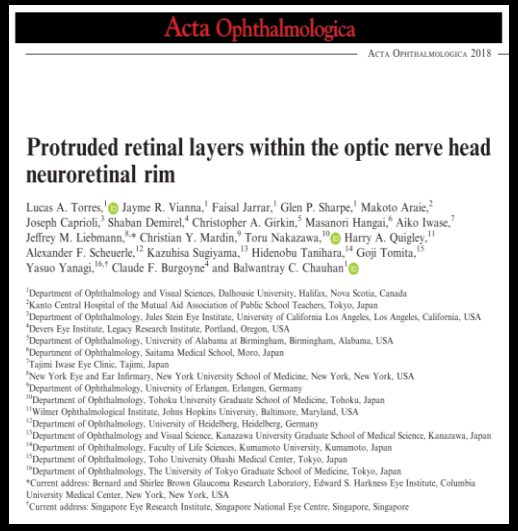

Acta Ophthalmologica

Protruded retinal layers within the optic nerve head neuroretinal rim

Torres et al, Acta Ophthal 2018

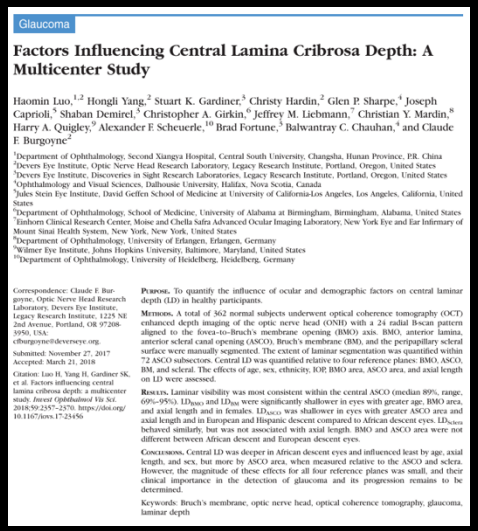

Glaucoma

Factors Influencing Central Lamina Cribrosa Depth: A Multicenter Study

Luo et al, IOVS 2018

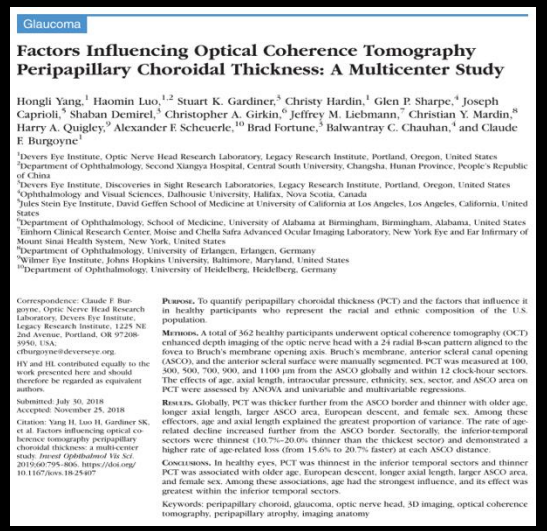

Glaucoma

Factors Influencing Optical Coherence Tomography Peripapillary Choroidal Thickness: A Multicenter Study

Yang et al, IOVS 2018

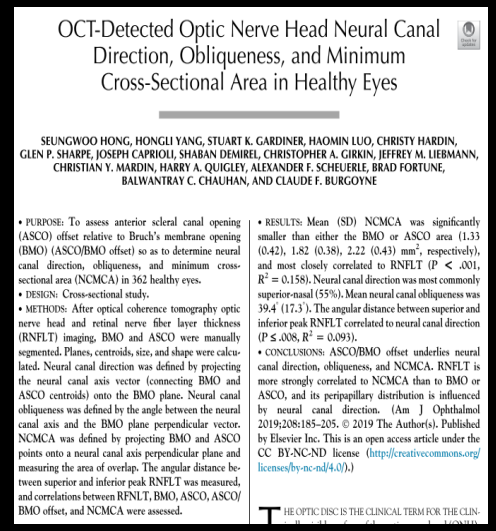

OCT-Detected Optic Nerve Head Neural Canal Direction, Obliqueness, and Minimum Cross-Sectional Area in Healthy Eyes

Hong et al, IOVS 2019

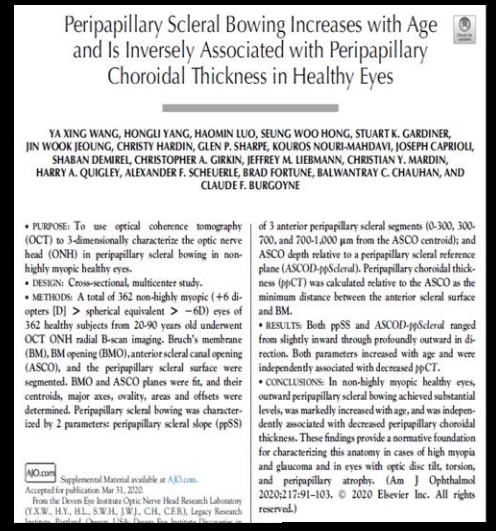

Peripapillary Scleral Bowing Increases with Age and Is Inversely Associated with Peripapillary Choroidal Thickness in Healthy Eyes

Wang et al, AJO 2020

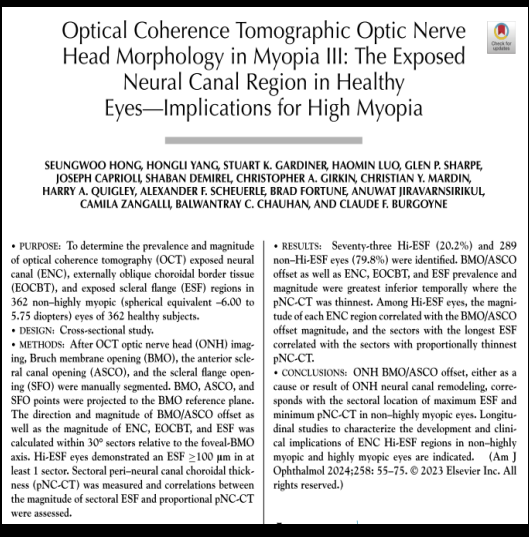

Optical Coherence Tomographic Optic Nerve Head Morphology in Myopia III: The Exposed Neural Canal Region in Healthy Eyes—Implications for High Myopia

Hong et al, AJO 2024

Burgoyne–2024 Goldmann–GRS Website

FoBMO Deep ONH/pNC OCT Structural Phenotyping – Detecting Glaucoma

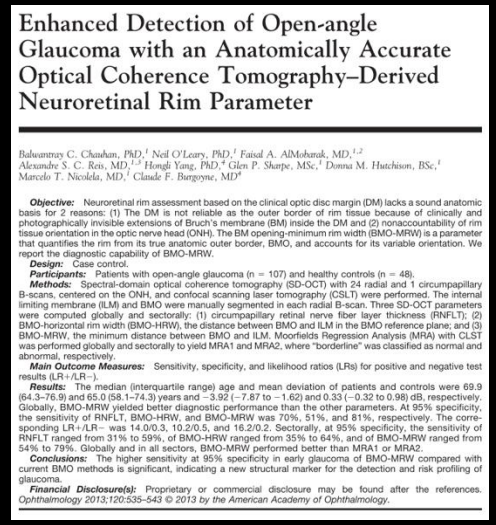

Enhanced Detection of Open-angle Glaucoma with an Anatomically Accurate Optical Coherence Tomography–Derived Neuroretinal Rim Parameter

Balwantray C. Chauhan, PhD,[1] Neil O'Leary, PhD,[1] Faisal A. AlMobarak, MD,[1,2] Alexandre S. C. Reis, MD,[1,3] Hongli Yang, PhD,[4] Glen P. Sharpe, MSc,[1] Donna M. Hutchison, BSc,[1] Marcelo T. Nicolela, MD,[1] Claude F. Burgoyne, MD[4]

Objective: Neuroretinal rim assessment based on the clinical optic disc margin (DM) lacks a sound anatomic basis for 2 reasons: (1) The DM is not reliable as the outer border of rim tissue because of clinically and photographically invisible extensions of Bruch's membrane (BM) inside the DM and (2) nonaccountability of rim tissue orientation in the optic nerve head (ONH). The BM opening-minimum rim width (BMO-MRW) is a parameter that quantifies the rim from its true anatomic outer border, BMO, and accounts for its variable orientation. We report the diagnostic capability of BMO-MRW.

Design: Case control.

Participants: Patients with open-angle glaucoma (n = 107) and healthy controls (n = 48).

Methods: Spectral-domain optical coherence tomography (SD-OCT) with 24 radial and 1 circumpapillary B-scans, centered on the ONH, and confocal scanning laser tomography (CSLT) were performed. The internal limiting membrane (ILM) and BMO were manually segmented in each radial B-scan. Three SD-OCT parameters were computed globally and sectorally: (1) circumpapillary retinal nerve fiber layer thickness (RNFLT); (2) BMO-horizontal rim width (BMO-HRW), the distance between BMO and ILM in the BMO reference plane; and (3) BMO-MRW, the minimum distance between BMO and ILM. Moorfields Regression Analysis (MRA) with CLST was performed globally and sectorally to yield MRA1 and MRA2, where "borderline" was classified as normal and abnormal, respectively.

Main Outcome Measures: Sensitivity, specificity, and likelihood ratios (LRs) for positive and negative test results (LR+/LR−).

Results: The median (interquartile range) age and mean deviation of patients and controls were 69.9 (64.3–76.9) and 65.0 (58.1–74.3) years and −3.92 (−7.87 to −1.62) and 0.33 (−0.32 to 0.98) dB, respectively. Globally, BMO-MRW yielded better diagnostic performance than the other parameters. At 95% specificity, the sensitivity of RNFLT, BMO-HRW, and BMO-MRW was 70%, 51%, and 81%, respectively. The corresponding LR+/LR− was 14.0/0.3, 10.2/0.5, and 16.2/0.2. Sectorally, at 95% specificity, the sensitivity of RNFLT ranged from 31% to 59%, of BMO-HRW ranged from 35% to 64%, and of BMO-MRW ranged from 54% to 79%. Globally and in all sectors, BMO-MRW performed better than MRA1 or MRA2.

Conclusions: The higher sensitivity at 95% specificity in early glaucoma of BMO-MRW compared with current BMO methods is significant, indicating a new structural marker for the detection and risk profiling of glaucoma.

Financial Disclosure(s): Proprietary or commercial disclosure may be found after the references.
Ophthalmology 2013;120:535–543 © 2013 by the American Academy of Ophthalmology.

Chauhan et al, Ophthalmology 2013

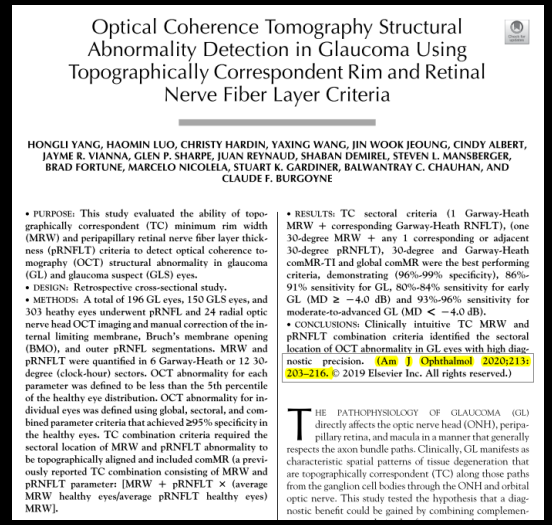

Optical Coherence Tomography Structural Abnormality Detection in Glaucoma Using Topographically Correspondent Rim and Retinal Nerve Fiber Layer Criteria

HONGLI YANG, HAOMIN LUO, CHRISTY HARDIN, YAXING WANG, JIN WOOK JEOUNG, CINDY ALBERT, JAYME R. VIANNA, GLEN P. SHARPE, JUAN REYNAUD, SHABAN DEMIREL, STEVEN L. MANSBERGER, BRAD FORTUNE, MARCELO NICOLELA, STUART K. GARDINER, BALWANTRAY C. CHAUHAN, AND CLAUDE F. BURGOYNE

• PURPOSE: This study evaluated the ability of topographically correspondent (TC) minimum rim width (MRW) and peripapillary retinal nerve fiber layer thickness (pRNFLT) criteria to detect optical coherence tomography (OCT) structural abnormality in glaucoma (GL) and glaucoma suspect (GLS) eyes.
• DESIGN: Retrospective cross-sectional study.
• METHODS: A total of 196 GL eyes, 150 GLS eyes, and 303 healthy eyes underwent pRNFL and 24 radial optic nerve head OCT imaging and manual correction of the internal limiting membrane, Bruch's membrane opening (BMO), and outer pRNFL segmentations. MRW and pRNFLT were quantified in 6 Garway-Heath or 12 30-degree (clock-hour) sectors. OCT abnormality for each parameter was defined to be less than the 5th percentile of the healthy eye distribution. OCT abnormality for individual eyes was defined using global, sectoral, and combined parameter criteria that achieved ≥95% specificity in the healthy eyes. TC combination criteria required the sectoral location of MRW and pRNFLT abnormality to be topographically aligned and included comMR (a previously reported TC combination consisting of MRW and pRNFLT parameter: [MRW + pRNFLT × (average MRW healthy eyes/average pRNFLT healthy eyes) MRW].
• RESULTS: TC sectoral criteria (1 Garway-Heath MRW + corresponding Garway-Heath RNFLT), (one 30-degree MRW + any 1 corresponding or adjacent 30-degree pRNFLT), 30-degree and Garway-Heath comMR-TI and global comMR were the best performing criteria, demonstrating (96%-99% specificity), 86%-91% sensitivity for GL, 80%-84% sensitivity for early GL (MD ≥ −4.0 dB) and 93%-96% sensitivity for moderate-to-advanced GL (MD < −4.0 dB).
• CONCLUSIONS: Clinically intuitive TC MRW and pRNFLT combination criteria identified the sectoral location of OCT abnormality in GL eyes with high diagnostic precision. (Am J Ophthalmol 2020;213:203–216. © 2019 Elsevier Inc. All rights reserved.)

THE PATHOPHYSIOLOGY OF GLAUCOMA (GL) directly affects the optic nerve head (ONH), peripapillary retina, and macula in a manner that generally respects the axon bundle paths. Clinically, GL manifests as characteristic spatial patterns of tissue degeneration that are topographically correspondent (TC) along those paths from the ganglion cell bodies through the ONH and orbital optic nerve. This study tested the hypothesis that a diagnostic benefit could be gained by combining complemen-

Yang et al, AJO 2010

FoBMO Deep ONH/pNC OCT Structural Phenotyping – Detecting Myopic Remodeling

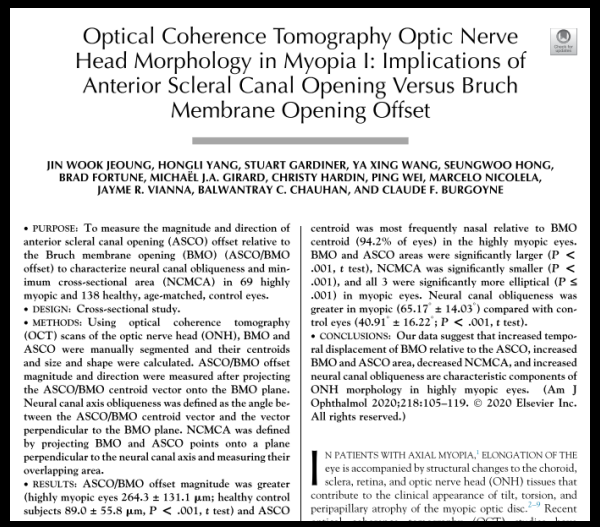

Optical Coherence Tomography Optic Nerve Head Morphology in Myopia I: Implications of Anterior Scleral Canal Opening Versus Bruch Membrane Opening Offset

JIN WOOK JEOUNG, HONGLI YANG, STUART GARDINER, YA XING WANG, SEUNGWOO HONG, BRAD FORTUNE, MICHAËL J.A. GIRARD, CHRISTY HARDIN, PING WEI, MARCELO NICOLELA, JAYME R. VIANNA, BALWANTRAY C. CHAUHAN, AND CLAUDE F. BURGOYNE

• PURPOSE: To measure the magnitude and direction of anterior scleral canal opening (ASCO) offset relative to the Bruch membrane opening (BMO) (ASCO/BMO offset) to characterize neural canal obliqueness and minimum cross-sectional area (NCMCA) in 69 highly myopic and 138 healthy, age-matched, control eyes.
• DESIGN: Cross-sectional study.
• METHODS: Using optical coherence tomography (OCT) scans of the optic nerve head (ONH), BMO and ASCO were manually segmented and their centroids and size and shape were calculated. ASCO/BMO offset magnitude and direction were measured after projecting the ASCO/BMO centroid vector onto the BMO plane. Neural canal axis obliqueness was defined as the angle between the ASCO/BMO centroid vector and the vector perpendicular to the BMO plane. NCMCA was defined by projecting BMO and ASCO points onto a plane perpendicular to the neural canal axis and measuring their overlapping area.
• RESULTS: ASCO/BMO offset magnitude was greater (highly myopic eyes 264.3 ± 131.1 μm; healthy control subjects 89.0 ± 55.8 μm, $P < .001$, t test) and ASCO centroid was most frequently nasal relative to BMO centroid (94.2% of eyes) in the highly myopic eyes. BMO and ASCO areas were significantly larger ($P < .001$, t test), NCMCA was significantly smaller ($P < .001$), and all 3 were significantly more elliptical ($P \leq .001$) in myopic eyes. Neural canal obliqueness was greater in myopic (65.17° ± 14.03°) compared with control eyes (40.91° ± 16.22°; $P < .001$, t test).
• CONCLUSIONS: Our data suggest that increased temporal displacement of BMO relative to the ASCO, increased BMO and ASCO area, decreased NCMCA, and increased neural canal obliqueness are characteristic components of ONH morphology in highly myopic eyes. (Am J Ophthalmol 2020;218:105–119. © 2020 Elsevier Inc. All rights reserved.)

IN PATIENTS WITH AXIAL MYOPIA,[1] ELONGATION OF THE eye is accompanied by structural changes to the choroid, sclera, retina, and optic nerve head (ONH) tissues that contribute to the clinical appearance of tilt, torsion, and peripapillary atrophy of the myopic optic disc.[2–9] Recent

Jeoung et al, AJO 2020

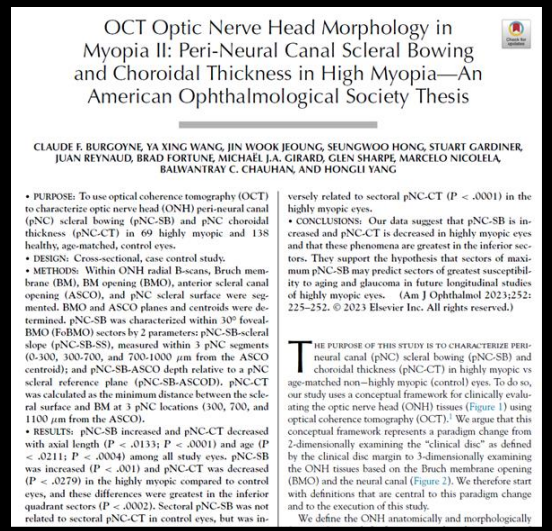

OCT Optic Nerve Head Morphology in Myopia II: Peri-Neural Canal Scleral Bowing and Choroidal Thickness in High Myopia—An American Ophthalmological Society Thesis

CLAUDE F. BURGOYNE, YA XING WANG, JIN WOOK JEOUNG, SEUNGWOO HONG, STUART GARDINER, JUAN REYNAUD, BRAD FORTUNE, MICHAËL J.A. GIRARD, GLEN SHARPE, MARCELO NICOLELA, BALWANTRAY C. CHAUHAN, AND HONGLI YANG

• PURPOSE: To use optical coherence tomography (OCT) to characterize optic nerve head (ONH) peri-neural canal (pNC) scleral bowing (pNC-SB) and pNC choroidal thickness (pNC-CT) in 69 highly myopic and 138 healthy, age-matched, control eyes.
• DESIGN: Cross-sectional, case control study.
• METHODS: Within ONH radial B-scans, Bruch membrane (BM), BM opening (BMO), anterior scleral canal opening (ASCO), and pNC scleral surface were segmented. BMO and ASCO planes and centroids were determined. pNC-SB was characterized within 30° foveal-BMO (FoBMO) sectors by 2 parameters: pNC-SB-scleral slope (pNC-SB-SS), measured within 3 pNC segments (0-300, 300-700, and 700-1000 μm from the ASCO centroid); and pNC-SB-ASCO depth relative to a pNC scleral reference plane (pNC-SB-ASCOD). pNC-CT was calculated as the minimum distance between the scleral surface and BM at 3 pNC locations (300, 700, and 1100 μm from the ASCO).
• RESULTS: pNC-SB increased and pNC-CT decreased with axial length ($P < .0133$; $P < .0001$) and age ($P < .0211$; $P < .0004$) among all study eyes. pNC-SB was increased ($P < .001$) and pNC-CT was decreased ($P < .0279$) in the highly myopic compared to control eyes, and these differences were greatest in the inferior quadrant sectors ($P < .0002$). Sectoral pNC-SB was not related to sectoral pNC-CT in control eyes, but was inversely related to sectoral pNC-CT ($P < .0001$) in the highly myopic eyes.
• CONCLUSIONS: Our data suggest that pNC-SB is increased and pNC-CT is decreased in highly myopic eyes and that these phenomena are greatest in the inferior sectors. They support the hypothesis that sectors of maximum pNC-SB may predict sectors of greatest susceptibility to aging and glaucoma in future longitudinal studies of highly myopic eyes. (Am J Ophthalmol 2023;252:225–252. © 2023 Elsevier Inc. All rights reserved.)

THE PURPOSE OF THIS STUDY IS TO CHARACTERIZE PERIneural canal (pNC) scleral bowing (pNC-SB) and choroidal thickness (pNC-CT) in highly myopic vs age-matched non–highly myopic (control) eyes. To do so, our study uses a conceptual framework for clinically evaluating the optic nerve head (ONH) tissues (Figure 1) using optical coherence tomography (OCT).[1] We argue that this conceptual framework represents a paradigm change from 2-dimensionally examining the "clinical disc" as defined by the clinical disc margin to 3-dimensionally examining the ONH tissues based on the Bruch membrane opening (BMO) and the neural canal (Figure 2). We therefore start with definitions that are central to this paradigm change and to the execution of this study.

We define the ONH anatomically and morphologically

Burgoyne et al. AJO. 2023

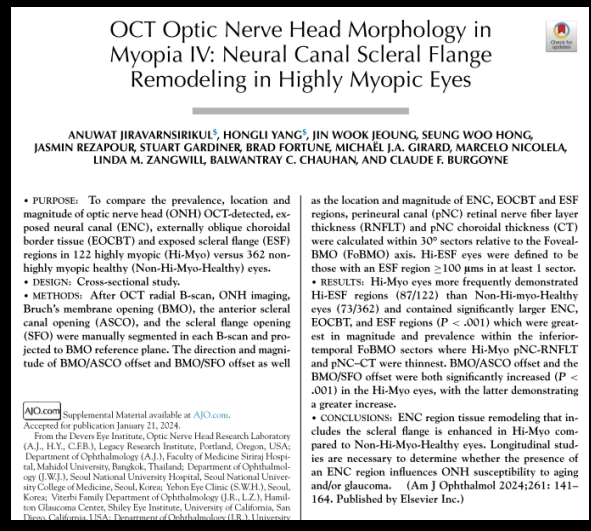

OCT Optic Nerve Head Morphology in Myopia IV: Neural Canal Scleral Flange Remodeling in Highly Myopic Eyes

ANUWAT JIRAVARNSIRIKUL[$], HONGLI YANG[$], JIN WOOK JEOUNG, SEUNG WOO HONG, JASMIN REZAPOUR, STUART GARDINER, BRAD FORTUNE, MICHAËL J.A. GIRARD, MARCELO NICOLELA, LINDA M. ZANGWILL, BALWANTRAY C. CHAUHAN, AND CLAUDE F. BURGOYNE

• PURPOSE: To compare the prevalence, location and magnitude of optic nerve head (ONH) OCT-detected, exposed neural canal (ENC), externally oblique choroidal border tissue (EOCBT) and exposed scleral flange (ESF) regions in 122 highly myopic (Hi-Myo) versus 362 non-highly myopic healthy (Non-Hi-Myo-Healthy) eyes.
• DESIGN: Cross-sectional study.
• METHODS: After OCT radial B-scan, ONH imaging, Bruch's membrane opening (BMO), the anterior scleral canal opening (ASCO), and the scleral flange opening (SFO) were manually segmented in each B-scan and projected to BMO reference plane. The direction and magnitude of BMO/ASCO offset and BMO/SFO offset as well as the location and magnitude of ENC, EOCBT and ESF regions, perineural canal (pNC) retinal nerve fiber layer thickness (RNFLT) and pNC choroidal thickness (CT) were calculated within 30° sectors relative to the Foveal-BMO (FoBMO) axis. Hi-ESF eyes were defined to be those with an ESF region ≥100 μms in at least 1 sector.
• RESULTS: Hi-Myo eyes more frequently demonstrated Hi-ESF regions (87/122) than Non-Hi-myo-Healthy eyes (73/362) and contained significantly larger ENC, EOCBT, and ESF regions ($P < .001$) which were greatest in magnitude and prevalence within the inferior-temporal FoBMO sectors where Hi-Myo pNC-RNFLT and pNC–CT were thinnest. BMO/ASCO offset and the BMO/SFO offset were both significantly increased ($P < .001$) in the Hi-Myo eyes, with the latter demonstrating a greater increase.
• CONCLUSIONS: ENC region tissue remodeling that includes the scleral flange is enhanced in Hi-Myo compared to Non-Hi-Myo-Healthy eyes. Longitudinal studies are necessary to determine whether the presence of an ENC region influences ONH susceptibility to aging and/or glaucoma. (Am J Ophthalmol 2024;261:141–164. Published by Elsevier Inc.)

AJO.com Supplemental Material available at AJO.com.

Accepted for publication January 21, 2024.

From the Devers Eye Institute, Optic Nerve Head Research Laboratory (A.J., H.Y., C.F.B.), Legacy Research Institute, Portland, Oregon, USA; Department of Ophthalmology (A.J.), Faculty of Medicine Siriraj Hospital, Mahidol University, Bangkok, Thailand; Department of Ophthalmology (J.W.J.), Seoul National University Hospital, Seoul National University College of Medicine, Seoul, Korea; Yebon Eye Clinic (S.W.H.), Seoul, Korea; Viterbi Family Department of Ophthalmology (J.R., L.Z.), Hamilton Glaucoma Center, Shiley Eye Institute, University of California, San Diego, California, USA; Department of Ophthalmology (J.R.), University

Jiravarnsirikul et al, AJO 2024

OCT Structural Abnormality in High Myopia and Glaucoma

Glaucoma/Myopia OCT Phenotyping Consortium (GMOPC)

Cohort 1	Cohort 2	Cohort 3
Highly Myopic	*Highly Myopic*	*Non-Highly Myopic*
<u>without</u> GL	*<u>with</u> GL*	*<u>early</u> GL*

Balwantray Chauhan, PhD
GMOPC Co-Principal Investigator
Clinical Review Reading Center Director
Mathers Professor of Ophthalmology
Dalhousie University

Linda Zangwill, PhD
GMOPC Co-Principal Investigator
OCT Reading Center Director
Richard K. Lansche M.D. and Tatiana A. Lansche Endowed Professor
University of California – San Diego

Claude Burgoyne, MD
Past - GMOPC Principal Investigator
OCT Anatomy/Morphology Consultation
Van Buskirk Chair for Ophthalmic Research
Devers Eye Institute

The GMOPC is an Investigator Initiated Study which includes Heidelberg Engineering as an Industry partner

Outline

- Professor Hans Goldmann
- Disclosures and Acknowledgements
- Revisiting 3D Optic Nerve Head Anatomy and Morphology
- The Optic Nerve Head in Glaucoma
- What Defines a Glaucomatous Optic Neuropathy?
- 3D Histomorphometric Structural Phenotyping in Monkey Glaucoma
- 3D OCT Structural Phenotyping in Monkey and Human Glaucoma
- Our qIHC / *3D* SBEM Cellular Mechanism Studies in Monkey Early EG
- Summary / Implications
- A Final Acknowledgement

Our work first focused on laminar connective tissue remodeling and co-incident myelin disruption

Glaucoma

Optic Nerve Head Myelin-Related Protein, GFAP, and Iba1 Alterations in Non-Human Primates With Early to Moderate Experimental Glaucoma

Priya Chaudhary,[1,2] Cheri Stowell,[1,2] Juan Reynaud,[1,2] Stuart K. Gardiner,[2] Hongli Yang,[1,2] Galen Williams,[1,2] Imee Williams,[1,2] Nicholas Marsh-Armstrong,[3] and Claude F. Burgoyne[1,2]

[1]Optic Nerve Head Research Laboratory, Devers Eye Institute, Legacy Research Institute, Portland, Oregon, United States
[2]Discoveries in Sight, Devers Eye Institute, Legacy Research Institute, Portland, Oregon, United States
[3]Department of Ophthalmology, University of California - Davis, California, United States

Correspondence: Claude F. Burgoyne, Optic Nerve Head Research Laboratory, Devers Eye Institute, Legacy Research Institute, 1225 NE 2nd Avenue, Portland, OR 97232, USA;
cfburgoyne@deverseye.org.

Received: May 17, 2022
Accepted: September 8, 2022
Published: October 14, 2022

Citation: Chaudhary P, Stowell C, Reynaud J, et al. Optic nerve head myelin-related protein, GFAP, and Iba1 alterations in non-human primates with early to moderate experimental glaucoma. *Invest Ophthalmol Vis Sci.* 2022;63(11):9. https://doi.org/10.1167/iovs.63.11.9

Purpose. The purpose of this study was to test if optic nerve head (ONH) myelin basic protein (MBP), 2′,3′-cyclic nucleotide 3′-phosphodiesterase (CNPase), glial fibrillary acidic protein (GFAP), and ionized calcium binding adaptor molecule 1 (Iba1) proteins are altered in non-human primate (NHP) early/moderate experimental glaucoma (EG).

Methods. Following paraformaldehyde perfusion, control and EG eye ONH tissues from four NHPs were paraffin embedded and serially (5 µm) vertically sectioned. Anti-MBP, CNPase, GFAP, Iba1, and nuclear dye-stained sections were imaged using sub-saturating light intensities. Whole-section images were segmented creating anatomically consistent laminar (L) and retrolaminar (RL) regions/sub-regions. EG versus control eye intensity/pixel-cluster density data within L and two RL regions (RL1 [1-250 µm]/RL2 [251-500 µm] from L) were compared using random effects models within the statistical program "R."

Results. EG eye retinal nerve fiber loss ranged from 0% to 20%. EG eyes' MBP and CNPase intensity were decreased within the RL1 (MBP = 31.4%, $P < 0.001$; CNPase =62.3%, $P < 0.001$) and RL2 (MBP = 19.6%, $P < 0.001$; CNPase = 56.1%, $P = 0.0004$) regions. EG eye GFAP intensity was decreased in the L (41.6%, $P < 0.001$) and RL regions (26.7% for RL1, and 28.4% for RL2, both $P < 0.001$). Iba1+ and NucBlue pixel-cluster density were increased in the laminar (28.2%, $P = 0.03$ and 16.6%, $P = 0.008$) and both RL regions (RL1 = 37.3%, $P = 0.01$ and 23.7%, $P = 0.0002$; RL2 = 53.7%, $P = 0.002$ and 33.2%, $P < 0.001$).

Conclusions. Retrolaminar myelin disruption occurs early in NHP EG and may be accompanied by laminar and retrolaminar decreases in astrocyte process labeling and increases in microglial/ macrophage density. The mechanistic and therapeutic implications of these findings warrant further study.

Keywords: immunohistochemistry, optic nerve head (ONH), lamina cribrosa, myelin, microglia, macrophages, monkey, experimental glaucoma (EG), astrocytes

Quantitative IHC

Glaucoma

Retrolaminar Demyelination of Structurally Intact Axons in Nonhuman Primate Experimental Glaucoma

Priya Chaudhary,[1,2] Howard Lockwood,[1,2] Cheri Stowell,[1,2] Eric Bushong,[3] Juan Reynaud,[1,2] Hongli Yang,[1,2] Stuart K. Gardiner,[2] Galen Wiliams,[1,2] Imee Williams,[1,2] Mark Ellisman,[3] Nick Marsh-Armstrong,[4] and Claude Burgoyne[1,2]

[1]Optic Nerve Head Research Laboratory, Legacy Devers Eye Institute, Legacy Research Institute, Portland, Oregon, United States
[2]Discoveries in Sight, Devers Eye Institute, Legacy Research Institute, Portland, Oregon, United States
[3]National Center for Microscopy & Imaging Research, UCSD, La Jolla, California, United States
[4]Department of Ophthalmology, University of California, Davis, California, United States

Correspondence: Claude F. Burgoyne, Optic Nerve Head Research Laboratory, Devers Eye Institute, Legacy Research Institute, 1225 NE 2nd Avenue, Portland, OR 97232, USA;
cfburgoyne@deverseye.org.

Received: November 2, 2023
Accepted: January 28, 2024
Published: February 26, 2024

Citation: Chaudhary P, Lockwood H, Stowell C, et al. Retrolaminar demyelination of structurally intact axons in nonhuman primate experimental glaucoma. *Invest Ophthalmol Vis Sci.* 2024;65(2):36. https://doi.org/10.1167/iovs.65.2.36

Purpose. To determine if structurally intact, retrolaminar optic nerve (RON) axons are demyelinated in nonhuman primate (NHP) experimental glaucoma (EG).

Methods. Unilateral EG NHPs ($n = 3$) were perfusion fixed, EG and control eyes were enucleated, and foveal Bruch's membrane opening (FoBMO) 30° sectoral axon counts were estimated. Optic nerve heads were trephined; serial vibratome sections (VSs) were imaged and colocalized to a fundus photograph establishing their FoBMO location. The peripheral neural canal region within $n = 5$ EG versus control eye VS comparisons was targeted for scanning block-face electron microscopic reconstruction (SBEMR) using micro–computed tomographic reconstructions (µCTRs) of each VS. Posterior laminar beams within each µCTR were segmented, allowing a best-fit posterior laminar surface (PLS) to be colocalized into its respective SBEMR. Within each SBEMR, up to 300 axons were randomly traced until they ended (nonintact) or left the block (intact). For each intact axon, myelin onset was identified and myelin onset distance (MOD) was measured relative to the PLS. For each EG versus control SBEMR comparison, survival analyses compared EG and control MOD.

Results. MOD calculations were successful in three EG and five control eye SBEMRs. Within each SBEMR comparison, EG versus control eye axon loss was −32.9%, −8.3%, and −15.2% (respectively), and MOD was increased in the EG versus control SBEMR ($P < 0.0001$ for each EG versus control SBEMR comparison). When data from all three EG eye SBEMRs were compared to all five control eye SBEMRs, MOD was increased within the EG eyes.

Conclusions. Structurally intact, RON axons are demyelinated in NHP early to moderate EG. Studies to determine their functional status are indicated.

Keywords: serial block-face scanning electron microscopy, nonhuman primate, monkey, glaucoma, lamina cribrosa, myelin, demyelination

Quantitative *3D* SBEM

(scanning block-face electron microscopy)

Priya Chaudhary, PhD

Cheri Stowell, PhD

Nick Marsh-Armstrong, PhD

Mark Ellisman, PhD
Eric Bushong, PhD Generated all 3D SBEM Reconstructions

Our work first focused on laminar connective tissue remodeling and co-incident myelin disruption

Glaucoma

Optic Nerve Head Myelin-Related Protein, GFAP, and Iba1 Alterations in Non-Human Primates With Early to Moderate Experimental Glaucoma

Priya Chaudhary,[1,2] Cheri Stowell,[1,2] Juan Reynaud,[1,2] Stuart K. Gardiner,[2] Hongli Yang,[1,2] Galen Williams,[1,2] Imee Williams,[1,2] Nicholas Marsh-Armstrong,[3] and Claude F. Burgoyne[1,2]

[1]Optic Nerve Head Research Laboratory, Devers Eye Institute, Legacy Research Institute, Portland, Oregon, United States
[2]Discoveries in Sight, Devers Eye Institute, Legacy Research Institute, Portland, Oregon, United States
[3]Department of Ophthalmology, University of California - Davis, California, United States

Correspondence: Claude F. Burgoyne, Optic Nerve Head Research Laboratory, Devers Eye Institute, Legacy Research Institute, 1225 NE 2nd Avenue, Portland, OR 97232, USA;
cfburgoyne@deverseye.org.

Received: May 17, 2022
Accepted: September 8, 2022
Published: October 14, 2022

Citation: Chaudhary P, Stowell C, Reynaud J, et al. Optic nerve head myelin-related protein, GFAP, and Iba1 alterations in non-human primates with early to moderate experimental glaucoma. *Invest Ophthalmol Vis Sci.* 2022;63(11):9. https://doi.org/10.1167/iovs.63.11.9

Purpose. The purpose of this study was to test if optic nerve head (ONH) myelin basic protein (MBP), 2′,3′-cyclic nucleotide 3′-phosphodiesterase (CNPase), glial fibrillary acidic protein (GFAP), and ionized calcium binding adaptor molecule 1 (Iba1) proteins are altered in non-human primate (NHP) early/moderate experimental glaucoma (EG).

Methods. Following paraformaldehyde perfusion, control and EG eye ONH tissues from four NHPs were paraffin embedded and serially (5 µm) vertically sectioned. Anti-MBP, CNPase, GFAP, Iba1, and nuclear dye-stained sections were imaged using sub-saturating light intensities. Whole-section images were segmented creating anatomically consistent laminar (L) and retrolaminar (RL) regions/sub-regions. EG versus control eye intensity/pixel-cluster density data within L and two RL regions (RL1 [1-250 µm]/RL2 [251-500 µm] from L) were compared using random effects models within the statistical program "R."

Results. EG eye retinal nerve fiber loss ranged from 0% to 20%. EG eyes' MBP and CNPase intensity were decreased within the RL1 (MBP = 31.4%, $P < 0.001$; CNPase =62.3%, $P < 0.001$) and RL2 (MBP = 19.6%, $P < 0.001$; CNPase = 56.1%, $P = 0.0004$) regions. EG eye GFAP intensity was decreased in the L (41.6%, $P < 0.001$) and RL regions (26.7% for RL1, and 28.4% for RL2, both $P < 0.001$). Iba1+ and NucBlue pixel-cluster density were increased in the laminar (28.2%, $P = 0.03$ and 16.6%, $P = 0.008$) and both RL regions (RL1 = 37.3%, $P = 0.01$ and 23.7%, $P = 0.0002$; RL2 = 53.7%, $P = 0.002$ and 33.2%, $P < 0.001$).

Conclusions. Retrolaminar myelin disruption occurs early in NHP EG and may be accompanied by laminar and retrolaminar decreases in astrocyte process labeling and increases in microglial/ macrophage density. The mechanistic and therapeutic implications of these findings warrant further study.

Keywords: immunohistochemistry, optic nerve head (ONH), lamina cribrosa, myelin, microglia, macrophages, monkey, experimental glaucoma (EG), astrocytes

Quantitative IHC

Glaucoma

Retrolaminar Demyelination of Structurally Intact Axons in Nonhuman Primate Experimental Glaucoma

Priya Chaudhary,[1,2] Howard Lockwood,[1,2] Cheri Stowell,[1,2] Eric Bushong,[3] Juan Reynaud,[1,2] Hongli Yang,[1,2] Stuart K. Gardiner,[2] Galen Wiliams,[1,2] Imee Williams,[1,2] Mark Ellisman,[3] Nick Marsh-Armstrong,[4] and Claude Burgoyne[1,2]

[1]Optic Nerve Head Research Laboratory, Legacy Devers Eye Institute, Legacy Research Institute, Portland, Oregon, United States
[2]Discoveries in Sight, Devers Eye Institute, Legacy Research Institute, Portland, Oregon, United States
[3]National Center for Microscopy & Imaging Research, UCSD, La Jolla, California, United States
[4]Department of Ophthalmology, University of California, Davis, California, United States

Correspondence: Claude F. Burgoyne, Optic Nerve Head Research Laboratory, Devers Eye Institute, Legacy Research Institute, 1225 NE 2nd Avenue, Portland, OR 97232, USA;
cfburgoyne@deverseye.org.

Received: November 2, 2023
Accepted: January 28, 2024
Published: February 26, 2024

Citation: Chaudhary P, Lockwood H, Stowell C, et al. Retrolaminar demyelination of structurally intact axons in nonhuman primate experimental glaucoma. *Invest Ophthalmol Vis Sci.* 2024;65(2):36. https://doi.org/10.1167/iovs.65.2.36

Purpose. To determine if structurally intact, retrolaminar optic nerve (RON) axons are demyelinated in nonhuman primate (NHP) experimental glaucoma (EG).

Methods. Unilateral EG NHPs ($n = 3$) were perfusion fixed, EG and control eyes were enucleated, and foveal Bruch's membrane opening (FoBMO) 30° sectoral axon counts were estimated. Optic nerve heads were trephined; serial vibratome sections (VSs) were imaged and colocalized to a fundus photograph establishing their FoBMO location. The peripheral neural canal region within $n = 5$ EG versus control eye VS comparisons was targeted for scanning block-face electron microscopic reconstruction (SBEMR) using micro–computed tomographic reconstructions (µCTRs) of each VS. Posterior laminar beams within each µCTR were segmented, allowing a best-fit posterior laminar surface (PLS) to be colocalized into its respective SBEMR. Within each SBEMR, up to 300 axons were randomly traced until they ended (nonintact) or left the block (intact). For each intact axon, myelin onset was identified and myelin onset distance (MOD) was measured relative to the PLS. For each EG versus control SBEMR comparison, survival analyses compared EG and control MOD.

Results. MOD calculations were successful in three EG and five control eye SBEMRs. Within each SBEMR comparison, EG versus control eye axon loss was −32.9%, −8.3%, and −15.2% (respectively), and MOD was increased in the EG versus control SBEMR ($P < 0.0001$ for each EG versus control SBEMR comparison). When data from all three EG eye SBEMRs were compared to all five control eye SBEMRs, MOD was increased within the EG eyes.

Conclusions. Structurally intact, RON axons are demyelinated in NHP early to moderate EG. Studies to determine their functional status are indicated.

Keywords: serial block-face scanning electron microscopy, nonhuman primate, monkey, glaucoma, lamina cribrosa, myelin, demyelination

Quantitative *3D* SBEM

(scanning block-face electron microscopy)

Priya Chaudhary, PhD

Cheri Stowell, PhD

Nick Marsh-Armstrong, PhD

Mark Ellisman, PhD
Eric Bushong, PhD Generated all 3D SBEM Reconstructions

Our work first focused on laminar connective tissue remodeling and co-incident myelin disruption

Glaucoma

Optic Nerve Head Myelin-Related Protein, GFAP, and Iba1 Alterations in Non-Human Primates With Early to Moderate Experimental Glaucoma

Priya Chaudhary,[1,2] Cheri Stowell,[1,2] Juan Reynaud,[1,2] Stuart K. Gardiner,[2] Hongli Yang,[1,2] Galen Williams,[1,2] Imee Williams,[1,2] Nicholas Marsh-Armstrong,[3] and Claude F. Burgoyne[1,2]

[1]Optic Nerve Head Research Laboratory, Devers Eye Institute, Legacy Research Institute, Portland, Oregon, United States
[2]Discoveries in Sight, Devers Eye Institute, Legacy Research Institute, Portland, Oregon, United States
[3]Department of Ophthalmology, University of California - Davis, California, United States

Correspondence: Claude F. Burgoyne, Optic Nerve Head Research Laboratory, Devers Eye Institute, Legacy Research Institute, 1225 NE 2nd Avenue, Portland, OR 97232, USA;
cfburgoyne@deverseye.org.

Received: May 17, 2022
Accepted: September 8, 2022
Published: October 14, 2022

Citation: Chaudhary P, Stowell C, Reynaud J, et al. Optic nerve head myelin-related protein, GFAP, and Iba1 alterations in non-human primates with early to moderate experimental glaucoma. *Invest Ophthalmol Vis Sci.* 2022;63(11):9. https://doi.org/10.1167/iovs.63.11.9

Purpose. The purpose of this study was to test if optic nerve head (ONH) myelin basic protein (MBP), 2′,3′-cyclic nucleotide 3′-phosphodiesterase (CNPase), glial fibrillary acidic protein (GFAP), and ionized calcium binding adaptor molecule 1 (Iba1) proteins are altered in non-human primate (NHP) early/moderate experimental glaucoma (EG).

Methods. Following paraformaldehyde perfusion, control and EG eye ONH tissues from four NHPs were paraffin embedded and serially (5 µm) vertically sectioned. Anti-MBP, CNPase, GFAP, Iba1, and nuclear dye-stained sections were imaged using sub-saturating light intensities. Whole-section images were segmented creating anatomically consistent laminar (L) and retrolaminar (RL) regions/sub-regions. EG versus control eye intensity/pixel-cluster density data within L and two RL regions (RL1 [1-250 µm]/RL2 [251-500 µm] from L) were compared using random effects models within the statistical program "R."

Results. EG eye retinal nerve fiber loss ranged from 0% to 20%. EG eyes' MBP and CNPase intensity were decreased within the RL1 (MBP = 31.4%, $P < 0.001$; CNPase =62.3%, $P < 0.001$) and RL2 (MBP = 19.6%, $P < 0.001$; CNPase = 56.1%, $P = 0.0004$) regions. EG eye GFAP intensity was decreased in the L (41.6%, $P < 0.001$) and RL regions (26.7% for RL1, and 28.4% for RL2, both $P < 0.001$). Iba1+ and NucBlue pixel-cluster density were increased in the laminar (28.2%, $P = 0.03$ and 16.6%, $P = 0.008$) and both RL regions (RL1 = 37.3%, $P = 0.01$ and 23.7%, $P = 0.0002$; RL2 = 53.7%, $P = 0.002$ and 33.2%, $P < 0.001$).

Conclusions. Retrolaminar myelin disruption occurs early in NHP EG and may be accompanied by laminar and retrolaminar decreases in astrocyte process labeling and increases in microglial/ macrophage density. The mechanistic and therapeutic implications of these findings warrant further study.

Keywords: immunohistochemistry, optic nerve head (ONH), lamina cribrosa, myelin, microglia, macrophages, monkey, experimental glaucoma (EG), astrocytes

Quantitative IHC

Glaucoma

Retrolaminar Demyelination of Structurally Intact Axons in Nonhuman Primate Experimental Glaucoma

Priya Chaudhary,[1,2] Howard Lockwood,[1,2] Cheri Stowell,[1,2] Eric Bushong,[3] Juan Reynaud,[1,2] Hongli Yang,[1,2] Stuart K. Gardiner,[2] Galen Wiliams,[1,2] Imee Williams,[1,2] Mark Ellisman,[3] Nick Marsh-Armstrong,[4] and Claude Burgoyne[1,2]

[1]Optic Nerve Head Research Laboratory, Legacy Devers Eye Institute, Legacy Research Institute, Portland, Oregon, United States
[2]Discoveries in Sight, Devers Eye Institute, Legacy Research Institute, Portland, Oregon, United States
[3]National Center for Microscopy & Imaging Research, UCSD, La Jolla, California, United States
[4]Department of Ophthalmology, University of California, Davis, California, United States

Correspondence: Claude F. Burgoyne, Optic Nerve Head Research Laboratory, Devers Eye Institute, Legacy Research Institute, 1225 NE 2nd Avenue, Portland, OR 97232, USA;
cfburgoyne@deverseye.org.

Received: November 2, 2023
Accepted: January 28, 2024
Published: February 26, 2024

Citation: Chaudhary P, Lockwood H, Stowell C, et al. Retrolaminar demyelination of structurally intact axons in nonhuman primate experimental glaucoma. *Invest Ophthalmol Vis Sci.* 2024;65(2):36. https://doi.org/10.1167/iovs.65.2.36

Purpose. To determine if structurally intact, retrolaminar optic nerve (RON) axons are demyelinated in nonhuman primate (NHP) experimental glaucoma (EG).

Methods. Unilateral EG NHPs ($n = 3$) were perfusion fixed, EG and control eyes were enucleated, and foveal Bruch's membrane opening (FoBMO) 30° sectoral axon counts were estimated. Optic nerve heads were trephined; serial vibratome sections (VSs) were imaged and colocalized to a fundus photograph establishing their FoBMO location. The peripheral neural canal region within $n = 5$ EG versus control eye VS comparisons was targeted for scanning block-face electron microscopic reconstruction (SBEMR) using micro–computed tomographic reconstructions (µCTRs) of each VS. Posterior laminar beams within each µCTR were segmented, allowing a best-fit posterior laminar surface (PLS) to be colocalized into its respective SBEMR. Within each SBEMR, up to 300 axons were randomly traced until they ended (nonintact) or left the block (intact). For each intact axon, myelin onset was identified and myelin onset distance (MOD) was measured relative to the PLS. For each EG versus control SBEMR comparison, survival analyses compared EG and control MOD.

Results. MOD calculations were successful in three EG and five control eye SBEMRs. Within each SBEMR comparison, EG versus control eye axon loss was −32.9%, −8.3%, and −15.2% (respectively), and MOD was increased in the EG versus control SBEMR ($P < 0.0001$ for each EG versus control SBEMR comparison). When data from all three EG eye SBEMRs were compared to all five control eye SBEMRs, MOD was increased within the EG eyes.

Conclusions. Structurally intact, RON axons are demyelinated in NHP early to moderate EG. Studies to determine their functional status are indicated.

Keywords: serial block-face scanning electron microscopy, nonhuman primate, monkey, glaucoma, lamina cribrosa, myelin, demyelination

Quantitative *3D* SBEM

(scanning block-face electron microscopy)

Priya Chaudhary, PhD

Cheri Stowell, PhD

Nick Marsh-Armstrong, PhD

Mark Ellisman, PhD
Eric Bushong, PhD Generated all 3D SBEM Reconstructions

Using our 3D Laminar Reconstructions – Engineering finite element modeling suggested that the thickened lamina contained an increased number of laminar beams

Remodeling of the Connective Tissue Microarchitecture of the Lamina Cribrosa in Early Experimental Glaucoma

Michael D. Roberts,[1] Vicente Grau,[2] Jonathan Grimm,[3] Juan Reynaud,[3] Anthony J. Bellezza,[4] Claude F. Burgoyne,[3] and J. Crawford Downs[1]

Purpose. To characterize the trabeculated connective tissue microarchitecture of the lamina cribrosa (LC) in terms of total connective tissue volume (CTV), connective tissue volume fraction (CTVF), predominant beam orientation, and material anisotropy in monkeys with early experimental glaucoma (EG).

Methods. The optic nerve heads from three monkeys with unilateral EG and four bilaterally normal monkeys were three dimensionally reconstructed from tissues perfusion fixed at an intraocular pressure of 10 mm Hg. A three-dimensional segmentation algorithm was used to extract a binary, voxel-based representation of the porous LC connective tissue microstructure that was regionalized into 45 subvolumes, and the following quantities were calculated: total CTV within the LC, mean and regional CTVF, regional predominant beam orientation, and mean and regional material anisotropy.

Results. Regional variation within the laminar microstructure was considerable within the normal eyes of all monkeys. The laminar connective tissue was generally most dense in the central and superior regions for the paired normal eyes, and laminar beams were radially oriented at the periphery for all eyes considered. CTV increased substantially in EG eyes compared with contralateral normal eyes (82%, 44%, 45% increases; $P < 0.05$), but average CTVF changed little (−7%, 1%, and −2% in the EG eyes). There were more laminar beams through the thickness of the LC in the EG eyes than in the normal controls (46%, 18%, 17% increases).

Conclusions. The substantial increase in laminar CTV with little change in CTVF suggests that significant alterations in connective and nonconnective tissue components in the laminar region occur in the early stages of glaucomatous damage. (*Invest Ophthalmol Vis Sci.* 2009;50:681–690) DOI:10.1167/iovs.08-1792

A biomechanical paradigm for the development and progression of glaucoma has been proposed that posits that the load-bearing tissues of the lamina cribrosa (LC), peripapillary sclera, and sclera are central to the underlying pathogenesis of the disease and that the manner in which they bear and respond to load is an important component of susceptibility to glaucoma.[1,2] In this paradigm, the mechanical stress and strain borne by the load-bearing tissues of the posterior pole are of special interest because they link the tissue-level mechanical environment of the optic nerve head (ONH) to the intraocular pressure (IOP) in the eye. Thus, characterization of the geometric and material properties of the connective tissue structures in the LC is a necessary step for the quantification of tissue level changes caused by experimental perturbation of IOP and for the development of mathematical models to describe the mechanical environment to which the tissues are exposed.

The LC has been implicated as the primary site of axonal damage in glaucoma, with disruption of axoplasmic transport, impaired blood flow, and mechanically mediated tissue remodeling proposed as possible underlying etiological mechanisms.[2–6] Using the monkey model of experimental glaucoma (EG) and standard two-dimensional (2D) histology, we have previously shown that permanent posterior deformation and thickening of the LC occurs soon after the induction of chronic elevated IOP.[7] More recently, we developed a three-dimensional (3D) histomorphometric technique to quantify various aspects of ONH anatomy and structure.[8–10] We have used this technique to demonstrate significant morphologic changes in the neural canal, subarachnoid space, LC, peripapillary sclera, and prelaminar neural tissues in EG monkey eyes. These studies demonstrate that changes in connective tissue occur at the earliest stages of glaucomatous damage and provide supporting evidence for a biomechanical basis of the disease.

The arrangement of the connective tissue of the LC bears

Roberts et al, IOVS 2009

Mike Roberts, PhD

Crawford Downs, PhD

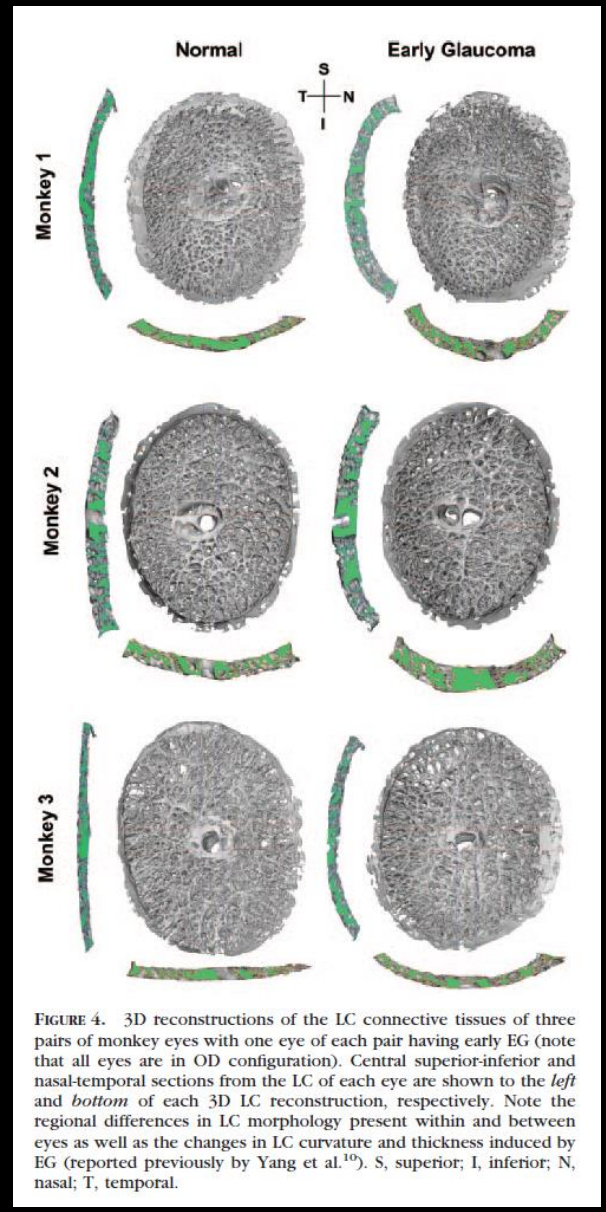

Figure 4. 3D reconstructions of the LC connective tissues of three pairs of monkey eyes with one eye of each pair having early EG (note that all eyes are in OD configuration). Central superior-inferior and nasal-temporal sections from the LC of each eye are shown to the *left* and *bottom* of each 3D LC reconstruction, respectively. Note the regional differences in LC morphology present within and between eyes as well as the changes in LC curvature and thickness induced by EG (reported previously by Yang et al.[10]). S, superior; I, inferior; N, nasal; T, temporal.

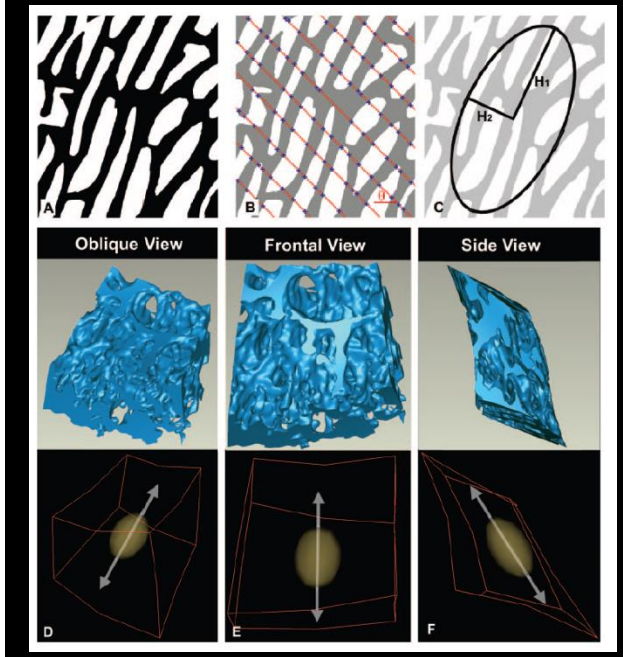

Burgoyne–2024 Goldmann–GRS Website

Laminar Thickening / Retrolaminar Septal Recruitment and Myelin Disruption

Remodeling of the Connective Tissue Microarchitecture of the Lamina Cribrosa in Early Experimental Glaucoma

Michael D. Roberts,[1] Vicente Grau,[2] Jonathan Grimm,[3] Juan Reynaud,[3] Anthony J. Bellezza,[4] Claude F. Burgoyne,[3] and J. Crawford Downs[1]

Purpose. To characterize the trabeculated connective tissue microarchitecture of the lamina cribrosa (LC) in terms of total connective tissue volume (CTV), connective tissue volume fraction (CTVF), predominant beam orientation, and material anisotropy in monkeys with early experimental glaucoma (EG).

Methods. The optic nerve heads from three monkeys with unilateral EG and four bilaterally normal monkeys were three dimensionally reconstructed from tissues perfusion fixed at an intraocular pressure of 10 mm Hg. A three-dimensional segmentation algorithm was used to extract a binary, voxel-based representation of the porous LC connective tissue microstructure that was regionalized into 45 subvolumes, and the following quantities were calculated: total CTV within the LC, mean and regional CTVF, regional predominant beam orientation, and mean and regional material anisotropy.

Results. Regional variation within the laminar microstructure was considerable within the normal eyes of all monkeys. The laminar connective tissue was generally most dense in the central and superior regions for the paired normal eyes, and laminar beams were radially oriented at the periphery for all eyes considered. CTV increased substantially in EG eyes compared with contralateral normal eyes (82%, 44%, 45% increases; $P < 0.05$), but average CTVF changed little (−7%, 1%, and −2% in the EG eyes). There were more laminar beams through the thickness of the LC in the EG eyes than in the normal controls (46%, 18%, 17% increases).

Conclusions. The substantial increase in laminar CTV with little change in CTVF suggests that significant alterations in connective and nonconnective tissue components in the laminar region occur in the early stages of glaucomatous damage. (*Invest Ophthalmol Vis Sci.* 2009;50:681–690) DOI:10.1167/iovs.08-1792

A biomechanical paradigm for the development and progression of glaucoma has been proposed that posits that the load-bearing tissues of the lamina cribrosa (LC), peripapillary sclera, and sclera are central to the underlying pathogenesis of the disease and that the manner in which they bear and respond to load is an important component of susceptibility to glaucoma.[1,2] In this paradigm, the mechanical stress and strain borne by the load-bearing tissues of the posterior pole are of special interest because they link the tissue-level mechanical environment of the optic nerve head (ONH) to the intraocular pressure (IOP) in the eye. Thus, characterization of the geometric and material properties of the connective tissue structures in the LC is a necessary step for the quantification of tissue level changes caused by experimental perturbation of IOP and for the development of mathematical models to describe the mechanical environment to which the tissues are exposed.

The LC has been implicated as the primary site of axonal damage in glaucoma, with disruption of axoplasmic transport, impaired blood flow, and mechanically mediated tissue remodeling proposed as possible underlying etiological mechanisms.[2–6] Using the monkey model of experimental glaucoma (EG) and standard two-dimensional (2D) histology, we have previously shown that permanent posterior deformation and thickening of the LC occurs soon after the induction of chronic elevated IOP.[7] More recently, we developed a three-dimensional (3D) histomorphometric technique to quantify various aspects of ONH anatomy and structure.[8–10] We have used this technique to demonstrate significant morphologic changes in the neural canal, subarachnoid space, LC, peripapillary sclera, and prelaminar neural tissues in EG monkey eyes. These studies demonstrate that changes in connective tissue occur at the earliest stages of glaucomatous damage and provide supporting evidence for a biomechanical basis of the disease.

The arrangement of the connective tissue of the LC bears

Roberts et al, IOVS 2009

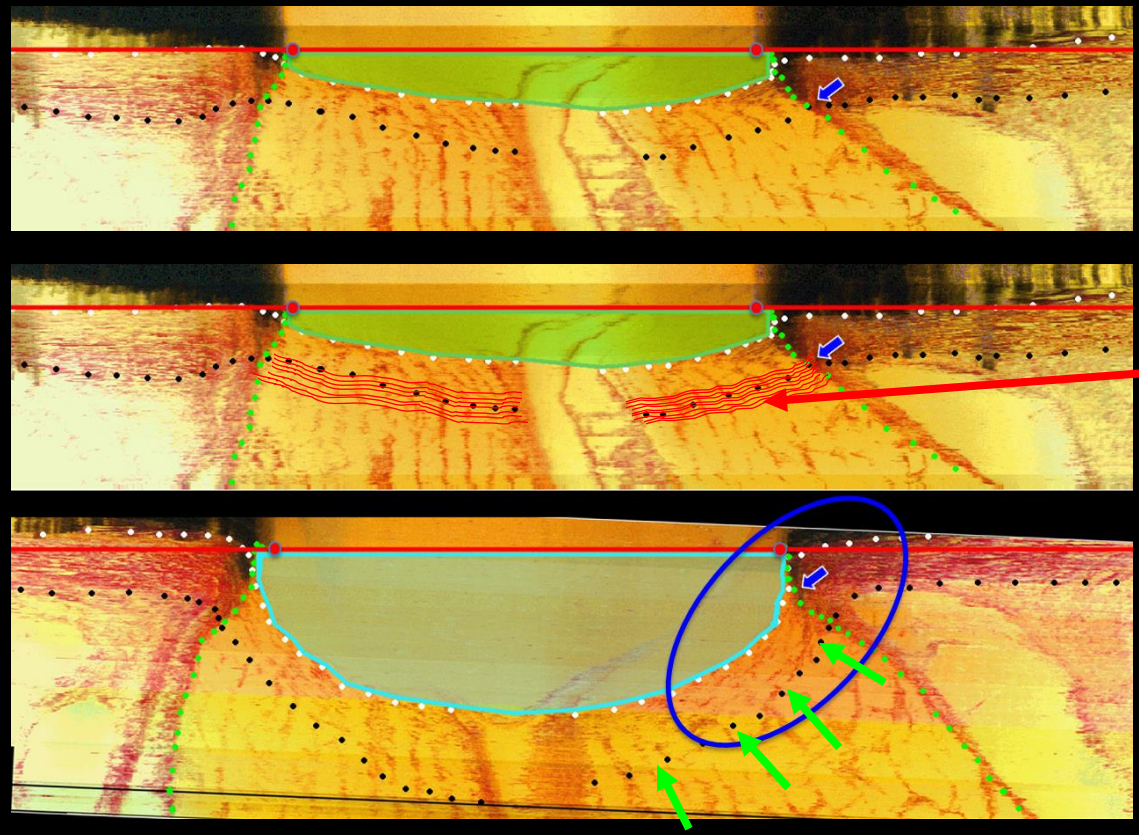

Healthy

Early Ocular HTN
Transverse Connectivity added to Longitudinal Retrolaminar Septa

Thickened and Migrated Lamina Cribrosa

Laminar Thickening / Retrolaminar Septal Recruitment and Myelin Disruption

Remodeling of the Connective Tissue Microarchitecture of the Lamina Cribrosa in Early Experimental Glaucoma

Michael D. Roberts,[1] Vicente Grau,[2] Jonathan Grimm,[3] Juan Reynaud,[3] Anthony J. Bellezza,[4] Claude F. Burgoyne,[3] and J. Crawford Downs[1]

Purpose. To characterize the trabeculated connective tissue microarchitecture of the lamina cribrosa (LC) in terms of total connective tissue volume (CTV), connective tissue volume fraction (CTVF), predominant beam orientation, and material anisotropy in monkeys with early experimental glaucoma (EG).

Methods. The optic nerve heads from three monkeys with unilateral EG and four bilaterally normal monkeys were three dimensionally reconstructed from tissues perfusion fixed at an intraocular pressure of 10 mm Hg. A three-dimensional segmentation algorithm was used to extract a binary, voxel-based representation of the porous LC connective tissue microstructure that was regionalized into 45 subvolumes, and the following quantities were calculated: total CTV within the LC, mean and regional CTVF, regional predominant beam orientation, and mean and regional material anisotropy.

Results. Regional variation within the laminar microstructure was considerable within the normal eyes of all monkeys. The laminar connective tissue was generally most dense in the central and superior regions for the paired normal eyes, and laminar beams were radially oriented at the periphery for all eyes considered. CTV increased substantially in EG eyes compared with contralateral normal eyes (82%, 44%, 45% increases; $P < 0.05$), but average CTVF changed little (−7%, 1%, and −2% in the EG eyes). There were more laminar beams through the thickness of the LC in the EG eyes than in the normal controls (46%, 18%, 17% increases).

Conclusions. The substantial increase in laminar CTV with little change in CTVF suggests that significant alterations in connective and nonconnective tissue components in the laminar region occur in the early stages of glaucomatous damage. (*Invest Ophthalmol Vis Sci.* 2009;50:681–690) DOI:10.1167/iovs.08-1792

A biomechanical paradigm for the development and progression of glaucoma has been proposed that posits that the load-bearing tissues of the lamina cribrosa (LC), peripapillary sclera, and sclera are central to the underlying pathogenesis of the disease and that the manner in which they bear and respond to load is an important component of susceptibility to glaucoma.[1,2] In this paradigm, the mechanical stress and strain borne by the load-bearing tissues of the posterior pole are of special interest because they link the tissue-level mechanical environment of the optic nerve head (ONH) to the intraocular pressure (IOP) in the eye. Thus, characterization of the geometric and material properties of the connective tissue structures in the LC is a necessary step for the quantification of tissue level changes caused by experimental perturbation of IOP and for the development of mathematical models to describe the mechanical environment to which the tissues are exposed.

The LC has been implicated as the primary site of axonal damage in glaucoma, with disruption of axoplasmic transport, impaired blood flow, and mechanically mediated tissue remodeling proposed as possible underlying etiological mechanisms.[2–6] Using the monkey model of experimental glaucoma (EG) and standard two-dimensional (2D) histology, we have previously shown that permanent posterior deformation and thickening of the LC occurs soon after the induction of chronic elevated IOP.[7] More recently, we developed a three-dimensional (3D) histomorphometric technique to quantify various aspects of ONH anatomy and structure.[8–10] We have used this technique to demonstrate significant morphologic changes in the neural canal, subarachnoid space, LC, peripapillary sclera, and prelaminar neural tissues in EG monkey eyes. These studies demonstrate that changes in connective tissue occur at the earliest stages of glaucomatous damage and provide supporting evidence for a biomechanical basis of the disease.

The arrangement of the connective tissue of the LC bears

Roberts et al, IOVS 2009

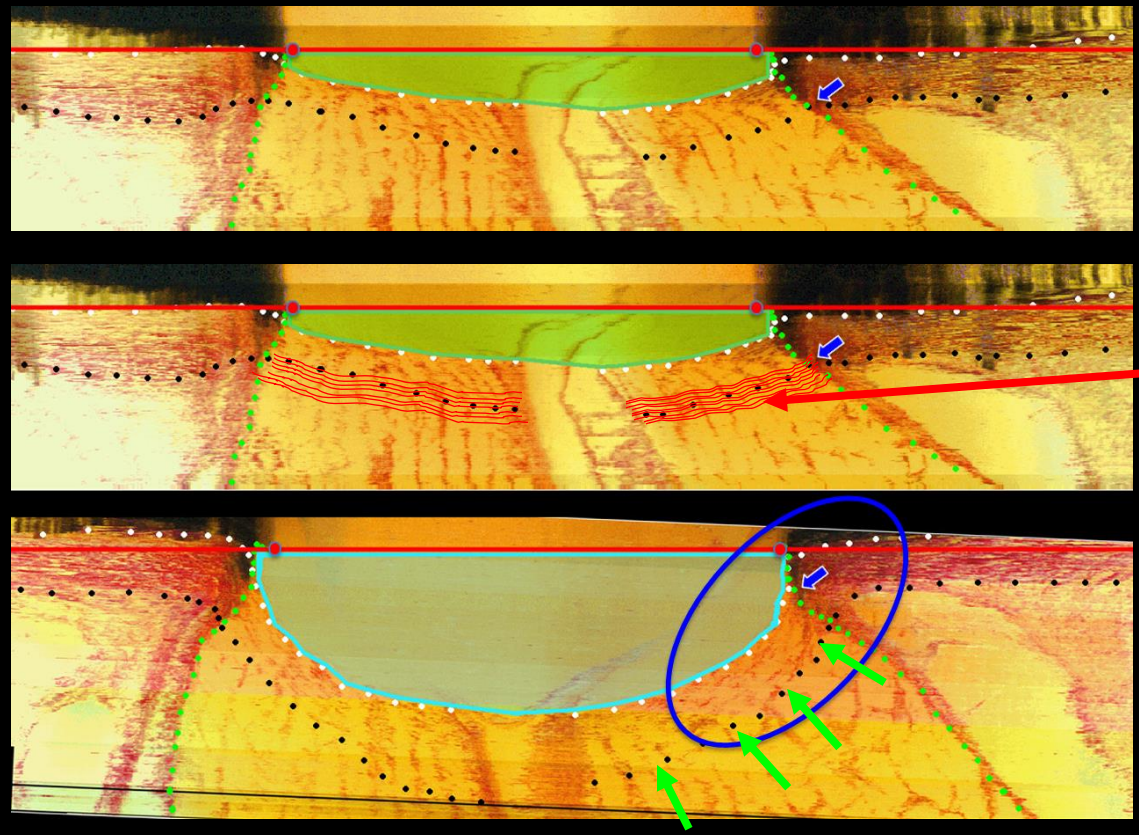

Healthy

Early Ocular HTN
Transverse Connectivity added to Longitudinal Retrolaminar Septa

Thickened and Migrated Lamina Cribrosa

If this occurs - does it disrupt retro-laminar myelin homeostasis

Quantitative IHC demonstrated retrolaminar myelin disruption in Early to Moderate NHP Experimental Glaucoma

Glaucoma

Optic Nerve Head Myelin-Related Protein, GFAP, and Iba1 Alterations in Non-Human Primates With Early to Moderate Experimental Glaucoma

Priya Chaudhary,[1,2] Cheri Stowell,[1,2] Juan Reynaud,[1,2] Stuart K. Gardiner,[2] Hongli Yang,[1,2] Galen Williams,[1,2] Imee Williams,[1,2] Nicholas Marsh-Armstrong,[3] and Claude F. Burgoyne[1,2]

[1]Optic Nerve Head Research Laboratory, Devers Eye Institute, Legacy Research Institute, Portland, Oregon, United States
[2]Discoveries in Sight, Devers Eye Institute, Legacy Research Institute, Portland, Oregon, United States
[3]Department of Ophthalmology, University of California - Davis, California, United States

Correspondence: Claude F. Burgoyne, Optic Nerve Head Research Laboratory, Devers Eye Institute, Legacy Research Institute, 1225 NE 2nd Avenue, Portland, OR 97232, USA; cfburgoyne@deverseye.org.

Received: May 17, 2022
Accepted: September 8, 2022
Published: October 14, 2022

Citation: Chaudhary P, Stowell C, Reynaud J, et al. Optic nerve head myelin-related protein, GFAP, and Iba1 alterations in non-human primates with early to moderate experimental glaucoma. *Invest Ophthalmol Vis Sci.* 2022;63(11):9. https://doi.org/10.1167/iovs.63.11.9

Purpose. The purpose of this study was to test if optic nerve head (ONH) myelin basic protein (MBP), 2′,3′-cyclic nucleotide 3′-phosphodiesterase (CNPase), glial fibrillary acidic protein (GFAP), and ionized calcium binding adaptor molecule 1 (Iba1) proteins are altered in non-human primate (NHP) early/moderate experimental glaucoma (EG).

Methods. Following paraformaldehyde perfusion, control and EG eye ONH tissues from four NHPs were paraffin embedded and serially (5 µm) vertically sectioned. Anti-MBP, CNPase, GFAP, Iba1, and nuclear dye-stained sections were imaged using sub-saturating light intensities. Whole-section images were segmented creating anatomically consistent laminar (L) and retrolaminar (RL) regions/sub-regions. EG versus control eye intensity/pixel-cluster density data within L and two RL regions (RL1 [1-250 µm]/RL2 [251-500 µm] from L) were compared using random effects models within the statistical program "R."

Results. EG eye retinal nerve fiber loss ranged from 0% to 20%. EG eyes' MBP and CNPase intensity were decreased within the RL1 (MBP = 31.4%, $P < 0.001$; CNPase =62.3%, $P < 0.001$) and RL2 (MBP = 19.6%, $P < 0.001$; CNPase = 56.1%, $P = 0.0004$) regions. EG eye GFAP intensity was decreased in the L (41.6%, $P < 0.001$) and RL regions (26.7% for RL1, and 28.4% for RL2, both $P < 0.001$). Iba1+ and NucBlue pixel-cluster density were increased in the laminar (28.2%, $P = 0.03$ and 16.6%, $P = 0.008$) and both RL regions (RL1 = 37.3%, $P = 0.01$ and 23.7%, $P = 0.0002$; RL2 = 53.7%, $P = 0.002$ and 33.2%, $P < 0.001$).

Conclusions. Retrolaminar myelin disruption occurs early in NHP EG and may be accompanied by laminar and retrolaminar decreases in astrocyte process labeling and increases in microglial/ macrophage density. The mechanistic and therapeutic implications of these findings warrant further study.

Keywords: immunohistochemistry, optic nerve head (ONH), lamina cribrosa, myelin, microglia, macrophages, monkey, experimental glaucoma (EG), astrocytes

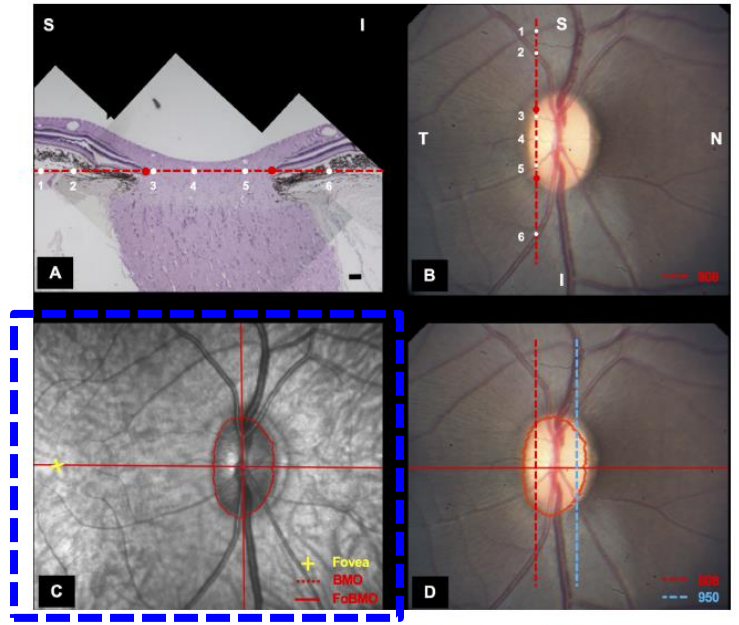

Figure 2. Estimating the clinical location of temporal and nasal "cardinal" ONH paraffin sections relative to the OCT foveal-BMO (FoBMO) axis. See the Methods section for our definition of the ONH and neural canal. (**A**) The temporal cardinal section (number 808 - *red dotted line* in panels **A**, **B**, and **D**) from the left (control) eye (shown in the right eye orientation) of NHP 3 was stained using hematoxylin and eosin (H&E) and the location of each blood vessel (6 *white circles* numbered 1 to 6 also in *white*) and BMO point (*red circles*) was identified and projected to the BMO reference line (*red dotted line* in panels **A**, **B**, and **D**). (**B**) The superior (S) versus inferior (I) orientation and temporal versus nasal location of the section (*red dotted line*) is estimated by adjusting the angle of the section line until the best fit of the BMO and vessel points (1 to 6 in *white* from panel **A**) to the photograph is accomplished. Estimating the location of a nasal cardinal section (section 950 – *blue dotted line* in panel **D**) was then performed in a similar manner. (**C**) The OCT-determined foveal to BMO centroid (FoBMO) axis as projected onto the infrared (IR) image acquired at the time of OCT image acquisition during the pre-euthanasia imaging session. (**D**) The location and orientation of the temporal (808) and nasal (950) cardinal tissue sections relative to the OCT-determined FoBMO axis is achieved by colocalizing the color fundus image containing their locations to the OCT IR image using the retinal vessels. The nasal/temporal position and S versus I orientation of each individual IHC section is then approximated relative to the cardinal sections by using the section number and fine-tuned using the vessel crossings and BMO points as outlined above.

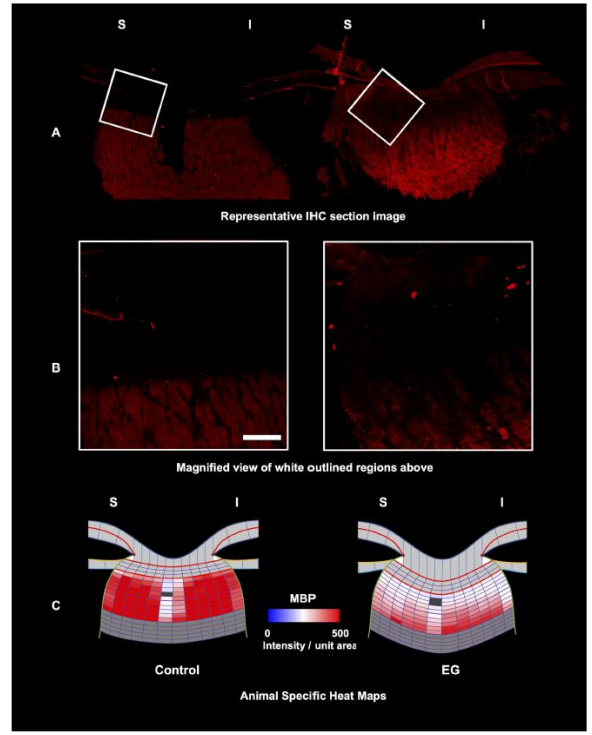

Figure 6. **MBP intensity decreased in the EG eye retrolaminar regions.** Representative control (*left*) and EG (*right*) eye single IHC section images (**A**, **B**) and animal-specific mean intensity heat maps (**C**) for MBP for NHP2. **A** Control and EG eye fluorescent full section images (see Fig. 3A for the clinical location of these sections), with magnified views of the white outlined regions shown in **B**. (**C**) MBP intensity heat maps for NHP2 based on mean data for four section images from each eye reveal diffuse qualitative decreases in both retrolaminar RL1 and RL2 subregions (see Fig. 3), which achieve significance by statistical analysis (see Table 2, Supplementary Table S1). *Dark grey* color denotes blood vessels.

Chaudhary et al, IOVS, 2022

Quantitative IHC

Burgoyne–2024 Goldmann–GRS Website

Quantitative IHC demonstrated retrolaminar myelin disruption in Early to Moderate NHP Experimental Glaucoma – so what???? Wouldn't we expect myelin to be disrupted if axons are degenerating????

Glaucoma

Optic Nerve Head Myelin-Related Protein, GFAP, and Iba1 Alterations in Non-Human Primates With Early to Moderate Experimental Glaucoma

Priya Chaudhary,[1,2] Cheri Stowell,[1,2] Juan Reynaud,[1,2] Stuart K. Gardiner,[2] Hongli Yang,[1,2] Galen Williams,[1,2] Imee Williams,[1,2] Nicholas Marsh-Armstrong,[3] and Claude F. Burgoyne[1,2]

[1]Optic Nerve Head Research Laboratory, Devers Eye Institute, Legacy Research Institute, Portland, Oregon, United States
[2]Discoveries in Sight, Devers Eye Institute, Legacy Research Institute, Portland, Oregon, United States
[3]Department of Ophthalmology, University of California - Davis, California, United States

Correspondence: Claude F. Burgoyne, Optic Nerve Head Research Laboratory, Devers Eye Institute, Legacy Research Institute, 1225 NE 2nd Avenue, Portland, OR 97232, USA;
cfburgoyne@deverseye.org.

Received: May 17, 2022
Accepted: September 8, 2022
Published: October 14, 2022

Citation: Chaudhary P, Stowell C, Reynaud J, et al. Optic nerve head myelin-related protein, GFAP, and Iba1 alterations in non-human primates with early to moderate experimental glaucoma. *Invest Ophthalmol Vis Sci.* 2022;63(11):9.
https://doi.org/10.1167/iovs.63.11.9

Purpose. The purpose of this study was to test if optic nerve head (ONH) myelin basic protein (MBP), 2′,3′-cyclic nucleotide 3′-phosphodiesterase (CNPase), glial fibrillary acidic protein (GFAP), and ionized calcium binding adaptor molecule 1 (Iba1) proteins are altered in non-human primate (NHP) early/moderate experimental glaucoma (EG).

Methods. Following paraformaldehyde perfusion, control and EG eye ONH tissues from four NHPs were paraffin embedded and serially (5 µm) vertically sectioned. Anti-MBP, CNPase, GFAP, Iba1, and nuclear dye-stained sections were imaged using sub-saturating light intensities. Whole-section images were segmented creating anatomically consistent laminar (L) and retrolaminar (RL) regions/sub-regions. EG versus control eye intensity/pixel-cluster density data within L and two RL regions (RL1 [1-250 µm]/RL2 [251-500 µm] from L) were compared using random effects models within the statistical program "R."

Results. EG eye retinal nerve fiber loss ranged from 0% to 20%. EG eyes' MBP and CNPase intensity were decreased within the RL1 (MBP = 31.4%, $P < 0.001$; CNPase =62.3%, $P < 0.001$) and RL2 (MBP = 19.6%, $P < 0.001$; CNPase = 56.1%, $P = 0.0004$) regions. EG eye GFAP intensity was decreased in the L (41.6%, $P < 0.001$) and RL regions (26.7% for RL1, and 28.4% for RL2, both $P < 0.001$). Iba1+ and NucBlue pixel-cluster density were increased in the laminar (28.2%, $P = 0.03$ and 16.6%, $P = 0.008$) and both RL regions (RL1 = 37.3%, $P = 0.01$ and 23.7%, $P = 0.0002$; RL2 = 53.7%, $P = 0.002$ and 33.2%, $P < 0.001$).

Conclusions. Retrolaminar myelin disruption occurs early in NHP EG and may be accompanied by laminar and retrolaminar decreases in astrocyte process labeling and increases in microglial/ macrophage density. The mechanistic and therapeutic implications of these findings warrant further study.

Keywords: immunohistochemistry, optic nerve head (ONH), lamina cribrosa, myelin, microglia, macrophages, monkey, experimental glaucoma (EG), astrocytes

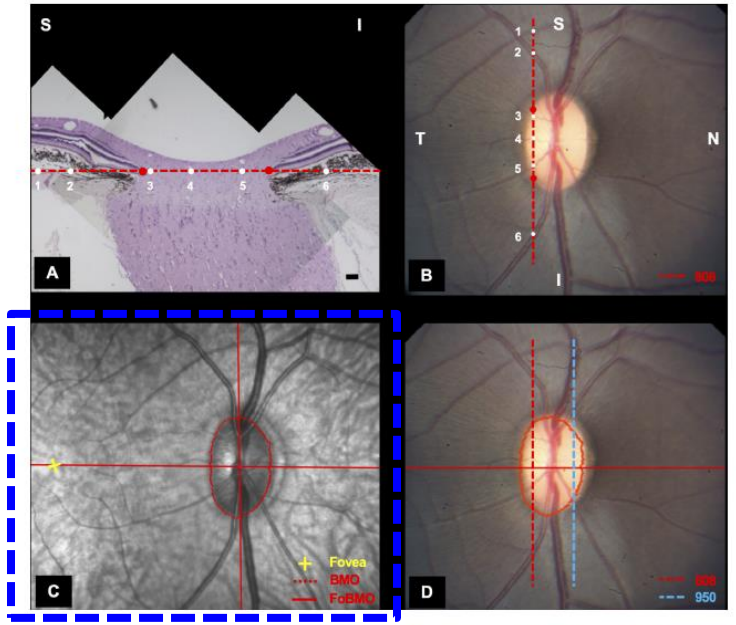

Figure 2. Estimating the clinical location of temporal and nasal "cardinal" ONH paraffin sections relative to the OCT foveal-BMO (FoBMO) axis. See the Methods section for our definition of the ONH and neural canal. (**A**) The temporal cardinal section (number 808 - *red dotted line* in panels **A**, **B**, and **D**) from the left (control) eye (shown in the right eye orientation) of NHP 3 was stained using hematoxylin and eosin (H&E) and the location of each blood vessel (6 *white circles* numbered 1 to 6 also in *white*) and BMO point (*red circles*) was identified and projected to the BMO reference line (*red dotted line* in panels **A**, **B**, and **D**). (**B**) The superior (S) versus inferior (I) orientation and temporal versus nasal location of the section (*red dotted line*) is estimated by adjusting the angle of the section line until the best fit of the BMO and vessel points (1 to 6 in *white* from panel **A**) to the photograph is accomplished. Estimating the location of a nasal cardinal section (section 950 – *blue dotted line* in panel **D**) was then performed in a similar manner. (**C**) The OCT-determined foveal to BMO centroid (FoBMO) axis as projected onto the infrared (IR) image acquired at the time of OCT image acquisition during the pre-euthanasia imaging session. (**D**) The location and orientation of the temporal (808) and nasal (950) cardinal tissue sections relative to the OCT-determined FoBMO axis is achieved by colocalizing the color fundus image containing their locations to the OCT IR image using the retinal vessels. The nasal/temporal position and S versus I orientation of each individual IHC section is then approximated relative to the cardinal sections by using the section number and fine-tuned using the vessel crossings and BMO points as outlined above.

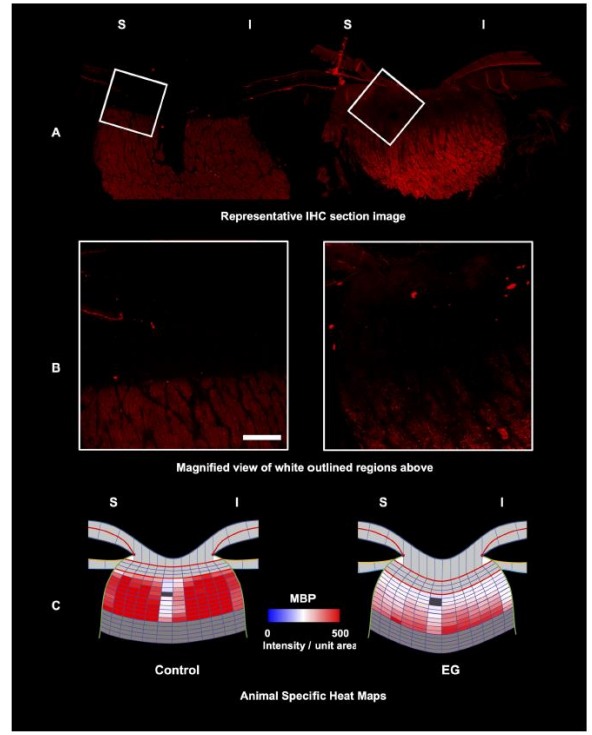

Figure 6. MBP intensity decreased in the EG eye retrolaminar regions. Representative control (*left*) and EG (*right*) eye single IHC section images (**A**, **B**) and animal-specific mean intensity heat maps (**C**) for MBP for NHP2. **A** Control and EG eye fluorescent full section images (see Fig. 3A for the clinical location of these sections), with magnified views of the white outlined regions shown in **B**. (**C**) MBP intensity heat maps for NHP2 based on mean data for four section images from each eye reveal diffuse qualitative decreases in both retrolaminar RL1 and RL2 subregions (see Fig. 3), which achieve significance by statistical analysis (see Table 2, Supplementary Table S1). *Dark grey* color denotes blood vessels.

Chaudhary et al, IOVS, 2022

Quantitative IHC

Quantitative SBEM axon tracing suggests that structurally-intact, retrolaminar axons are demyelinated in NHP experimental glaucoma.

Glaucoma

Retrolaminar Demyelination of Structurally Intact Axons in Nonhuman Primate Experimental Glaucoma

Priya Chaudhary,[1,2] Howard Lockwood,[1,2] Cheri Stowell,[1,2] Eric Bushong,[3] Juan Reynaud,[1,2] Hongli Yang,[1,2] Stuart K. Gardiner,[2] Galen Wiliams,[1,2] Imee Williams,[1,2] Mark Ellisman,[3] Nick Marsh-Armstrong,[4] and Claude Burgoyne[1,2]

[1]Optic Nerve Head Research Laboratory, Legacy Devers Eye Institute, Legacy Research Institute, Portland, Oregon, United States
[2]Discoveries in Sight, Devers Eye Institute, Legacy Research Institute, Portland, Oregon, United States
[3]National Center for Microscopy & Imaging Research, UCSD, La Jolla, California, United States
[4]Department of Ophthalmology, University of California, Davis, California, United States

Correspondence: Claude F. Burgoyne, Optic Nerve Head Research Laboratory, Devers Eye Institute, Legacy Research Institute, 1225 NE 2nd Avenue, Portland, OR 97232, USA; cfburgoyne@deverseye.org.

Received: November 2, 2023
Accepted: January 28, 2024
Published: February 26, 2024

Citation: Chaudhary P, Lockwood H, Stowell C, et al. Retrolaminar demyelination of structurally intact axons in nonhuman primate experimental glaucoma. *Invest Ophthalmol Vis Sci.* 2024;65(2):36. https://doi.org/10.1167/iovs.65.2.36

Purpose. To determine if structurally intact, retrolaminar optic nerve (RON) axons are demyelinated in nonhuman primate (NHP) experimental glaucoma (EG).

Methods. Unilateral EG NHPs ($n = 3$) were perfusion fixed, EG and control eyes were enucleated, and foveal Bruch's membrane opening (FoBMO) 30° sectoral axon counts were estimated. Optic nerve heads were trephined; serial vibratome sections (VSs) were imaged and colocalized to a fundus photograph establishing their FoBMO location. The peripheral neural canal region within $n = 5$ EG versus control eye VS comparisons was targeted for scanning block-face electron microscopic reconstruction (SBEMR) using micro–computed tomographic reconstructions (μCTRs) of each VS. Posterior laminar beams within each μCTR were segmented, allowing a best-fit posterior laminar surface (PLS) to be colocalized into its respective SBEMR. Within each SBEMR, up to 300 axons were randomly traced until they ended (nonintact) or left the block (intact). For each intact axon, myelin onset was identified and myelin onset distance (MOD) was measured relative to the PLS. For each EG versus control SBEMR comparison, survival analyses compared EG and control MOD.

Results. MOD calculations were successful in three EG and five control eye SBEMRs. Within each SBEMR comparison, EG versus control eye axon loss was −32.9%, −8.3%, and −15.2% (respectively), and MOD was increased in the EG versus control SBEMR ($P < 0.0001$ for each EG versus control SBEMR comparison). When data from all three EG eye SBEMRs were compared to all five control eye SBEMRs, MOD was increased within the EG eyes.

Conclusions. Structurally intact, RON axons are demyelinated in NHP early to moderate EG. Studies to determine their functional status are indicated.

Keywords: serial block-face scanning electron microscopy, nonhuman primate, monkey, glaucoma, lamina cribrosa, myelin, demyelination

Chaudhary et al, IOVS, 2024

Quantitative *3D* SBEM

(scanning block-face electron microscopy)

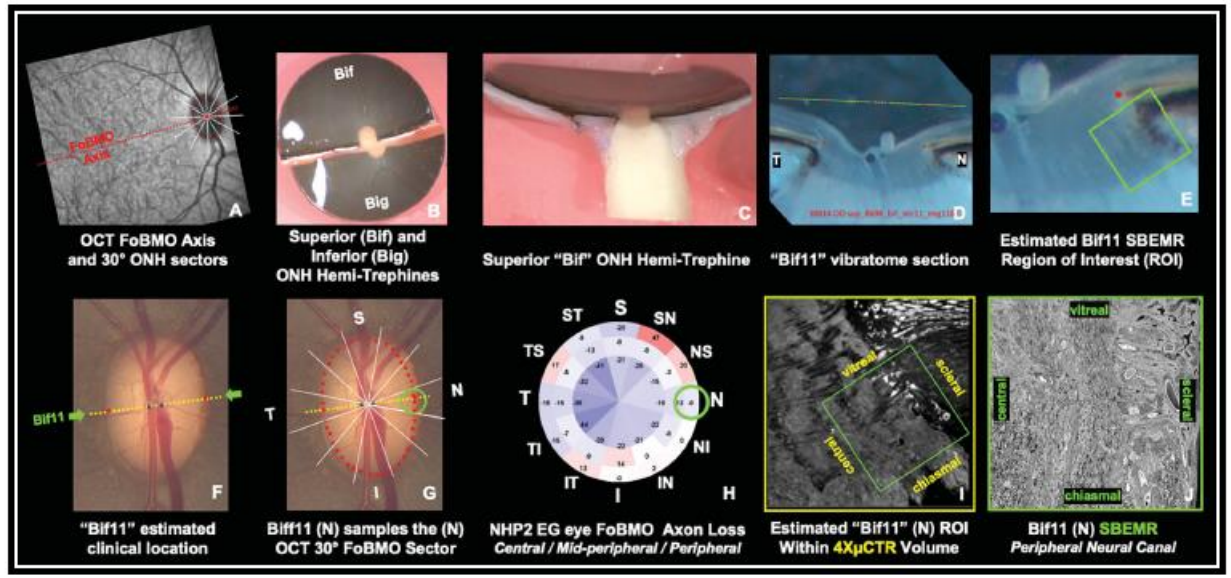

Figure 3. Post-mortem tissue processing part 2: controlling the anatomic location of the NHP2 Bif11 EG eye nasal (N) (Table 2) SBEMR so as to sample the peripheral-most axon bundles within the laminar and RON regions of the nasal (N) FoBMO 30° sector (ON axon loss 8.3%). (**A–H**) The clinical and anatomic locations of the SBEMR are shown. (**A**) The infrared (IR) image acquired at the time of OCT acquisition showing the FoBMO axis (*red dotted line*) extending from the OCT-detected center of the fovea through the OCT-detected BMO (*small red dots*) and centroid (*large red dot*). The OCT FoBMO ONH 30° sectors (*white lines*) are also shown. (**B**) Manual transection of the 10.0-mm ONH trephine along a line approximating the FoBMO axis into superior (tissue number "Bif") and inferior (tissue number "Big") hemi-trephines for serial 100-μm vibratome sectioning. (**C**) Cut-face of the superior hemi-trephine. (**D**) For each vibratome section, BMO points (*red dots*) and vessel locations (*blue dots*) are used to identify the section's location within a clinical fundus photo (*green arrows* in **F**). (**E**) Closeup of the nasal side of the Bif11 vibratome section in **D**, in which the SBEMR ROI has been tentatively identified (*white square*). (**F**) Each individual vibratome section is colocalized to the clinical ONH photograph using the histologic BMO (*red*) and vessel (*blue*) points identified in **D** (see Methods). (**G**) The OCT FoBMO 30° sectors are imposed onto the fundus photo after it has been colocalized to the OCT IR, allowing the FoBMO sectoral location of the SBEMR to be estimated. (**H**) Estimated FoBMO EG eye axon count differences from control (−8% for the peripheral subsector of the [N] 30° sector [*green circle*]). The 30° sectoral acronyms are defined at the end of this legend. (**I**) A single optical section image from a 4× microscopic x-ray computed tomographic reconstruction (μCTR) of the vibratome section is used to finalize the x-y-z location (*green box*) of the 200 × 200 × 50-μm SBEMR within the 100-μm thick vibratome section. (**J**) Single SBEMR block-face image at the starting point of the reconstruction. The chiasmal, vitreous, central, and scleral surfaces of the reconstruction are identified in **I** and **J**. See Figure 2H for the definition of the FoBMO 30° sectoral acronyms. See Table 1 for acronym definitions.

Axon transport studies to show that demyelinated axons are functionally intact are now indicated.

Glaucoma

Retrolaminar Demyelination of Structurally Intact Axons in Nonhuman Primate Experimental Glaucoma

Priya Chaudhary,[1,2] Howard Lockwood,[1,2] Cheri Stowell,[1,2] Eric Bushong,[3] Juan Reynaud,[1,2] Hongli Yang,[1,2] Stuart K. Gardiner,[2] Galen Wiliams,[1,2] Imee Williams,[1,2] Mark Ellisman,[3] Nick Marsh-Armstrong,[4] and Claude Burgoyne[1,2]

[1]Optic Nerve Head Research Laboratory, Legacy Devers Eye Institute, Legacy Research Institute, Portland, Oregon, United States
[2]Discoveries in Sight, Devers Eye Institute, Legacy Research Institute, Portland, Oregon, United States
[3]National Center for Microscopy & Imaging Research, UCSD, La Jolla, California, United States
[4]Department of Ophthalmology, University of California, Davis, California, United States

Correspondence: Claude F. Burgoyne, Optic Nerve Head Research Laboratory, Devers Eye Institute, Legacy Research Institute, 1225 NE 2nd Avenue, Portland, OR 97232, USA; cfburgoyne@deverseye.org.

Received: November 2, 2023
Accepted: January 28, 2024
Published: February 26, 2024

Citation: Chaudhary P, Lockwood H, Stowell C, et al. Retrolaminar demyelination of structurally intact axons in nonhuman primate experimental glaucoma. *Invest Ophthalmol Vis Sci.* 2024;65(2):36. https://doi.org/10.1167/iovs.65.2.36

Purpose. To determine if structurally intact, retrolaminar optic nerve (RON) axons are demyelinated in nonhuman primate (NHP) experimental glaucoma (EG).

Methods. Unilateral EG NHPs ($n = 3$) were perfusion fixed, EG and control eyes were enucleated, and foveal Bruch's membrane opening (FoBMO) 30° sectoral axon counts were estimated. Optic nerve heads were trephined; serial vibratome sections (VSs) were imaged and colocalized to a fundus photograph establishing their FoBMO location. The peripheral neural canal region within $n = 5$ EG versus control eye VS comparisons was targeted for scanning block-face electron microscopic reconstruction (SBEMR) using micro–computed tomographic reconstructions (μCTRs) of each VS. Posterior laminar beams within each μCTR were segmented, allowing a best-fit posterior laminar surface (PLS) to be colocalized into its respective SBEMR. Within each SBEMR, up to 300 axons were randomly traced until they ended (nonintact) or left the block (intact). For each intact axon, myelin onset was identified and myelin onset distance (MOD) was measured relative to the PLS. For each EG versus control SBEMR comparison, survival analyses compared EG and control MOD.

Results. MOD calculations were successful in three EG and five control eye SBEMRs. Within each SBEMR comparison, EG versus control eye axon loss was −32.9%, −8.3%, and −15.2% (respectively), and MOD was increased in the EG versus control SBEMR ($P < 0.0001$ for each EG versus control SBEMR comparison). When data from all three EG eye SBEMRs were compared to all five control eye SBEMRs, MOD was increased within the EG eyes.

Conclusions. Structurally intact, RON axons are demyelinated in NHP early to moderate EG. Studies to determine their functional status are indicated.

Keywords: serial block-face scanning electron microscopy, nonhuman primate, monkey, glaucoma, lamina cribrosa, myelin, demyelination

Chaudhary et al, IOVS, 2024

Quantitative *3D* SBEM

(scanning block-face electron microscopy)

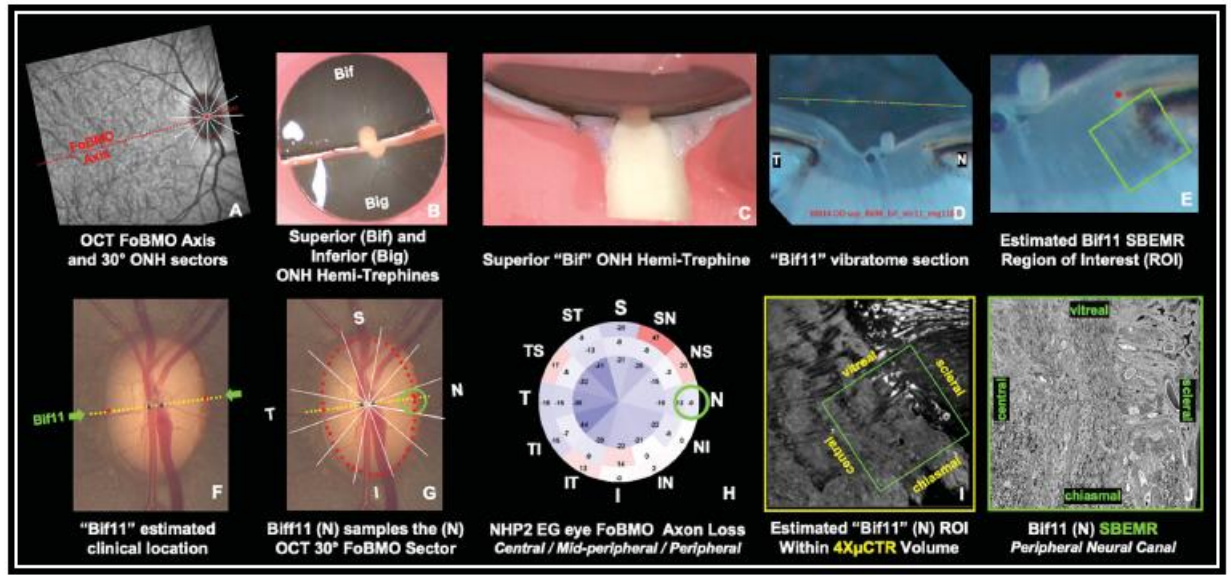

Figure 3. Post-mortem tissue processing part 2: controlling the anatomic location of the NHP2 Bif11 EG eye nasal (N) (Table 2) SBEMR so as to sample the peripheral-most axon bundles within the laminar and RON regions of the nasal (N) FoBMO 30° sector (ON axon loss 8.3%). (**A–H**) The clinical and anatomic locations of the SBEMR are shown. (**A**) The infrared (IR) image acquired at the time of OCT acquisition showing the FoBMO axis (*red dotted line*) extending from the OCT-detected center of the fovea through the OCT-detected BMO (*small red dots*) and centroid (*large red dot*). The OCT FoBMO ONH 30° sectors (*white lines*) are also shown. (**B**) Manual transection of the 10.0-mm ONH trephine along a line approximating the FoBMO axis into superior (tissue number "Bif") and inferior (tissue number "Big") hemi-trephines for serial 100-μm vibratome sectioning. (**C**) Cut-face of the superior hemi-trephine. (**D**) For each vibratome section, BMO points (*red dots*) and vessel locations (*blue dots*) are used to identify the section's location within a clinical fundus photo (*green arrows* in **F**). (**E**) Closeup of the nasal side of the Bif11 vibratome section in **D**, in which the SBEMR ROI has been tentatively identified (*white square*). (**F**) Each individual vibratome section is colocalized to the clinical ONH photograph using the histologic BMO (*red*) and vessel (*blue*) points identified in **D** (see Methods). (**G**) The OCT FoBMO 30° sectors are imposed onto the fundus photo after it has been colocalized to the OCT IR, allowing the FoBMO sectoral location of the SBEMR to be estimated. (**H**) Estimated FoBMO EG eye axon count differences from control (−8% for the peripheral subsector of the [N] 30° sector [*green circle*]). The 30° sectoral acronyms are defined at the end of this legend. (**I**) A single optical section image from a 4× microscopic x-ray computed tomographic reconstruction (μCTR) of the vibratome section is used to finalize the x-y-z location (*green box*) of the 200 × 200 × 50-μm SBEMR within the 100-μm thick vibratome section. (**J**) Single SBEMR block-face image at the starting point of the reconstruction. The chiasmal, vitreous, central, and scleral surfaces of the reconstruction are identified in **I** and **J**. See Figure 2H for the definition of the FoBMO 30° sectoral acronyms. See Table 1 for acronym definitions.

This work continues employing new technologies under Priya Chaudhary's direction in collaboration with Brad Fortune OD, PhD and Nick Marsh-Armstrong, PhD

Glaucoma

Optic Nerve Head Myelin-Related Protein, GFAP, and Iba1 Alterations in Non-Human Primates With Early to Moderate Experimental Glaucoma

Priya Chaudhary,[1,2] Cheri Stowell,[1,2] Juan Reynaud,[1,2] Stuart K. Gardiner,[2] Hongli Yang,[1,2] Galen Williams,[1,2] Imee Williams,[1,2] Nicholas Marsh-Armstrong,[3] and Claude F. Burgoyne[1,2]

[1]Optic Nerve Head Research Laboratory, Devers Eye Institute, Legacy Research Institute, Portland, Oregon, United States
[2]Discoveries in Sight, Devers Eye Institute, Legacy Research Institute, Portland, Oregon, United States
[3]Department of Ophthalmology, University of California - Davis, California, United States

Correspondence: Claude F. Burgoyne, Optic Nerve Head Research Laboratory, Devers Eye Institute, Legacy Research Institute, 1225 NE 2nd Avenue, Portland, OR 97232, USA;
cfburgoyne@deverseye.org.

Received: May 17, 2022
Accepted: September 8, 2022
Published: October 14, 2022

Citation: Chaudhary P, Stowell C, Reynaud J, et al. Optic nerve head myelin-related protein, GFAP, and Iba1 alterations in non-human primates with early to moderate experimental glaucoma. *Invest Ophthalmol Vis Sci.* 2022;63(11):9. https://doi.org/10.1167/iovs.63.11.9

Purpose. The purpose of this study was to test if optic nerve head (ONH) myelin basic protein (MBP), 2′,3′-cyclic nucleotide 3′-phosphodiesterase (CNPase), glial fibrillary acidic protein (GFAP), and ionized calcium binding adaptor molecule 1 (Iba1) proteins are altered in non-human primate (NHP) early/moderate experimental glaucoma (EG).

Methods. Following paraformaldehyde perfusion, control and EG eye ONH tissues from four NHPs were paraffin embedded and serially (5 µm) vertically sectioned. Anti-MBP, CNPase, GFAP, Iba1, and nuclear dye-stained sections were imaged using sub-saturating light intensities. Whole-section images were segmented creating anatomically consistent laminar (L) and retrolaminar (RL) regions/sub-regions. EG versus control eye intensity/pixel-cluster density data within L and two RL regions (RL1 [1-250 µm]/RL2 [251-500 µm] from L) were compared using random effects models within the statistical program "R."

Results. EG eye retinal nerve fiber loss ranged from 0% to 20%. EG eyes' MBP and CNPase intensity were decreased within the RL1 (MBP = 31.4%, $P < 0.001$; CNPase =62.3%, $P < 0.001$) and RL2 (MBP = 19.6%, $P < 0.001$; CNPase = 56.1%, $P = 0.0004$) regions. EG eye GFAP intensity was decreased in the L (41.6%, $P < 0.001$) and RL regions (26.7% for RL1, and 28.4% for RL2, both $P < 0.001$). Iba1+ and NucBlue pixel-cluster density were increased in the laminar (28.2%, $P = 0.03$ and 16.6%, $P = 0.008$) and both RL regions (RL1 = 37.3%, $P = 0.01$ and 23.7%, $P = 0.0002$; RL2 = 53.7%, $P = 0.002$ and 33.2%, $P < 0.001$).

Conclusions. Retrolaminar myelin disruption occurs early in NHP EG and may be accompanied by laminar and retrolaminar decreases in astrocyte process labeling and increases in microglial/ macrophage density. The mechanistic and therapeutic implications of these findings warrant further study.

Keywords: immunohistochemistry, optic nerve head (ONH), lamina cribrosa, myelin, microglia, macrophages, monkey, experimental glaucoma (EG), astrocytes

Quantitative IHC

Glaucoma

Retrolaminar Demyelination of Structurally Intact Axons in Nonhuman Primate Experimental Glaucoma

Priya Chaudhary,[1,2] Howard Lockwood,[1,2] Cheri Stowell,[1,2] Eric Bushong,[3] Juan Reynaud,[1,2] Hongli Yang,[1,2] Stuart K. Gardiner,[2] Galen Wiliams,[1,2] Imee Williams,[1,2] Mark Ellisman,[3] Nick Marsh-Armstrong,[4] and Claude Burgoyne[1,2]

[1]Optic Nerve Head Research Laboratory, Legacy Devers Eye Institute, Legacy Research Institute, Portland, Oregon, United States
[2]Discoveries in Sight, Devers Eye Institute, Legacy Research Institute, Portland, Oregon, United States
[3]National Center for Microscopy & Imaging Research, UCSD, La Jolla, California, United States
[4]Department of Ophthalmology, University of California, Davis, California, United States

Correspondence: Claude F. Burgoyne, Optic Nerve Head Research Laboratory, Devers Eye Institute, Legacy Research Institute, 1225 NE 2nd Avenue, Portland, OR 97232, USA;
cfburgoyne@deverseye.org.

Received: November 2, 2023
Accepted: January 28, 2024
Published: February 26, 2024

Citation: Chaudhary P, Lockwood H, Stowell C, et al. Retrolaminar demyelination of structurally intact axons in nonhuman primate experimental glaucoma. *Invest Ophthalmol Vis Sci.* 2024;65(2):36. https://doi.org/10.1167/iovs.65.2.36

Purpose. To determine if structurally intact, retrolaminar optic nerve (RON) axons are demyelinated in nonhuman primate (NHP) experimental glaucoma (EG).

Methods. Unilateral EG NHPs ($n = 3$) were perfusion fixed, EG and control eyes were enucleated, and foveal Bruch's membrane opening (FoBMO) 30° sectoral axon counts were estimated. Optic nerve heads were trephined; serial vibratome sections (VSs) were imaged and colocalized to a fundus photograph establishing their FoBMO location. The peripheral neural canal region within $n = 5$ EG versus control eye VS comparisons was targeted for scanning block-face electron microscopic reconstruction (SBEMR) using micro–computed tomographic reconstructions (µCTRs) of each VS. Posterior laminar beams within each µCTR were segmented, allowing a best-fit posterior laminar surface (PLS) to be colocalized into its respective SBEMR. Within each SBEMR, up to 300 axons were randomly traced until they ended (nonintact) or left the block (intact). For each intact axon, myelin onset was identified and myelin onset distance (MOD) was measured relative to the PLS. For each EG versus control SBEMR comparison, survival analyses compared EG and control MOD.

Results. MOD calculations were successful in three EG and five control eye SBEMRs. Within each SBEMR comparison, EG versus control eye axon loss was −32.9%, −8.3%, and −15.2% (respectively), and MOD was increased in the EG versus control SBEMR ($P < 0.0001$ for each EG versus control SBEMR comparison). When data from all three EG eye SBEMRs were compared to all five control eye SBEMRs, MOD was increased within the EG eyes.

Conclusions. Structurally intact, RON axons are demyelinated in NHP early to moderate EG. Studies to determine their functional status are indicated.

Keywords: serial block-face scanning electron microscopy, nonhuman primate, monkey, glaucoma, lamina cribrosa, myelin, demyelination

Quantitative *3D* SBEM

(scanning block-face electron microscopy)

Priya Chaudhary, PhD

Nick Marsh-Armstrong, PhD

Brad Fortune OD, PhD

Outline

- Professor Hans Goldmann
- Disclosures and Acknowledgements
- Revisiting 3D Optic Nerve Head Anatomy and Morphology
- The Optic Nerve Head in Glaucoma
- What Defines a Glaucomatous Optic Neuropathy?
- 3D Histomorphometric Structural Phenotyping in Monkey Glaucoma
- 3D OCT Structural Phenotyping in Monkey and Human Glaucoma
- qIHC and SBEM in Monkey EG
- Summary / Implications
- A Final Acknowledgement

Summary / Implications

- Current Pathophysiologic Definitions of Glaucoma should emphasize:
  - Primary Alterations of ONH /pNC Scleral / Posterior Scleral Connective Tissue Mechanobiology
  - Disruption of ONH RGC axon homeostasis that may precede or coincide with connective tissue changes
  - RGC Somal and Axon Projection Pathophysiology that may precede or coincide with ONH changes
  - Longitudinal OCT studies to confirm Deep ONH connective tissue remodeling in Humans are required
- *All* ONH Cellular Mechanisms remain unknown:
  - Altered ONH Neural/Connective Tissue Mechanobiology
  - altered ONH homeostasis
  - RGC axon insult
  - Mechanism by which Aging / Myopic Structural Remodeling / African Descent *increase* ONH susceptibility
  - All/Some of the above should provide targets for ONH-targeted neuroprotective interventions in glaucoma
- ONH Biomechanics Prospective / Retrospective Prediction of ONH susceptibility:
  - Not yet accomplished clinically or experimentally
  - OCT tools /concepts / techniques may be ready for prospective /retrospective monkey/human studies

Summary / Implications

- Current Pathophysiologic Definitions of Glaucoma should emphasize:
  - Primary Alterations of ONH Neural/Connective Tissue Mechanobiology
  - Disruption of ONH RGC axon homeostasis that may precede or coincide with connective tissue changes
  - RGC Somal and Axon Projection Pathophysiology that may precede or coincide with ONH changes
  - Longitudinal OCT studies to confirm Deep ONH connective tissue remodeling in Humans are required
- *All* ONH Cellular Mechanisms remain unknown:
  - Altered ONH Neural/Connective Tissue Mechanobiology
  - altered ONH homeostasis
  - RGC axon insult
  - Mechanism by which Aging / Myopic Structural Remodeling / African Descent *increase* ONH susceptibility
  - All/Some of the above should provide targets for ONH-targeted neuroprotective interventions in glaucoma
- ONH Biomechanics Prospective / Retrospective Prediction of ONH susceptibility:
  - Not yet accomplished clinically or experimentally
  - OCT tools /concepts / techniques may be ready for prospective /retrospective monkey/human studies

Cross-Sectionally - Lamina Cribrosa Thickness is increased in Human OHT eyes

Jpn J Ophthalmol (2016) 60:14–19
DOI 10.1007/s10384-015-0407-z

THE OFFICIAL INTERNATIONAL JOURNAL OF THE JAPANESE OPHTHALMOLOGICAL SOCIETY

CrossMark

CLINICAL INVESTIGATION

Evaluation of lamina cribrosa thickness and depth in ocular hypertension

Jong Chul Han[1] · Da-Ye Choi[1] · Young Kyo Kwun[1] · Wool Suh[2] · Changwon Kee[1]

Received: 28 April 2015 / Accepted: 21 July 2015 / Published online: 11 September 2015
© Japanese Ophthalmological Society 2015

Abstract

Purpose To investigate the differences in thickness and depth of the lamina cribrosa (LC) between ocular hypertension (OH) patients and normal control subjects, using enhanced depth imaging (EDI) spectral-domain optical coherence tomography (SD-OCT).

Methods EDI-OCT data were obtained from the subjects in a cross-sectional analysis of data from a retrospective study. After IOP correction according to central corneal thickness (CCT), we divided the OH patients into two groups based on the corrected IOP (cIOP) — OH with lower IOP (OH-L; cIOP < 23 mmHg) and OH with higher IOP (OH-H; cIOP ≥ 23 mmHg). Comparisons of LC thickness and depth among three groups were performed.

Results Seventy-four OH patients and 45 normal control subjects were included in the analysis. Among the 74 OH patients, 41 were included in the OH-L group and 33 were included in the OH-H group. LC thickness was thicker in the OH-H group compared to normal controls both in superior ($P = 0.02$) and inferior ($P = 0.01$) portions. However, no difference was found in LC depth among the three groups in any portion ($P = 0.36$; $P = 0.44$; $P = 0.31$, respectively).

Conclusion OH patients may have a thicker LC than normal control subjects, especially in OH with definite high IOP.

Keywords Ocular hypertension · Lamina cribrosa · Optical coherence tomography · Lamina cribrosa thickness

Introduction

Axonal injury in the lamina cribrosa (LC) is thought to be the most important factor in glaucoma pathogenesis [1–4]. Structural differences in the LC may be responsible for the differential effects of intraocular pressure (IOP) within the tissues and lamina cribrosa of the optic nerve head (ONH) [5]. Several studies investigated the associations between glaucoma and the thickness of LC measured by enhanced depth imaging (EDI) spectral domain (SD) optical coherent tomography (OCT) [6–11]. In these studies, eyes with glaucoma are reported to have a thinner LC than normal controls [6, 10]. In those studies, a thin LC was regarded as a structural weakness, explaining why NTG eyes show glaucomatous progression even under normal IOP.

Han, JC et al. JPN J Ophthalmol. 2016

Conclusion OH patients may have a thicker LC than normal control subjects, especially in OH with definite high IOP.

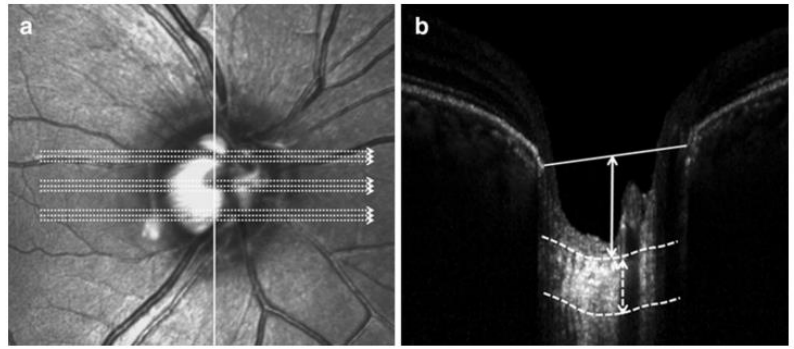

Fig. 1 Delineation of the border of the lamina cribrosa (LC). **a** Lamina cribrosa (LC) thickness and depth were measured at the presumed vertical center of three areas (superior, center, and inferior). **b** LC thickness was defined as the distance between the anterior and posterior borders of the LC (*dashed white arrow*). LC depth was defined as the distance between the reference line connecting both Bruch's membrane openings and the anterior border of the LC (*solid white arrow*)

Table 3 Mean thickness and depth of the lamina cribrosa

	Normal controls (*A*) ($n = 45$)	Ocular hypertension		*P*	Post hoc analysis		
		cIOP < 23 (*B*) ($n = 41$)	cIOP ≥ 23 (*C*) ($n = 33$)		*A–B*	*A–C*	*B–C*
Thickness (μm)							
Superior	232.1 ± 22.9 (195–279)	242.8 ± 23.3 (201–299)	254.9 ± 24.7 (211–310)	0.03	0.31	0.02	0.34
Middle	233.7 ± 23.2 (192–285)	241.1 ± 24.0 (198–302)	248.2 ± 24.2 (201–302)	0.11			
Inferior	230.6 ± 20.5 (197–272)	245.4 ± 23.8 (205–310)	253.5 ± 23.9 (213–307)	0.02	0.12	0.01	0.58
Depth (μm)							
Superior	431.2 ± 106.9 (179–640)	452.7 ± 89.3 (191–653)	452.6 ± 90.1 (185–651)	0.36			
Middle	442.8 ± 105.5 (165–653)	458.6 ± 95.4 (193–659)	462.2 ± 102.2 (192–655)	0.44			
Inferior	435.1 ± 110.2 (167–645)	449.3 ± 90.8 (188–638)	458.8 ± 101.0 (190–645)	0.31			

cIOP corrected intraocular pressure

Cross-Sectionally - Lamina Cribrosa Thickness is increased in Human OHT eyes

Glaucoma

Comparison of Lamina Cribrosa Morphology in Eyes with Ocular Hypertension and Normal-Tension Glaucoma

Ji-Ah Kim,[1] Tae-Woo Kim,[1] Eun Ji Lee,[1] Michaël J. A. Girard,[2,3] and Jean Martial Mari[4]

[1]Department of Ophthalmology, Seoul National University College of Medicine, Seoul National University Bundang Hospital, Seongnam, Korea
[2]Department of Biomedical Engineering, National University of Singapore, Singapore
[3]Singapore Eye Research Institute, Singapore National Eye Centre, Singapore
[4]GePaSud, Université de la Polynésie Française, Tahiti, French Polynesia

Correspondence: Tae-Woo Kim, Department of Ophthalmology, Seoul National University College of Medicine, Seoul National University Bundang Hospital, 82, Gumi-ro, 173 Beon-gil, Bundang-gu, Seongnam, Gyeonggi-do 463-707, Korea; twkim7@snu.ac.kr.

Received: May 8, 2019
Accepted: January 29, 2020
Published: April 9, 2020

Citation: Kim J-A, Kim T-W, Lee EJ, Girard MJA, Mari JM. Comparison of lamina cribrosa morphology in eyes with ocular hypertension and normal-tension glaucoma. *Invest Ophthalmol Vis Sci.* 2020;61(4):4. https://doi.org/10.1167/iovs.61.4.4

Purpose. To characterize differences in the lamina cribrosa (LC) morphology between healthy, ocular hypertension (OHT), and naive normal-tension glaucoma (NTG) eyes.

Methods. Each group consisted of 80 eyes of 80 participants who were matched for age, sex, and axial length. The participants underwent enhanced-depth-imaging volume scanning of the optic nerve head using spectral-domain optical coherence tomography. The lamina cribrosa curvature index (LCCI) and lamina cribrosa thickness (LCT) were measured in horizontal B-scan images spaced equidistantly across the vertical diameter of the optic disc.

Results. The LCCIs in all seven planes were smaller in both OHT and healthy eyes than in NTG eyes (all $P < 0.001$), and did not differ significantly between the OHT and healthy eyes. The LCTs in all three planes were greatest in OHT eyes followed by healthy and then NTG eyes (all $P < 0.001$). Overall, the larger LCCI was associated with smaller LCT ($P < 0.001$).

Conclusions. The LC was thin and steeply curved in NTG eyes than in healthy and OHT eyes. In OHT eyes, the LC was thick, and its curvature was comparable to healthy eyes. Longitudinal studies are required to examine whether the straight and thickened LCs in OHT eyes precede the onset of OHT or are a protective response to elevated intraocular pressure.

Keywords: ocular hypertension, normal-tension glaucoma, lamina cribrosa

Kim, JA, et al. IOVS. 2020

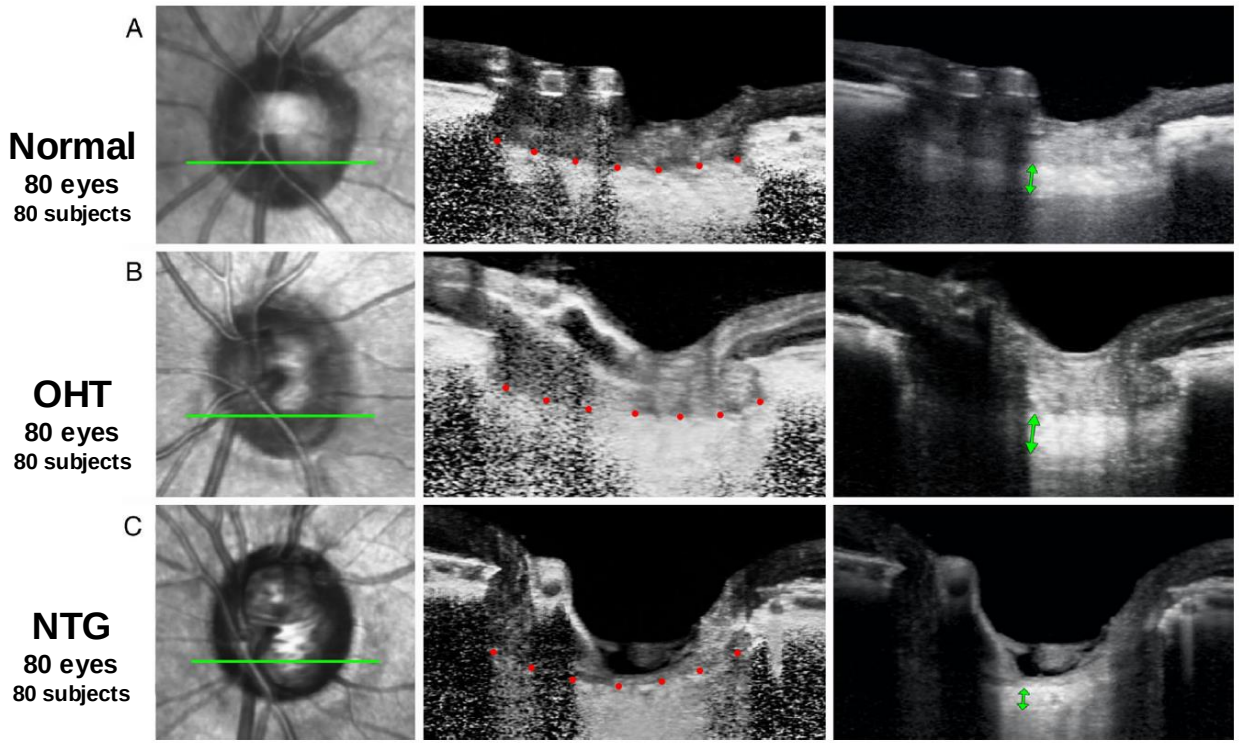

Figure 2. Three representative cases. (*Left*) En face images of the left eyes of a 62-year-old man with a healthy eye (**A**), a 60-year-old man with an OHT eye (**B**), and a 62-year-old man with an NTG eye (**C**), respectively. (*Middle*) B-scan images postprocessed using adaptive compensation in the plane indicated by the *green lines* in the en face images. Note that the degree of posterior bowing of the anterior LC surface (*red dots*) was greatest in the NTG eye. (*Right*) MIP images. Note that the LC thickness (*green arrows*) was greatest in the OHT eye and smallest in the NTG eye.

Conclusions. The LC was thin and steeply curved in NTG eyes than in healthy and OHT eyes. In OHT eyes, the LC was thick, and its curvature was comparable to healthy eyes. Longitudinal studies are required to examine whether the straight and thickened LCs in OHT eyes precede the onset of OHT or are a protective response to elevated intraocular pressure.

longitudinal studies are required

Summary / Implications

- Pathophysiologic Definitions of Glaucoma should clearly state:
  - Primary Alterations of ONH Neural/Connective Tissue Mechanobiology
  - Primary and/or Secondary Disruption of ONH RGC axon homeostasis
  - RGC Somal and Axon Projection Pathophysiology that may precede or coincide with ONH changes
  - Longitudinal OCT studies to confirm Deep ONH connective tissue remodeling in Humans are required
- *All* ONH Cellular Mechanisms remain unknown:
  - Altered ONH Neural/Connective Tissue Mechanobiology
  - Altered ONH/RGC axon homeostasis
  - RGC axon insult
  - Mechanism by which Aging / Myopic Structural Remodeling / African Descent *increase* ONH susceptibility
  - Genetic contributions to all of the above
- ONH Biomechanics Prospective / Retrospective Prediction of ONH susceptibility:
  - Not yet accomplished clinically or experimentally in our own work or the work of others…….
  - OCT tools /concepts / techniques may be ready for prospective /retrospective monkey/human studies

Summary / Implications

- Pathophysiologic Definitions of Glaucoma should clearly state:
  - Primary Alterations of ONH Neural/Connective Tissue Mechanobiology
  - Primary and/or Secondary Disruption of ONH RGC axon homeostasis
  - RGC Somal and Axon Projection Pathophysiology that may precede or coincide with ONH changes
  - Longitudinal OCT studies to confirm Deep ONH connective tissue remodeling in Humans are required
- *All* ONH Cellular Mechanisms remain unknown:
  - altered ONH Mechanobiology
  - altered ONH homeostasis
  - RGC axon insult
  - Mechanism by which Aging / Myopic Structural Remodeling / African Descent increase ONH susceptibility
  - All/Some of the above should provide targets for ONH-targeted neuroprotective interventions in glaucoma
- ONH Morphologic/Finite Element Modeling based Prediction of ONH susceptibility:
  - Not yet accomplished clinically or experimentally in our own work or the work of others…….
  - OCT Tools /Concepts / Parameters may be ready for prospective /retrospective monkey/human studies

Outline

- Professor Hans Goldmann
- Disclosures and Acknowledgements
- Revisiting 3D Optic Nerve Head Anatomy and Morphology
- The Optic Nerve Head in Glaucoma
- What Defines a Glaucomatous Optic Neuropathy?
- FoBMO 3D Histomorphometric Structural Phenotyping in Monkey Glaucoma
- FoBMO 3D OCT Structural Phenotyping in Monkey and Human Glaucoma
- FoBMO qIHC and SBEM in Monkey EG
- Summary / Implications
- A Final Acknowledgement

My wife Vicki Smith – for 26 years of collaboration

My wife Vicki Smith – for 26 years of collaboration and FUN!!!

How Optic Nerve Head Biomechanics has Clarified the Defining Pathophysiology and OCT Structural Phenotype of Human Glaucoma

The Goldmann Lecture

2024 Glaucoma Research Society Meeting
Siam Reap, Cambodia

November 15, 2024

Thank You!

Claude Burgoyne, MD
Emeritus Van Buskirk Chair in Ophthalmic Research
Past-Director, Optic Nerve Head Research Laboratory
Legacy Devers Eye Institute
Portland, OR
cfburgoyne@gmail.org

How Optic Nerve Head Biomechanics has Clarified the Defining Pathophysiology and OCT Structural Phenotype of Human Glaucoma

The Goldmann Lecture

2024 Glaucoma Research Society Meeting
Siam Reap, Cambodia

November 15, 2024

GRS Website Version - Please request permission to replicate in any form.

Claude Burgoyne, MD
Emeritus Van Buskirk Chair for Ophthalmic Research
Past-Director, Optic Nerve Head Research Laboratory
Legacy Devers Eye Institute
Portland, OR
cfburgoyne@gmail.org

Jack Cioffi and the 3 Ring Binder

(….If it doesn't kill you it will make you stronger…..)

How Optic Nerve Head Biomechanics has Clarified the Defining Pathophysiology and OCT Structural Phenotype of Human Glaucoma

The Goldmann Lecture

2024 Glaucoma Research Society Meeting
Siam Reap, Cambodia

November 15, 2024

Thank You!

Claude Burgoyne, MD
Emeritus Van Buskirk Chair in Ophthalmic Research
Past-Director, Optic Nerve Head Research Laboratory
Legacy Devers Eye Institute
Portland, OR
cfburgoyne@gmail.org